ISHAM, LINCOLN & BEALE
COUNSELORS AT LAW

THREE FIRST NATIONAL PLAZA
CHICAGO, ILLINOIS 60602
TELEPHONE 312 558 7500
TELEX 2 5288

EDWARD S. ISHAM, 1872-1902
ROBERT T. LINCOLN, 1872-1889
WILLIAM G. BEALE, 1885-1923

WASHINGTON OFFICE
1120 CONNECTICUT AVENUE, N.W.
SUITE 840
WASHINGTON, D.C. 20036
202 833-9730

August 1, 1983

In the Matter of)	
)	Docket Nos. 50-329-OM
CONSUMERS POWER COMPANY)	50-330-OM
)	50-329-OL
(Midland Plant, Units 1)	50-330-OL
and 2))	

Charles Bechhoefer, Esq.
Atomic Safety & Licensing Board Panel
U.S. Nuclear Regulatory Commission
Washington, D. C. 20555

Dr. Jerry Harbour
Atomic Safety & Licensing Board Panel
U.S. Nuclear Regulatory Commission
Washington, D. C. 20555

Dr. Frederick P. Cowan
6152 N. Verde Trail
Apt. B-125
Boca Raton, Florida 33433

Dear Administrative Judges:

Pursuant to the duty of full disclosure, enclosed is the latest volume of the Seismic Margin Review which deals with the Auxiliary Building, together with a cover letter from Consumers Power Company to the NRC Staff.

Sincerely,

Philip P. Steptoe

PPS:es

enc.

cc Service List (with enclosure)

DS03

Frederick W Buckman
Executive Manager
Midland Project Office

General Offices: 1945 West Parnall Road, Jackson, MI 49201 • (517) 788-1933

July 22, 1983

Harold R Denton, Director
Office of Nuclear Reactor Regulation
US Nuclear Regulatory Commission
Washington, DC 20555

MIDLAND ENERGY CENTER
MIDLAND DOCKET NOS 50-329, 50-330
SEISMIC MARGIN REVIEW REPORT
FILE: B3.7.1 SERIAL: 23861
ENCLOSURE: VOLUME III - AUXILIARY BUILDING (25 COPIES)

REFERENCE: LETTER FROM J W COOK TO H R DENTON
SERIAL 21010, DATED FEBRUARY 4, 1983

As an attachment to our letter, Serial 21010, dated February 4, 1983, we submitted the criteria for the Seismic Margin Review, Volume I, for the Staff's review and it was subsequently discussed in a meeting on February 8, 1983 in Bethesda. The firm of Structural Mechanics Associates (SMA) of Newport Beach, CA, under the direction of Dr R P Kennedy, was assigned the task of performing the Seismic Margin Review per the criteria in Volume I. Volume III, dealing with the evaluation of the Seismic Margins in the Auxiliary Building is submitted for the Staff's review as an attachment to this letter.

Volume III of the Seismic Margin Review Report titled, "Auxiliary Building" describes in detail the method of analysis and the resulting seismic margins. The underpinning walls of the Electrical Penetration Areas (EPA) and the Control Tower were included in this evaluation for their margins. A wide range of relative soil stiffnesses between the main Auxiliary Building and the EPA were considered in the margin evaluation. In spite of the wide range of soils stiffnesses mentioned above, this evaluation shows that there is still a considerable amount of margin in the design. The lowest margin identified for the underpinning walls was conservatively estimated at 1.6 with respect to code allowables. The lowest margin identified in the rest of the structure was conservatively estimated at 1.2 with respect to code allowables.

oc0783-0516a100

Future volumes of the Seismic Margin Review Report dealing with structures and systems will be submitted as they become available.

Frederick W Buckman

FWB/BFH/bjb

CC FJCook, Midland Resident Inspector
JGKeppler, Administrator, NRC Region III
DSHood, NRC
FRinaldi, NRC
GHarstead, Harstead Engineering

oc0783-0516a100

BCC TABuczwinski, Midland
DBMiller, Midland, (3)
TABuczwinski, Midland
DMBudzik, P-24-517
PPSteptoe, IL&B (21)
PJGriffin, P-24-513
NRC Correspondence File, P-24-517
LGraber, LIS
FRHand, P-14-417
BFHenley, P-14-212
Dr R P Kennedy, SMA
TRThiruvengadam, P-14-400
KBRazdan
UFI, P-24-517A
BJWalraven, P-24-517

CONSUMERS POWER COMPANY
Midland Units 1 and 2
Docket No 50-329, 50-330

Letter Serial 23861 Dated July 22, 1983

At the request of the Commission and pursuant to the Atomic Energy Act of 1954, and the Energy Reorganization Act of 1974, as amended and the Commission's Rules and Regulations thereunder, Consumers Power Company submits Volume III of the Seismic Margin Review titled, "Auxiliary Building".

CONSUMERS POWER COMPANY

By /s/ F W Buckman
F W Buckman, Executive Manager
Midland Project Office

Sworn and subscribed before me this 22nd day of July, 1983

/s/ Pamela J Griffin
Notary Public
Jackson County, Michigan

My Commission Expires Sept 8, 1984

oc0783-0516a100

NRC LICENSING CORRESPONDENCE - RECORD SUMMARY

DATE: July 19, 1983

DOCKET NUMBERS 50-329, 50-330
MIDLAND UNITS 1 & 2

SUMMARY: (State why letter is written)
To transmit Volume III of the Seismic Margin Review Report titled, "Auxiliary Building" for the Staff to review.

COMMITMENTS MADE: (LCP items will be made for these items by Safety & Licensing; Site commitments will be identified separately).

None

PREVIOUS NRC/CPCO CORRESPONDENCE (References)

JWCook to HRDenton Serial 23197 dated July 11, 1983

File/UFI NO.

B3.7.1

INDIVIDUALS PROVIDING INFORMATION (Including Consultants)

Dr R P Kennedy of Structural Mechanics Associates

CONCURRENCES (normally name of section or department head and name of any site personnel who concurred)

TRThiruvengadam

ORIGINATOR (Preparer)

BFHenley

SPECIAL DISTRIBUTION

US Mail [X]

Federal Express [ ]

Telecopy [ ]

To Whom:

INDIVIDUALS ASSIGNED RESPONSIBILITY FOR IMPLEMENTING COMMITMENTS:

TRThiruvengadam

LCP item(s) or SER open item(s) this correspondence closes:

None

Attachments or Enclosures?

Yes [X] How Many: 1

No [ ]

SMA 13701.05R003(VOLUME III)

SEISMIC MARGIN REVIEW

VOLUME III

AUXILIARY BUILDING

prepared for

CONSUMERS POWER COMPANY
Jackson, Michigan

June, 1983

STRUCTURAL MECHANICS ASSOCIATES
A Calif. Corp.

5160 Birch Street, Newport Beach, Calif. 92660 (714) 833-7552

SMA 13701.05R003(VOLUME III)

SEISMIC MARGIN REVIEW

VOLUME III

AUXILIARY BUILDING

by

D. A. Wesley
R. P. Kennedy
R. H. Kincaid
P. S. Hashimoto
R. D. Thrasher
W. H. Tong

Approved: D A Wesley for
R. P. Kennedy
President

Approved: Thomas R. Kipp
T. R. Kipp
Manager of
Quality Assurance

prepared for

CONSUMERS POWER COMPANY
Jackson, Michigan

June, 1983

STRUCTURAL MECHANICS ASSOCIATES
A Calif. Corp.
5160 Birch Street, Newport Beach, Calif. 92660 (714) 833-7552

REVISIONS

Document Number SMA 13701.05R003(VOLUME III)

Title Seismic Margin Review

Volume III

Auxiliary Building

Rev.	Description	QA	Project Manager
8/1982	Draft for Review	Thomas R. Kipp 3/30/82	D A Wesley 8/30/82
3/1983	Initial Issue	Thomas R. Kipp 3/7/83	D A Wesley 3/7/83
5/1983	Revised to include discussion of thermal stress, soil bearing capacity, and editorial changes Elevation 659' floor slab modification	Thomas R. Kipp 5/17/83	D A Wesley 5/16/83

SEISMIC MARGIN REVIEW
MIDLAND ENERGY CENTER PROJECT

TABLE OF CONTENTS

TABLE OF CONTENTS

TABLE OF CONTENTS (Continued)

1. INTRODUCTION

A seismic margin evaluation of the Midland Energy Center has been conducted. The purpose of this assessment was to provide confidence in the safety and structural integrity of critical structures and equipment required to remain operational during an earthquake in order to achieve safe shutdown. This volume presents the results of the seismic analysis conducted for the auxiliary building complex.

The plant was designed in accordance with criteria and codes described in the FSAR (Reference 1). Recently, the expected seismic input at the Midland site has been reevaluated using current methodology (Reference 3, 4 and 5). Seismic inputs applicable for the auxiliary building were determined in terms of site specific response spectra at the original ground surface. These site specific response spectra as well as the overall methodology used to develop the seismic models and in-structure response spectra for equipment evaluation are contained in Volume I of this report (Reference 6). This volume of the report presents the results of the auxiliary building seismic analysis.

1.1 BUILDING FUNCTION

The auxiliary building is located between the two reactor containment building structures and provides essential control and service facilities for the reactor buildings. The auxiliary building contains the control room, access control room, cable spreading rooms, engineered safeguards systems, switchgear equipment, and facilities for fuel handling, storage and shipment (Reference 1). The areas containing engineered safeguards equipment are partitioned into separate rooms to provide protection against postulated accidents. The structure was designed to Seismic Category I criteria.

1.2 DESCRIPTION OF THE STRUCTURE

The auxiliary building at the Midland Nuclear Generating Station is a reinforced concrete structure consisting of the main auxiliary building, the control tower, and the east and west electrical penetration wing areas. The auxiliary building complex contains the control room, access control room, cable spreading room, engineered safeguards systems, switchgear equipment, and facilities for fuel handling, storage and shipment. A schematic representation of the concrete portion of this complex structure is presented in Figure III-1-1.

The auxiliary building is a reinforced concrete shear wall structure with structural steel framing above Elevation 659'-0" in the main auxiliary building. The geometry of the auxiliary building is a relatively complex building because of the many diverse functions this structure performs. Exterior walls, the spent fuel pool, and some interior walls are all part of the vertical load-carrying system. Many of the interior walls in the structure are of reinforced concrete block. These walls are designed to provide separation of building facilities only and were designed to have no load-carrying capacity. Reinforced concrete floor slabs supported on steel beams and integrally connected to the shear walls are used throughout the structure as part of the vertical load-carrying system and provide diaphragm action to distribute the lateral forces resulting from seismic response. The structural steel frame above Elevation 659' in the main auxiliary building is used to support a 125 ton main crane and a 15 ton auxiliary crane.

The main auxiliary building is supported by a 6-foot thick reinforced concrete mat approximately 158' long and 79' wide, founded on glacial till at Elevation 562 feet. Beneath the control tower and electrical penetration wings, remedial underpinning (Figures III-1-1 and III-1-2) has been designed which transfers all loads from the control tower and electrical penetration wings to the undisturbed glacial till. The underpinning beneath the electrical penetration wing areas are 6-foot thick, reinforced concrete walls, 38 feet high, belled out to 10-feet

thick at the bottom. The underpinning walls beneath the control tower are 6-foot thick, reinforced concrete walls, varying from 41 to 47 feet high. These walls bell outward to 14-feet thick at the base. Individual piers are provided to underpin interior columns of the building. The bottom of the underpinning beneath the control tower is at Elevation 562 feet. Beneath the electrical penetration wings, the bottom of the underpinning is at Elevation 571 feet.

1.3 GROUND MOTION

The auxiliary building base mat and foundation remedial structure beneath the control tower and electrical penetration wings are founded on the natural material (glacial till) at the Midland site. The SME ground response spectra appropriate for use with structures founded on the original ground were presented in Volume I of this report and are shown in Figure III-1-3 for reference.

1.4 SOIL PROPERTIES

The auxiliary building is founded on glacial till deposits. These deposits consist of very stiff to hard cohesive soils, with some very dense sandy soils near the bedrock. The details of site geology are discussed in the FSAR (Reference 1). The site characteristics for the Midland plant have been discussed in Volume I of this report. Figures III-1-4 and III-1-5 present the soft site and stiff site profiles, respectively. In addition, Figure III-1-6 presents an intermediate profile. The development of the intermediate profile as well as the low strain shear moduli, strain degradation effects and other engineering characteristics used in the Seismic Margin Review (SMR) are discussed in Volume I (Reference 6). Use of this wide range of soil characteristics in the seismic analysis of the auxiliary building ensures conservative response results in both the structure loads and in-structure response spectra.

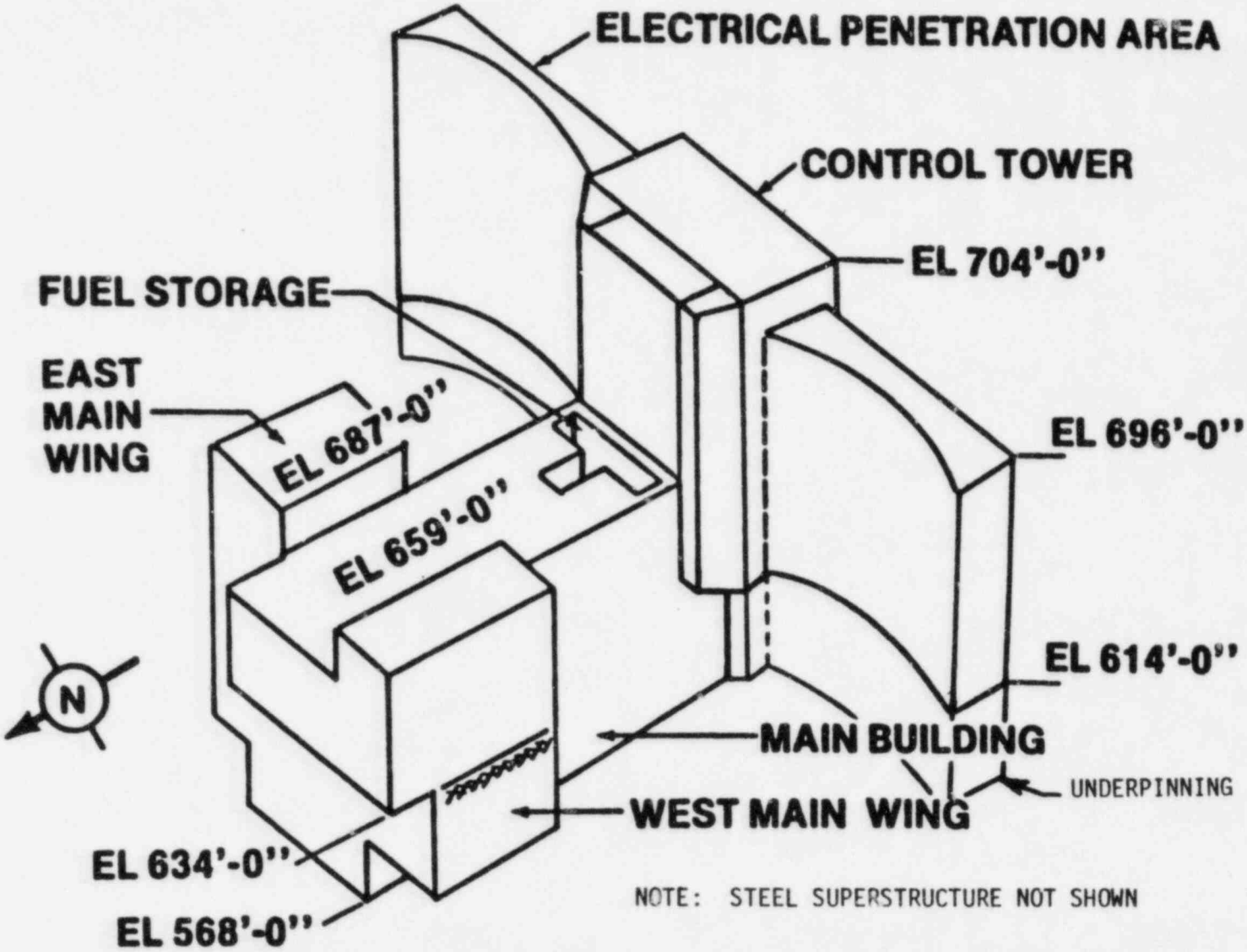

FIGURE III-1-1. SCHEMATIC REPRESENTATION OF AUXILIARY BUILDING AND CONTROL TOWER

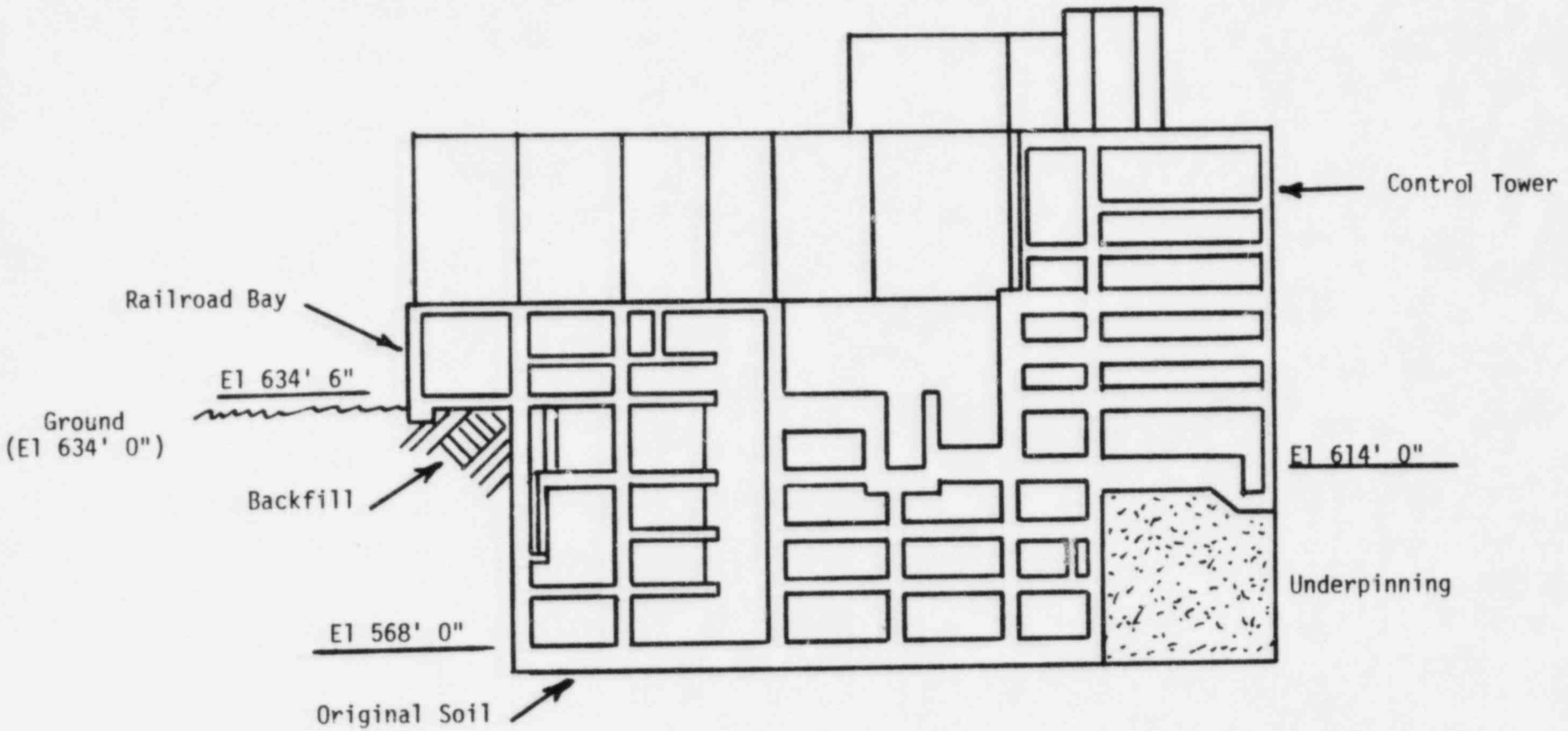

FIGURE III-1-2. SECTIONAL VIEW OF AUXILIARY BUILDING AND CONTROL TOWER SHOWING UNDERPINNING

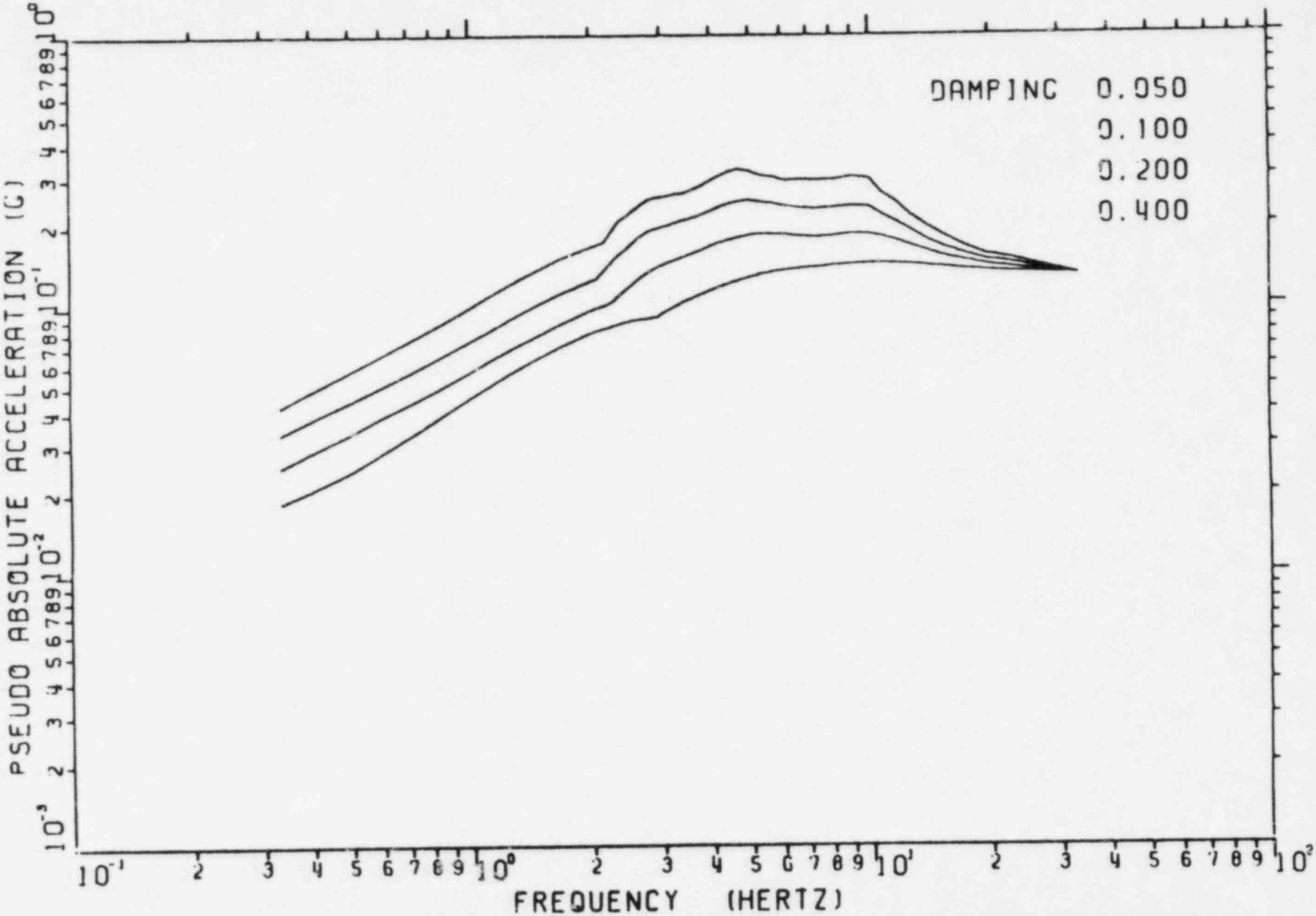

FIGURE III-1-3. SEISMIC MARGIN EARTHQUAKE ORIGINAL GROUND SURFACE ENVELOPE RESPONSE SPECTRA

Elevation

634 — Top of Grade

603 — Original Ground

Glacial Till

W_s = 135 pcf
ν = 0.47
V_s = 1290 fps

G_{max} = $7 \cdot 10^6$ psf
G_{SME} = $2 \cdot 10^6$ psf

550

Glacial Till

W_s = 135 pcf
ν = 0.47
V_s = 1690 fps

G_{max} = $12 \cdot 10^6$ psf
G_{SME} = $4.2 \cdot 10^6$ psf

410

Dense Cohesionless Material

W_s = 135 pcf
ν = 0.34
V_s = 2540 fps

G_{max} = $27 \cdot 10^6$ psf
G_{SME} = $17.8 \cdot 10^6$ psf

Elevation 410

V_s = 2970 fps

G_{max} = $37 \cdot 10^6$ psf
G_{SME} = $25.2 \cdot 10^6$ psf

Elevation 260

260

Bedrock

W_s = 150 pcf
ν = 0.33
V_s = 5000 fps

FIGURE III-1-4. SOIL LAYERING PROFILE FOR SOFT SITE

Elevation

634 — Top of Grade

603 — Original Ground

Aux. Bldg. - 570
Reactor Bldg. - 568
SWPS - 585

Glacial Till
W_s = 120 pcf
ν = 0.49 V_s = 1400 fps
G_{max} = $7.3 \cdot 10^6$ psf
G_{SME} = $3.65 \cdot 10^6$ psf

Glacial Till
W_s = 135 pcf
ν = 0.42
V_s = 2300 fps
G_{max} = $22.2 \cdot 10^6$ psf
G_{SME} = $13.3 \cdot 10^6$ psf

463

Glacial Till
W_s = 135 pcf
ν = 0.42
V_s = 3000 fps
G_{max} = $37.8 \cdot 10^6$ psf
G_{SME} = $25.0 \cdot 10^6$ psf

363

Dense Cohesionless Material
W_s = 135 pcf
ν = 0.34
V_s = 3000 fps
G_{max} = $37.8 \cdot 10^6$ psf
G_{SME} = $31.0 \cdot 10^6$ psf

263

Bedrock
W_s = 150 pcf
ν = 0.33
V_s = 5000 fps

FIGURE III-1-5. SOIL LAYERING PROFILE FOR STIFF SITE

Elevation

634 — Top of Grade

603 — Original Ground

Glacial Till

W_s = 110 pcf

ν = 0.49

V_s = 1500 fps

G_{max} = $7.7 \cdot 10^6$ psf

G_{SME} = $4.08 \cdot 10^6$ psf

553

Glacial Till

W_s = 135 pcf

ν = 0.42

V_s = 1890 fps

G_{max} = $15 \cdot 10^6$ psf

G_{SME} = $7.95 \cdot 10^6$ psf

463

Dense Cohesionless Material

W_s = 135 pcf

ν = 0.34

V_s = 2468 fps

G_{max} = $25.6 \cdot 10^6$ psf

G_{SME} = $13.6 \cdot 10^6$ psf

263

Bedrock

W_s = 145 pcf

ν = 0.33

V_s = 5000 fps

FIGURE III-1-6. INTERMEDIATE SOIL PROFILE

2. SEISMIC ANALYSIS

2.1 STRUCTURE DYNAMIC MODEL

The auxiliary building is represented by a three-dimensional, lumped-mass multi-stick model (with additional detail in the electrical penetration areas (EPA) provided by plate elements) which preserves the physical geometry of the various building components. The auxiliary building mathematical model was developed by Bechtel (Reference 13). As part of the SME evaluation, this model was reviewed to ensure that the overall dynamic characteristics of the structure are expected to be adequately represented. The auxiliary building dynamic model described herein was used to evaluate overall building response to seismic loadings as well as to generate the in-structure response spectra. The overall building dynamic responses developed from this model were also used to develop forces in the individual structural elements.

Figure III-2-1 presents a schematic plan of the auxiliary building. This building can be subdivided into a main auxiliary building, a control tower, and two EPA, all of which are interconnected. The overall dynamic response of the auxiliary building was calculated from a model developed using a series of vertical beam elements, each representing a major portion of the building (Figures III-2-2 through III-2-4). The stiffness and mass characteristics of the main auxiliary building (north of column line G) were modeled as one vertical beam. The control tower was also modeled as a vertical beam. Flexible beam elements at each floor elevation between column lines G and H are used to model the flexible interconnectivity between the control tower and the main auxiliary building. The stiffnesses for these connecting beam elements reflect both the floor properties and any interconnecting shear walls between column lines G and H. Rigid elements were used as connection members between column line H and the control tower beam, and between column line G and the main auxiliary building to reflect the actual geometry of the structure.

The wing areas are made up of a major vertical wall along the external south side of the structure with several intermediate cross walls. The south walls were represented by a series of plate elements with three beams per wing to reflect the intermediate cross walls. The individual EPA beams are connected by horizontal beam elements whose stiffness represents the existing floor properties. The EPA boundary nearest the control tower is connected to the control beam by rigid elements, representing the geometric distance to the control tower model.

Figures III-2-5 and III-2-6 present the overall auxiliary building dynamic model. The weights associated with major floors and walls throughout the structures were represented by lumped masses. The masses include concrete, steel, blockwalls, major equipment and 25% of the floor design live loading. The center of mass was established for each floor level and mass nodes were placed at these centers of mass. For the wing areas, the masses associated with each plate element were lumped in accordance with the plate thicknesses and the remaining mass associated with each EPA lumped at the floor elevations along the six sticks. Beam elements in Figure III-2-5 define the stiffness characteristics of the structural systems being represented. The elements were located at the calculated centers of rigidity and are thus horizontally offset from the mass points and from each other. These offsets (eccentricities) are included to properly account for torsional response.

The proposed underpinning design underneath the control tower was accounted for in the section properties of the control tower model below Elevation 614 feet. The underpinning wall layout was connected to the existing column line H wall to make up the extension of the control tower model to Elevation 562 feet. This portion of the control tower stick was also connected to the main auxiliary model by beam elements representing the floor properties and interconnecting shear walls in the same manner as the higher elevations. The mass associated with this portion of the control tower model includes both the concrete and any effective entrapped soil.

The EPA underpinning was represented by a series of plate elements having section properties equivalent to the underpinning concrete sections. The EPA underpinning plates were connected to the structural EPA beams and plates by rigid beams to maintain the geometric location and continuity of stiffness between the underpinning and existing structure. The underpinning plates were connected to the control tower model by rigid elements to reflect the geometry. The mass associated with the EPA underpinning was lumped at the nodes connecting the plate elements. This mass includes the actual concrete volume and the effective entrapped soil.

Soil-structure interaction impedance functions (represented by springs and dashpots) are attached to the structural model at the foundation mass points (■) shown in Figures III-2-5 and III-2-6. A single set of soil-structure interaction impedance functions is used for the main auxiliary and control tower portions of the foundation and are attached at the center of resistance for this foundation system. Individual impedance functions are placed at distributed node points at the base of the underpinning system for the EPA as shown in Figure III-2-3.

2.2 SOIL-STRUCTURE INTERACTION

2.2.1 Layered Site Analyses

The effects of the layered site characteristics on the auxiliary building seismic response were evaluated by developing equivalent elastic half-space soil impedances based on layered site analyses. These equivalent elastic half-space impedance functions were then modified to account for embedment effects and non-standard foundation shapes and were used in conjunction with the structure model described in Section 2.1 to perform the soil-structure interaction analysis of the auxiliary building complex. The layered site soil profiles presented in the previous section were used in conducting layered site analyses using the program CLASSI (Reference 7) to calculate the frequency-dependent soil impedances for the structure. The auxiliary building foundation geometry was

idealized as a 140' by 236' rectangular foundation as shown in Figure III-2-7 in all CLASSI analyses. This idealized foundation is founded at Elevation 562 feet.

The results of the CLASSI analyses are presented in Figures III-2-8 to III-2-25 for the three soil profiles studied. Soil impedances were developed for all global translational and rotational degrees-of-freedom. Both the real (stiffness) and imaginary (damping) portions of the soil impedances are presented in these figures for a range of soil-structure frequencies varying from 0 to 10 hertz. Figures III-2-8 to III-2-13 present the CLASSI layered site soil impedances for the soft site soil profile while Figures III-2-14 to III-2-19 and Figures III-2-20 to III-2-25 present the corresponding CLASSI results for the intermediate soil profile and the stiff site soil profile, respectively.

Examination of stiffness and damping terms for the soft site soil profile (Figures III-2-6 to III-2-13) shows there is some frequency dependence and resonance due to layering effects for horizontal translation degrees-of-freedom. The vertical translation and rocking degrees-of-freedom exhibit much stronger frequency dependence with layering effects particularly important in the vertical translation damping term. Torsional response of the structure is relatively unaffected by layering or frequency-dependent effects at all frequencies. Observations regarding layering effects for both the intermediate and stiff site soil profiles are similar. It should be noted that because CLASSI incorporates the five percent soil material damping in the layered site analysis, (References 6 and 7) the damping coefficient terms are not zero for the static case (0 hertz) as would be expected if only geometric damping was considered in the analysis.

2.2.2 Effective Elastic Half-Space Shear Moduli

The results of the CLASSI layered site analyses were used to develop effective elastic half-space shear moduli, G_{eff}, for all degrees-of-freedom of the structure (horizontal and vertical translation,

rocking, and torsion). The effective elastic half-space shear moduli were then used to develop soil impedances which accounted for actual foundation geometry, embedment effects, and soil layering. The procedure used to develop effective elastic half-space shear moduli from the CLASSI layered site analysis is presented in Volume I. Appendix A of this report presents a sample calculation of G_{eff} to demonstrate the procedure.

Table III-2-1 presents the effective soil shear moduli for each of the three soil profiles studied as determined from the CLASSI layered site analyses. For the auxiliary building, an effective soil shear modulus was developed which adequately represented the site characteristics for both the horizontal translation and torsional response modes of the structure for each soil case. Similarly, one shear modulus value was developed which was applicable to the vertical translation and rocking degrees-of-freedom of the structure.

Comparison of G_{eff} values tabulated in Table III-2-1 to the layered soil profiles presented in Figures III-1-4 to III-1-6 used in the CLASSI layered site analyses demonstrates some general trends. For the soft site soil profile, the G_{eff} of 3200 ksf associated with the horizontal translational and torsional response of the structure is influenced by the 12-foot thick layer of softer glacial till material beneath the structure from Elevation 550' to 562' shown in Figure III-1-4. For vertical translation and rocking, however, the G_{eff} of 4000 ksf is almost entirely due to the influence of the 140-foot thick layer of glacial till from Elevation 410' to 550' which has a degraded shear modulus of 4200 ksf.

Results for the intermediate soil case are similar. The effective soil shear modulus, G_{eff}, of 7100 ksf associated with horizontal translation and torsional response of the structure is slightly influenced by the soft layer of glacial till immediately beneath the structure. This layer tends to reduce to effective stiffness of the

half-space. The effective soil shear modulus, G_{eff}, of 8600 ksf determined for vertical translation and rocking of the structure is primarily due to the till material from Elevation 463' to 553'. Some minor influence of material below Elevation 463' is also reflected in the G_{eff} determined for these degrees-of-freedom.

The effective soil shear modulus values determined from the stiff site soil profiles reflect that the G_{eff} values of 13,900 ksf for horizontal translation and torsion, and 14,400 ksf for vertical translation and rocking degrees-of-freedom, are almost entirely due to the 99-foot thick layer of glacial till located between Elevation 463' to 562'. The stiffer material below Elevation 463' has a relatively minor influence on the G_{eff} values determined for this profile.

Upper and lower bound soil cases were developed for the auxiliary building based on the effective elastic half-space shear moduli presented in Table III-2-1. The upper and lower bound soil cases represent bounds the range of soil properties which might be possible at the Midland site. This is considered to adequately account for the variability from such factors as uncertainty in strain degradation effects, uncertainty in modeling soil-structure interaction, and the uncertainty in the knowledge of soil characteristics in the soil profiles studied. Based on these uncertainties, it was determined that $0.6 \times G_{eff}$ based on the soft site soil profile represented a realistic lower bound soil case for use in the SME. Similarly, $1.3 \times G_{eff}$ based on the stiff site soil profile was considered to be a realistic upper bound soil case for this structure. The details of the procedure used in developing the upper and lower bounds are presented in Section 4.3 of Volume I of this report. The intermediate soil case was not modified since it was considered to be a median representation of site conditions. Table III-2-2 presents the G_{eff} values used for the lower, intermediate, and upper bound soil cases used in the auxiliary building SME analysis.

2.2.3 Energy Entrapment Due to Layering

Two types of damping may be defined for the soil. The first type, known as material or hysteretic damping, is due to energy absorption by the soil due to straining of the material. For the Midland site, this damping has been conservatively estimated to be five percent of critical damping for the SME. Material damping is not significantly affected by layering. The second type of soil damping, known as geometric or radiation damping, involves the wave propagation of energy through the soil away from the structure. For an elastic half-space, these waves will propagate outwards to infinity. Layered soil profiles, however, tend to trap and reflect some of the energy back up towards the structure due to impedance mismatch at the layer interfaces. One of the principal reasons for conducting a layered site analysis for the SME was to determine the effect of layering on the geometric damping from the structure. In effect, the geometric damping for the layered profile is reduced to some percentage of the damping which would be determined for an equivalent elastic half-space. This decrease in geometric damping may be determined through the use of a factor defined as:

$$F_{Layer} = \frac{C(\text{CLASSI layered site analysis})}{C(\text{theoretical elastic half-space})}$$

where C (CLASSI layered site analysis) is the frequency-dependent damping including layering effects determined by the CLASSI layered site analysis. The term C (theoretical elastic half-space) represents the geometric damping which would be calculated for the structure based on the effective elastic half-space shear moduli and idealized foundation shape presented in Table III-2-1 and Figure III-2-7, respectively. This ratio is indicative of the amount of energy entrapped beneath the structure due to layering. The procedure for calculating F_{Layer} is presented in Volume I. A sample calculation of F_{Layer} is presented in Appendix A of this report.

Layering factors were determined for all three soil cases for the auxiliary building. Results showed that it was possible to define one set of layering factors for this structure applicable to all three soil profiles. Layering factors were conservatively limited to a maximum of 75 percent of theoretical elastic half-space geometric damping for all degrees-of-freedom where F_{Layer} was determined to be greater than 0.75. This conservative cutoff on geometric damping was based on results presented in Reference 8. These factors were defined for the auxiliary building as follows:

Structure Degree-of-Freedom	Layering Factor, F_{Layer}
Horizontal Translation and Torsion	0.75
Vertical Translation	0.75
Rocking	0.50

The results for this structure indicated that soil site layering was not significant for horizontal and vertical translations and the torsional degrees-of-freedom. For motions in these directions, the geometric damping of the structure was primarily determined by the thick glacial till layers below Elevation 550' shown in Figures III-1-4 to III-1-6. For rocking of the structure, however, layering effects were more important resulting in a reduction to 50 percent of theoretical elastic half-space damping. Rocking response of low-rise shear wall type structures such as the auxiliary building is relatively unimportant, however, and the lower calculated rocking geometric damping has a negligible effect on the overall responses.

2.2.4 Development of Global Soil Stiffnesses and Dashpots

Soil springs modeling the stiffness of the soil beneath the auxiliary building were developed based on the effective soil shear modulus values presented in Table III-2-2 and the actual building foundation geometry. Soil stiffnesses were calculated from the frequency-dependent elastic half-space equations shown in Table III-2-3. These equations and frequency-dependent coefficients are presented in References 9 to 12.

The auxiliary building foundation geometry used in determining the global soil stiffnesses for the structure is shown in Figure III-2-7. For the horizontal translation and torsional degrees-of-freedom, the entrapped soil beneath the control tower was assumed to act integrally with the foundation base mat. For vertical translation and rocking degrees-of-freedom, the geometric properties of the foundation were developed based on foundation contact area only.

The use of elastic half-space equations to calculate soil impedances required the development of equivalent base slab rectangles and circles for the auxiliary building based on the actual foundation geometry. The equivalent rectangles developed for the horizontal translation and rocking degrees-of-freedom were developed based on equivalence between the actual foundation geometric properties and the geometric properties of the rectangle. In the vertical direction, an equivalent rectangle was calculated based on area equivalence between the rectangle and the auxiliary building foundation contact area. The equivalent circle used to calculate the torsional soil stiffness was developed based on equivalence of polar moments of inertia between a circle and the actual foundation geometry.

The majority of the auxiliary building foundation is founded on glacial till at Elevation 562' and the G_{eff} values presented in Table III-2-2 are considered to be an appropriate representation of the effective soil shear modulus beneath most of the structure. However, the railroad bay is founded on softer fill material at approximately Elevation 630.5'. Use of the overall structure geometry including the railroad bay and the effective soil shear modulus values associated with Elevation 562' would overpredict soil stiffnesses beneath the auxiliary building. In order to approximately account for the softer material beneath the railroad bay, a weighted average soil stiffness was developed. The weighting procedure used to account for soil beneath the railroad bay is as follows:

1. Based on the overall foundation geometry including the railroad bay (Figure III-2-7) and the G_{eff} values shown in Table III-2-2 calculate the unembedded soil stiffness K* for the degree-of-freedom of interest.

2. Calculate an unembedded soil stiffness K' based on the structure foundation geometry neglecting the railroad bay for the same degree-of-freedom and use the same G_{eff} as in 1 above.

3. Determine the global soil stiffness for the degree-of-freedom by:

$$K_G = K' + (K^*-K') \frac{G_{eff} \text{ (railroad bay)}}{G_{eff} \text{ (Elevation 562')}} \qquad (2\text{-}1)$$

where G_{eff} (railroad bay) represents the effective soil shear modulus beneath the railroad bay and G_{eff} (Elevation 562') is the effective soil shear modulus presented in Table III-2-2.

This procedure was used for all degrees-of-freedom for the auxiliary building and is illustrated in Appendix A. Unembedded soil stiffnesses for each of the three soil cases studied are shown in Table III-2-4.

Embedment effects were considered to be applied as a multiplier to the unembedded frequency-dependent elastic half-space soil stiffnesses. Embedment effects considered both the soil in physical contact with the sides of the structure and stiffening of the soil due to the weight of adjacent structures. The procedure used to calculate embedment effects for the SME is described in Section 4.3 of Volume I. Appendix A of this volume presents a sample soil stiffness calculation including embedment effects.

As shown by Table III-2-4, embedment effects for the auxiliary building soil stiffnesses are relatively small. Translational degrees-of-freedom are stiffened by about 10 percent while rotational degrees-of-freedom show an increase on the order of 20 to 25 percent. Thus, the corresponding fundamental soil-structure frequencies would be expected to

increase in the range of 5 to 10 percent due to embedment effects. The final global soil stiffnesses for the structure including embedment effects are presented in Table III-2-4 for each of the three soil cases studied.

Dashpots modeling soil geometric and material damping were developed using the elastic half-space equations presented in Table III-2-3. Material damping of 5 percent of critical damping was assumed for the soil. Soil dashpots were calculated accounting for both layering and embedment effects as discussed in Volume I on methodology and criteria (Reference 6). A sample calculation of an embedded dashpot is presented in Appendix A of this report.

Table III-2-5 presents the unembedded dashpots and embedment factors for this structure. Embedment effects for damping increased translational dashpots 10 to 25 percent above their unembedded values. Rotational dashpots were increased by about 45 to 50 percent due to the stiffening effects from the surrounding soil. The embedded dashpots including 5 percent material damping are presented in Table III-2-5.

2.2.5 Relative Spring Stiffnesses Beneath the Electrical Penetration Areas

The global soil impedances presented in the previous section were based on the full auxiliary building foundation geometry. Examination of Figure III-2-7 shows this building has a fairly complex foundation shape. This structure has a thick base mat with many large interior shear walls stiffening the foundation. The structure base mat under the main structure is expected to act rigidly, and the global soil compliances for the structure were developed on this basis. However, because the EPA are long and narrow (Figures III-2-1 and III-2-2), there was concern that for seismic excitation there may be some slight flexibility of the EPA foundations relative to the main auxiliary/control tower foundation. Though this flexibility would not substantially affect the global soil impedances calculated by elastic half-space theory, flexing of the EPA relative to

the main auxiliary building and control tower could substantially influence the loads in the EPA underpinnings and possibly the in-structure response spectra calculated at locations in the EPA. Therefore, in order to conservatively define the loadings and in-structure spectra in the EPA, it was considered necessary to evaluate the effects of various approximations concerning the distribution of the portion of overall soil spring stiffness that supports them. Consideration was given to distributing the soil stiffness under the wings to the nodal points in the mathematical model representing the EPA foundation rather then lump all the soil stiffness at a single location beneath the auxiliary building foundation.

Because of these concerns, a parametric study was conducted in order to determine the effect on loads and in-structure response spectra of the distribution of the soil impedance beneath the EPA. Three cases were analyzed. The first case studied, defined as the global stiffness case, assumed that the soil compliance functions were developed using the overall structure foundation geometry and were located at the base mat centroid. Separate soil springs were not located beneath the EPA for this case. In the second case, defined as the lower bound relative wing stiffness case, a procedure was developed that calculated the lowest reasonable relative stiffnesses for the springs beneath the EPA. Soil springs were then distributed beneath the EPA and under the main auxiliary building/control tower foundation as shown schematically in Figure III-2-3. Equilibrium of the overall model was considered in order to ensure this case had the same global soil characteristics as defined by case one above. The final case, defined as the upper bound relative EPA stiffness case, used a procedure that calculated the highest reasonable relative stiffness for soil springs under them. As in case two, the soil stiffnesses beneath the auxiliary building/control tower foundation were adjusted to maintain the same global model characteristics defined by case one above. Using these models, comparisons of in-structure response spectra, peak accelerations, and peak displacements for each of the three models were made in order to determine the influence of modeling assumptions for the soil beneath the EPA.

The results of the parametric study investigating the influence of relative soil stiffness beneath the EPA are presented in Appendix B of this report. The relative soil springs beneath the EPA were developed using the methodology presented in Reference 28. Upper and lower bound relative EPA stiffnesses are presented in Tables III-2-6 to III-2-8 for each of the three soil cases studied for the SME. Locations of structural nodes referenced in these tables are shown in Figures III-2-5 and III-2-6.

The basic conclusions reached in this study were that for all locations studied, the in-structure response spectra, accelerations, and displacements were virtually identical for each of the three cases studied. The results indicated that the structure base mat was translating and rotating as a rigid body. Conservative in-structure response spectra can be calculated using the global stiffness case since the inclusion of relative soil springs beneath the EPA did not significantly influence structure response. Local load distributions were more sensitive to the assumptions. In developing structure dynamic response loads, moments and shears throughout the structure are conservatively taken as the envelope of results from both the lower bound relative wing stiffness case and the upper bound relative EPA stiffness case for each of the soil cases studied (lower bound, intermediate, and upper bound).

TABLE III-2-1

Auxiliary Building Seismic Margin Evaluation
Equivalent Elastic Half-Space Shear Moduli

Structure Degree-of-Freedom	Dynamic Soil Shear Modulus, G_{eff}		
	Soft Site Soil Profile (KSF)	Intermediate Soil Profile (KSF)	Stiff Site Soil Profile (KSF)
Horizontal Translation, Torsion	3,200	7,100	13,900
Vertical Translation, Rocking	4,000	8,600	14,900

TABLE III-2-2

Auxiliary Building Seismic Margin Evaluation
Equivalent Elastic Half-Space Shear Moduli

Structure Degree-of-Freedom	Dynamic Soil Shear Modulus, G_{eff}		
	Lower Bound Soil Case (KSF)	Intermediate Soil Case (KSF)	Upper Bound Soil Case (KSF)
Horizontal Translation, Torsion	1,900	7,100	18,100
Vertical Translation, Rocking	2,400	8,600	19,400

TABLE III-2-3

Frequency Dependent Elastic Half-Space Impedance

Direction of Motion	Equivalent Spring Constant For Rectangular Footing	Equivalent Spring Constant For Circular Footing	Equivalent Damping Coefficient
Horizontal	$k_x=k_1 2(1+\nu)G\beta_x\sqrt{BL}$	$k_x=k_1 \frac{32(1-\nu)GR}{7-8\nu}$	$c_x=c_1 k_x(\text{static})R\sqrt{\rho/G}$
Rocking	$k_\psi=k_2 \frac{G}{1-\nu}\beta_\psi B^2 L$	$k_\psi=k_2 \frac{8GR^3}{3(1-\nu)}$	$c_\psi=c_2 k_\psi(\text{static})R\sqrt{\rho/G}$
Vertical	$k_z=k_3 \frac{G}{1-\nu}\beta_z\sqrt{BL}$	$k_z=k_3 \frac{4GR}{1-\nu}$	$c_z=c_3 k_z(\text{static})R\sqrt{\rho/G}$
Torsion	———	$k_\theta=k_4 \frac{16}{3}GR^3$	$c_t=c_4 k_t(\text{static})R\sqrt{\rho/G}$

in which:

ν = Poisson's ratio of foundation medium,

G = shear modulus of foundation medium,

R = radius of the circular base mat,

ρ = density of foundation medium,

B = width of the base mat in the plane of horizontal excitation,

L = length of the base mat perpendicular to the plane of horizontal excitation,

k_1, k_2, k_3, k_4
c_1, c_2, c_3, c_4 = frequency dependent coefficients modifying the static stiffness or damping.

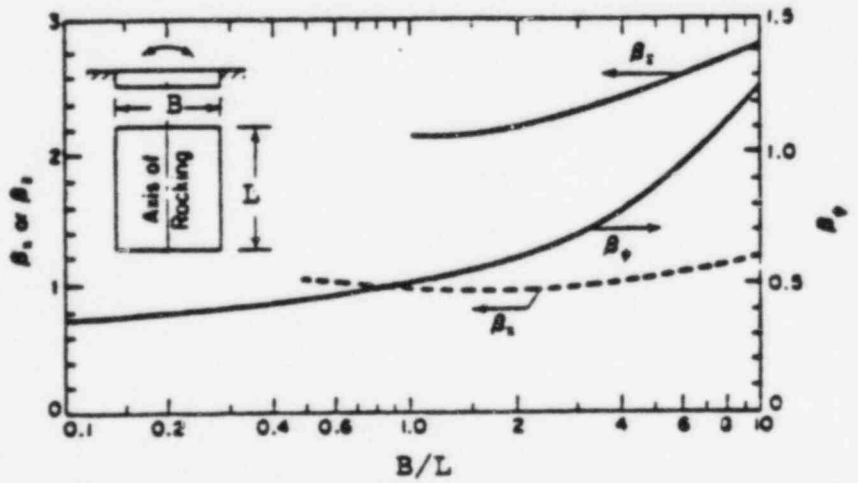

Constants β_x, β_ψ and β_z for Rectangular Bases

TABLE III-2-4

Auxiliary Building Soil Stiffnesses Developed For SME

Motion	Non Embedded Soil Stiffness			Embedment Factor	Embedded Soil Stiffness		
	Lower Bound Soil	Intermediate Soil	Upper Bound Soil		Lower Bound Soil	Intermediate Soil	Upper Bound Soil
Translational							
North-South	$0.90 \cdot 10^6$	$3.21 \cdot 10^6$	$8.18 \cdot 10^6$	1.11	$1.00 \cdot 10^6$	$3.56 \cdot 10^6$	$9.08 \cdot 10^6$
East-West	$0.93 \cdot 10^6$	$3.36 \cdot 10^6$	$8.54 \cdot 10^6$	1.10	$1.02 \cdot 10^6$	$3.70 \cdot 10^6$	$9.40 \cdot 10^6$
Vertical	$1.18 \cdot 10^6$	$3.64 \cdot 10^6$	$8.07 \cdot 10^6$	1.09	$1.28 \cdot 10^6$	$3.97 \cdot 10^6$	$8.80 \cdot 10^6$
Rotational							
North-South	$1.14 \cdot 10^{10}$	$3.73 \cdot 10^{10}$	$8.41 \cdot 10^{10}$	1.24	$1.41 \cdot 10^{10}$	$4.63 \cdot 10^{10}$	$10.4 \cdot 10^{10}$
East-West	$0.87 \cdot 10^{10}$	$2.85 \cdot 10^{10}$	$6.25 \cdot 10^{10}$	1.22	$1.06 \cdot 10^{10}$	$3.48 \cdot 10^{10}$	$7.63 \cdot 10^{10}$
Torsional	$0.94 \cdot 10^{10}$	$3.48 \cdot 10^{10}$	$8.92 \cdot 10^{10}$	1.21	$1.13 \cdot 10^{10}$	$4.21 \cdot 10^{10}$	$10.9 \cdot 10^{10}$

NOTES: 1. Units for Translational Soil Springs are K/ft.

2. Units for Rotational Soil Springs are K-ft./rad.

TABLE III-2-5

Auxiliary Building Damping Constants

Motion	Non Embedded Dashpot			Embedment Factor	Embedded Dashpot (3)		
	Lower Bound Soil	Intermediate Soil	Upper Bound Soil		Lower Bound Soil	Intermediate Soil	Upper Bound Soil
Translational							
North-South	$6.02 \cdot 10^4$	$1.12 \cdot 10^5$	$1.77 \cdot 10^5$	1.25	$8.33 \cdot 10^4$	$1.60 \cdot 10^5$	$2.58 \cdot 10^5$
East-West	$6.46 \cdot 10^4$	$1.22 \cdot 10^5$	$1.91 \cdot 10^5$	1.24	$8.82 \cdot 10^4$	$1.73 \cdot 10^5$	$2.76 \cdot 10^5$
Vertical	$1.41 \cdot 10^5$	$2.54 \cdot 10^5$	$3.74 \cdot 10^5$	1.11	$1.64 \cdot 10^5$	$2.97 \cdot 10^5$	$4.42 \cdot 10^5$
Rotational							
North-South	$2.17 \cdot 10^8$	$4.53 \cdot 10^8$	$5.65 \cdot 10^8$	1.44	$4.25 \cdot 10^8$	$9.07 \cdot 10^8$	$1.24 \cdot 10^9$
East-West	$9.80 \cdot 10^7$	$2.03 \cdot 10^8$	$2.55 \cdot 10^8$	1.46	$2.27 \cdot 10^8$	$5.01 \cdot 10^8$	$6.84 \cdot 10^8$
Torsional	$2.08 \cdot 10^8$	$3.79 \cdot 10^8$	$6.35 \cdot 10^8$	1.49	$4.01 \cdot 10^8$	$8.03 \cdot 10^8$	$1.39 \cdot 10^8$

NOTES: 1. Units for Translational Dashpots are K-sec/ft.

2. Units for Rotational Dashpots are K-sec-ft./rad.

3. Includes 5% Soil Hysteretic Damping.

TABLE III-2-6

NODAL SPRING STIFFNESS FOR

LOWER AND UPPER BOUND RELATIVE WING STIFFNESS CASES

LOWER BOUND SOIL CASE

Node Number	Direction	Motion	Lower Bound Relative Wing Stiffness Case	Upper Bound Relative Wing Stiffness Case
214,217	N-S	Translation	1.17×10^4	3.76×10^4
	E-W	Translation	1.19×10^4	3.35×10^4
	Vertical	Translation	1.61×10^4	4.51×10^4
	N-S	Rocking	3.29×10^6	1.41×10^7
211,220	N-S	Translation	1.26×10^4	4.05×10^4
	E-W	Translation	1.29×10^4	3.61×10^4
	Vertical	Translation	1.74×10^4	4.86×10^4
	N-S	Rocking	3.54×10^5	1.52×10^7
112,168	N-S	Translation	3.33×10^3	1.07×10^4
	E-W	Translation	3.39×10^3	9.52×10^3
	Vertical	Translation	4.58×10^3	1.28×10^4
	N-S	Rocking	9.35×10^5	4.02×10^6
208,223	N-S	Translation	7.04×10^3	2.26×10^4
	E-W	Translation	7.18×10^3	2.01×10^4
	Vertical	Translation	9.69×10^3	2.71×10^4
	N-S	Rocking	1.98×10^6	8.50×10^6
205,226	N-S	Translation	6.14×10^3	1.97×10^4
	E-W	Translation	6.26×10^3	1.76×10^4
	Vertical	Translation	8.45×10^3	2.36×10^4
	N-S	Rocking	1.72×10^6	7.41×10^6
269,272	N-S	Translation	1.52×10^3	4.88×10^3
	E-W	Translation	1.55×10^3	4.34×10^3
	Vertical	Translation	2.09×10^3	5.84×10^3
	N-S	Rocking	4.26×10^5	1.83×10^6
239	N-S	Translation	9.15×10^5	8.28×10^5
	E-W	Translation	9.34×10^5	7.78×10^5
	Vertical	Translation	1.16×10^6	9.54×10^5
	N-S	Rocking	9.67×10^9	8.08×10^9
	E-W	Rocking	1.28×10^{10}	9.31×10^9
	Torsion	Rocking	9.80×10^9	6.41×10^9

NOTE: 1. Units on translational springs are $^{kip}/_{ft}$

2. Units on rotational springs are $^{kip\text{-}ft}/_{rad}$

3. Node Locations are shown in Figures II-2-24 and II-2-25

TABLE III-2-7

NODAL SPRING STIFFNESS FOR

LOWER AND UPPER BOUND RELATIVE WING STIFFNESS CASES

INTERMEDIATE SOIL CASE

Node Number	Direction	Motion	Lower Bound Relative Wing Stiffness Case	Upper Bound Relative Wing Stiffness Case
214,217	N-S	Translation	$4.17 \cdot 10^4$	$1.41 \cdot 10^5$
	E-W	Translation	$4.33 \cdot 10^4$	$1.25 \cdot 10^5$
	Vertical	Translation	$5.00 \cdot 10^4$	$1.53 \cdot 10^5$
	N-S	Rocking	$1.02 \cdot 10^7$	$5.06 \cdot 10^7$
211,220	N-S	Translation	$4.49 \cdot 10^4$	$1.52 \cdot 10^5$
	E-W	Translation	$4.67 \cdot 10^4$	$1.35 \cdot 10^5$
	Vertical	Translation	$5.39 \cdot 10^4$	$1.65 \cdot 10^5$
	N-S	Rocking	$1.10 \cdot 10^7$	$5.46 \cdot 10^7$
112,168	N-S	Translation	$1.18 \cdot 10^4$	$4.00 \cdot 10^4$
	E-W	Translation	$1.23 \cdot 10^4$	$3.56 \cdot 10^4$
	Vertical	Translation	$1.42 \cdot 10^4$	$4.35 \cdot 10^4$
	N-S	Rocking	$2.90 \cdot 10^6$	$1.44 \cdot 10^7$
208,223	N-S	Translation	$2.50 \cdot 10^4$	$8.47 \cdot 10^4$
	E-W	Translation	$2.60 \cdot 10^4$	$7.53 \cdot 10^4$
	Vertical	Translation	$3.01 \cdot 10^4$	$9.20 \cdot 10^4$
	N-S	Rocking	$6.13 \cdot 10^6$	$3.04 \cdot 10^7$
205,226	N-S	Translation	$2.18 \cdot 10^4$	$7.38 \cdot 10^4$
	E-W	Translation	$2.27 \cdot 10^4$	$6.57 \cdot 10^4$
	Vertical	Translation	$2.62 \cdot 10^4$	$8.02 \cdot 10^4$
	N-S	Rocking	$5.35 \cdot 10^6$	$2.65 \cdot 10^7$
269,272	N-S	Translation	$5.40 \cdot 10^3$	$1.82 \cdot 10^4$
	E-W	Translation	$5.61 \cdot 10^3$	$1.62 \cdot 10^4$
	Vertical	Translation	$6.48 \cdot 10^3$	$1.98 \cdot 10^4$
	N-S	Rocking	$1.32 \cdot 10^6$	$6.56 \cdot 10^6$
239	N-S	Translation	$3.26 \cdot 10^6$	$2.54 \cdot 10^6$
	E-W	Translation	$3.38 \cdot 10^6$	$2.79 \cdot 10^6$
	Vertical	Translation	$3.61 \cdot 10^6$	$2.86 \cdot 10^6$
	N-S	Rocking	$3.20 \cdot 10^{10}$	$2.62 \cdot 10^{10}$
	E-W	Rocking	$4.23 \cdot 10^{10}$	$3.05 \cdot 10^{10}$
	Torsion	Rocking	$3.68 \cdot 10^{10}$	$2.39 \cdot 10^{10}$

NOTE: 1. Units on translational springs are $^{kip}/_{ft}$

2. Units on rotational springs are $^{kip\text{-}ft}/_{rad}$

3. Node Locations are shown in Figures II-2-24 and II-2-25

TABLE III-2-8

NODAL SPRING STIFFNESS FOR

LOWER AND UPPER BOUND RELATIVE WING STIFFNESS CASES

UPPER BOUND SOIL CASE

Node Number	Direction	Motion	Lower Bound Relative Wing Stiffness Case	Upper Bound Relative Wing Stiffness Case
214,217	N-S	Translation	1.06×10^5	3.60×10^5
	E-W	Translation	1.10×10^5	3.21×10^5
	Vertical	Translation	1.11×10^5	3.46×10^5
	N-S	Rocking	2.26×10^7	1.15×10^8
211,220	N-S	Translation	1.15×10^5	3.88×10^5
	E-W	Translation	1.19×10^5	3.46×10^5
	Vertical	Translation	1.19×10^5	3.73×10^5
	N-S	Rocking	2.44×10^7	1.23×10^8
112,168	N-S	Translation	3.02×10^4	1.02×10^5
	E-W	Translation	3.13×10^4	9.13×10^4
	Vertical	Translation	3.15×10^4	9.83×10^4
	N-S	Rocking	6.43×10^6	3.26×10^7
208,223	N-S	Translation	6.39×10^4	2.16×10^5
	E-W	Translation	6.61×10^4	1.93×10^5
	Vertical	Translation	6.66×10^4	2.08×10^5
	N-S	Rocking	1.36×10^7	6.89×10^7
205,226	N-S	Translation	5.57×10^4	1.89×10^5
	E-W	Translation	5.77×10^4	1.68×10^5
	Vertical	Translation	5.81×10^4	1.81×10^5
	N-S	Rocking	1.19×10^7	6.00×10^7
269,272	N-S	Translation	1.38×10^4	4.66×10^4
	E-W	Translation	1.43×10^4	4.16×10^4
	Vertical	Translation	1.44×10^4	4.48×10^4
	N-S	Rocking	2.93×10^6	1.48×10^7
239	N-S	Translation	8.31×10^6	6.48×10^6
	E-W	Translation	8.61×10^6	7.08×10^6
	Vertical	Translation	8.00×10^6	6.30×10^6
	N-S	Rocking	7.01×10^{10}	5.69×10^{10}
	E-W	Rocking	9.51×10^{10}	6.87×10^{10}
	Torsion	Rocking	9.56×10^{10}	6.25×10^{10}

NOTE: 1. Units on translational springs are $^{kip}/_{ft}$

2. Units on rotational springs are $^{kip\text{-}ft}/_{rad}$

3. Node Locations are shown in Figures II-2-24 and II-2-25

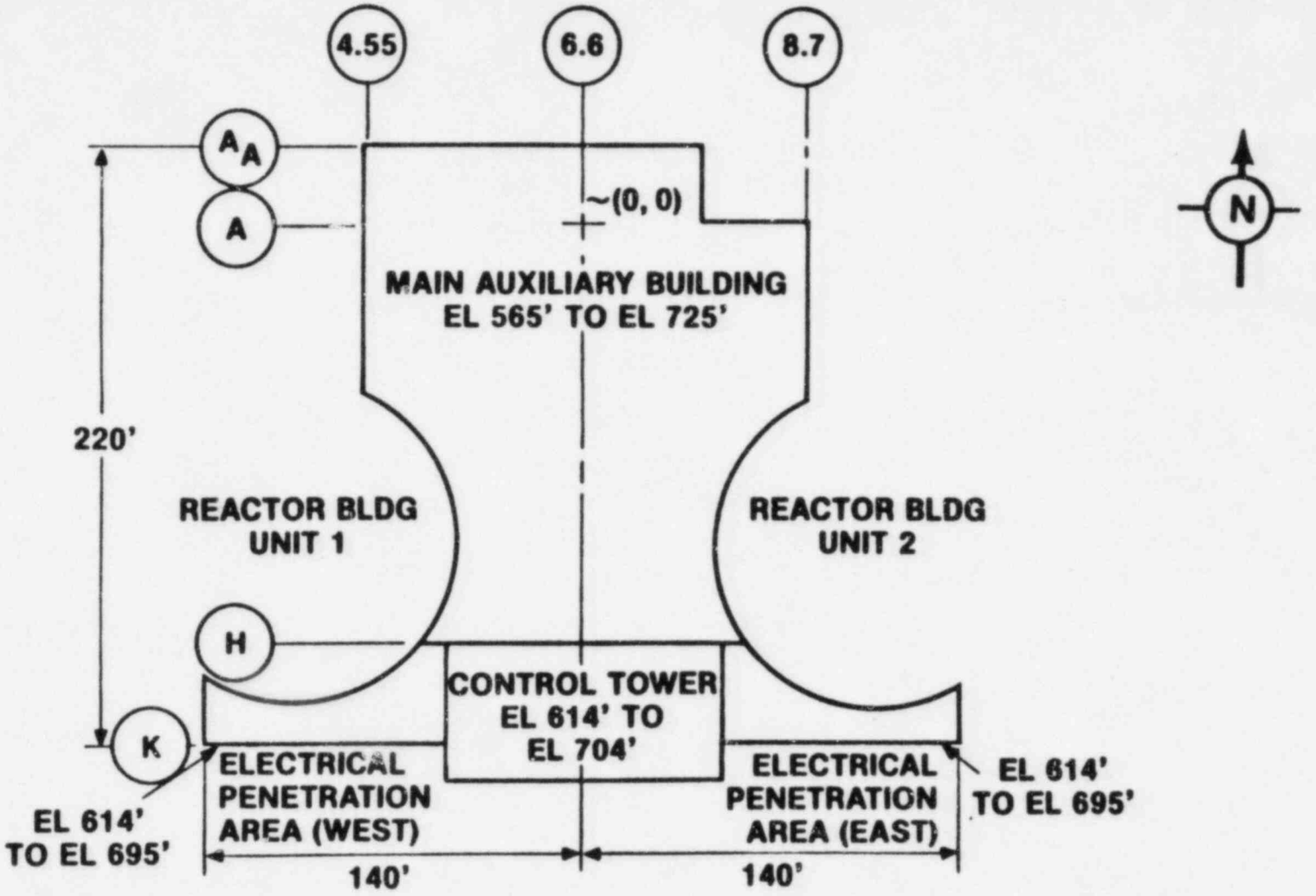

FIGURE III-2-1. SCHEMATIC PLAN VIEW OF AUXILIARY BUILDING, CONTROL TOWER AND ELECTRICAL PENETRATION AREAS

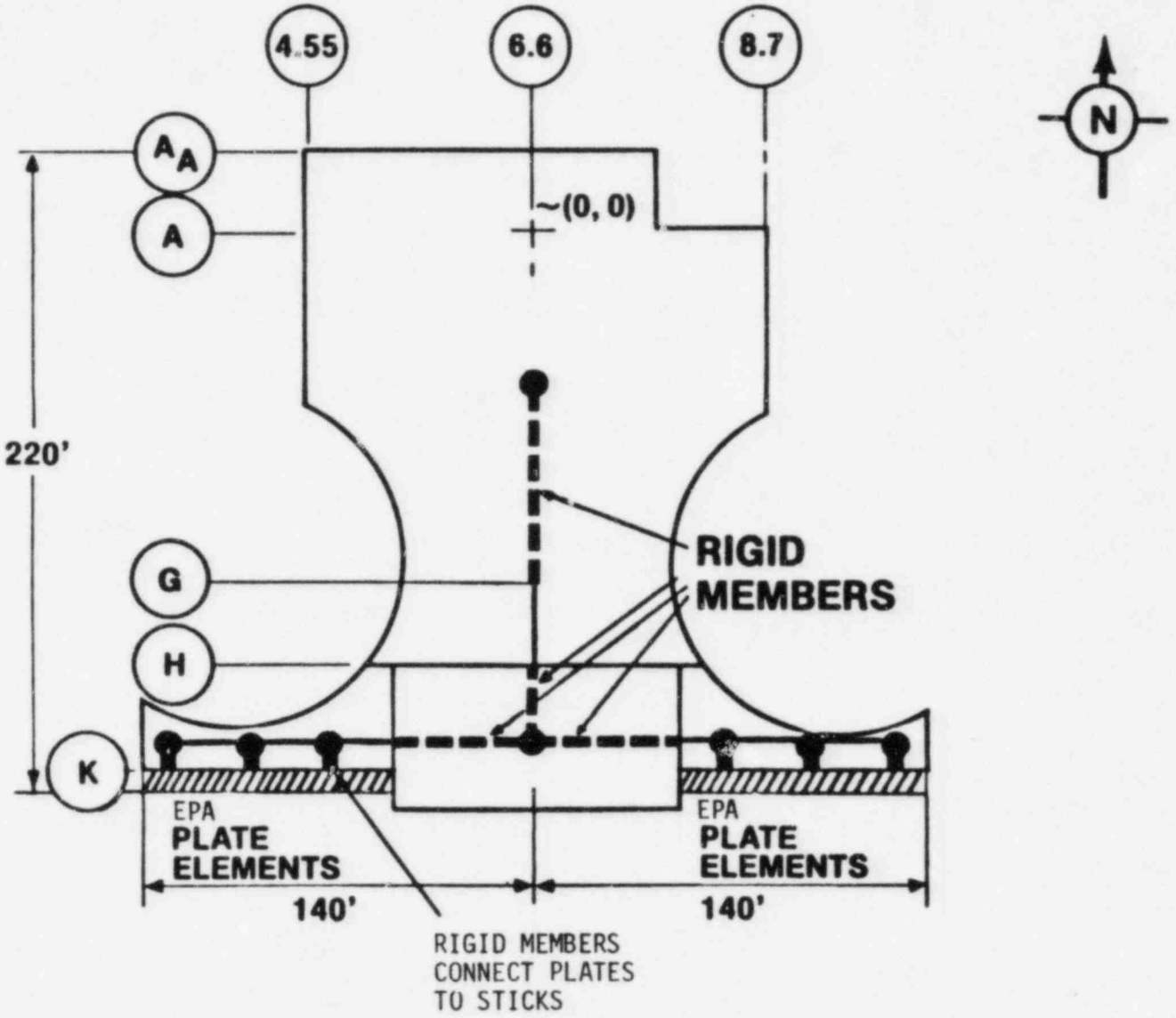

FIGURE III-2-2. PLAN VIEW OF AUXILIARY BUILDING, SHOWING LOCATION OF VERTICAL BEAMS MODELING MAJOR STRUCTURAL ELEMENTS

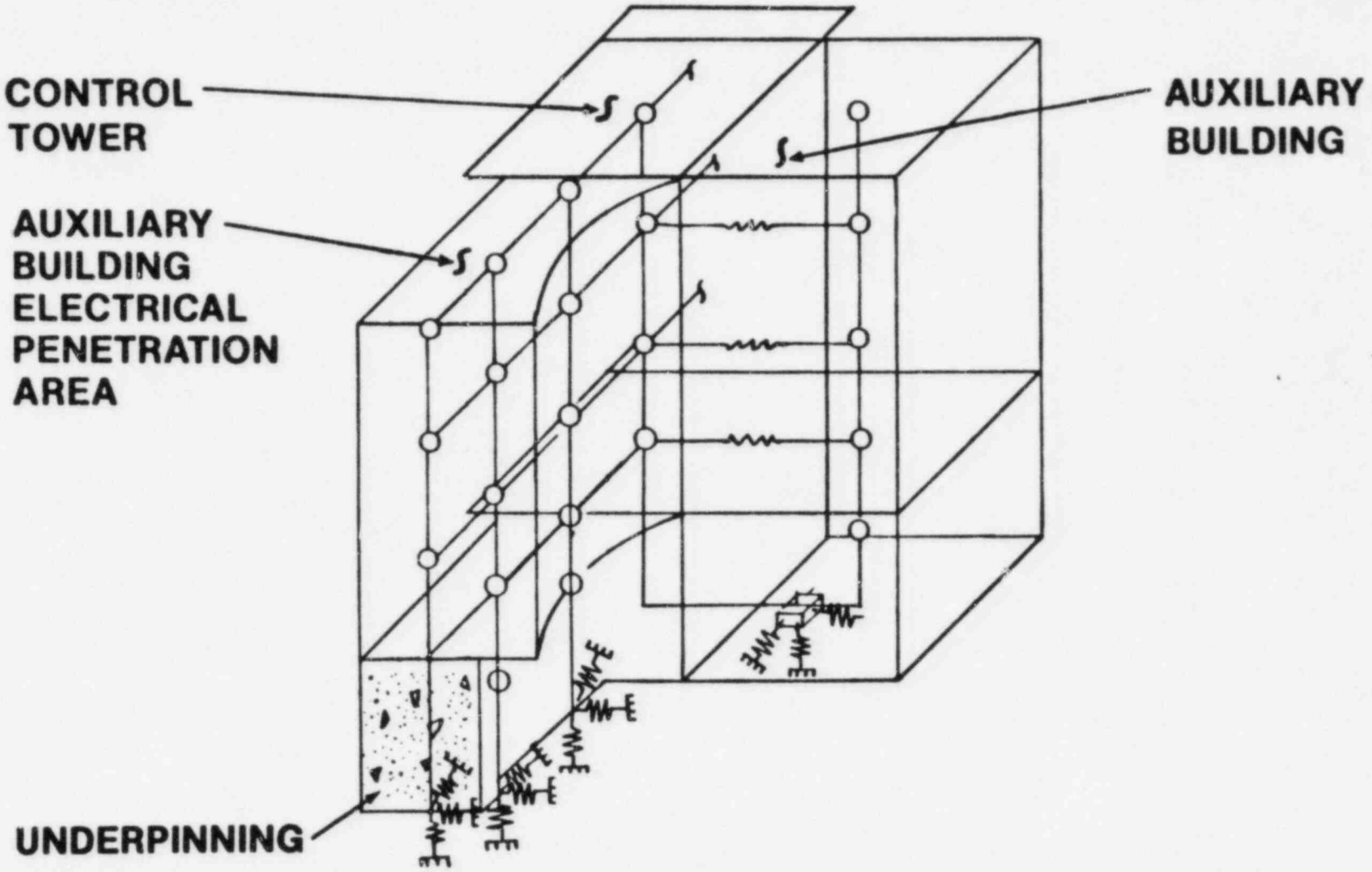

FIGURE III-2-3. AUXILIARY BUILDING CONCEPTUAL SEISMIC MODEL SHOWING LOCATION OF SOIL IMPEDANCE BENEATH STRUCTURES

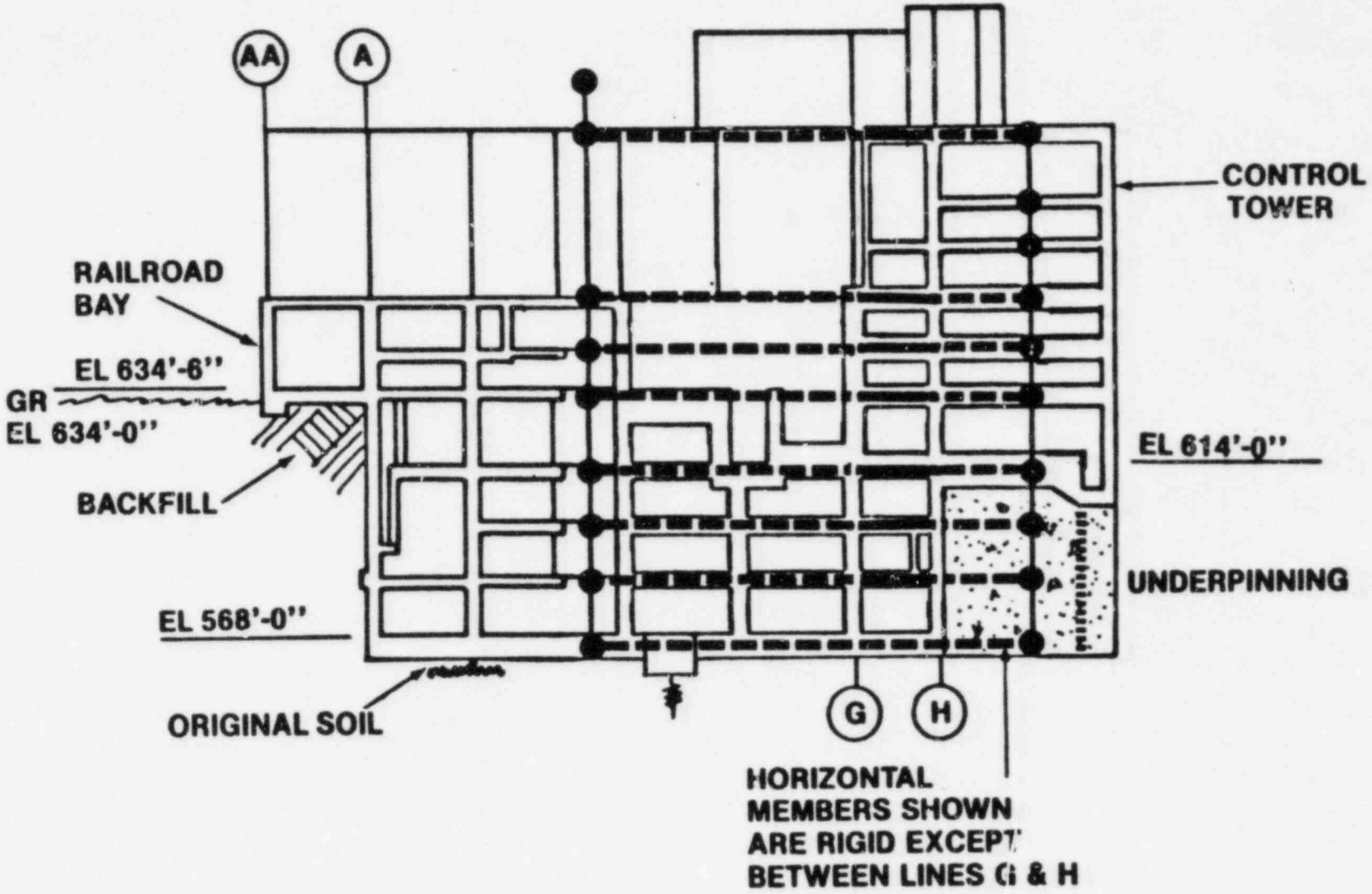

FIGURE III-2-4. SECTIONAL VIEW OF AUXILIARY BUILDING SHOWING CONNECTIVITY BETWEEN VERTICAL BEAMS OF DYNAMIC MODEL

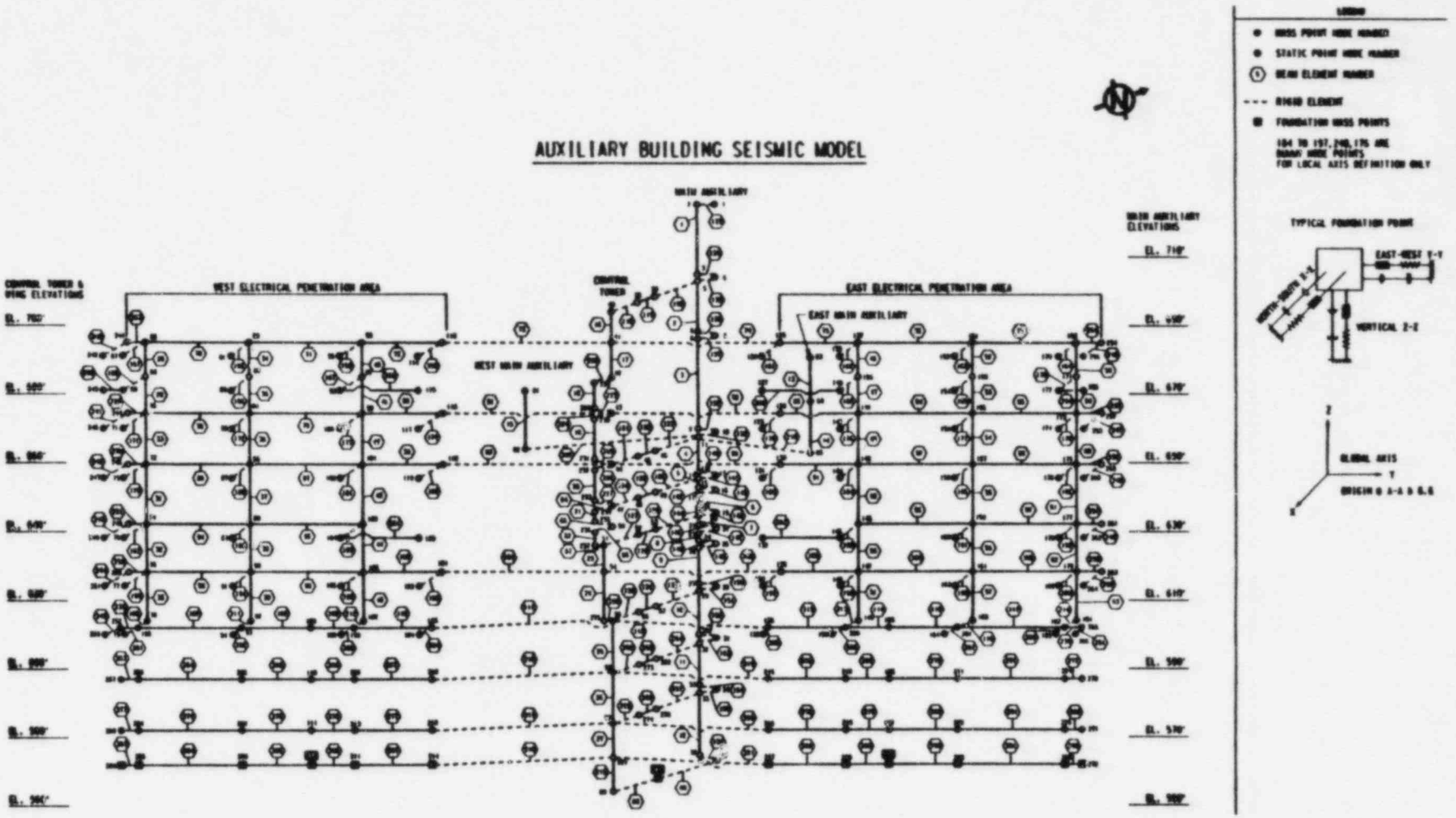

FIGURE III-2-5. AUXILIARY BUILDING DYNAMIC MODEL SHOWING BEAM ELEMENT MODELING FLOOR STIFFNESSES- ISOMETRIC VIEW LOOKING NORTH

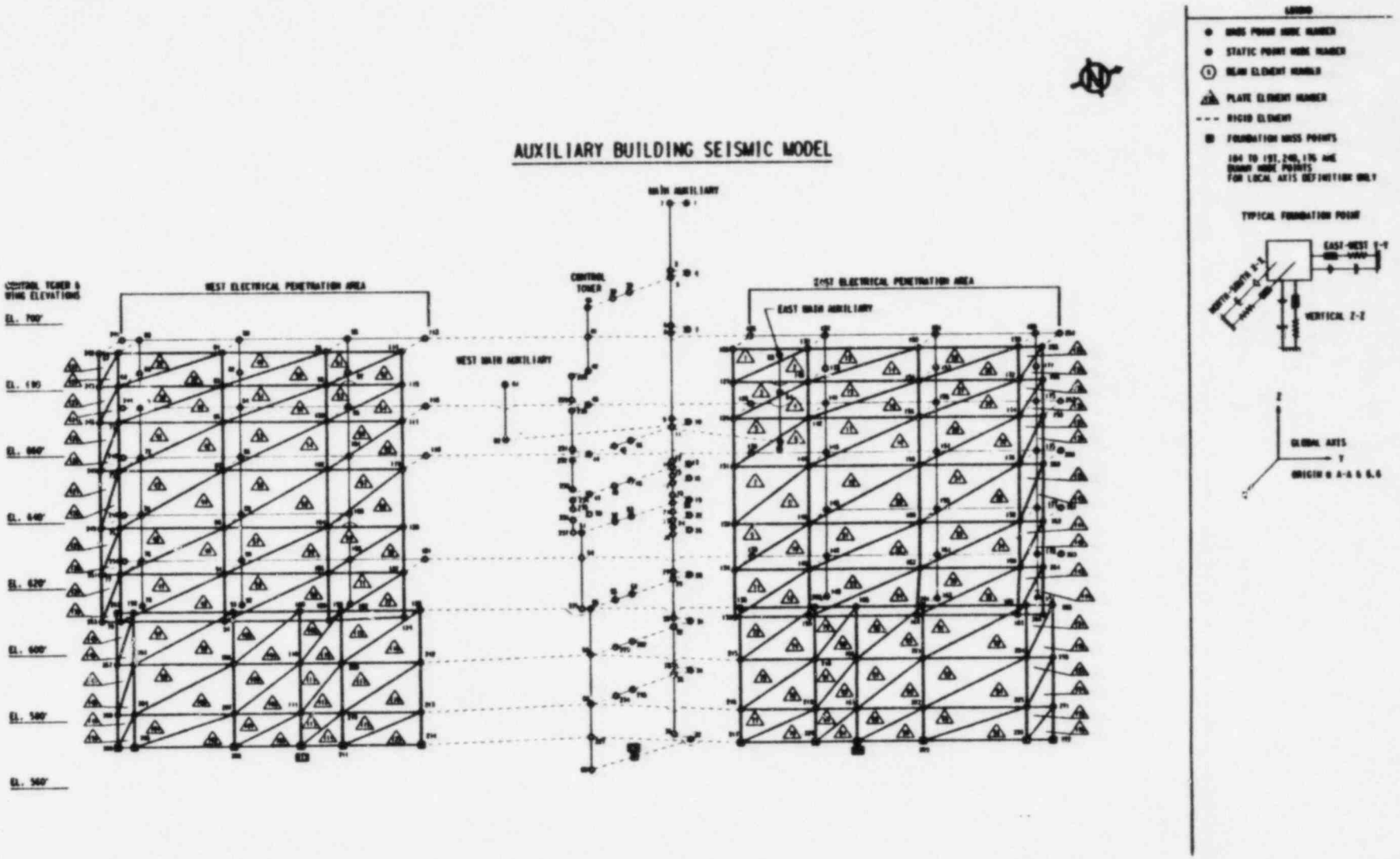

FIGURE III-2-6. AUXILIARY BUILDING DYNAMIC MODEL SHOWING PLATE ELEMENTS MODELING SOUTH WALL OF ELECTRICAL PENETRATION AREAS ISOMETRIC VIEW LOOKING NORTH

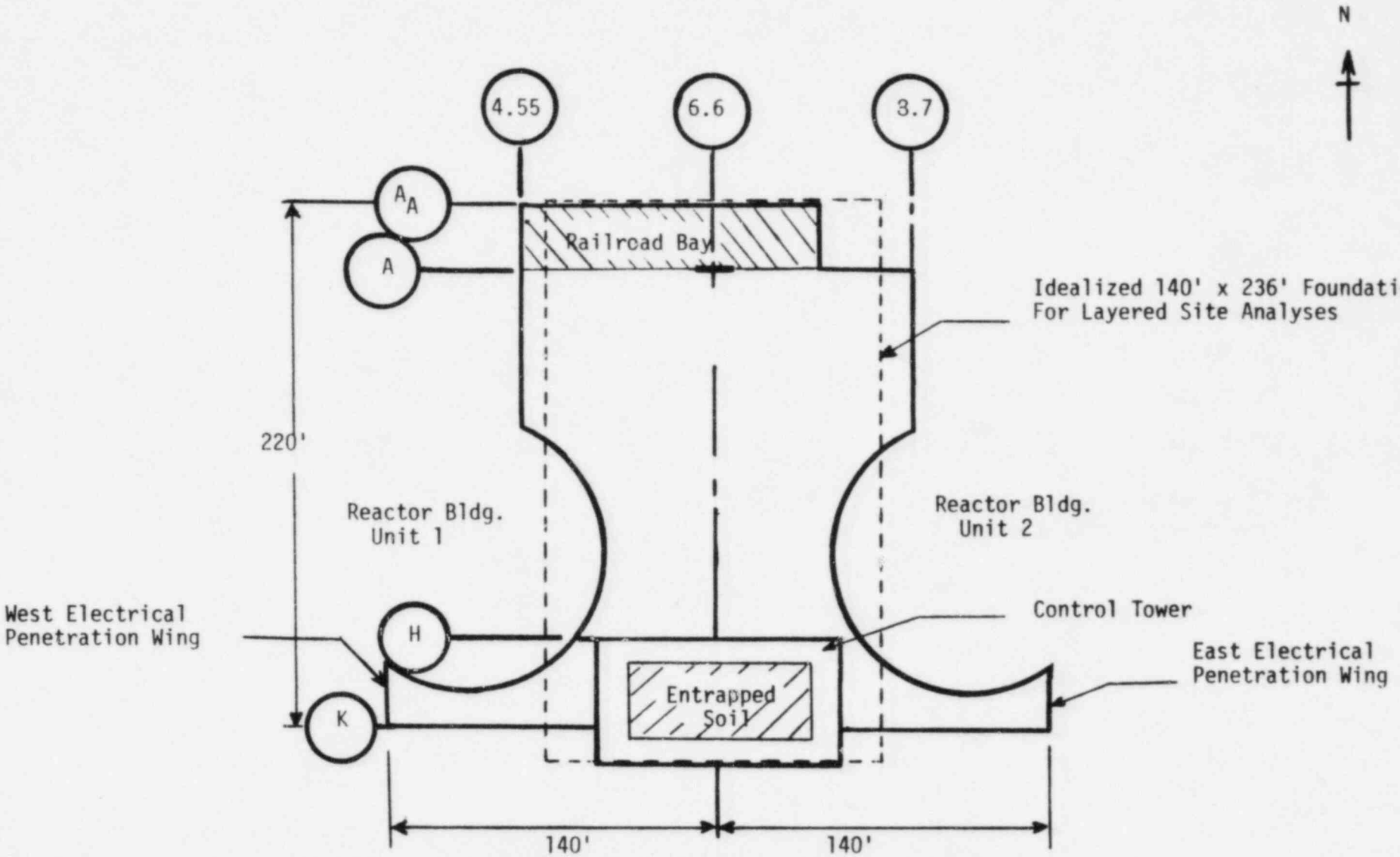

FIGURE III-2-7. SCHEMATIC REPRESENTATION OF AUXILIARY BUILDING FOUNDATION SHOWING IDEALIZED FOUNDATION USED IN LAYERED SITE ANALYSES

FIGURE III-2-8. NORTH-SOUTH TRANSLATION SOIL IMPEDANCE
SOFT SITE LAYERED SOIL PROFILE

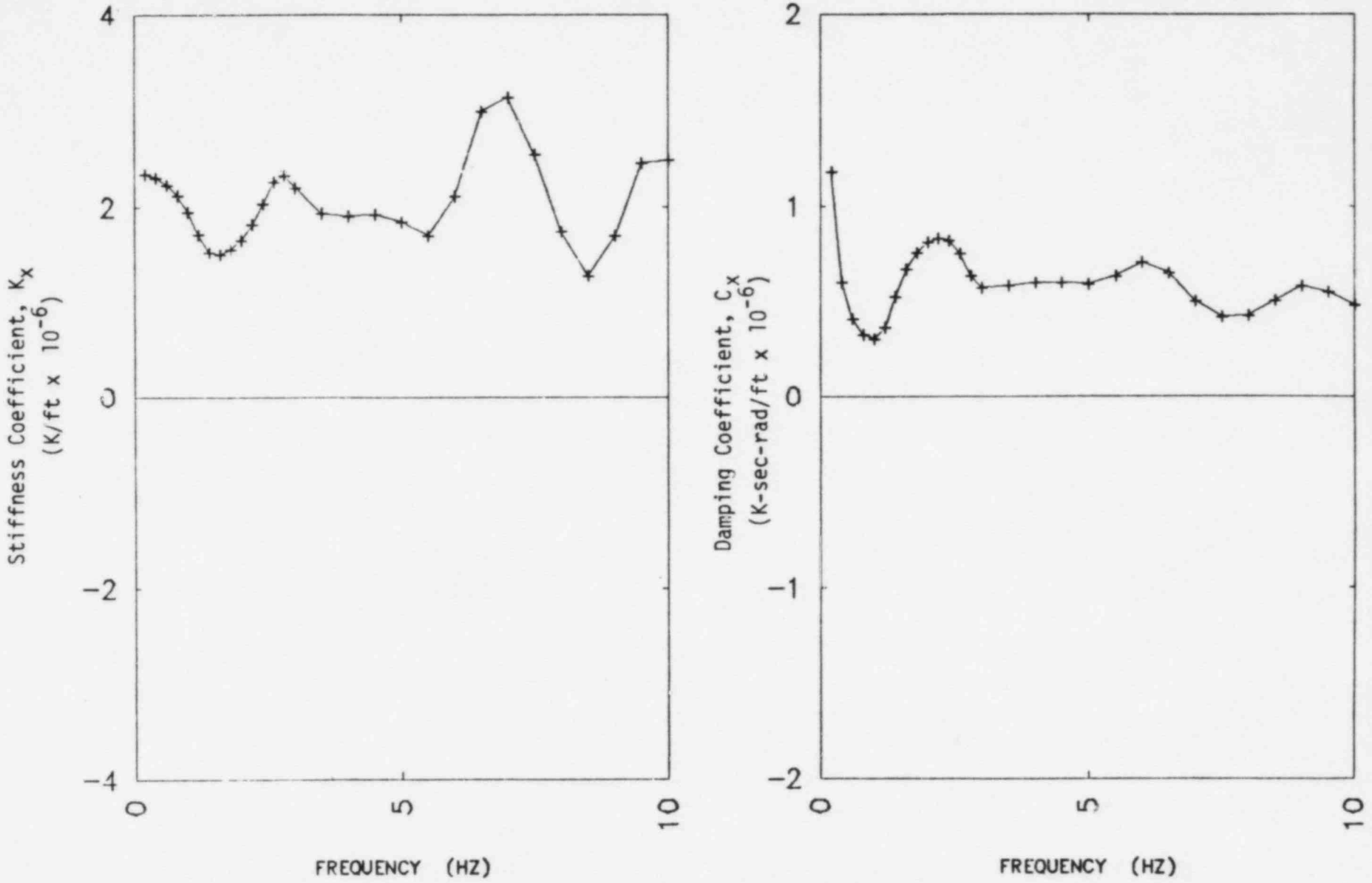

FIGURE III-2-9. EAST-WEST TRANSLATION SOIL IMPEDANCE
SOFT SITE LAYERED SOIL PROFILE

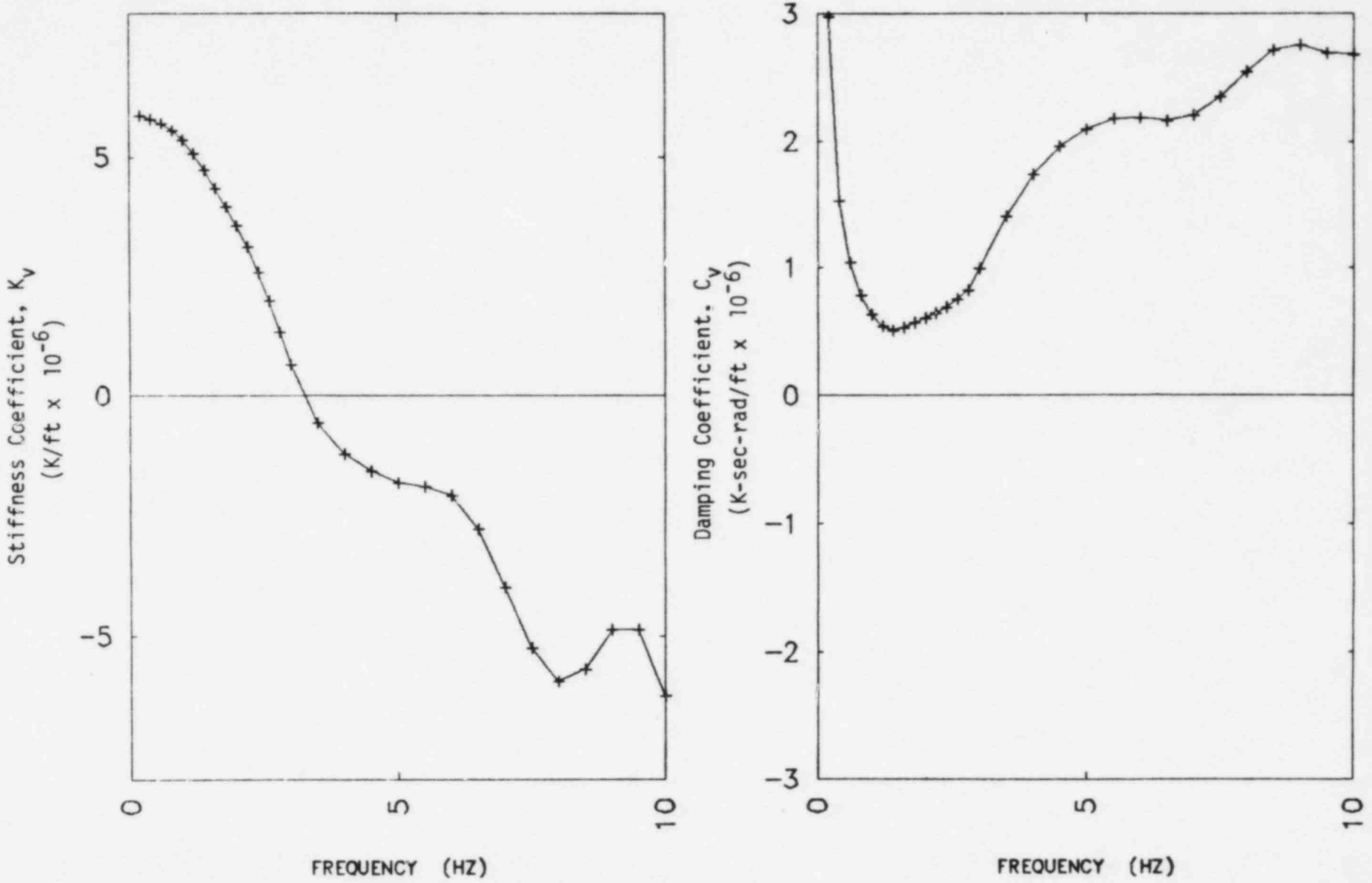

FIGURE III-2-10. VERTICAL TRANSLATION SOIL IMPEDANCE
SOFT SITE LAYERED SOIL PROFILE

FIGURE III-2-11. ROCKING ABOUT THE NORTH-SOUTH AXIS SOIL IMPEDANCE SOFT SITE LAYERED SOIL PROFILE

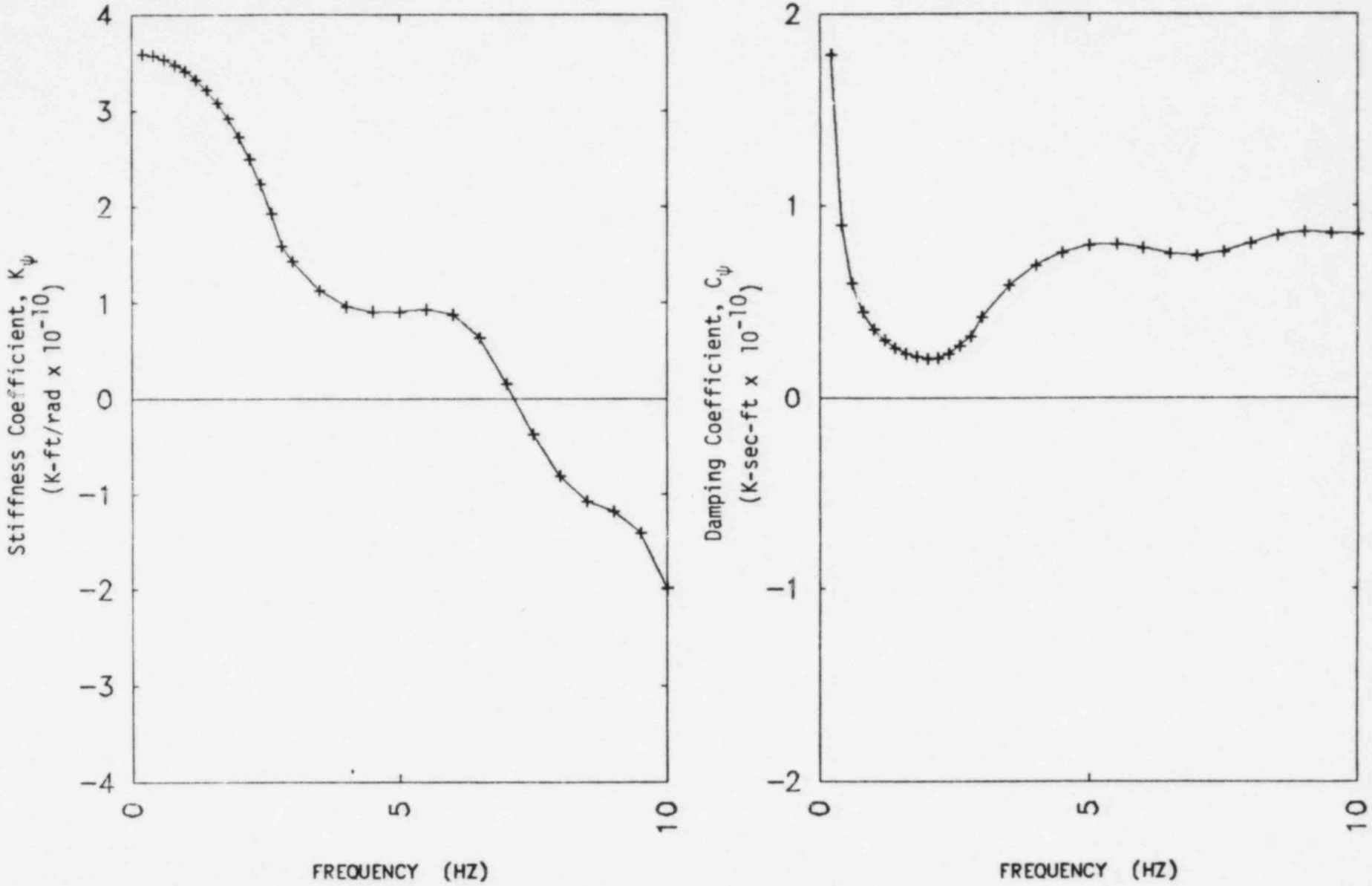

FIGURE III-2-12. ROCKING ABOUT THE EAST-WEST AXIS SOIL IMPEDANCE
SOFT SITE LAYERED SOIL PROFILE

FIGURE III-2-13. TORSIONAL RESPONSE SOIL IMPEDANCE
SOFT SITE LAYERED SOIL PROFILE

FIGURE III-2-14. NORTH-SOUTH TRANSLATION SOIL IMPEDANCE
INTERMEDIATE CASE LAYERED SOIL PROFILE

FIGURE III-2-15. EAST-WEST TRANSLATION SOIL IMPEDANCE
INTERMEDIATE CASE LAYERED SOIL PROFILE

FIGURE III-2-16. VERTICAL TRANSLATION SOIL IMPEDANCE
INTERMEDIATE CASE LAYERED SOIL PROFILE

FIGURE III-2-17. ROCKING ABOUT THE NORTH-SOUTH AXIS SOIL IMPEDANCE INTERMEDIATE CASE LAYERED SOIL PROFILE

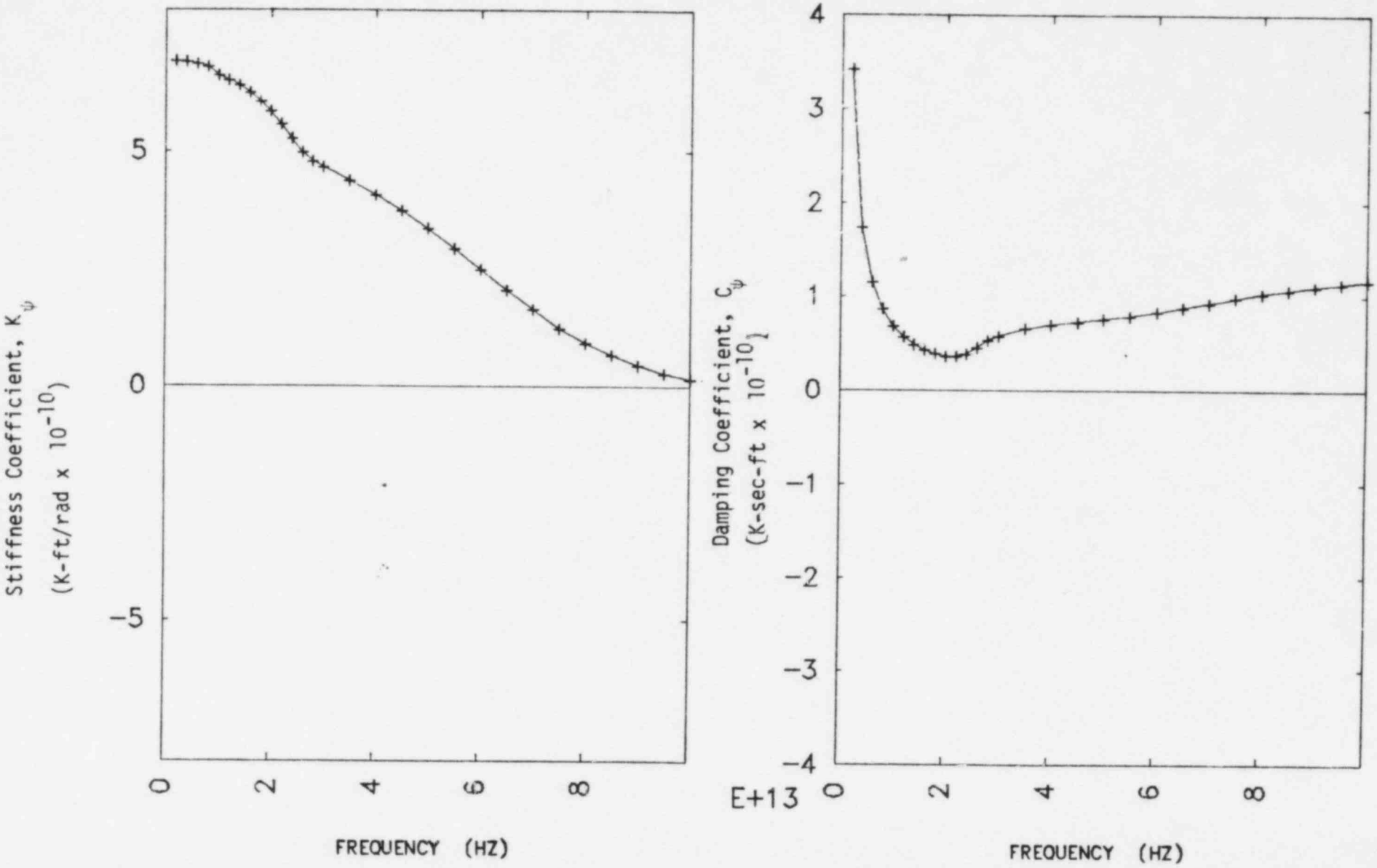

FIGURE III-2-18. ROCKING ABOUT THE EAST-WEST AXIS SOIL IMPEDANCE
INTERMEDIATE CASE LAYERED SOIL PROFILE

FIGURE III-2-19. TORSIONAL RESPONSE SOIL IMPEDANCE
INTERMEDIATE CASE LAYERED SOIL PROFILE

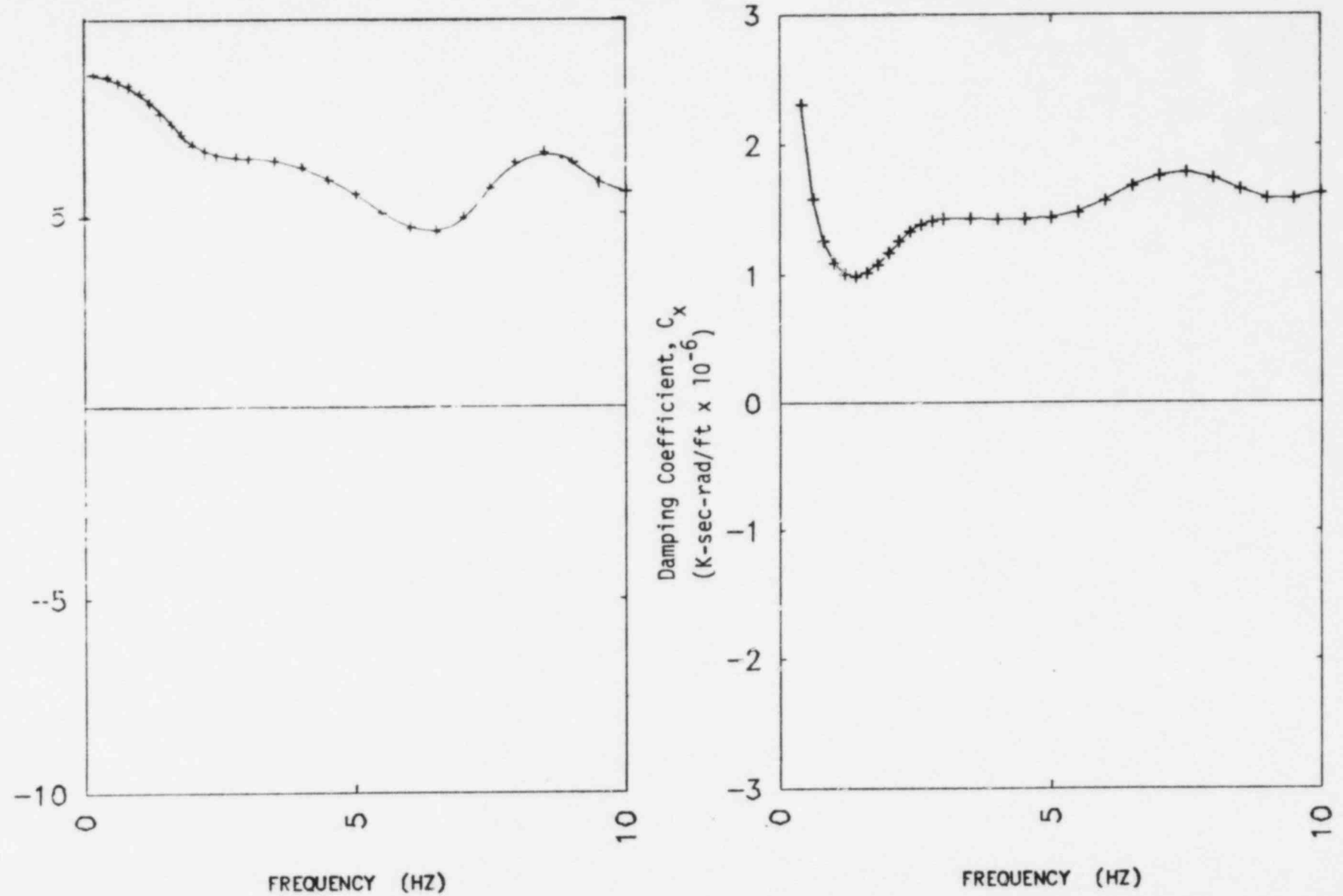

FIGURE III-2-20. NORTH-SOUTH TRANSLATION SOIL IMPEDANCE
STIFF SITE LAYERED SOIL PROFILE

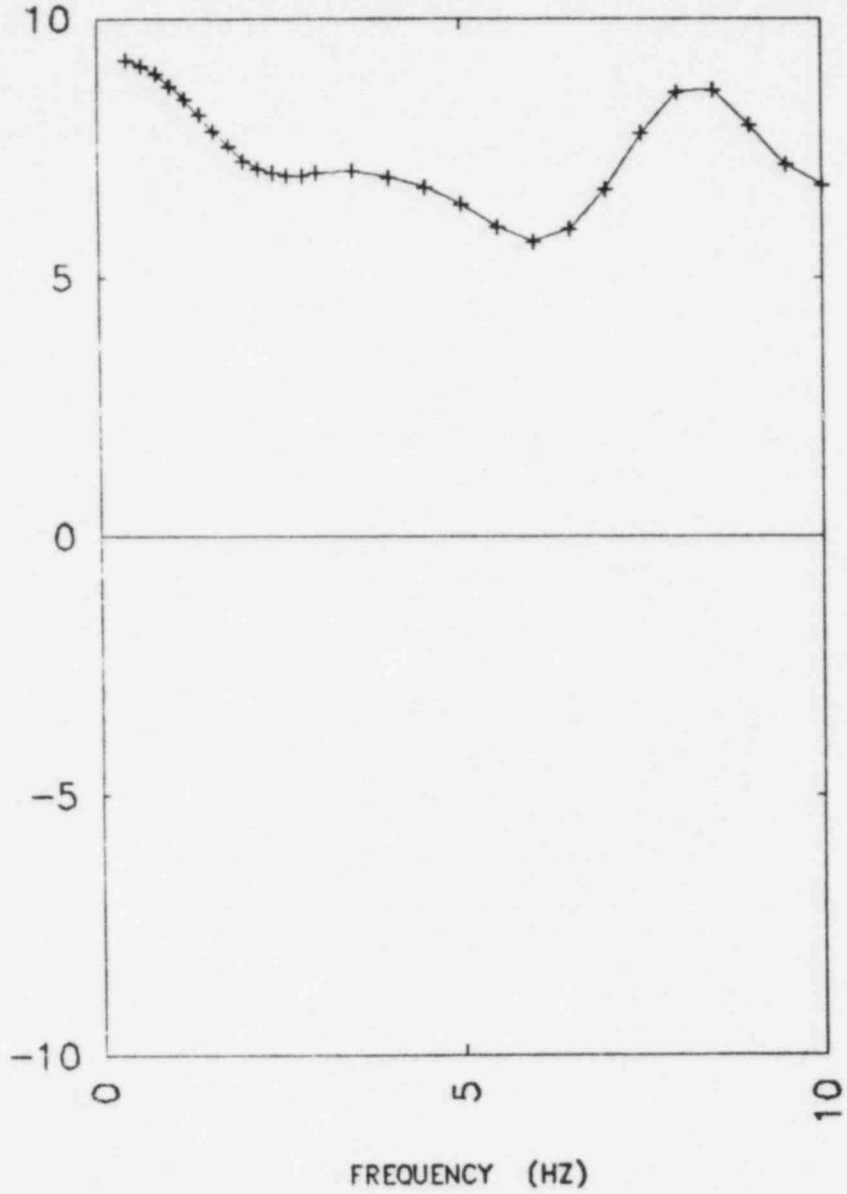

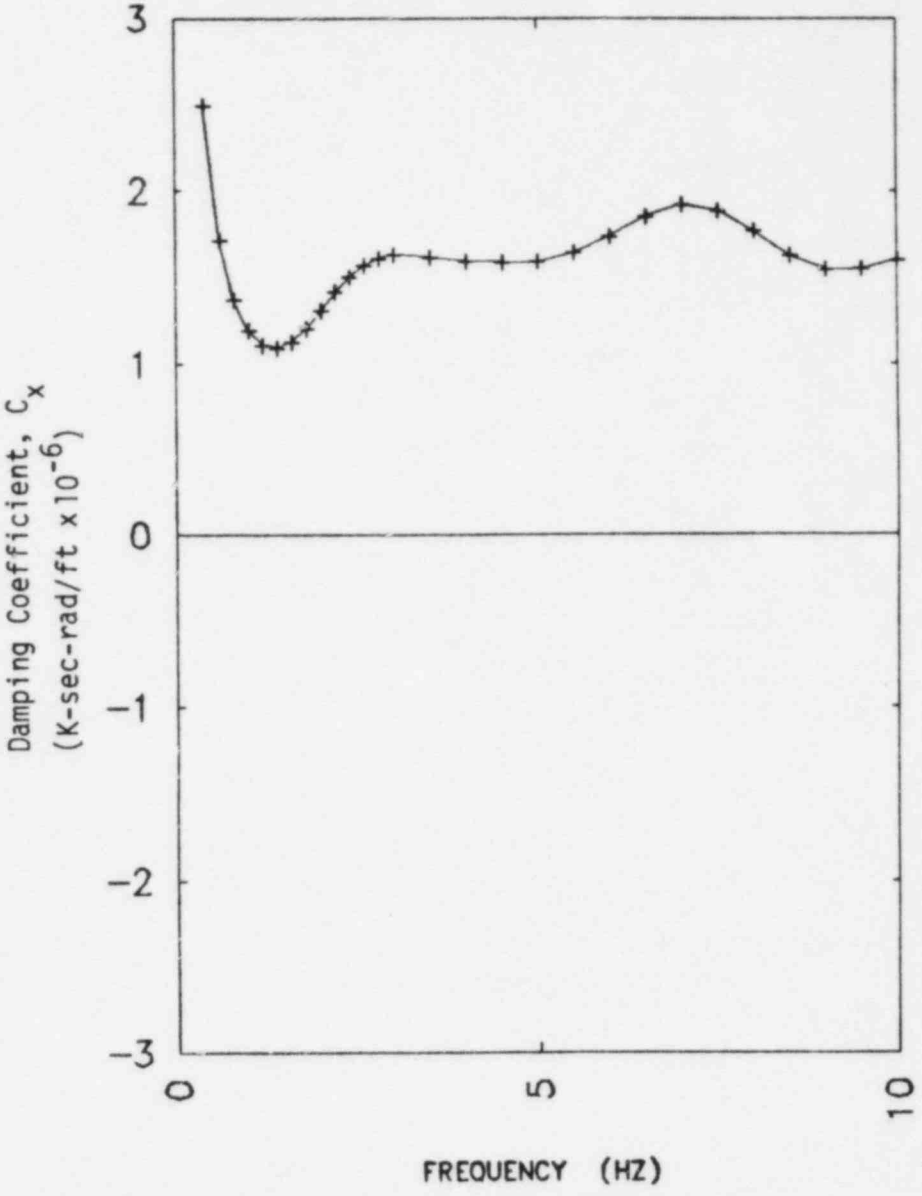

FIGURE III-2-21. EAST-WEST TRANSLATION SOIL IMPEDANCE
STIFF SITE LAYERED SOIL PROFILE

FIGURE III-2-22. VERTICAL TRANSLATION SOIL IMPEDANCE STIFF SITE LAYERED SOIL PROFILE

FIGURE III-2-23. ROCKING ABOUT THE NORTH-SOUTH AXIS SOIL IMPEDANCE STIFF SITE LAYERED SOIL PROFILE

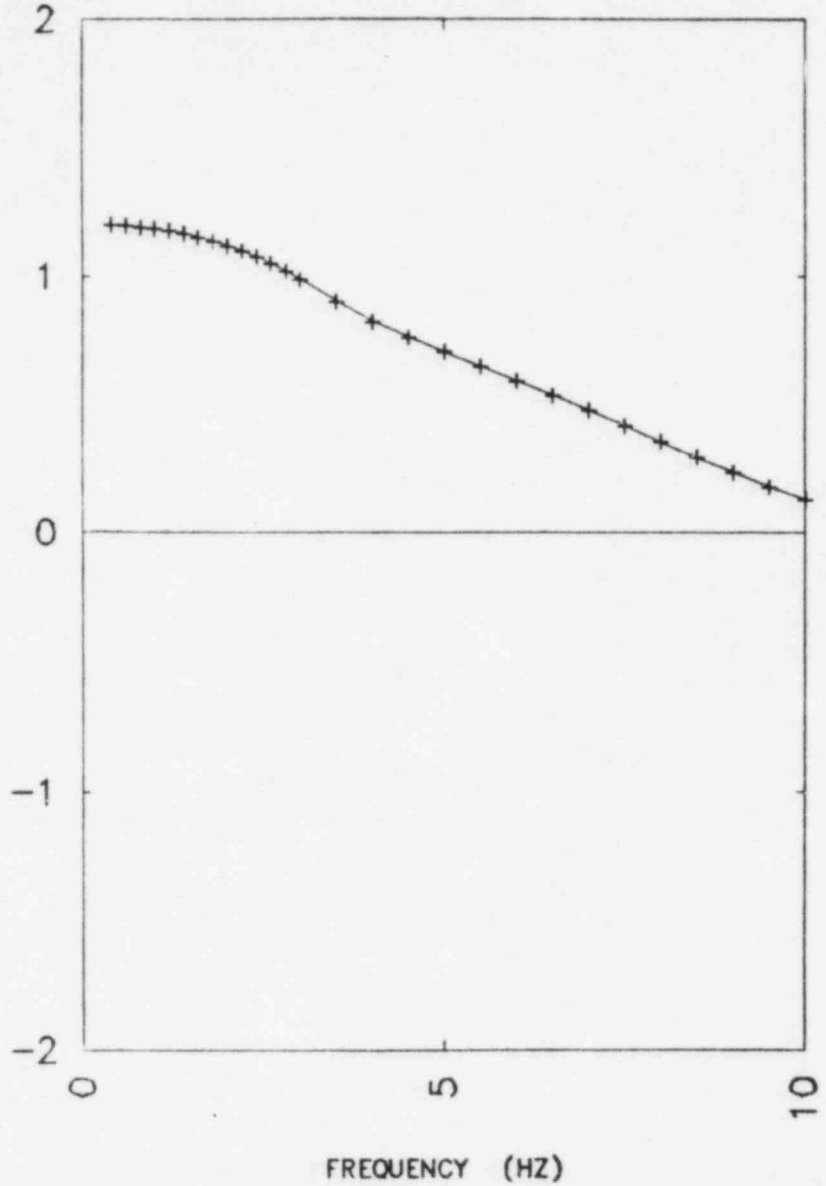

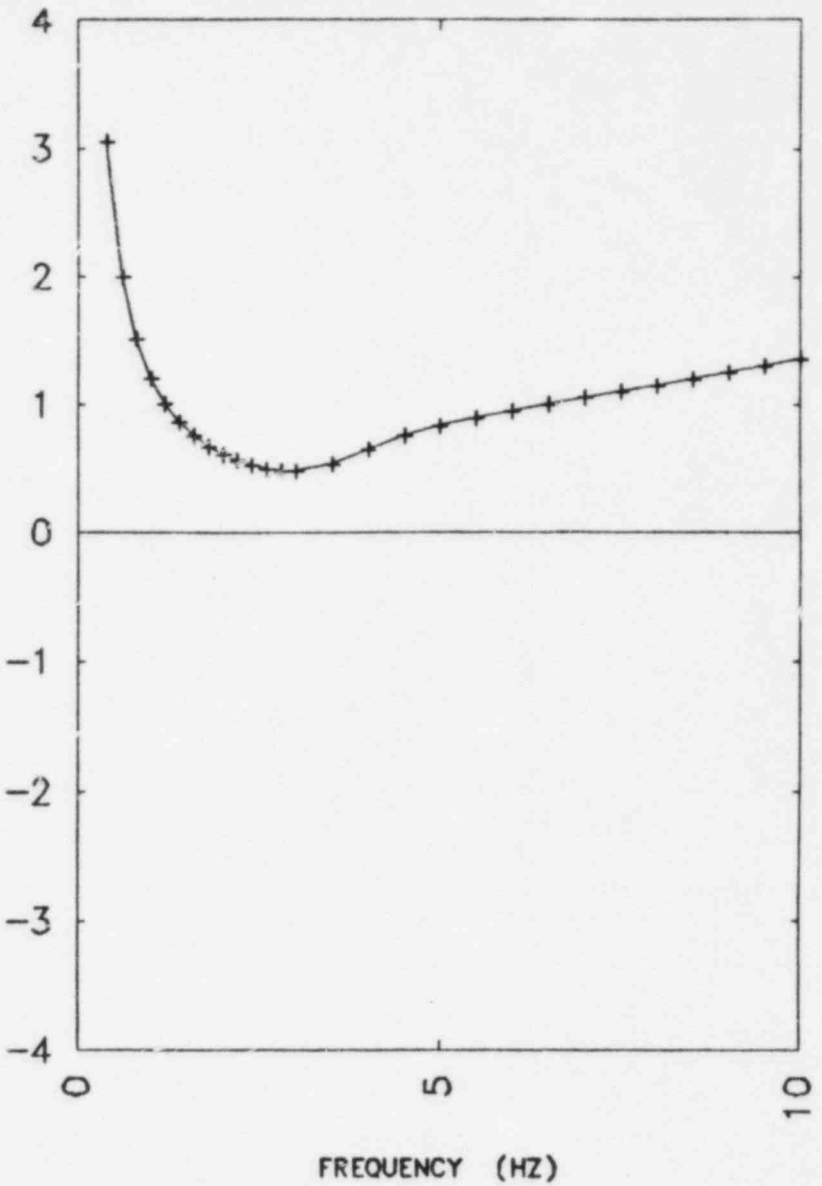

FIGURE III-2-24. ROCKING ABOUT THE EAST-WEST AXIS SOIL IMPEDANCE
STIFF SITE LAYERED SOIL PROFILE

FIGURE III-2-25. TORSIONAL RESPONSE SOIL IMPEDANCE
STIFF SITE LAYERED SOIL PROFILE

3. SEISMIC RESPONSE

3.1 MODAL CHARACTERISTICS

The auxiliary building natural frequencies, percentage of total structure mass participating in each mode, and mode description are presented in Tables III-3-1 to III-3-6. Using the results presented in these tables it can be noted that for the lower bound soil case, the fundamental East-West (E-W) translational frequency occurs at 1.52 hertz for the lower bound relative EPA stiffness case and 1.53 hertz for the upper bound relative EPA stiffness case. In the North-South (N-S) direction, the fundamental translational frequency occurs at 1.57 hertz and 1.60 hertz for the lower and upper bound relative EPA stiffness cases, respectively. Between 82 percent and 85 percent of the total structure mass participates in these coupled horizontal translational soil-structure modes. The fundamental vertical soil-structure mode occurs at 2.12 hertz for both relative EPA stiffness cases with approximately 93 percent of the total structure mass participating in this mode. Higher modes for these two relative EPA stiffness cases are virtually identical as shown by the natural frequencies, participating mass percentages, and mode descriptions. The higher modes for this soil case primarily represent out-of-phase soil-structure response in both the N-S and E-W directions. The percentage of mass participating in these higher modes ranges from a low of about 3 percent in the vertical direction to a high of 12 percentage for N-S response. In conducting the response spectrum analysis for this soil case, 30 modes of structure were used which resulted in at least 99.9 percent of the structure mass in each direction being included in all analyses.

The fundamental E-W translation frequency for the intermediate soil case occur at 2.66 hertz for the lower bound relative EPA stiffness case and 2.71 hertz for the upper bound relative EPA stiffness case. In the N-S direction, these frequencies occur at 2.71 hertz and 2.68 hertz

for the lower and upper bound relative EPA stiffness cases, respectively. Approximately 81 to 83 percent of the total structure mass participates in these fundamental horizontal translational soil-structure modes. The fundamental vertical frequency occurs at approximately 3.69 hertz with about 95 to 97 percent of the total structure mass responding in this vertical soil-structure mode. For the higher modes, a comparison of modal descriptions shows there are some minor shifting of modal frequencies and participating mass percentages between the lower and upper bound relative EPA stiffness cases. Higher modes are associated with both local structure response and out-of-phase soil-structure translational response in both the E-W and N-S directions. The percentage of mass participating in these higher modes (neglecting local modes) ranges from a low of about 2 percent in the vertical direction to a high of 13 percent for out-of-phase N-S soil structure response. Thirty modes of the structure were used in conducting the response spectrum analysis which resulted in at least 99.6 percent of the structure mass in each direction being included for this soil case.

For the upper bound soil case, the fundamental E-W translation frequency occurs at 3.72 hertz for the lower bound relative EPA stiffness case and 3.71 hertz for the upper bound relative EPA stiffness case. In the N-S direction, the corresponding fundamental frequencies are 3.65 and 3.63 hertz. The fundamental vertical translational mode occurs at approximately 5.34 hertz. Between 65 and 71 percent of the total structure mass participates in the fundamental horizontal translational soil-structure modes. In the vertical direction, between 91 and 95 percent of the total structure mass responds in this coupled soil-structure mode. A comparison of modal descriptions for the higher modes for the lower and upper bound relative EPA stiffness cases again shows some minor shifting of modal frequencies and participating mass percentages for these two cases. The higher modes for the upper bound soil case are associated with both local structure response and motion of the overall structure. In both the N-S and E-W directions, structural response is described by a number of smaller modes of the EPA, the

main auxiliary building and control tower. The percentage of mass participating in these higher modes (neglecting local modes) ranges from a low of about 1 percent in the vertical and N-S directions to a high of 12 percent in the N-S direction. Inclusion of 30 structure modes in the response spectrum analysis conducted for the upper bound soil case resulted in at least 97.6 percent of the total structure mass included in each direction.

Table III-3-7 presents a comparison of the fundamental soil-structure translational modes for both the lower and upper bound relative EPA stiffness cases for all three soil cases studied. In all cases, the fundamental soil structure frequencies for the lower and upper bound relative EPA stiffness cases are virtually identical. This close frequency comparison implies that the procedure used to develop relative EPA stiffnesses is not an important factor in determining global structure response. The substantial shift in fundamental structure frequencies for the three soil cases reflects the effects of the conservatively broad range of soil profiles evaluated for this structure.

3.2 COMPOSITE MODAL DAMPING

As discussed in Section 6 of Volume I of this report, both time history and response spectrum analyses were conducted for the SME. Time-history analyses were used to develop the in-structure response spectra used as input to floor mounted equipment. Response spectrum analyses were used to generate seismic response loads in the auxiliary building. By using response spectrum analyses to determine seismic response loads, excess conservatism was avoided since the SME ground response spectra are smooth and do not have the peaks and valleys associated with the spectra generated by the synthetic time histories. Use of response spectrum techniques to determine seismic response loads required the development of composite modal damping values for the structure. The procedure presented in Volume I of this report was used to define composite modal damping for the auxiliary building.

The method presented in Volume I is based on matching the response computed from the coupled equations of motion with the modal response at selected locations. Soil impedances are considered to act at the centroid of the overall foundation in determining structure dynamic characteristics. Structure response transfer functions are developed at a number of locations in the structure for both the rigorous and normal mode solutions. Modal damping values for the normal mode solution are iterated upon until the transfer functions for the two solutions match. By choosing locations which are sensitive to damping, composite modal damping values are determined which generally predict conservative response at all locations.

Composite modal damping values were determined using the program SOILST (Reference 14). The embedded stiffnesses and dashpots presented in Tables III-2-4 and III-2-5 defined the soil impedances beneath the structure in this analysis. The concrete structure was considered to be damped at 7 percent of critical damping consistent with SME damping for reinforced concrete structures above one-half yield.

Composite modal damping values were determined for a number of locations in the structure. Typical floors were chosen in both the main auxiliary building and the control tower that were relatively high in the structure and were judged to have dynamic responses sensitive to modal damping. Additional locations high in the EPA were also evaluated. Composite modal damping values for all modes were chosen based on a generally lower bound envelope of the modal damping values determined for all locations studied.

Composite modal damping values were determined only for modes contributing significantly to the dynamic response at the degree-of-freedom studied (in general more than about 10 percent of the total degree-of-freedom response). Damping for less significant modes of the auxiliary building was based on parametric studies of in-structure response spectra developed for the intermediate soil case. Because these

modes were typically associated with local, higher frequency response of the structure, overall seismic response loads were not particularly sensitive to the modal damping values used for the less significant modes. However, conservative modal damping values were chosen for these modes in order to avoid any underprediction of the auxiliary building response in some locations. In this study, in-structure response spectra were developed at typical locations in the structure by directly integrating the coupled equations of motion. These in-structure response spectra were then compared to the in-structure spectra determined from a modal superposition time history analysis of the structure. By appropriately modifying the damping of the less significant modes in the modal superposition time history analysis until close comparisons of the response spectra and zero period accelerations were obtained, conservative modal damping ratios were determined for these less significant modes. Based on these studies, high-frequency modes were damped at 3-1/2 percent of critical damping. These modes typically are associated with the local response of a small portion of the dynamic model. Lower frequency modes associated primarily with gross structure response were damped at 7 percent of critical damping consistent with the SME damping for concrete structures above one-half yield. Figure III-3-1 presents a comparison of typical in-structure response spectra determined in this manner.

The composite modal damping values used to determine the seismic response loads in the auxiliary building are presented in Tables III-3-1 to III-3-6. Damping associated with primarily horizontal translational soil modes ranges from a low of 12 percent of critical damping for the upper bound soil case to a high of 22 percent of critical damping in the lower bound soil case. Vertical soil modes were damped between 55 to 60 percent of critical damping. Because of the high percentages of structure mass participating in each of the 3 fundamental soil-structure modes, seismic response accelerations are primarily due to these fundamental modes and corresponding composite modal damping values. To further ensure that the composite modal damping values developed in the manner described above were conservatively chosen for all structure modes,

comparisons of structural response predicted by direct integration time history analysis using concentrated dashpots to model the soil damping were made with the seismic response determined by modal superposition using composite modal damping. Response accelerations at typical locations in the structure were determined from direct integration of the coupled equations of motion. At these same locations, response accelerations were then developed from a modal superposition time history analysis of the flexible base structure model using the modal damping values defined for each soil case by Tables III-3-1 to III-3-6. The same input time history was used in both time history analyses. Response accelerations from the two analyses were compared to ensure the accelerations based on the composite modal damping values approximately met or exceeded those determined from the direct integration time history analyses. Table III-3-8 presents comparisons of zero period accelerations in the structure obtained by these two procedures for the upper bound soil, upper bound relative EPA stiffness case. The upper bound relative EPA stiffness case is presented because seismic response loads throughout the structure are generally controlled by this relative EPA stiffness case as discussed in Section 3.3.1. Results for the other soil cases were similar.

3.3 STRUCTURE SEISMIC RESPONSE

Seismic loads throughout the auxiliary building structure were developed from the combined auxiliary building/control tower dynamic model. The overall seismic loads computed for the main auxiliary building and control tower model were distributed to the individual structural elements from which the lumped mass model was developed as described in Section 3.3.3 of this volume.

The seismic loads in the structure were determined using response spectrum modal analysis techniques. Earthquake excitation was specified as the SME ground response spectra for the original ground surface. The development of these spectra is described in Section 2.2 of Volume I of this report. The overall seismic loads were developed from

the SRSS of the modal responses including consideration of closely spaced modes as discussed in Section 6.5 of Volume I. The structural response loads were determined for each of the three earthquake directional components acting independently and then combined by the SRSS.

In addition to the three soil conditions considered, the effects of modeling assumptions on the relative soil stiffnesses under the EPA were evaluated as discussed in Section 2. Upper and lower bound EPA stiffness cases were analyzed for each of the three soil conditions, so that overall seismic loads were developed for the auxiliary building for a total of six cases. The effects of the different soil conditions and wing soil stiffness assumptions on the seismic response of the structure is discussed in the following subsection. For the SMR, the highest load computed for the structural element from any of the six cases was used to determine its code margin.

3.3.1 Effects of Soil Conditions on Seismic Loads

In general, the upper bound soil condition results in the highest seismic response loads throughout the structure. This applies to the main auxiliary building, the control tower, and the EPA. Shears, overturning moments, vertical axial forces, and torsion loads are all greatest for the upper bound soil condition. Only relative displacements between adjacent structures are maximized for the soft soil conditions.

The effects of the relative soil stiffness under the EPA show higher loads in some locations for the upper wing stiffness case and lower loads in other locations. Although the overall structure seismic response characteristics such as frequencies and mode shapes are not significantly altered by the EPA soil stiffness assumptions, local stiffness variations have a more pronounced effect on the local load distributions within the structure; particularly in the lower elevations of the EPA and control tower. In some locations, the upper EPA soil stiffness case results in loads being transmitted out of the control tower through the EPA while for the lower EPA soil stiffness, inertia

loads from the penetration wings are transferred into the control tower. For the soft soil condition, the local soil stiffness variations are much less significant than for the stiff and intermediate soils cases.

Plots of SRSS horizontal seismic shear forces and overturning moments for the main auxiliary building are shown in Figures III-3-2 through III-3-5. Figure III-3-6 shows the vertical axial force in the main auxiliary building and Figure III-3-7 shows the torsional response about the vertical axis. For the upper bound soil case, the upper bound EPA soil stiffness results in slightly higher response for most locations in the structure. On the other hand, for the intermediate soil condition, the lower bound EPA soil stiffness normally results in somewhat higher loads, with the exception of torsion, than the upper bound EPA soil stiffness. Structure response for the lower bound soil condition was found to be quite insensitive to the EPA soil stiffness modeling assumptions and only the upper bound EPA soil stiffness case is plotted. For the torsional response, the lower bound soil case produced somewhat higher responses than the intermediate soil condition.

Figures III-3-7 through III-3-13 show similar plots of the seismic response throughout the control tower. Again, the upper bound soil case is seen to result in the maximum seismic loads. For E-W and axial response, the upper bound soil with the lower bound EPA soil stiffness results in higher loads in the majority of locations while for N-S and torsional response the upper bound soil and upper bound EPA soil stiffness condition is generally controlling. The seismic code margin evaluation was based on the worst case condition for all elements, even though the worst case cannot occur simultaneously for a number of different elements.

3.3.2 Comparison of SME and FSAR Loads

One basis for selecting various elements for code margin evaluation for the SME was the ratio of SME seismic load to the seismic load used for design. In order to determine the relative magnitudes of

the SME loads to the corresponding FSAR SSE design loads, comparisons of the lateral shear forces, overturning moments, vertical axial forces, and torsional response throughout the structure are shown in Figures III-3-14 through III-3-28.

Figures III-3-14 through III-3-17 show comparisons of the lateral seismic shear forces and corresponding overturning moments throughout the main auxiliary building. With the exception of the steel superstructure above Elevation 659', the design shears and moments for the most part exceed the corresponding SME values in critical locations by approximately 15 to 25 percent. Somewhat higher response was obtained for the SME in the steel superstructure than was used for design. The axial forces in the vertical direction of the main auxiliary building calculated for design also exceed the corresponding SME values throughout most of the structure. The comparison is shown in Figure III-3-18. However, as shown in Figure III-3-19, the SME torsional response exceeds the design loads for all locations. This occurs because of the torsional resonance conditions developed from the upper bound soil condition, and results in increased lateral loads in the peripheral shear walls of the structure.

Figures III-3-20 through III-3-25 show similar comparisons of SME and design seismic loads throughout the control tower portion of the structure. For lateral shear forces and axial loads, the design loads exceed the corresponding SME loads in most locations. The upper bound EPA soil stiffness results in increased moments transmitted through the EPA, and these moments are reflected in moments in the control tower about the N-S axis which exceed the design values; even through the control tower shear forces are less. Figures III-3-26 through III-3-28 show comparisons of the in-plane shears and moments as well as the axial forces in the east exterior wall of the east EPA. Because of symmetry, similar results occur in the west EPA. As can be observed in these figures, the SME loads throughout the EPA considerably exceed the design values as a consequence of the upper bound EPA soil stiffness. Several elements in the EPA were evaluted to determine the effects of these increased loads on the code margins.

3.3.3 Element Loads

The dynamic model used for the seismic analysis of the auxiliary building consisted primarily of interconnected vertical beam elements representing the stiffness properties of the main auxiliary building, control tower, and EPA. Each vertical element typically modeled the combined stiffness of the structural members of the load-resisting system at that story. Overall seismic loads acting on the structure were developed for these elements from the response spectrum analyses. Distribution of the overall loads to the individual structural members was performed using techniques appropriate for each different load-resisting system evaluated. Soil bearing stresses were not evaluated as part of the SMR. SME overturning moments and vertical loads in both the main auxiliary building and control tower are less than those calculated for the FSAR SSE, so that maximum toe pressures are less than the corresponding design values.

The main auxiliary building and the control tower are composed primarily of concrete shear walls interconnected by concrete floor slabs. For this type of structural system, the floor slabs act as diaphragms transmitting the seismic inertial forces to the load-resisting shear walls. If the diaphragms have sufficient stiffness, the walls spanning a story are constrained to displace together in the lateral directions. The overall seismic lateral loads can then be distributed to the individual walls in proportion to their relative rigidities. This technique is commonly used to develop load distributions for the design of concrete shear wall/floor slab systems.

The rigid diaphragm approximation was judged to be adequate for the determination of lateral seismic loads acting on the shear walls of the main auxiliary building and the control tower. Load distributions to the individual structural elements were developed as described in Section 6.7 of Volume I. Structural elements included in these load distributions were typically those considered to be seismic load-resisting in calculations performed to determine the stiffness properties of the dynamic model. As an example, the walls between Elevation 614'-0" and Elevation

634'-6" that were accounted for in the dynamic model are shown in Figure III-3-29. In general, all exterior and interior concrete walls capable of resisting seismic loads were included. Masonry walls were not considered to be capable of resisting forces due to overall seismic response. The walls receiving seismic forces were identified by individual elements having rectangular dimensions in plan. Some walls were modeled by a series of continuous elements. Major wall openings were treated as complete discontinuities in the element layout with the openings effectively spanning the full story height.

Story stiffnesses for elements identified as being seismic load-resisting were calculated by Bechtel as part of the development of stiffness properties of the dynamic model. These story stiffnesses were determined as described in Section 6.7 of Volume I. Out-of-plane wall stiffnesses were not included so that conservative in-plane loads would be produced. In-plane wall story stiffnesses considered the effects of both shear and flexural deformations. As an approximation, the flexural wall story stiffnesses were based on a condition of rotational fixity imposed at the top and bottom of the stories. The influence of flexural deformations diminishes for walls whose lengths are greater than their story heights and the lateral deflections of these walls are due primarily to shear deformations. The distribution of lateral seismic load, therefore, is not expected to be sensitive to the treatment wall rotational boundary conditions.

Seismic in-plane shears and overturning moments for the walls of the main auxiliary building and the control tower were calculated following the methodology for shear wall/floor slab systems described in Section 6.7 of Volume I. Wall element relative rigidities associated with the rigid diaphragm approximation were based on the wall story stiffnesses. Individual wall shears due to overall structure shears and torsional moments were then calculated using equations presented in Reference 15. Load input to these equations consisted of shears and torsional moments predicted by the structure response spectrum analyses. For conservatism, the possibility of a reduction in structure seismic

load due to embedment effects was neglected. Seismic loads acting on the wall elements evaluated in this study are listed in Tables III-4-1 and III-4-2.

Overall axial loads due to seismic response were available from the results of the response spectrum analyses. For the vertical elements, these axial loads include the effects of vertical inertial forces and resistance to overturning provided by these elements acting together to form a moment couple. These axial loads were distributed to the walls in proportion to their cross-sectional areas. The axial loads have an effect on the capacities of the walls against shear and overturning moment. However, these capacities are not particularly sensitive to small changes in the axial loads due to seismic response. Axial loads determined in this manner were included in shear and overturning moment capacity calculations.

Modifications to the load input were made at the bottom story of the main auxiliary building. Part of the main auxiliary building is supported on the base mat at Elevation 584'-0" while the remainder is supported on the base mat at Elevation 568'-0". These slabs are 5'-0" thick and bear on the original ground soil material. The slabs are stiffened in the out-of-plane direction by the concrete walls. It would be overly conservative to assume that the base mat at Elevation 568'-0" transmits all of the seismic forces to the soil since the base mat at Elevation 584'-0" will also participate in this load transfer. Consistent with the derivation of the soil impedances for the dynamic model, the base mats at the different elevations were taken to form a single unit. Seismic forces transmitted through the main auxiliary building to its bottom story were reduced by the forces associated with the stresses at the soil-base mat interface at Elevation 584'-0". Shear stresses due to horizontal seismic shear and normal stresses due to vertical seismic load were treated as being uniformly distributed over the base mat plan area while normal stresses due to overturning moments were taken to be distributed linearly. For conservatism, the transfer of

seismic loads to the soil by the foundation beneath the railroad bay at Elevation 634'-6" was neglected due to the lower stiffness of the fill material compared to that of the original ground material.

The distinction made in the overall dynamic model between the portion of the structure defined as the main auxiliary building and that defined as the control tower was retained for consistency. The walls included in the stiffness property calculations for the main auxiliary building were subjected to forces associated with overall loads from the main auxiliary building stick of the dynamic model. A similar treatment was performed for the walls of the control tower.

The south exterior walls of the east and west EPA were represented in the dynamic model by a series of plate elements having both in-plane and out-of-plane stiffnesses. The stiffness properties of the other walls of the EPA were represented by three vertical beams for each EPA. Each beam typically modeled a single wall or a limited number of walls within a region of the EPA. The wall in the EPA selected for code evaluation was the exterior N-S wall of the east EPA. The stiffness of this wall was accounted for by the outermost vertical beam of the dynamic model. Since this wall typically provided the only contribution to the stiffness properties of this vertical beam, seismic loads were taken directly from the response spectrum analyses in performing the capacities evaluation.

The underpinning walls that are to be installed beneath the existing control tower and EPA structures were represented in the dynamic model. The stiffness properties of the control tower underpinning walls were included in the vertical beam elements modeling the control tower below Elevation 614'-0". Seismic loads acting on these walls were determined using the same methodology developed for the other walls of the auxiliary building. Individual wall stiffnesses were modified to conform to the current preliminary design configuration transmitted by Reference 23. Seismic loads acting on the control tower underpinning wall elements evaluated in this study are listed in Tables III-4-5 and III-4-6.

Each of the underpinning walls beneath the east and west EPA was represented by a series of triangular plate elements in the dynamic model. Connectivity to the control tower and the existing EPA structures was modeled by beam elements having large stiffnesses. Boundary elements along the bottom wall face modeled the soil stiffnesses. Seismic loads on the underpinning walls, consisting of axial loads, in-plane and out-of-plane shears, and in-plane and torsional moments, were determined by resolving the reactions from these beam and boundary elements into overall loads acting on the wall boundaries. As an example, the overall in-plane shear acting on the bottom face of the underpinning wall was found by summing the forces from the boundary elements acting in the in-plane direction. These overall loads were calculated on a mode-by-mode basis with modal responses combined by SRSS. This approach leads to greater accuracy compared to integration of the plate element stresses. Plate element out-of-plane moment distributions are more sensitive to wall flexibility so values were taken directly from the response spectrum analyses. Seismic loads acting on the EPA underpinning wall elements evaluated in this study are listed in Tables III-4-5 and III-4-6.

The concrete floor slab at a given elevation serves as a diaphragm distributing floor inertial forces to the load-resisting shear walls. The slab also redistributes seismic shears from the walls of the story above to the walls of the story below when there is an alteration in the relative wall stiffness distribution from story to story. The diaphragm can be idealized as a beam subjected to load comprised of the seismic floor inertial force and shears from the walls of the story above. Support reactions for the idealized beam consist of the shears for the walls of the story below. Diaphragm in-plane shears and moments at the critical sections were determined based on the these applied loads and reactions. For slabs framing into an exterior wall, the diaphragm shear at the wall is equal to the difference in wall shears between the story above and the story below. This treatment accounts for diaphragm loads due to both floor inertial forces and redistribution of lateral seismic loads due to changes in the stiffness distribution of the

vertical load-resisting elements. This is conservative since the diaphragm load calculated in this manner includes the inertial load associated with the wall itself which is not actually transmitted through the diaphragm. Diaphragm forces at the interface between the and the control tower were taken directly from results for the horizontal elements modeling this connectivity from the response spectrum analyses. Applied seismic loads acting on the diaphragms selected for evaluation in this study are listed in Tables III-4-3 and III-4-4.

The load combination used in the structures capacities evaluation is discussed in Section 7.1 of Volume I. The dead and live load cases account for loads occurring at normal operating conditions. Forces and stresses in the reinforced concrete structural members of the auxiliary building due to loads occurring at normal operating conditions were taken from the results of the static analyses supplied by Bechtel (Reference 16). Load cases used in the FSAR static analysis consisting of various combinations of dead, live, jacking preload, and settlement loads were available for the auxiliary building. The effects of thermal gradients through the walls and slabs are discussed in Section 4-8. The code margins for the structural elements were calculated for the worst case obtained from the following combinations:

$$U = D + P_L + SME$$
$$U = D + P_L + L + SME$$
$$U = D + P_L + L + T + SME$$
$$U = D + P_L + T + SME$$

where

D = Dead Loads
L = Live Loads
P_L = Jacking preload
T = Settlement Loads
SME = Seismic Margin Earthquake Loads

The three-dimensional finite element model used for these static analyses generally consisted of plate elements representing the walls and slabs and beam or truss elements representing the beams, columns, and diagonal braces. Applied loads accounted for the effects of dead weight, live load, hydrostatic pressure, lateral earth pressure, jacking preload, and differential settlement. Results from the static analyses for the plate elements modeling the concrete walls and slabs consisted of membrane normal and shear forces per unit length and out-of-plane bending and twisting moments per unit length. For the walls and slabs, net in-plane axial forces, shears, and moments were calculated by integrating the reported plate element membrane stresses along the cross-sections being evaluated. In-plane shears and moments due to loads occurring at normal operating conditions for the walls and diaphragms evaluated in this study are also listed in Tables III-4-1 to III-4-6. Out-of-plane moments predicted by the plate elements were taken directly from the analytical results.

The structural steel framing above Elevation 659'-0" of the auxiliary building was included in the three-dimensional static model as interconnected beam and truss elements. The rigid frames in the E-W direction, the vertical braced frames in the N-S direction, and the horizontal bracing at Elevation 704'-0" were included in the model. The concrete slab at Elevation 704'-0" that is supported by this framing was represented by plate elements. Member forces due to loads occurring at normal operating conditions were taken directly from the results reported for the static analyses. The steel framing above Elevation 659'-0" was represented in the dynamic model by a beam element rising vertically from the main auxiliary building. A horizontal element connects the steel framing element to the control tower at Elevation 704'-0". This element models the interaction between the control tower and the steel framing due to inertial forces and differential displacements between the control tower and the main auxiliary building. Examination of the SME modal responses for the elements modeling the steel framing and its connectivity to the control tower indicates that loads due to seismic response occur primarily in single modes for the two horizontal ground motion components.

Forces in the steel framing occur due to seismic inertial loads and differential displacements between the main auxiliary building and the control tower. Prediction of forces in the steel framing using a finite element model with fixed boundary conditions would not account for the effects due to the differential displacements. For this reason, member forces for the steel framing due to SME were determined by scaling the results of the static finite element model analysis performed by Bechtel for the design OBE. These results were included along with those for the normal operating condition loads and correspond to the SRSS combination of seven modes for Bechtel's mean soil case. The finite element model is able to account for the relative influence of seismic inertial forces and differential displacements between the main auxiliary building and the control tower on the members of the structural steel framing.

Since seismic forces in the elements of the dynamic model representing the steel framing and its connectivity to the control tower occur primarily in single horizontal modes, it is possible to define factors to scale the member forces predicted by the OBE static analysis. For the rigid frames in the E-W direction, a scale factor of 3.2 was based on the ratio of the SRSS E-W shear force in the horizontal diaphragm element due to the SME to the SRSS shear force due to the design OBE for Bechtel's mean soil case. The scale factor of 2.3 for the N-S vertical bracing members was similarly derived from the SRSS axial forces in the horizontal element. These scale factors were based on forces in the horizontal diaphragm element rather than the E-W and N-S shear forces in the vertical element modeling the steel framing because more conservative values resulted. Use of these scale factors accounts for differences in seismic input and modal characteristics between the dynamic analyses performed for the SME and the design OBE.

Table III-3-1

Auxiliary Building Natural Frequencies and Modal Mass

Lower Bound Relative EPA Stiffness Case

Lower Bound Soil

Mode Number	Modal Frequency (Hz)	Percentage of Total Structure Mass Participating in Each Mode			Modal Damping (% Critical)	Mode Description
		North-South Response	East-West Response	Vertical Response		
1	1.52	---	85.0	---	22	East-West (E/W) Soil-Structure Translation
2	1.57	84.7	---	2.8	21	North-South (N/S) Soil-Structure Translation
3	2.12	4.8	---	93.8	60	Vertical Soil-Structure Translation
4	2.20	---	3.6	---	2	E/W Response of Main Aux. Out-of-phase with Control Tower, EPA
5	3.18	10.2	---	3.3	7	Out-of-phase N/S Soil-Structure Mode
6	3.40	---	11.2	---	14	Out-of-phase E/W Soil-Structure Mode
7					3.5	
.					.	
.					.	
30					3.5	
	Total Mass For 30 Modes	99.9	99.9	99.9		

Participating mass percentages less than 1 percent are not shown.

Table III-3-2

Auxiliary Building Natural Frequencies and Modal Mass

Upper Bound Relative EPA Stiffness Case

Lower Bound Soil

Mode Number	Modal Frequency (Hz)	Percentage of Total Structure Mass Participating in Each Mode			Modal Damping (% Critical)	Mode Description
		North-South Response	East-West Response	Vertical Response		
1	1.53	---	85.3	---	22	East-West (E/W) Soil-Structure Translation
2	1.60	81.8	---	3.5	21	North-South (N/S) Soil-Structure Translation
3	2.12	5.7	---	93.3	60	Vertical Soil-Structure Translation
4	2.24	---	3.8	---	2	E/W Response of Main Aux. Out-of-phase with Control Tower, EPA
5	3.18	12.0	---	3.1	7	Out-of-phase N/S Soil-Structure Mode
6	3.45	---	10.7	---	14	Out-of-phase E/W Soil-Structure Mode
7					3.5	
.					.	
.					.	
30					3.5	
	Total Mass For 30 Modes	99.9	99.9	99.9		

Participating mass percentages less than 1 percent are not shown

Table III-3-3

Auxiliary Building Natural Frequencies and Modal Mass
Lower Bound Relative EPA Stiffness Case
Intermediate Soil

Mode Number	Modal Frequency (Hz)	Percentage of Total Structure Mass Participating in Each Mode			Modal Damping (% Critical)	Mode Description
		North-South Response	East-West Response	Vertical Response		
1	2.66	---	80.8	---	16	East-West (E/W) Soil-Structure Translation
2	2.71	81.2	---	2.1	16	North-South (N/S) Soil-Structure Translation
3	3.48	---	1.4	---	7	E/W Response of Main Aux. Out-of-Phase with Control Tower, EPA
4	3.68	3.4	---	95.2	55	Vertical Soil-Structure Translation
5	4.08	---	---	---	2	Local Mode
6	4.29	---	---	---	2	Local Mode
7	4.80	---	7.0	---	16	Out-of-Phase E/W Structure Mode
8	5.27	---	---	---	7	Local Mode
9	5.39	3.2	---	---	11	N/S EPA
10	5.60	10.9	---	2.0	18	Out-of-Phase N/S Soil-Structure Mode
11	6.06	---	9.7	---	18	Out-of-Phase E/W Soil-Structure Mode
12					3.5	
.					.	
30					3.5	
	Total Mass For 30 Modes	99.6	99.8	99.9		

Participating mass percentages less than 1 percent are not shown

Table III-3-4

Auxiliary Building Natural Frequencies and Modal Mass

Upper Bound Relative EPA Stiffness Case

Intermediate Soil

Mode Number	Modal Frequency (Hz)	Percentage of Total Structure Mass Participating in Each Mode			Modal Damping (% Critical)	Mode Description
		North-South Response	East-West Response	Vertical Response		
1	2.68	82.4	---	1.4	16	North-South (N/S) Soil-Structure Translation
2	2.71	---	82.9	---	16	East-West (E/W) Soil-Structure Translation
3	3.59	---	1.0	---	7	E/W Response of Main Aux. Out-of-Phase with Control Tower, EPA
4	3.69	2.5	---	96.7	55	Vertical Soil-Structure Translation
5	4.42	---	---	---	2	Local Mode
6	4.52	---	---	---	2	Local Mode
7	4.80	---	6.1	---	16	Out-of-Phase E/W Structure Mode
8	5.48	13.0	---	1.5	18	Out-of-Phase N/S Soil-Structure Mode
9	5.89	---	---	---	7	Local Mode
10	6.04	---	---	---	2	Local Mode
11	6.35	---	9.0	---	18	Out-of-Phase E/W Soil-Structure Mode
12					3.5	
.					.	
30					3.5	
	Total Mass For 30 Modes	99.6	99.8	99.9		

Participating mass percentages less than 1 percent are not shown

Table III-3-5

Auxiliary Building Natural Frequencies and Modal Mass
Lower Bound Relative EPA Stiffness Case
Upper Bound Soil

Mode Number	Modal Frequency (Hz)	Percentage of Total Structure Mass Participating in Each Mode			Modal Damping (% Critical)	Mode Description
		North-South Response	East-West Response	Vertical Response		
1	3.65	67.5	---	---	14	North-South (N/S) Soil-Structure Translation
2	3.72	1.0	65.9	---	12	East-West (E/W) Soil-Structure Translation
3	3.98	---	---	---	7	Local Mode
4	4.44	5.8	---	---	7	N/S In-Phase Corner Flap of EPA
5	4.88	---	6.9	---	12	E/W Structure Mode, Top of Main Aux. Out-of-Phase
6	5.26	---	9.9	---	12	E/W Response of Main Aux. Out-of-Phase with Control Tower, EPA
7	5.33	1.5	---	95.5	60	Vertical Soil-Structure Translation
8	5.74	---	---	---	7	Local Mode
9	5.87	1.1	---	---	13	N/S Motion of EPA
10	6.77	7.7	---	---	13	N/S Motion of Main Aux., Control Tower
11	7.93	---	5.3	---	3.5	Out-of-Phase E/W Soil-Structure Mode
12	8.26	12.4	---	1.2	3.5	N/S Response of EPA
.				.		
.				.		
30				3.5		
	Total Mass For 30 Modes	97.7	97.7	99.7		

Participating mass percentages less than 1 percent not shown

Auxiliary Building Natural Frequencies and Modal Mass
Upper Bound Relative EPA Stiffness Case
Upper Bound Soil

Mode Number	Modal Frequency (Hz)	Percentage of Total Structure Mass Participating in Each Mode			Modal Damping (% Critical)	Mode Description
		North-South Response	East-West Response	Vertical Response		
1	3.63	70.9	1.1	---	14	North-South (N/S) Soil-Structure Translation
2	3.71	1.4	64.8	---	12	East-West (E/W) Soil-Structure Translation
3	4.18	---	2.3	---	7	E/W Structure Mode, Main Aux. Out-of-Phase
4	4.71	3.7	---	---	7	N/S In-Phase Corner Flap of EPA
5	4.95	---	11.0	---	12	E/W Structure Mode, Top of Main Aux. Out-of-Phase
6	5.28	---	4.0	6.6	6	Coupled E/W, Vertical Structure Mode
7	5.34	1.0	---	90.9	60	Vertical Soil-Structure Translation
8	6.51	---	---	---	7	Local Mode
9	6.72	2.7	---	---	13	N/S Motion of EPA
10	6.79	5.6	---	---	13	N/S Motion of Main Aux., Control Tower
11	8.05	---	2.7	---	3.5	Out-of-Phase E/W Soil-Structure Mode
12	8.17	11.5	---	---	3.5	N/S Response of EPA
.					.	
.					.	
.					.	
30					3.5	
	Total Mass For 30 Modes	97.6%	98.8%	99.6%		

Participating mass percentages less than 1 percent not shown

Table III-3-7

AUXILIARY BUILDING FUNDAMENTAL NATURAL FREQUENCIES FOR SOIL CASES EVALUATED

Mode Description	Lower Bound Soil				Intermediate Soil				Upper Bound Soil			
	Lower Bound Relative EPA Stiffness Case		Upper Bound Relative EPA Stiffness Case		Lower Bound Relative EPA Stiffness Case		Upper Bound Relative EPA Stiffness Case		Lower Bound Relative EPA Stiffness Case		Upper Bound Relative EPA Stiffness Case	
	Frequency (Hertz)	Mode	Frequency (Hertz)	Mode	Frequency (Hertz)	Mode	Frequency (Hertz)	Mode	Frequency (Hertz)	Mode	Frequency (Hertz)	Mode
East-West Soil Translation	1.52	1	1.53	1	2.66	1	2.71	2	3.72	2	3.71	2
North-South Soil Translation	1.57	2	1.60	2	2.71	2	2.68	1	3.65	1	3.63	1
Vertical Soil Translation	2.12	3	2.12	3	3.68	4	3.69	4	5.33	7	5.34	7

Table III-3-8

Comparison of In-Structure Zero Period Accelerations Determined
by Direct Integration and Modal Superposition
Upper Bound Soil Case

Location	North-South Response Due to North-South Excitation		East-West Response Due to East-West Excitation		Vertical Response Due to Vertical Excitation	
	Direct Integration	Modal Superposition	Direct Integration	Modal Superposition	Direct Integration	Modal Superposition
Main Auxiliary Building Elevation 634.5'	0.172	0.186	0.177	0.213	0.098	0.111
Main Auxiliary Building Elevation 659'	0.180	0.210	0.195	0.238	0.100	0.111
Control Tower Elevation 634.5'	0.168	0.183	0.202	0.193	0.092	0.108
Control Tower Elevation 659'	0.201	0.231	0.240	0.267	0.098	0.109
Eastern Edge of East Electrical Penetration Elevation 642.6'	0.393	0.397	0.215	0.222	0.115	0.115
Eastern Edge of East Electrical Penetration Elevation 685'	0.665	0.613	0.293	0.346	0.115	0.115
Center of East Electrical Penetration, Elevation 659'	0.224	0.246	0.245	0.270	0.113	0.113

All accelerations are in G units.

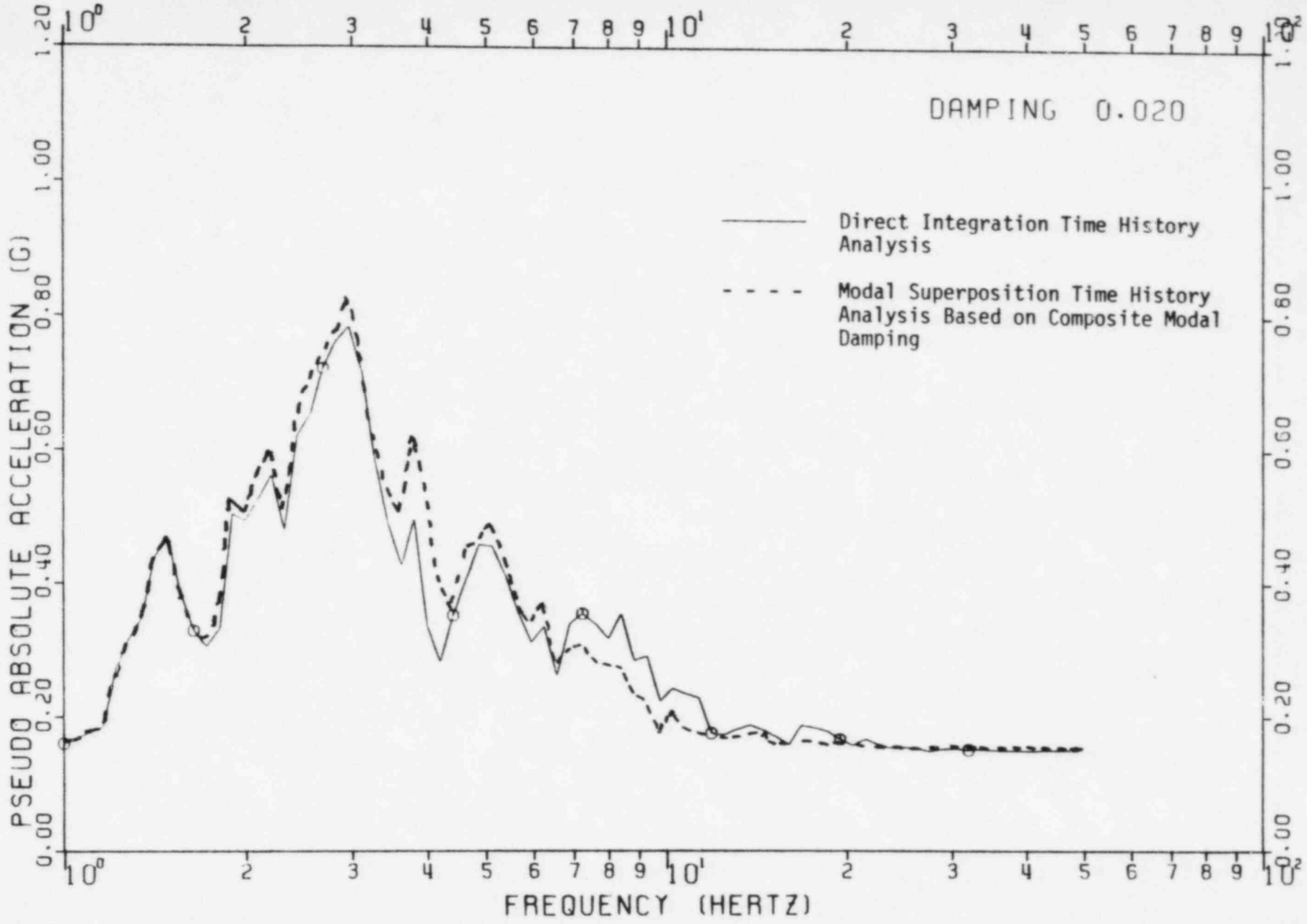

FIGURE III -3-1. COMPARISON OF IN-STRUCTURE RESPONSE SPECTRA, ELEVATION 628.6', MAIN AUXILIARY BUILDING, INTERMEDIATE SOIL CASE

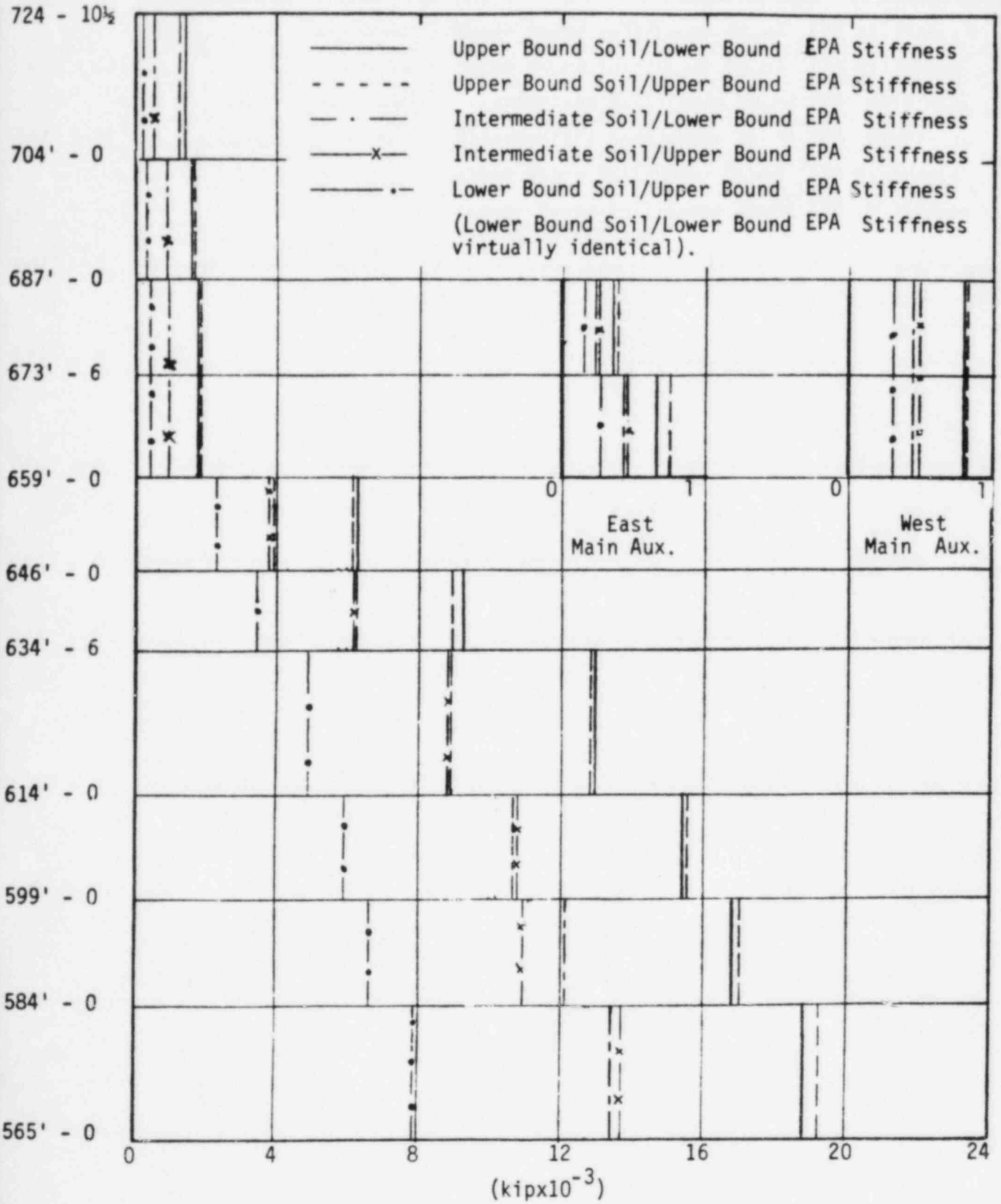

FIGURE III-3-2. MAIN AUXILIARY BUILDING E-W SRSS SHEAR

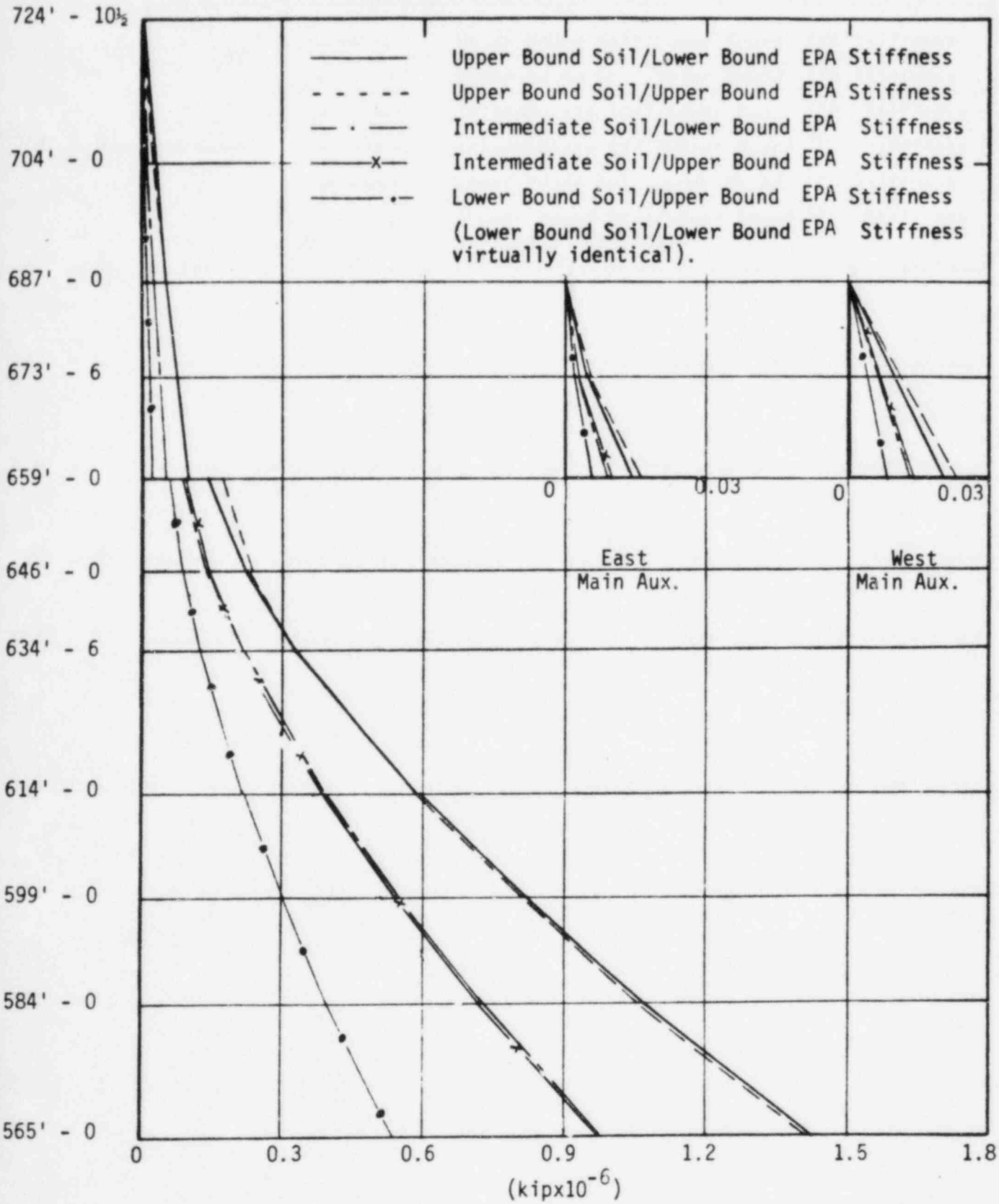

FIGURE III -3-3. MAIN AUXILIARY BUILDING SRSS MOMENT ABOUT N-S AXIS

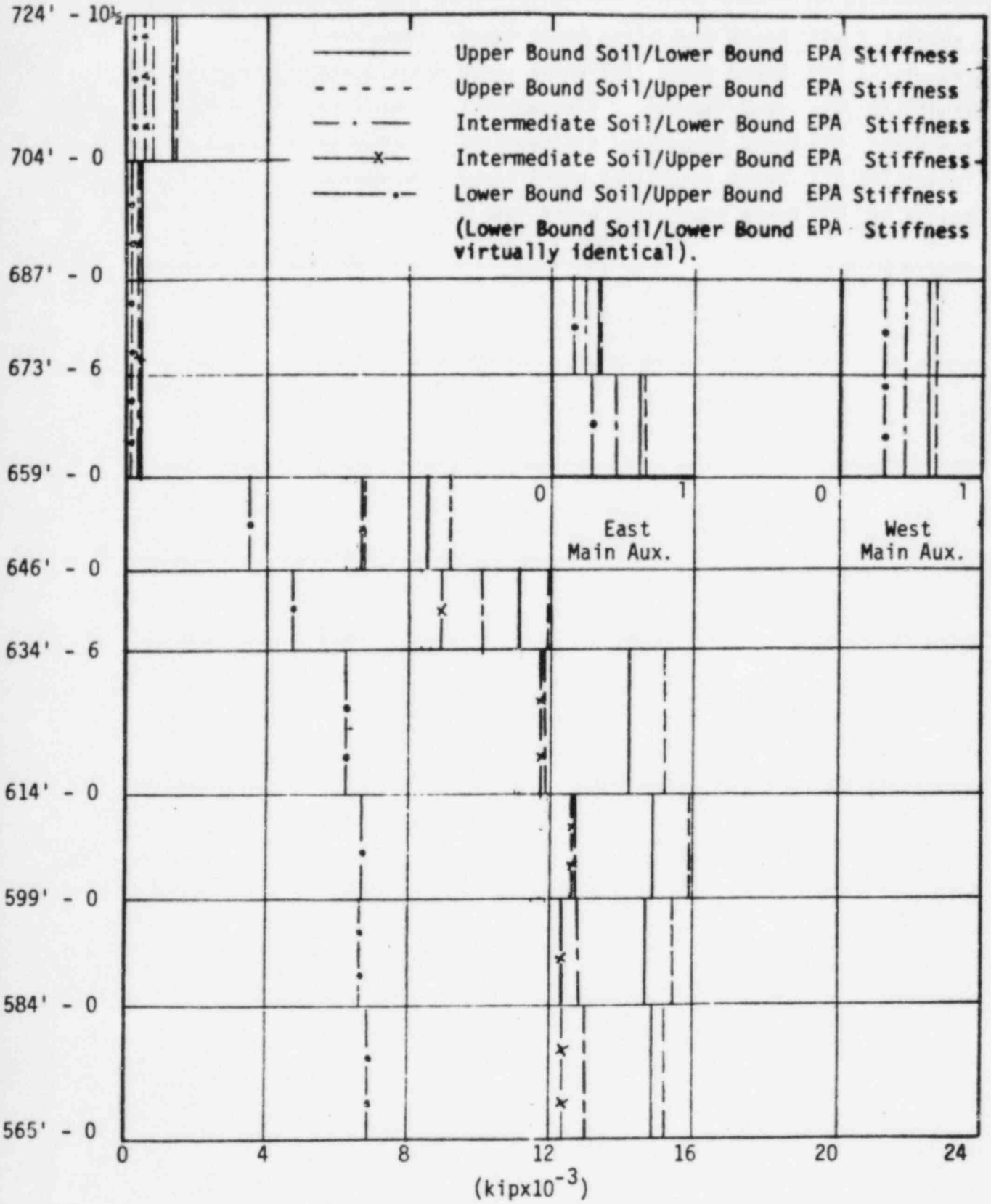

FIGURE III -3-4. MAIN AUXILIARY BUILDING N-S SRSS SHEAR

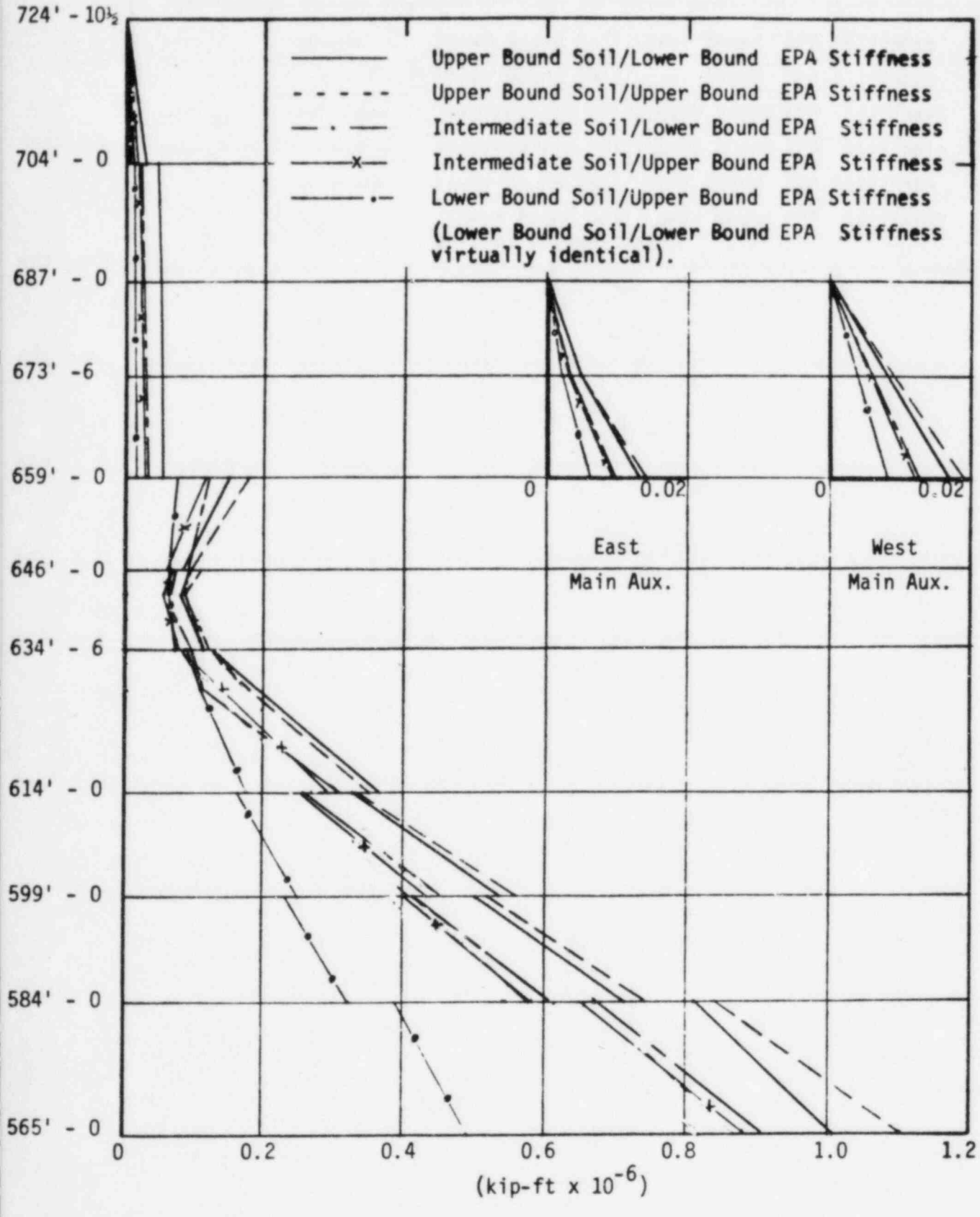

FIGURE III-3-5. MAIN AUXILIARY BUILDING SRSS MOMENT ABOUT E-W AXIS

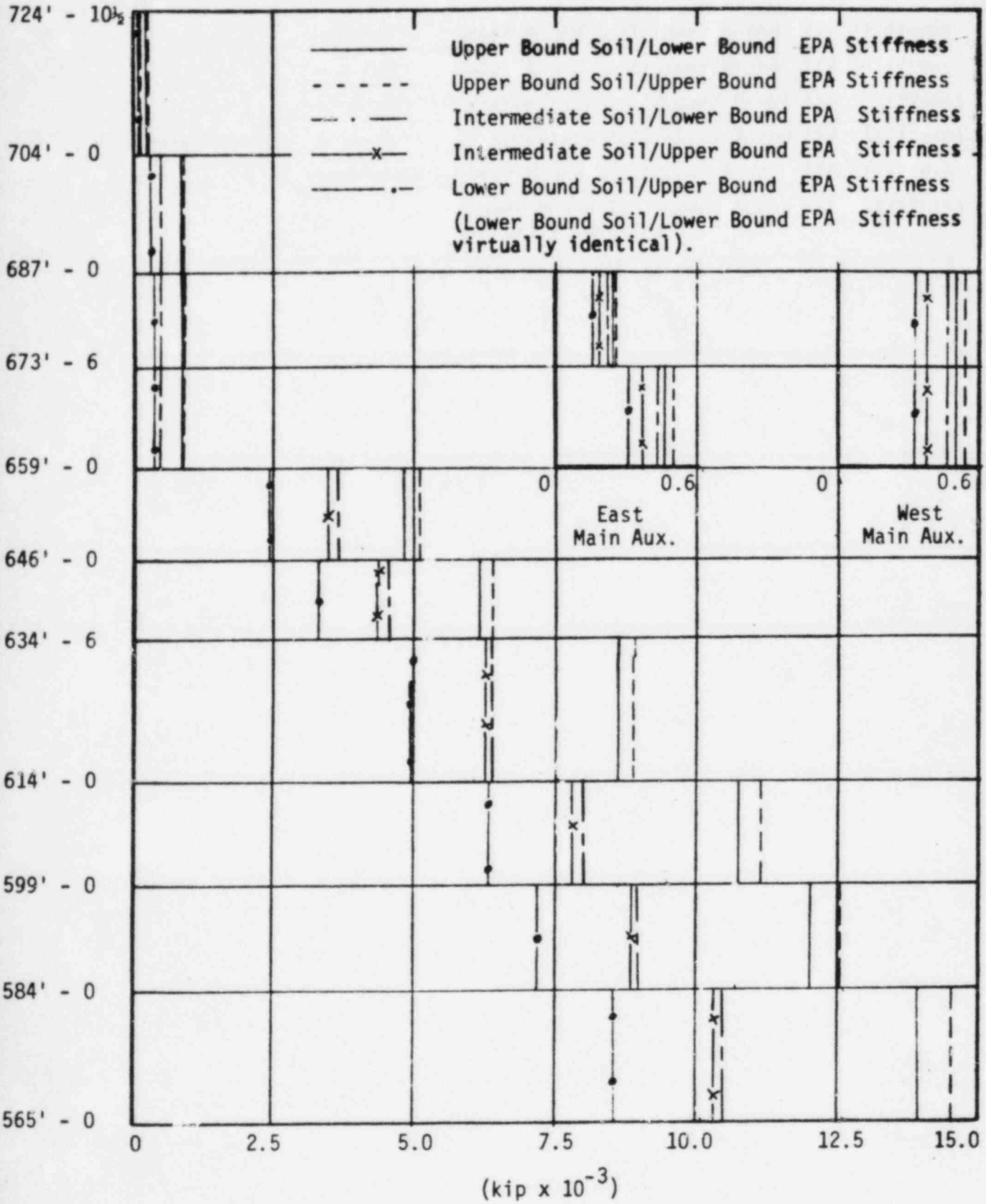

FIGURE III-3-6. MAIN AUXILIARY BUILDING SRSS AXIAL FORCE

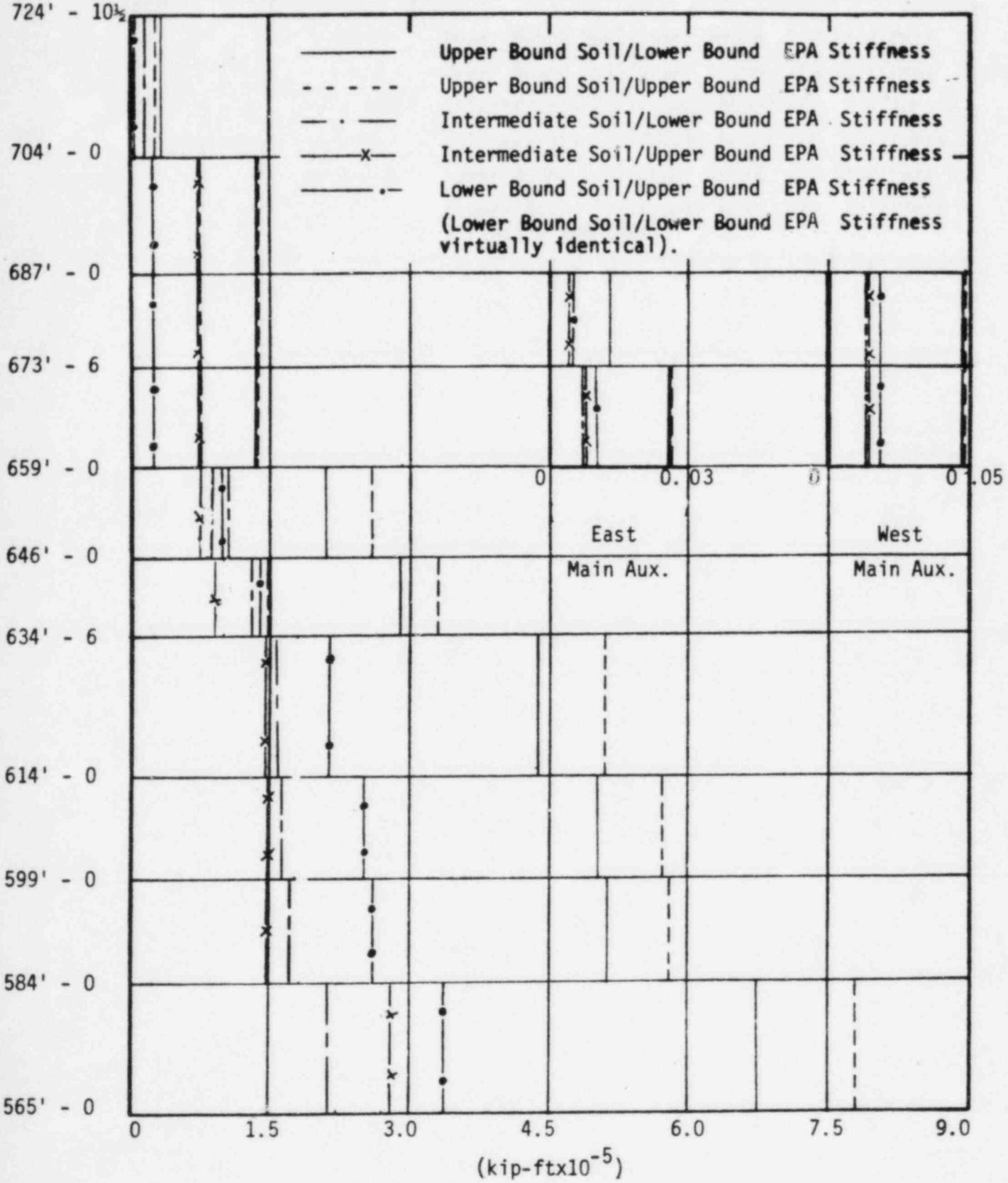

FIGURE III-3-7. MAIN AUXILIARY BUILDING SRSS TORSION

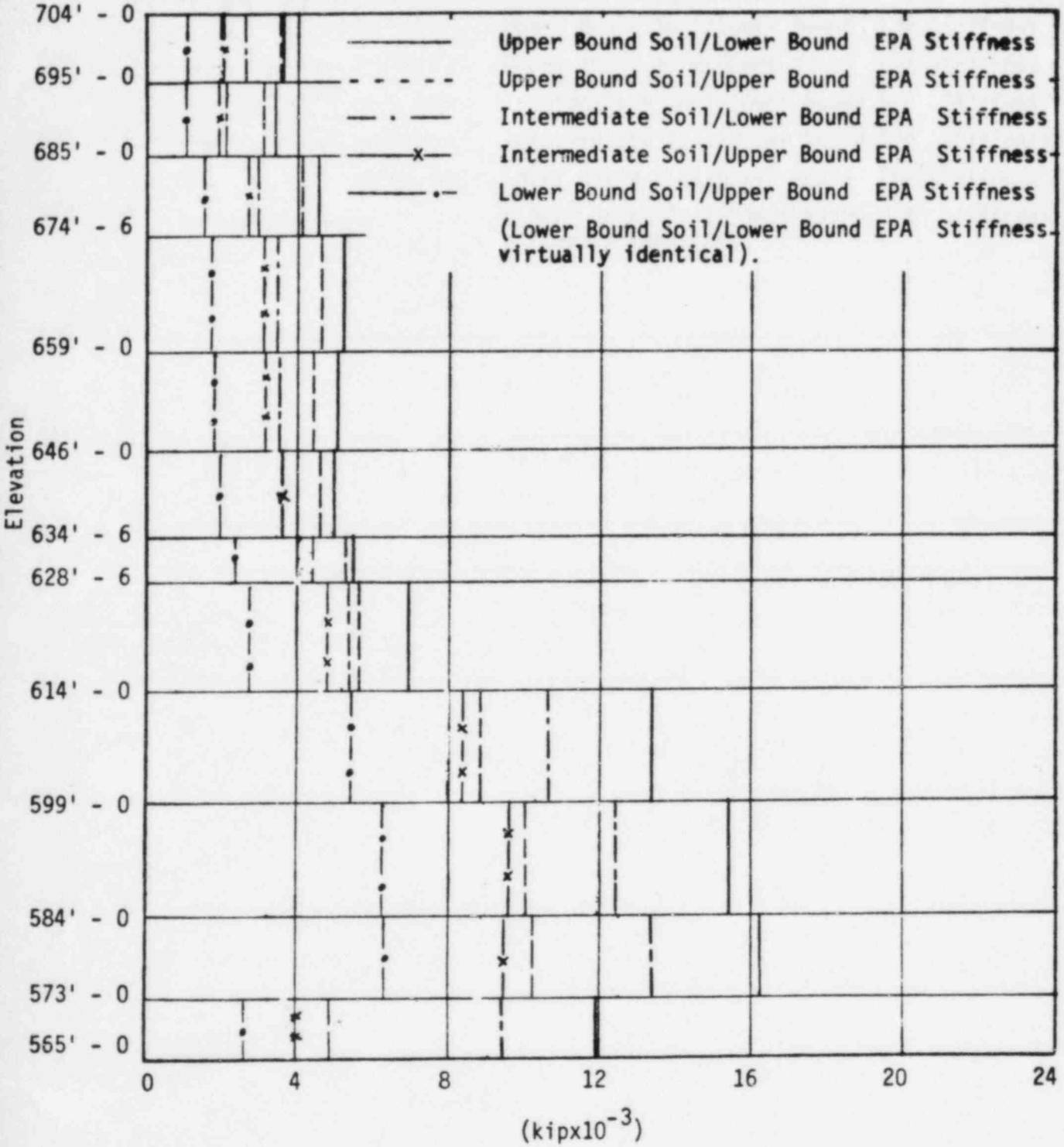

FIGURE III-3-8. CONTROL TOWER E-W SRSS SHEAR

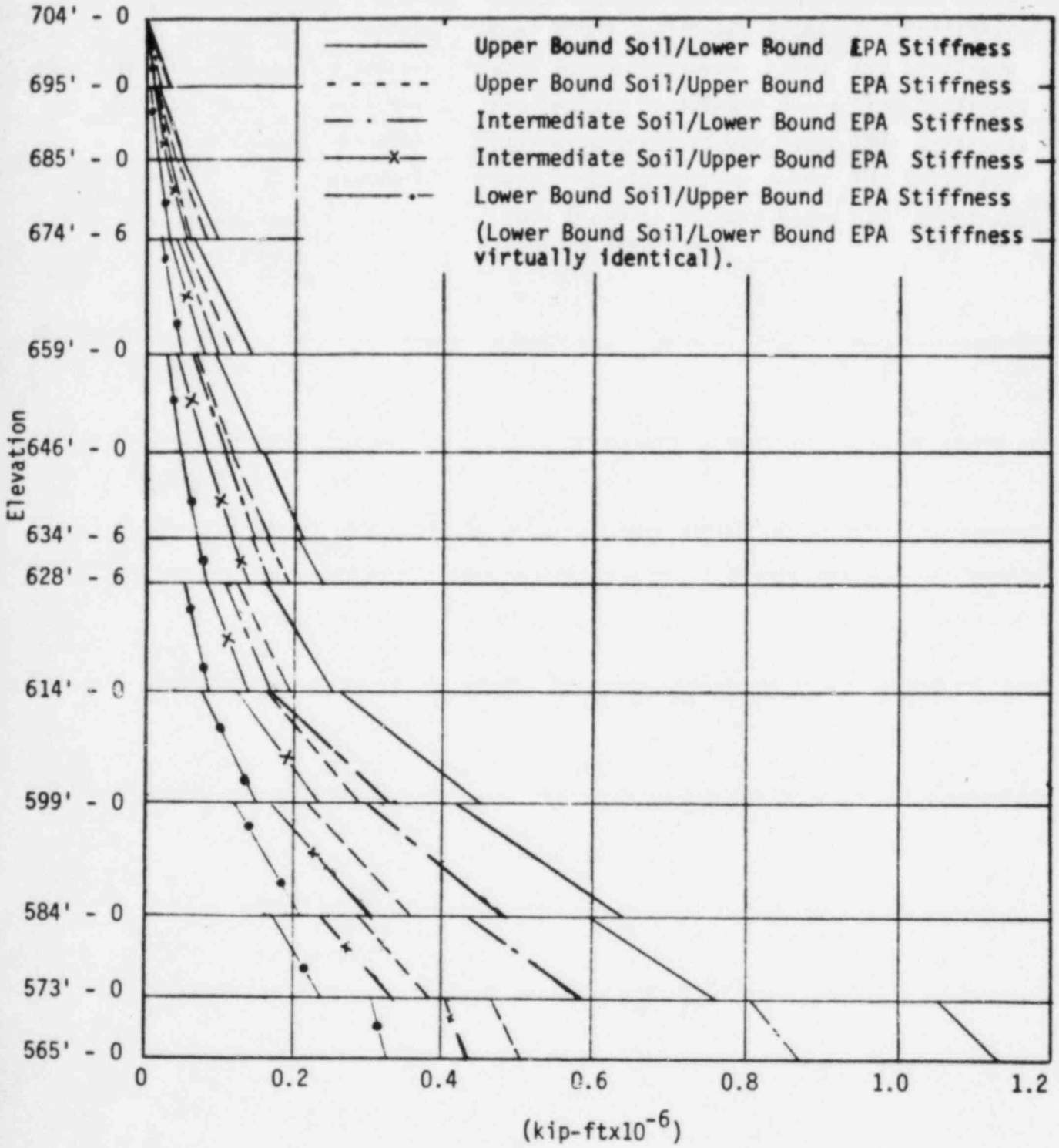

FIGURE III-3-9. CONTROL TOWER SRSS MOMENT ABOUT N-S AXIS

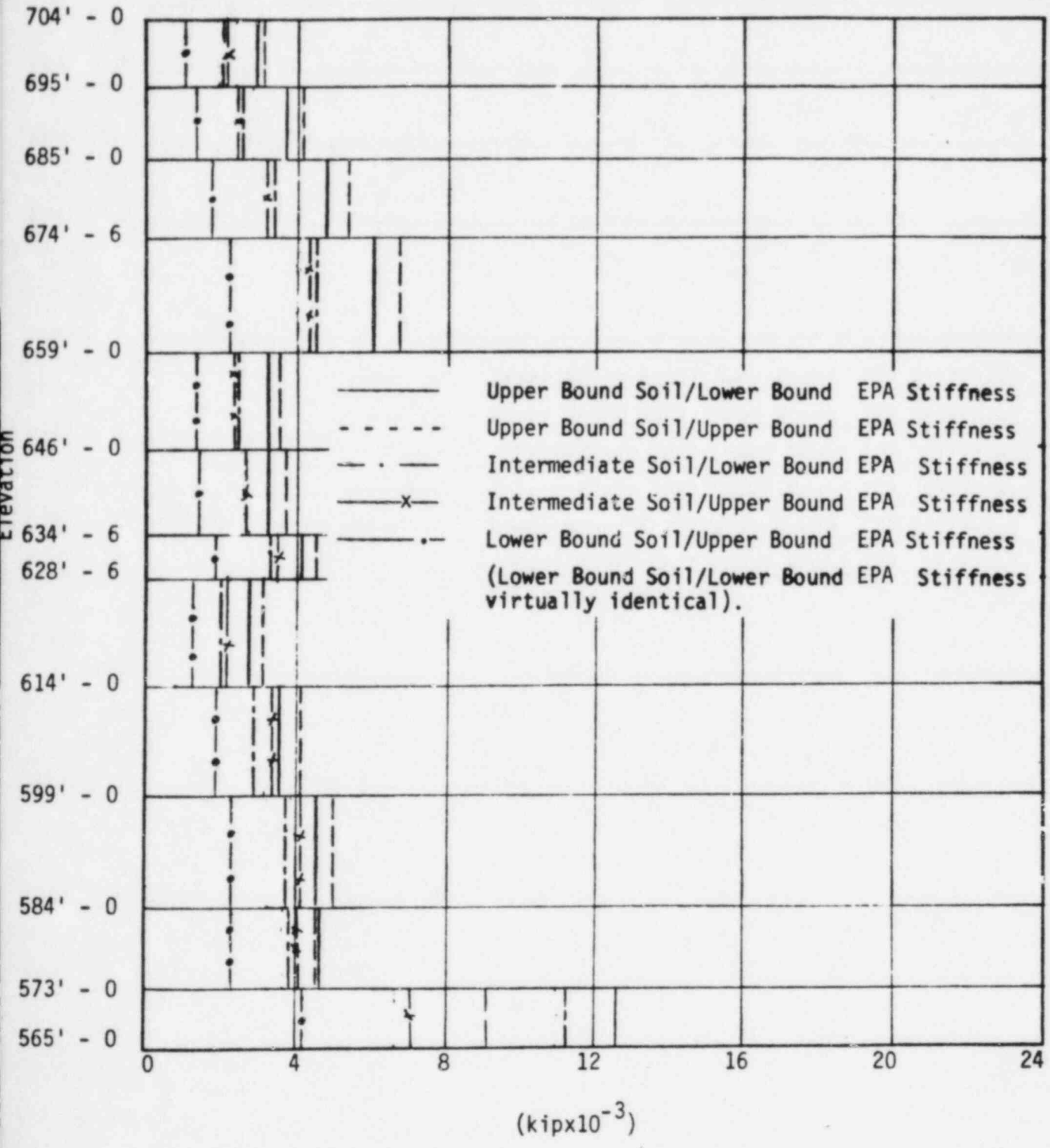

FIGURE III -3-10. CONTROL TOWER N-S SRSS SHEAR

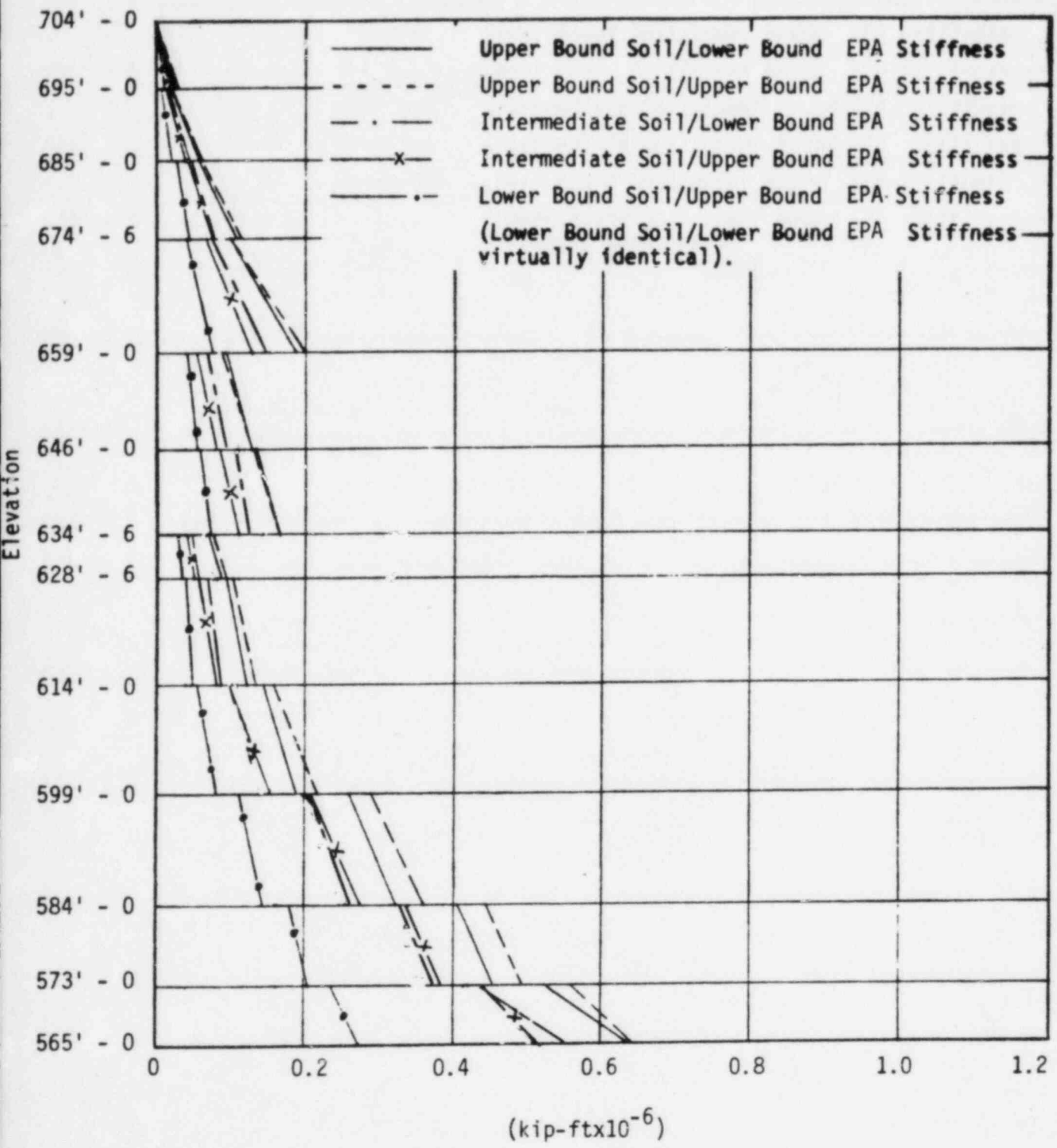

FIGURE III-3-11. CONTROL TOWER SRSS MOMENT ABOUT E-W AXIS

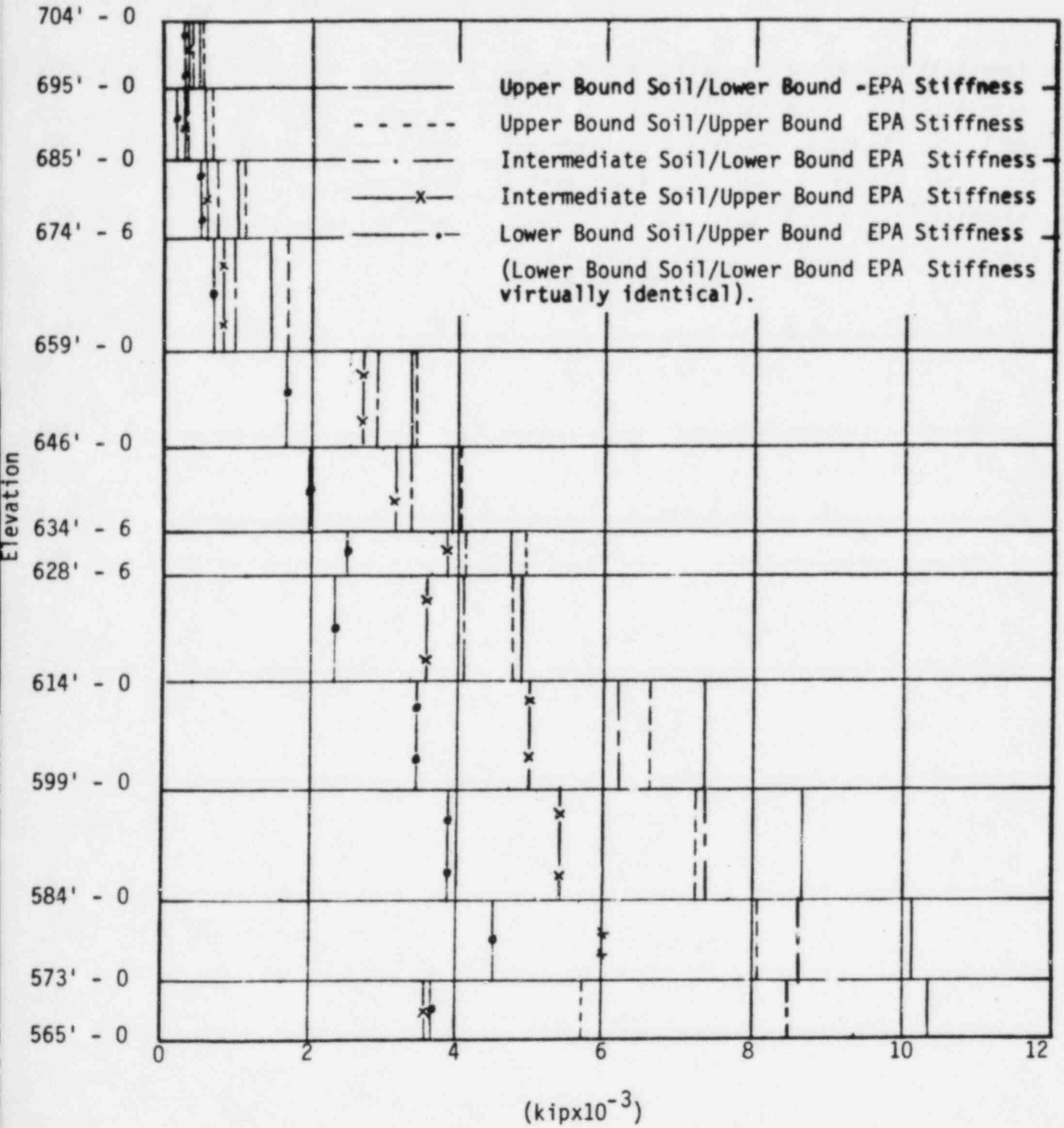

FIGURE III-3-12. CONTROL TOWER SRSS AXIAL FORCE

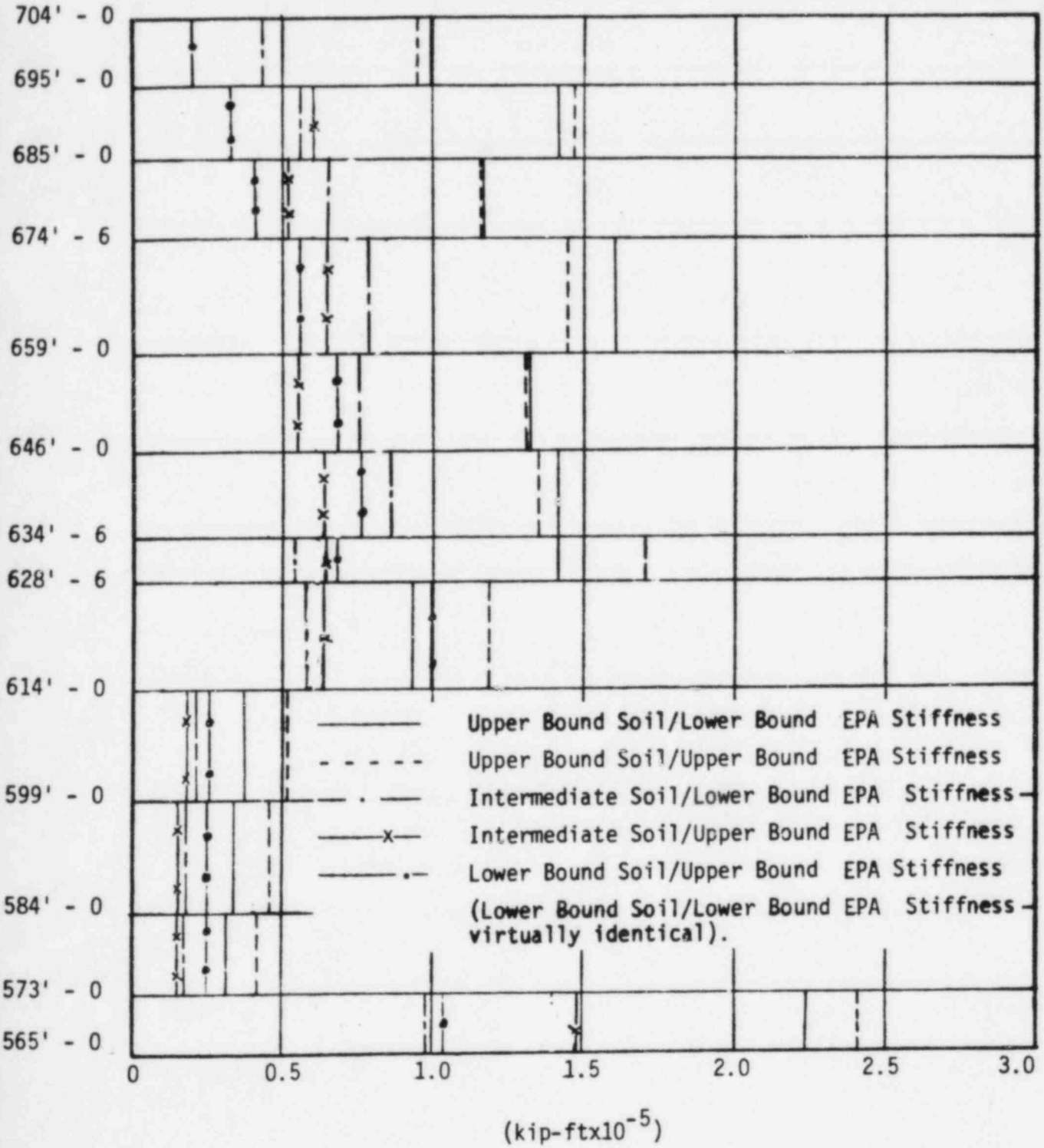

FIGURE III-3-13. CONTROL TOWER SRSS TORSION

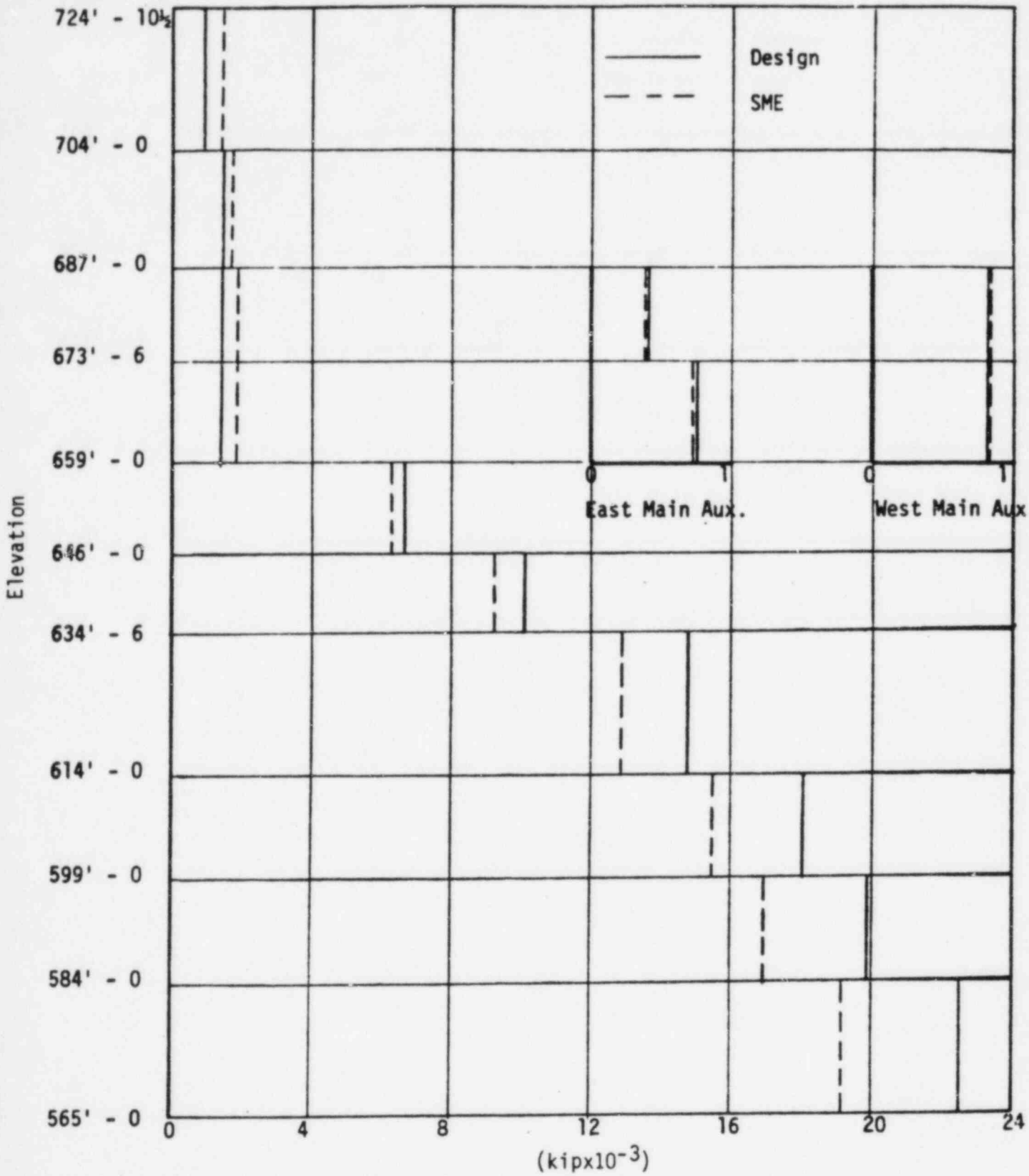

FIGURE III-3-14. MAIN AUXILIARY BUILDING E-W SHEAR COMPARISON

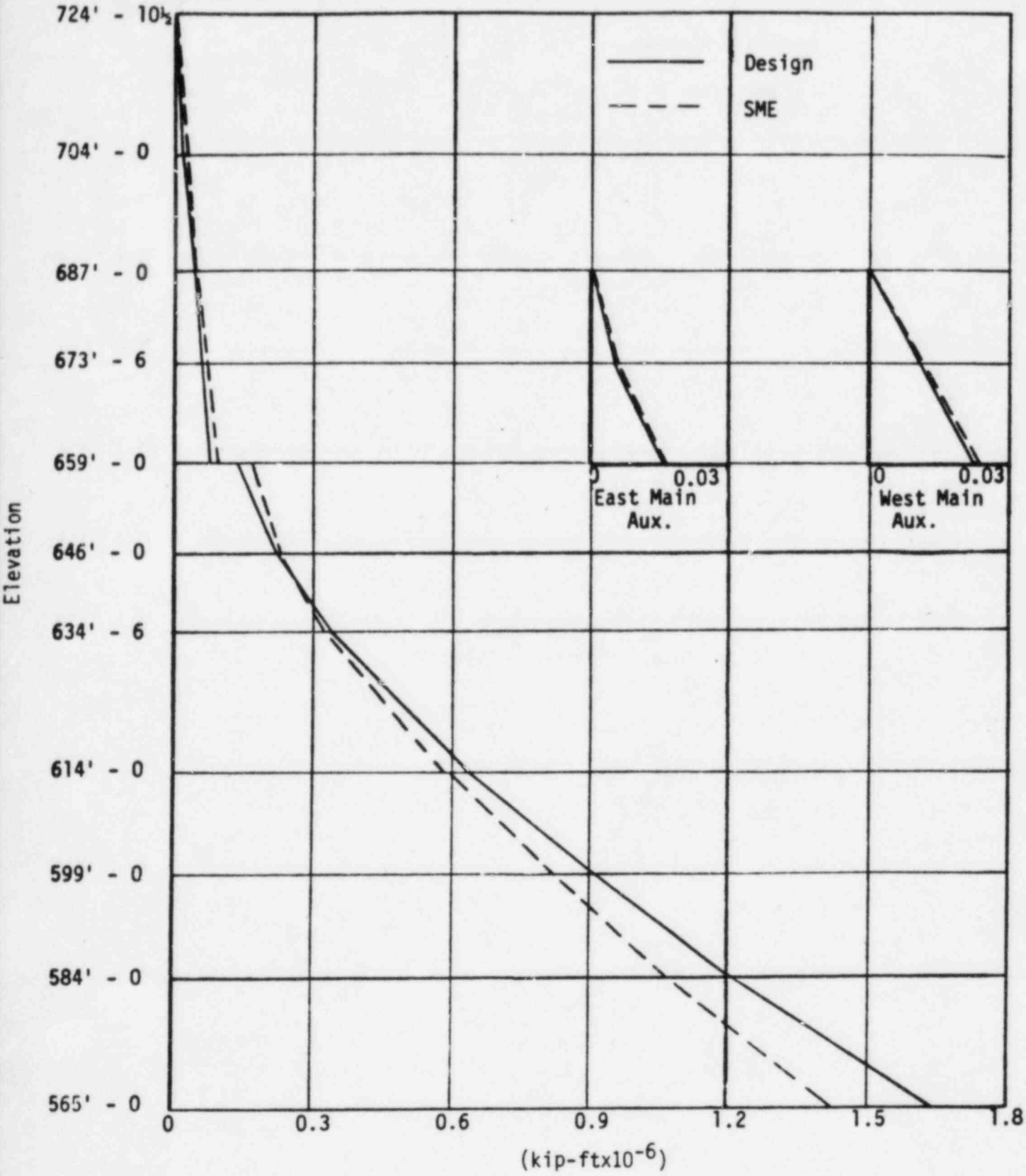

FIGURE III-3-15. MAIN AUXILIARY BUILDING MOMENT ABOUT N-S AXIS COMPARISON

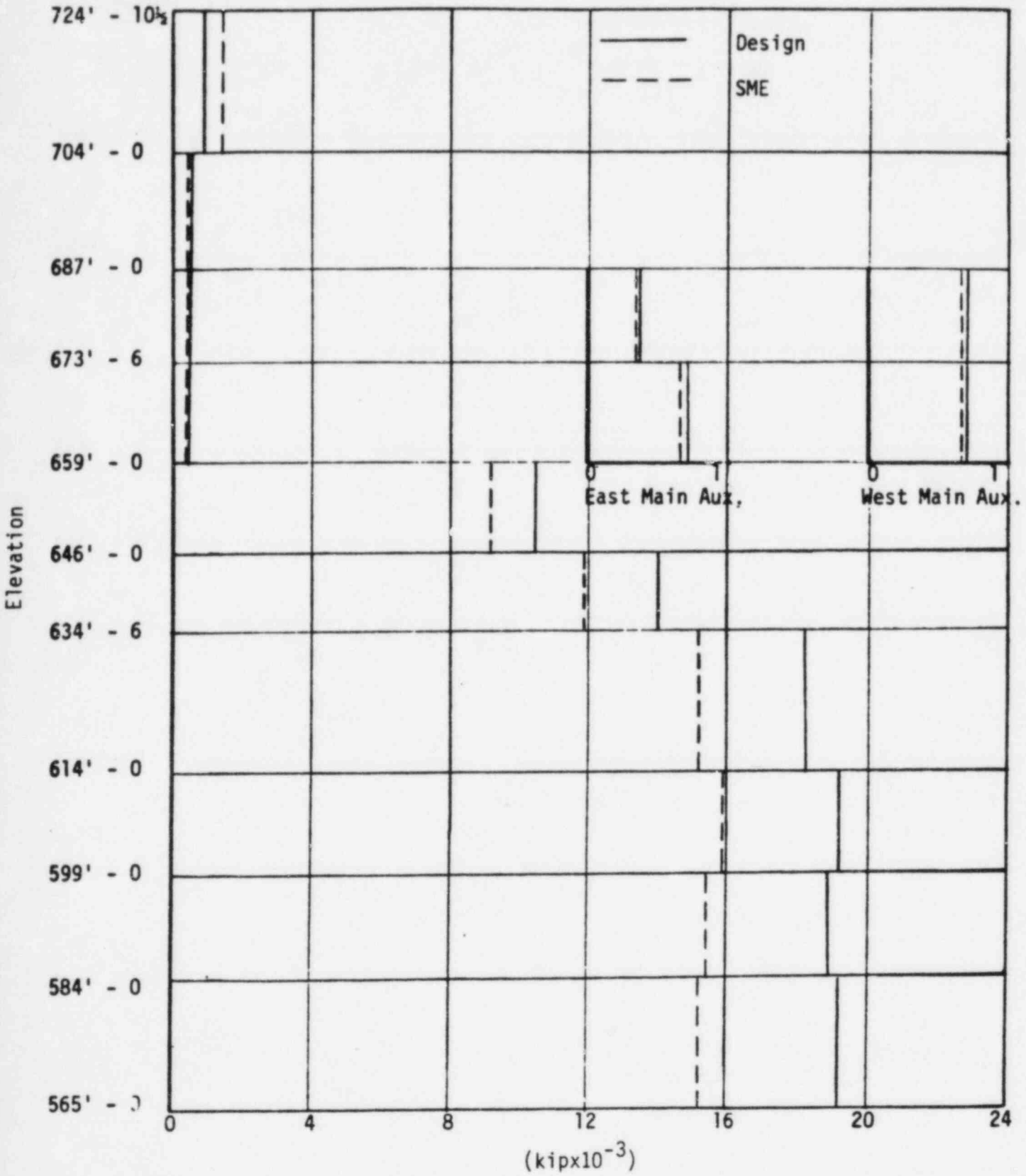

FIGURE III-3-16. MAIN AUXILIARY BUILDING N-S SHEAR COMPARISON

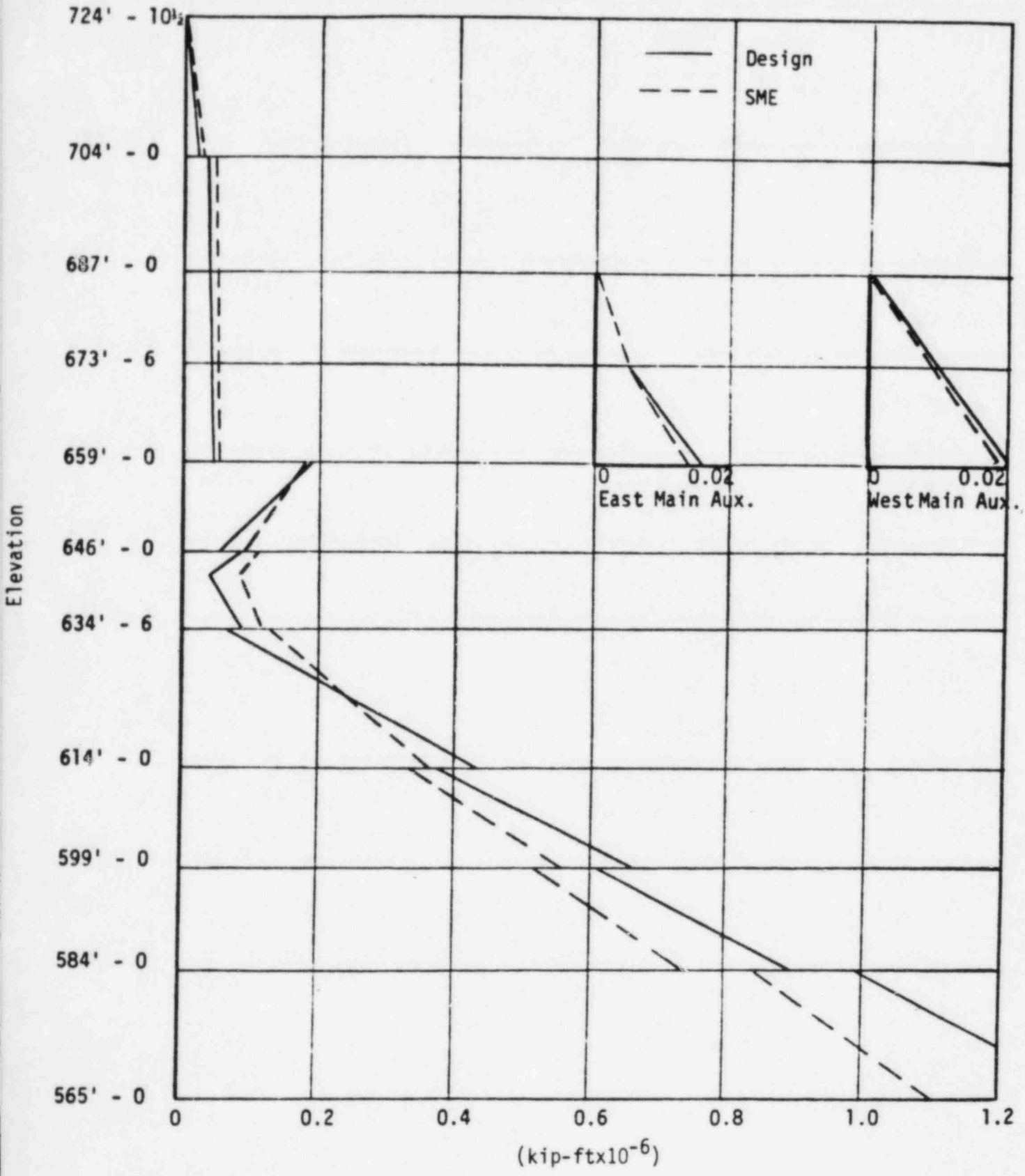

FIGURE III-3-17. MAIN AUXILIARY BUILDING MOMENT ABOUT E-W AXIS COMPARISON

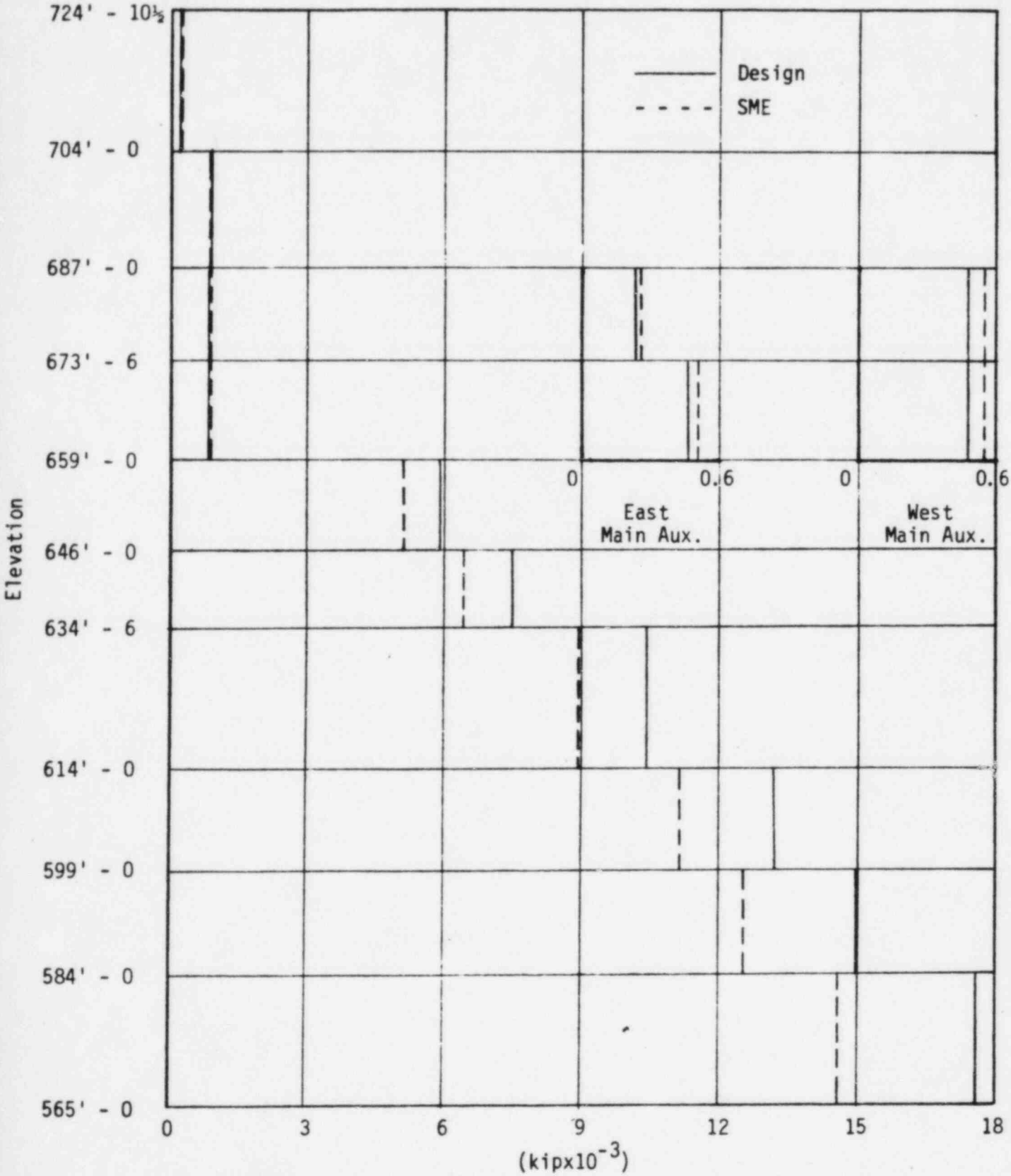

FIGURE III-3-18. MAIN AUXILIARY BUILDING AXIAL FORCE COMPARISON

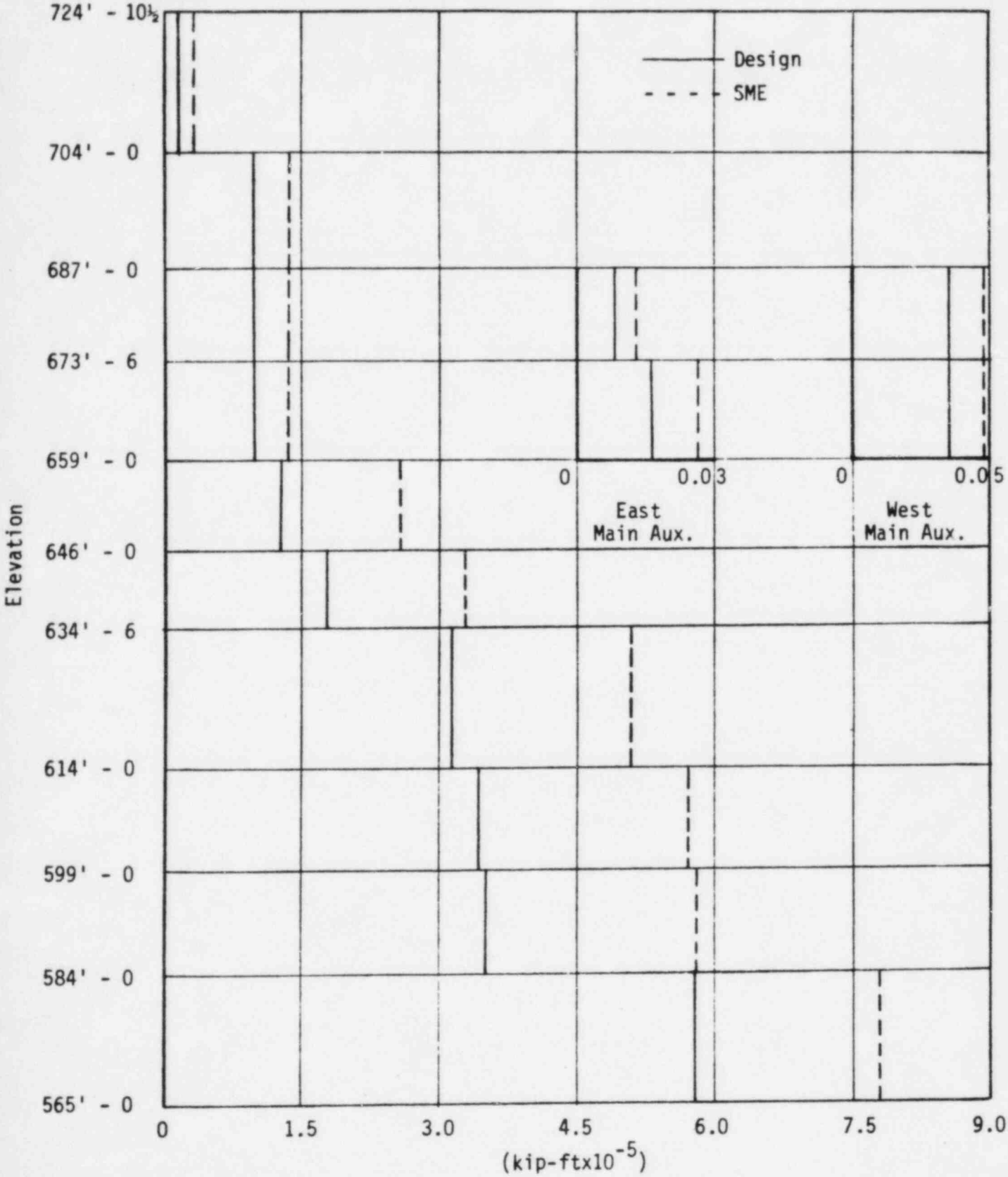

FIGURE III-3-19. MAIN AUXILIARY BUILDING TORSION COMPARISON

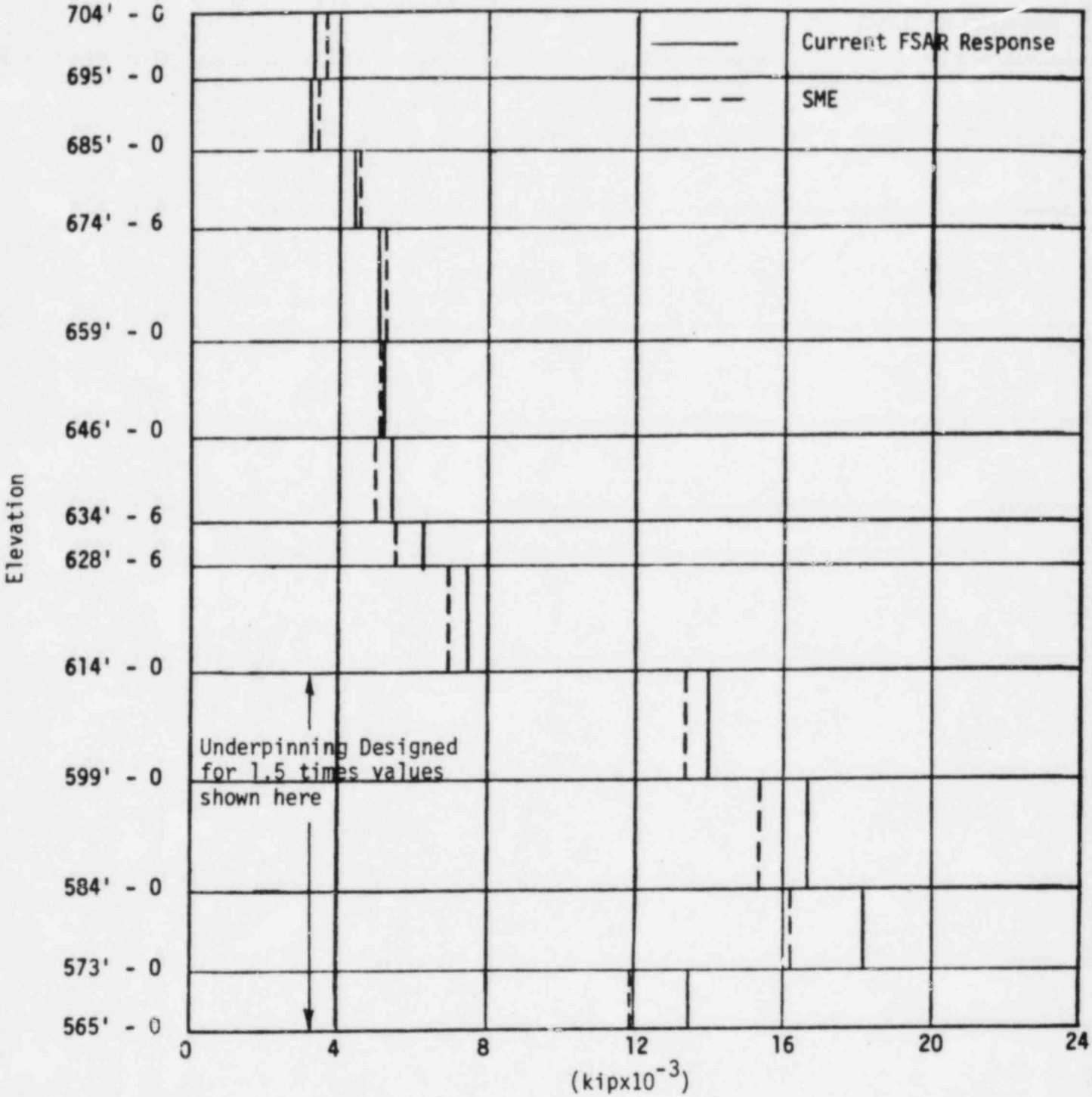

FIGURE III-3-20. CONTROL TOWER E-W SHEAR COMPARISON

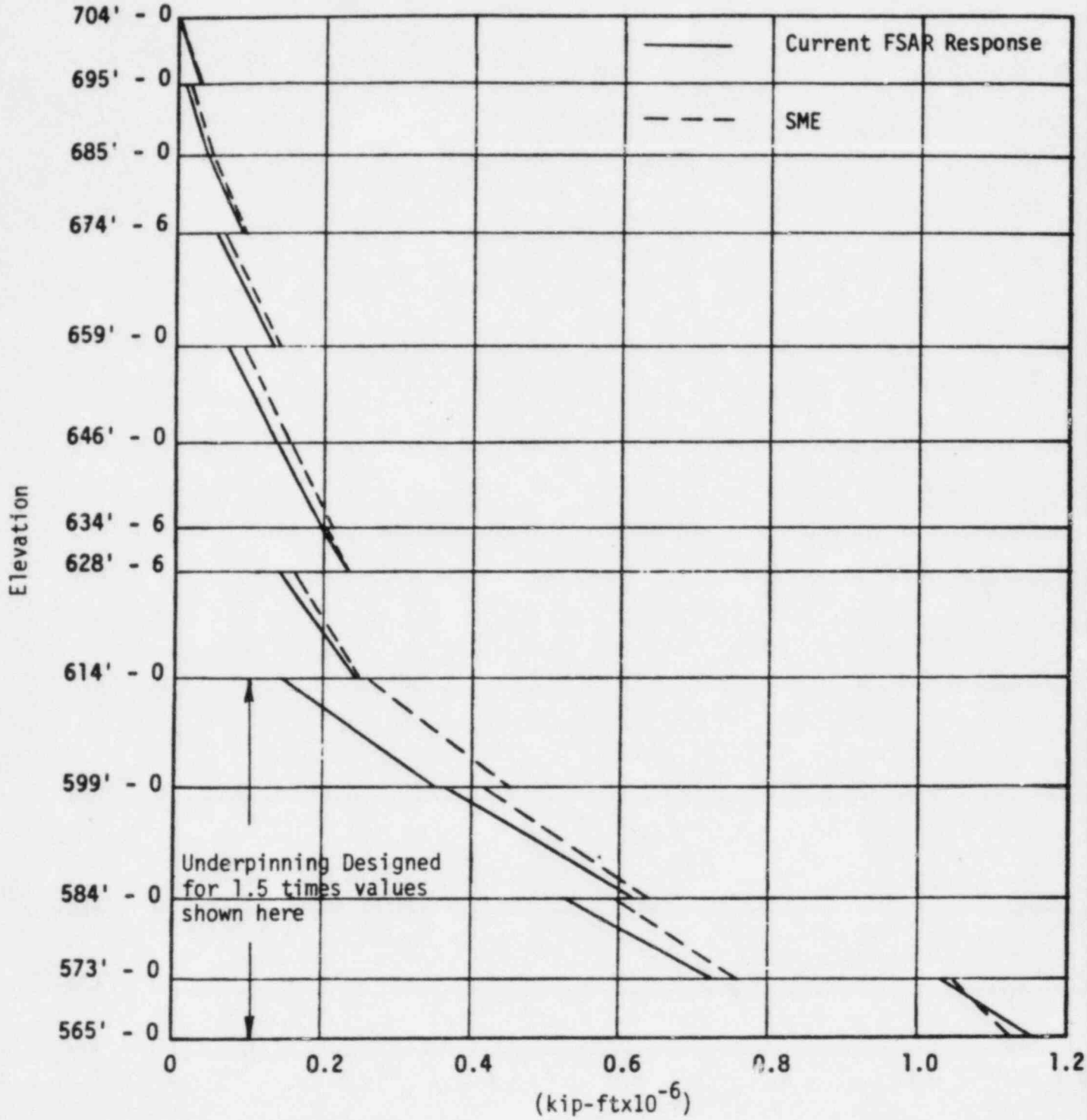

FIGURE III-3-21. CONTROL TOWER MOMENT ABOUT N-S AXIS COMPARISON

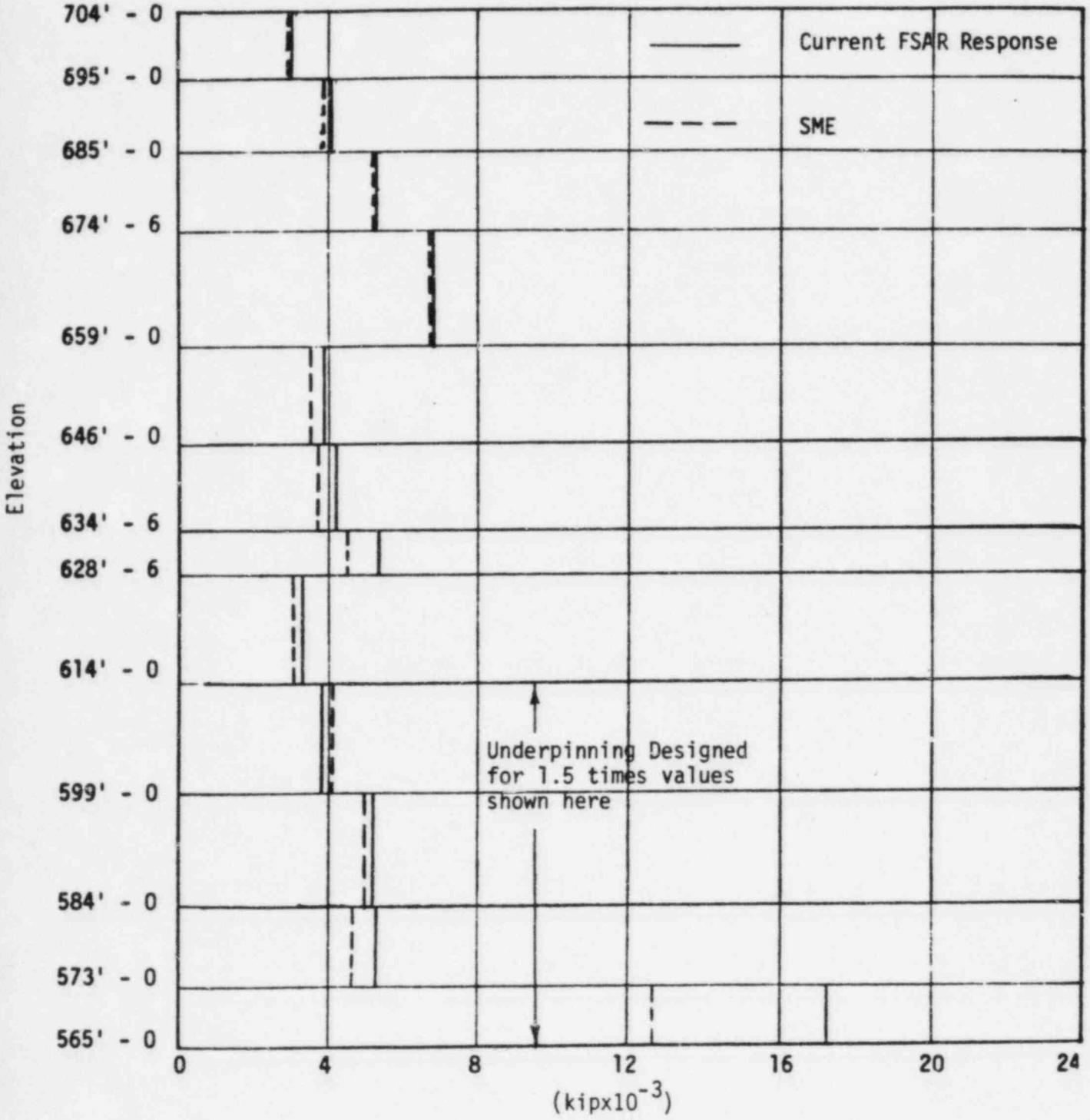

FIGURE III-3-22. CONTROL TOWER N-S SHEAR COMPARISON

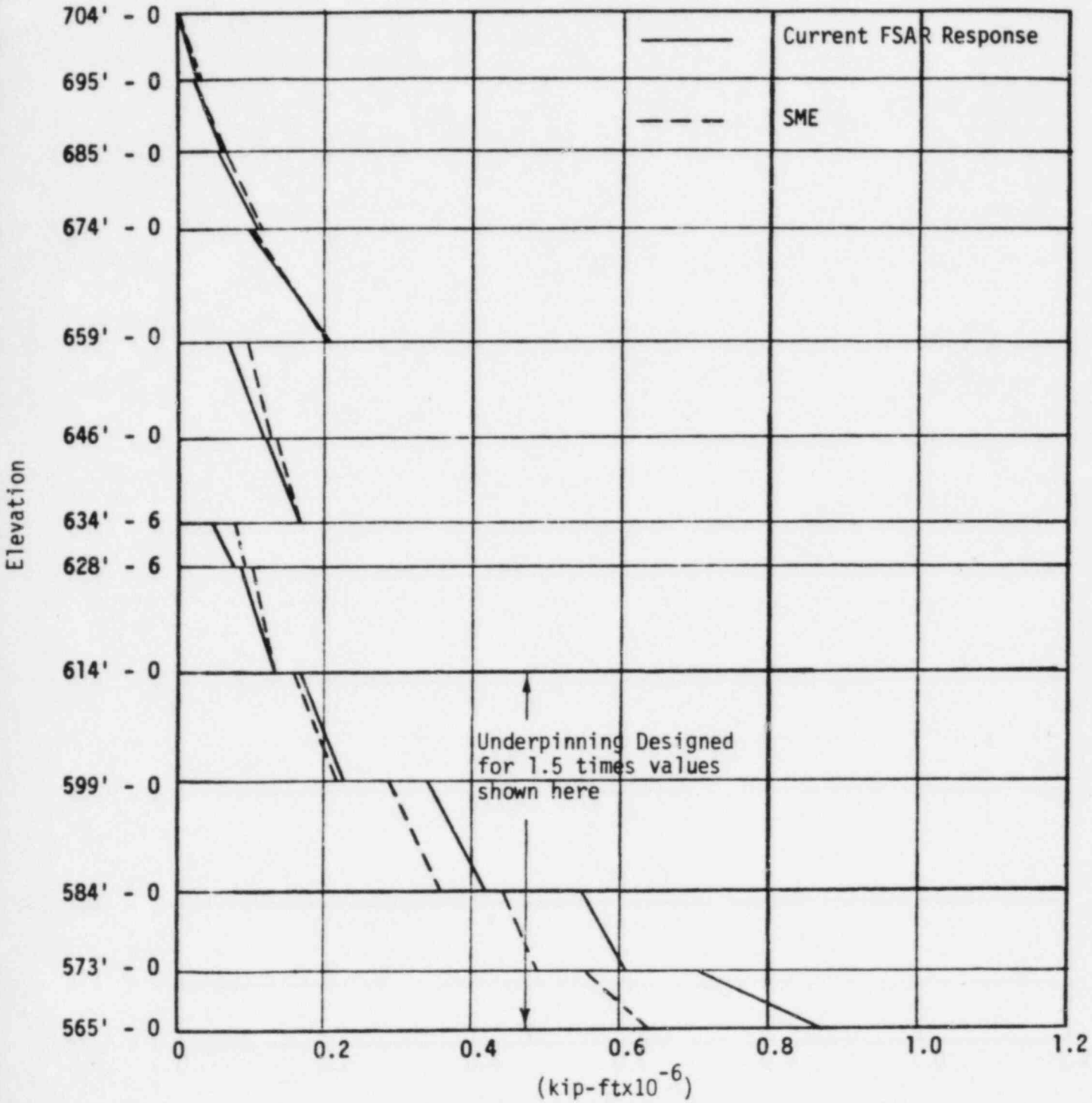

FIGURE III-3-23. CONTROL TOWER MOMENT ABOUT E-W AXIS COMPARISON

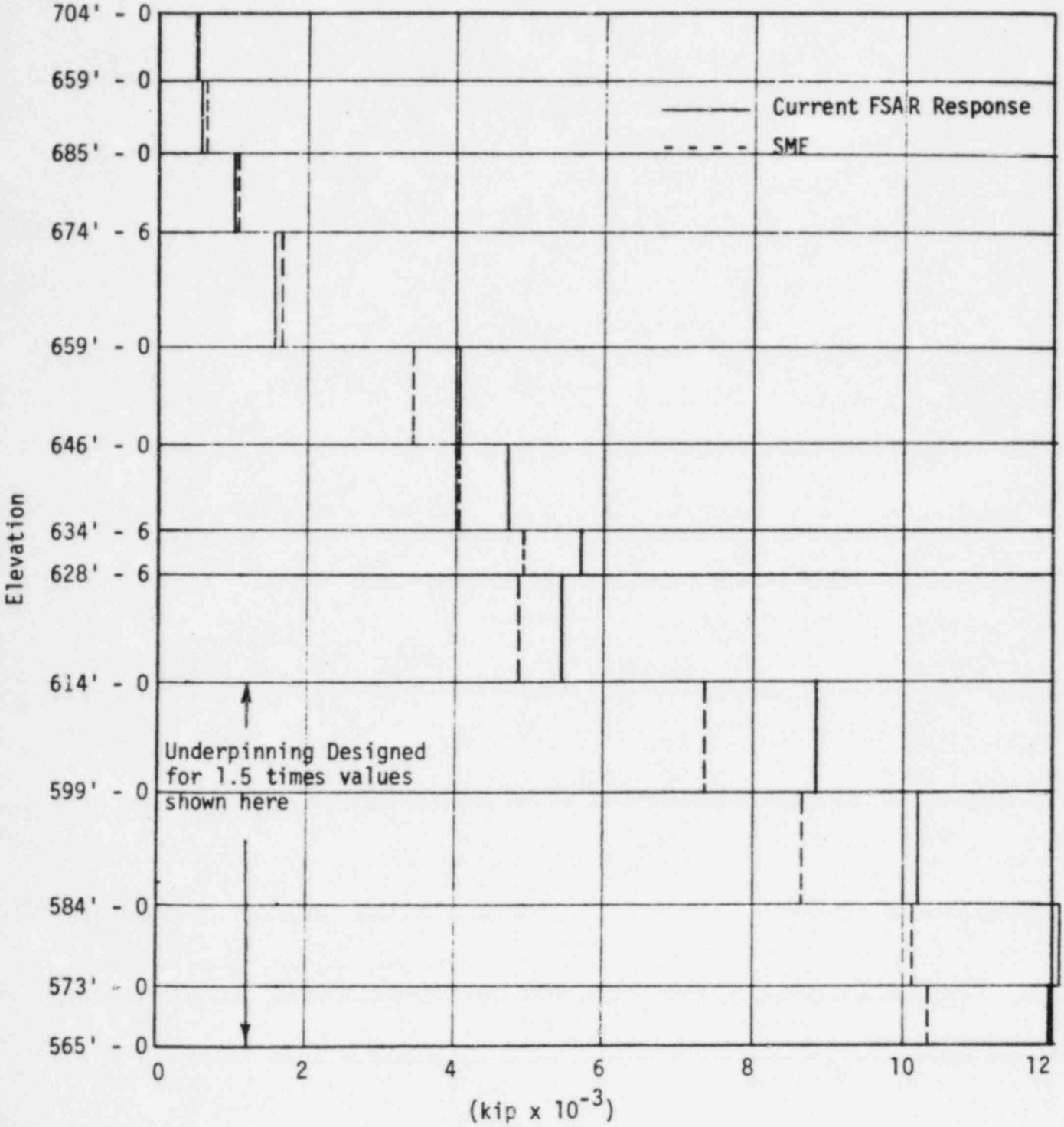

FIGURE III-3-24. CONTROL TOWER AXIAL FORCE COMPARISON

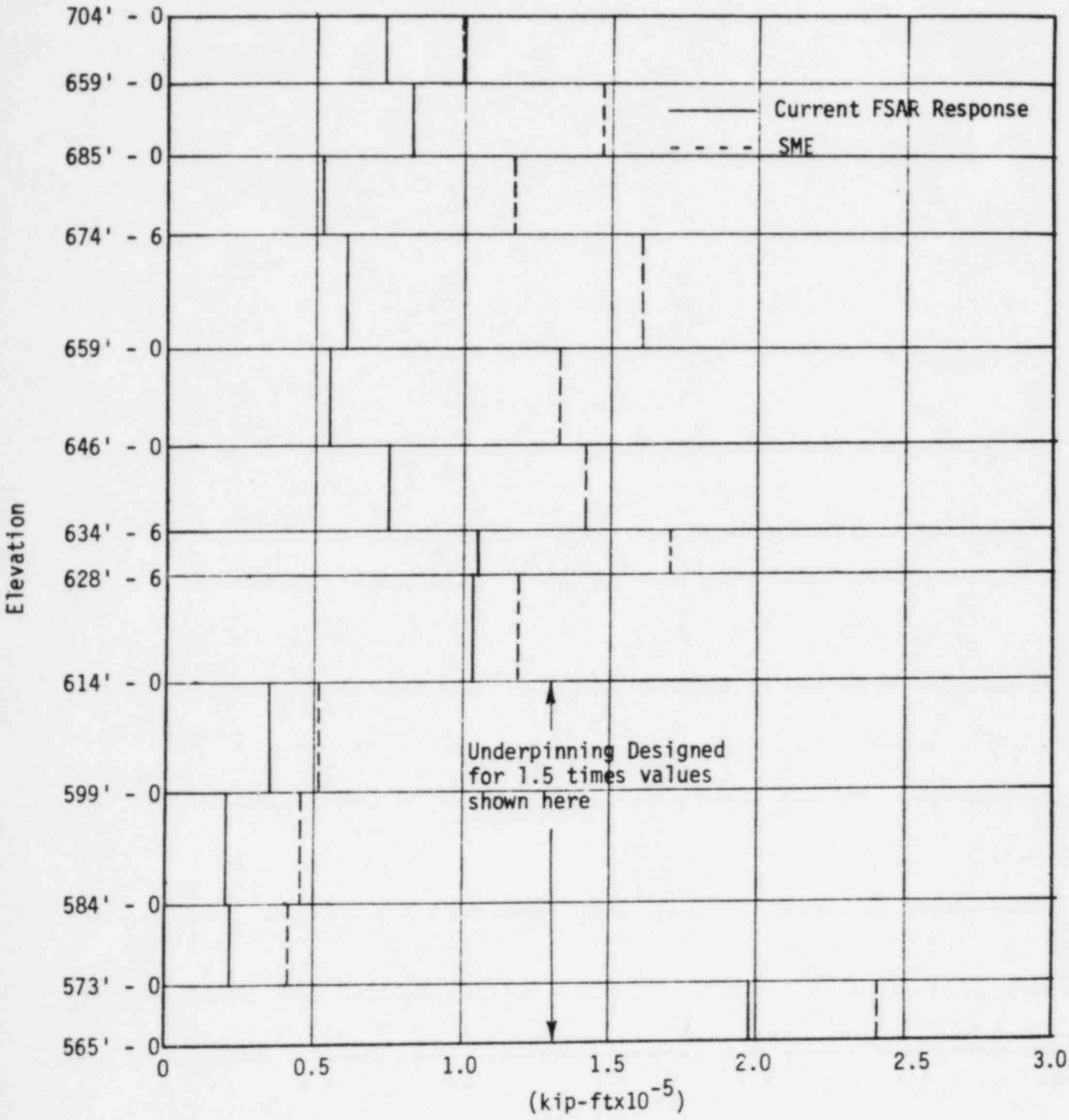

FIGURE III-3-25. CONTROL TOWER TORSION COMPARISON

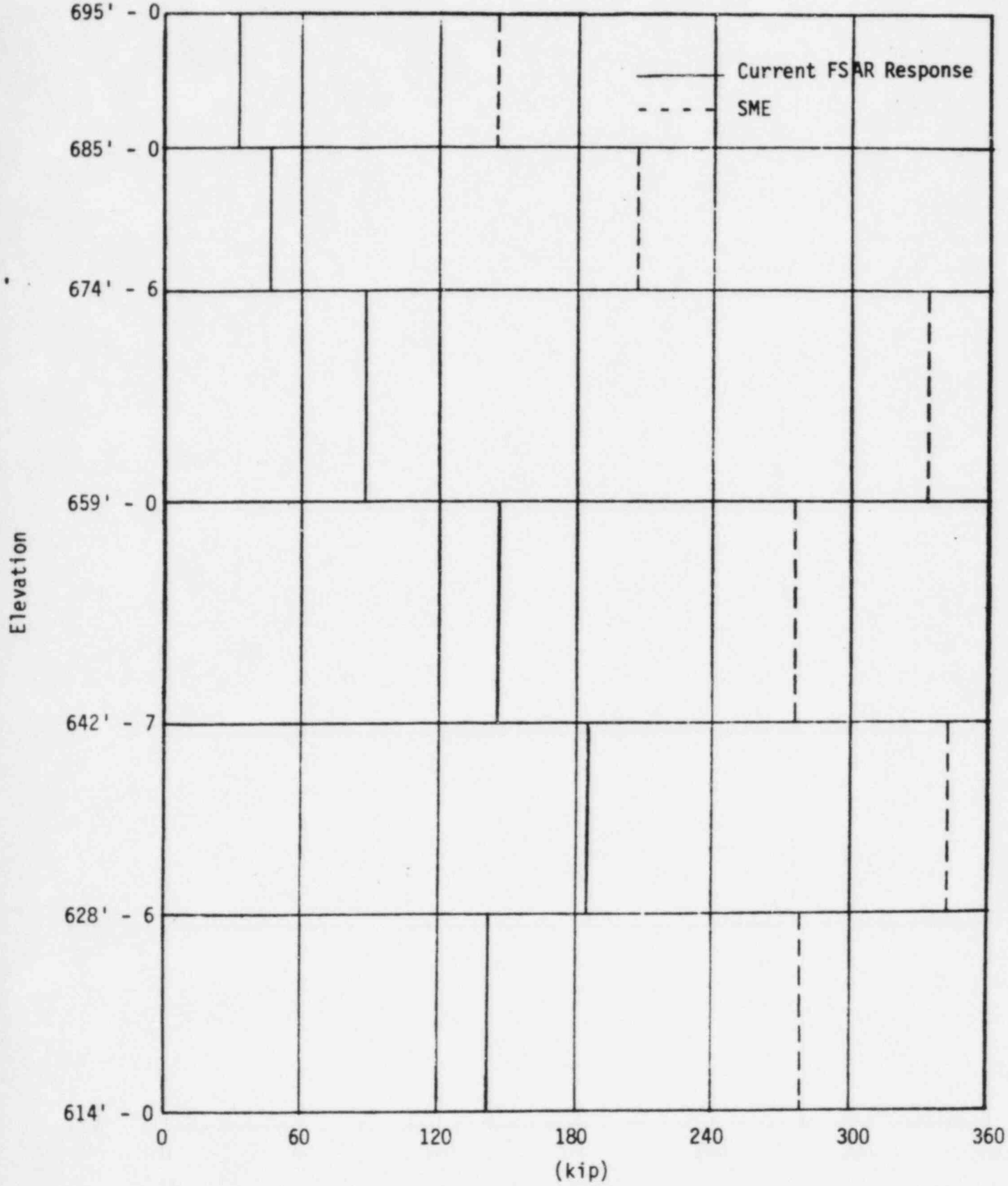

FIGURE III-3-26. PENETRATION WING EAST EXTERIOR WALL N-S SHEAR COMPARISON

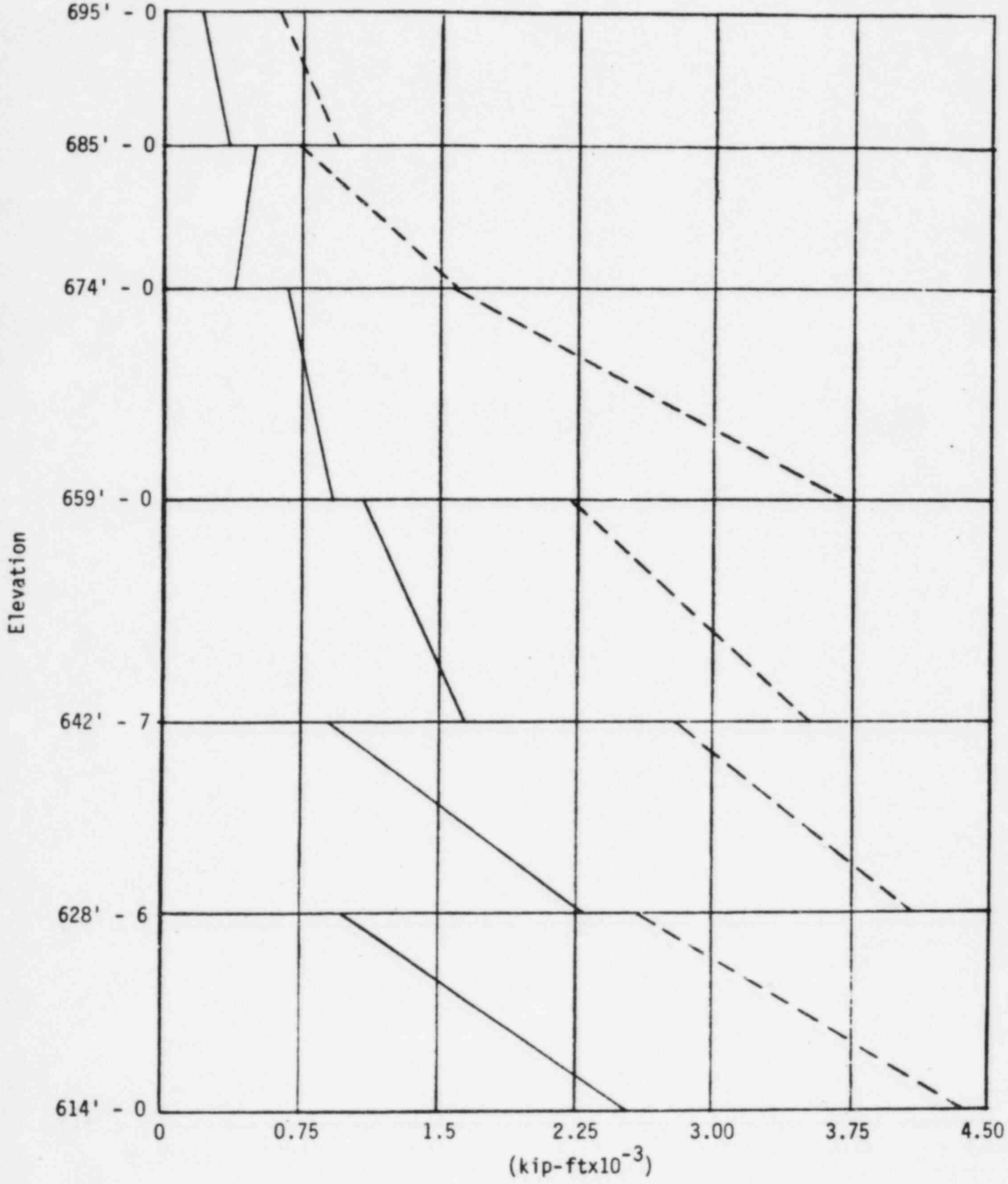

Figure III-3-27. PENETRATION WING EAST EXTERIOR WALL MOMENT ABOUT E-W AXIS COMPARISON

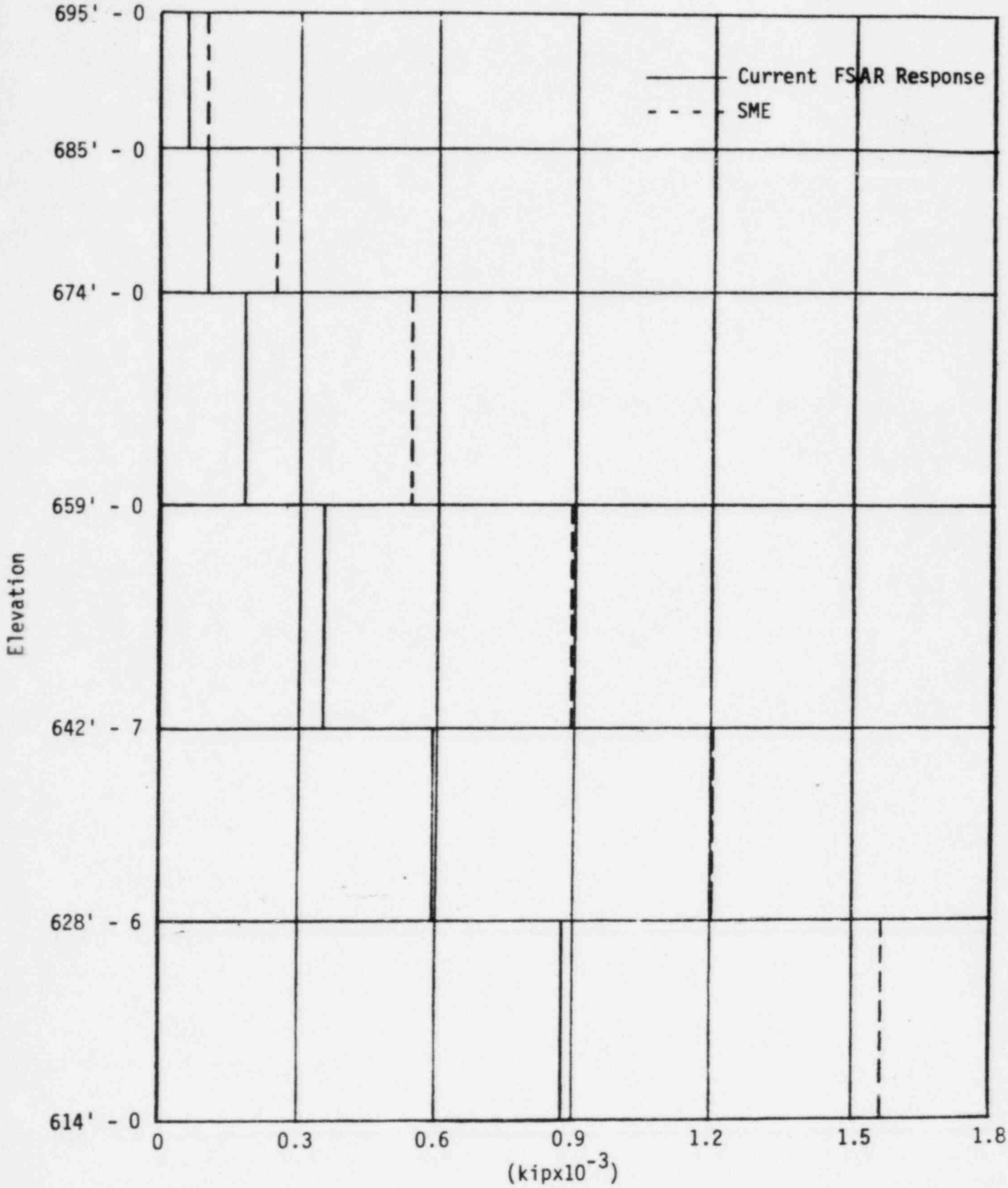

FIGURE III-3-28. PENETRATION WING EAST EXTERIOR WALL AXIAL FORCE COMPARISON

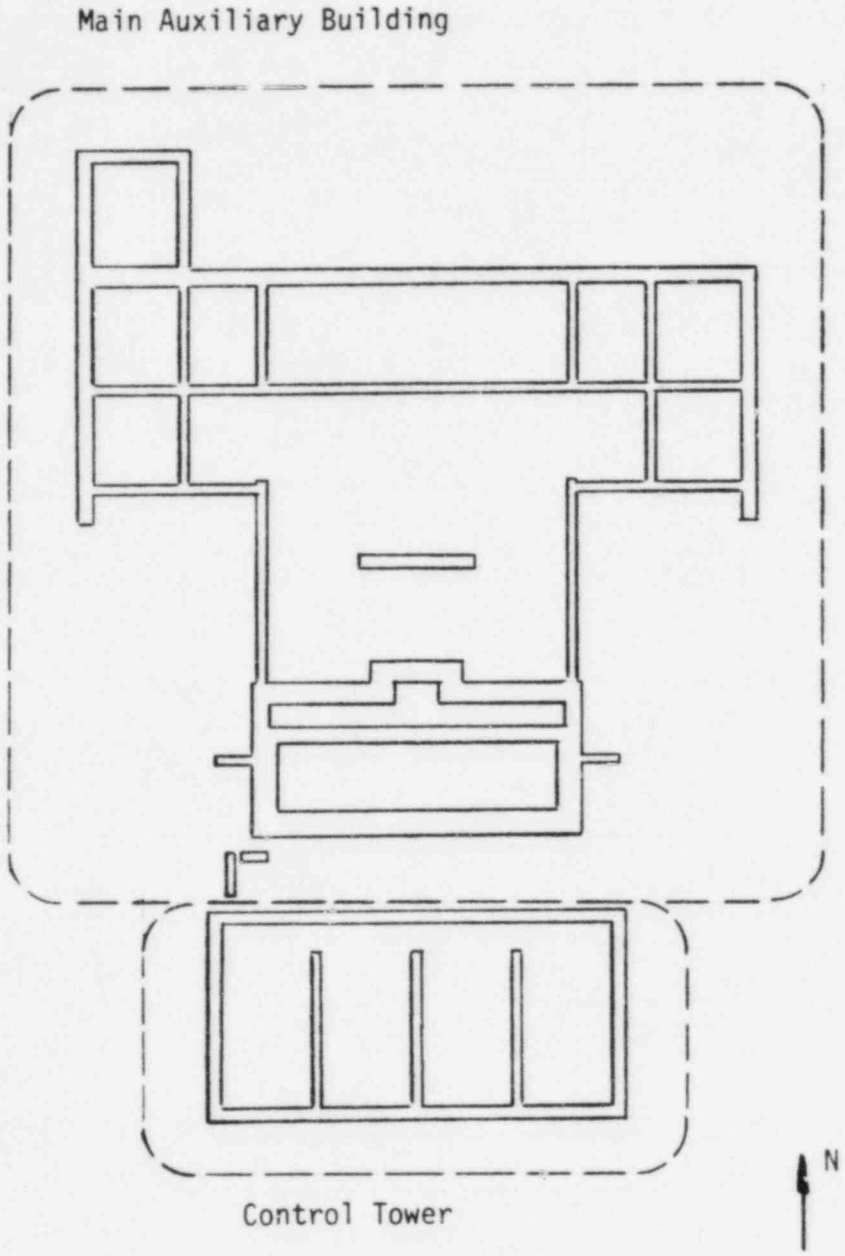

FIGURE III-3-29. IDEALIZED LAYOUT OF WALLS FROM ELEVATION 614'-0" TO ELEVATION 634'-6" INCLUDED IN LOAD DISTRIBUTIONS

4. CODE MARGINS

For the structure code margins evaluation, a number of structural elements were selected from locations throughout the auxiliary building to compare their capacities as prescribed by the acceptance criteria against their loads due to the SME combined with normal operating loads. The selected shear walls, floor diaphragms, and structural steel members are listed in Tables III-4-1 to III-4-9. Each wall and diaphragm is assigned an identification number in Tables III-4-1 to III-4-4. The location of the selected elements is then referenced by their identification numbers in Figures III-4-1 to III-4-8.

The structural elements selected for evaluation in this study are those expected to be more highly stressed due to seismic loads relative to other elements within the auxiliary building. General criteria used to identify structural elements to be included in the SMR structures capacities evaluation involved several considerations. The layout of the shear walls was reviewed to determine the distribution of walls throughout the structure and the availability of resistance to lateral load. The load distributions were compared to identify walls required to resist a significant portion of the seismic load at each story. The physical conditions of the walls were reviewed to provide an approximate assessment of the relative wall capacities. This included considerations such as wall thickness, reinforcement patterns, and the presence of openings which would tend to reduce the amount of material available for load resistance. An attempt was made to select a representative sample of walls through the height of the main auxiliary building and the control tower. Particular attention was given to the major walls since their relative rigidities are typically greater than smaller walls and consequently receive greater loads, and also to walls where the SME loads exceed the design loads. Also, walls located towards the perimeter of the structure receive greater seismic loads due to torsion as compared to walls in the interior.

Diaphragm elements were selected for detailed evaluation on a basis similar to that for the shear walls. Review of the shear wall layout through the structure also provided insight into the manner in which the floor slabs function as diaphragms in providing load paths to the walls. From the load distributions, locations of possible significant diaphragm stress were identified. The physical conditions of the slabs, including slab thickness, reinforcement pattern, and the presence of openings were reviewed to provide an approximate assessment of the relative diaphragm capacities. Attention was also given to reinforcement detailing that may have a significant impact on the ability of the diaphragms to transmit the required forces.

For the structural steel framing, different lateral load-resisting systems were supplied in the N-S and E-W directions. In the N-S direction, vertical diagonal bracing transmits seismic forces down to the floor at Elevation 659'-0". In the E-W direction, rigid frames resist both dead, live, and seismic loads. Representative elements from both of these systems were selected in a manner similar to that employed for the reinforced concrete elements.

Capacities for the structural elements selected for review were developed in accordance with the structural acceptance criteria described in Section 7.2 of Volume I. For the reinforced concrete portions of the auxiliary building, the ultimate strength design provisions of ACI 349-80, "Code Requirements for Nuclear Safety Related Concrete Structures" (Reference 17), were followed. Stresses in the structural steel framing were typically limited to 1.6 times the allowable stresses specified in Part 1 of the AISC "Specification for the Design, Fabrication, and Erection of Structural Steel for Buildings" (Reference 18). Shear stresses on steel members were limited to 0.55 times the minimum specified material yield stress in accordance with Section 2.5 of the AISC specifications. The ultimate strengths and allowable stresses were conservatively based on minimum specified crushing strengths or material yield stresses. The concrete used in the construction of the auxiliary building was typically specified to have a minimum compressive strength of 5000 psi for the base mat and walls and 4000 psi for the elevated floor slabs and interior

walls. Deviations from these typical values were noted on the structural drawings. Reinforcing steel used was required to conform to ASTM Designation A615, Grade 60 and has a specified minimum yield stress of 60,000 psi. Structural steel was typically required to conform to ASTM A36. Structural steel used in fabrication of the rigid frames was required to conform to ASTM A441.

4.1 SHEAR WALL CAPACITY OF EXISTING STRUCTURE

The in-plane shear strength provisions for concrete walls are contained in Section 11.10 of ACI 349-80. The total ultimate strength capacity is composed of separate contributions from the concrete and the steel reinforcement. ACI 349-80 provides alternative formulations with different levels of detail required for determining the concrete in-plane shear strength. Section 11.10.5 specifies the concrete shear strength as the value corresponding to an average shear stress of $2\sqrt{f'_c}$ (psi) acting on the effective area for walls in compression.

V_c = Nominal concrete shear strength, lb
$2\sqrt{f'_c}\, hd$ for walls in compression (4-1)

f'_c = Concrete compressive strength, psi

h = Wall thickness, in

d = Effective wall depth, in

This strength is subjected to a reduction if the wall is loaded in tension. This definition of the concrete shear strength was typically used to determine the wall capacities. As an alternative, Section 11.10.6 of ACI 349-80 permits the use of the lesser of the concrete in-plane shear strengths defined by the following two equations:

$$V_c = 3.3\sqrt{f'_c}\, hd + \frac{N_u d}{4L} \qquad (4\text{-}2)$$

or

$$V_c = \left[0.6\sqrt{f'_c} + \frac{L\left(1.25\sqrt{f'_c} + 0.2\,\frac{N_u}{Lh}\right)}{\frac{M_u}{V_u} - \frac{L}{2}} \right] hd \qquad (4\text{-}3)$$

L = Wall length, in

V_u = Shear force acting on the section, lb

N_u = Axial load occurring simultaneously with the shear force V_u, lb

M_u = Moment acting on the section, in-lb

As noted in Reference 19, Equation 4-2 reflects the concrete shear strength when web-shear cracking occurs as opposed to flexure-shear cracking which is represented by Equation 4-3. Walls whose concrete shear strengths were determined using Section 11.10.6 of ACI 349-80 are identified in Table III-4-1. For these walls, Equation 4-2 was generally found to be controlling. This is typically expected for low-rise shear walls such as those of the auxiliary building since shear rather than flexure is more significant. The wall in-plane shear strength contributed by the steel reinforcement was determined following the provisions of Section 11.10.9 of ACI 349-80. The steel shear strength was based on the horizontal reinforcement provided in each wall. The effective wall depth, d, was taken as 0.8 times the wall length as permitted by Section 11.10.4 of ACI 349-80. The wall ultimate shear strength was taken as the sum of the concrete and reinforcing steel shear strengths reduced by a strength reduction factor of 0.85. Some of the walls must also transmit out-of-plane shears due to lateral forces. Because the in-plane concrete shear strength was determined in accordance with Sections 11.10.2 to 11.10.8 of ACI 349-80, Section 11.10.1 eliminates the need to consider interaction between in-plane and out-of-plane shear. For walls separated into a series of piers by significant openings such as doorways, shear capacities were developed for the individual piers. The total seismic

shear acting on the wall was distributed to the piers in proportion to their relative rigidities using equations presented in Reference 15. A similar treatment was made for total shears due to the loads at normal operating conditions when the openings were not represented in Bechtel's static finite element model.

Shear wall resistance to overturning moment is provided by the internal couple consisting of the vertical wall reinforcement stressed in tension and the concrete stressed vertically in compression. An efficient means of developing overturning resistance is by concentrating the necessary vertical reinforcement at the ends of the wall so that the moment arm will be a maximum. As an example, this type of reinforcement was provided in the N-S exterior walls of the EPA. In general, however, vertical reinforcement of the auxiliary building walls was uniformly distributed along the lengths of the walls.

As noted in Reference 19, experimental results indicate that the flexural strengths of rectangular shear walls with height-to-length ratios equal to or greater than 1.0 and containing uniformly distributed vertical reinforcement are adequately predicted by the design provisions for reinforced concrete beams loaded axially and in bending. These provisions are contained in Section 10.2 of ACI 349-80. The flexural strength calculated using these provisions can be expressed by the following equation presented in Reference 19.

$$M_u = A_s f_y L \left[\left(1 + \frac{N_u}{A_s f_y} \right) \left(\frac{1}{2} - \frac{\beta_1 c}{2L} \right) \right. \qquad (4\text{-}1)$$

$$\left. - \frac{c^2}{L^2} \left(1 + \frac{\beta^2}{3} - \beta_1 \right) \right]$$

where $$\frac{c}{L} = \frac{q + \alpha}{2q + 0.85\beta_1}$$

$$q = \frac{A_s f_y}{Lhf'_c}$$

$$\alpha = \frac{N_u}{Lhf'_c} \text{ and } \beta = \frac{f_y}{87{,}000}$$

M_u = Design resisting moment a section, in. lb.

A_s = Total area of vertical reinforcement at section, sq. in.

f_y = Specified yield strength of vertical reinforcement, psi

L = Horizontal length of shear wall, in.

c = Distance from extreme compression fiber to neutral axis, in.

d = Distance from extreme compression fiber to resultant of tension force, in.

h = Thickness of shear wall, in.

N_u = Design axial load, positive if compression, lb.

f'_c = Specified compressive strength of concrete, psi

β_1 = 0.85 for strength f'_c up to 4000 psi and reduced continuously at a rate of 0.05 for each 1000 psi of strength in excess of 4000 psi

Reference 19 presented the following approximation to this equation:

$$M'_u = 0.5A_s f_y L \left(1 + \frac{N_u}{A_s f_y}\right)\left(1 - \frac{\beta_1 c}{L}\right) \qquad (4\text{-}5)$$

Upon inspection of Equation 4-5, it is apparent that this approximation is equivalent to obtaining the flexural strength of an underreinforced beam with the uniformly distributed reinforcement lumped at midlength of the wall.

Based on the findings of Reference 19, the design provisions in Section 10.2 of ACI 349-80 were used to determine the resistances to overturning moment for the walls of the auxiliary building having uniformly distributed vertical reinforcement. In accordance with Section 9.3.2 of ACI 349-80, the calculated overturning moment resistances, M_u', were modified by appropriate strength reduction factor ϕ.

$$M_u = \phi M_u'$$

where ϕ = strength reduction factor per Section 9.3.2 of ACI 349-80.

Most of the major walls of the auxiliary building are intersected at their ends by other walls oriented transversely. Due to deformational compatibility at the intersections, these transverse walls will behave similar to flanges of a wide-flanged steel beam. However, only the resistance to overturning moment provided by the web of the wall loaded in-plane was accounted for. This is conservative since the additional overturning resistance provided by the flanges may be significant due to their greater internal moment arms.

Some of the walls evaluated in this study contain small openings for doorways, pipe penetrations, etc. Typical details call for additional vertical reinforcement to be provided at the faces of the openings to make up for the reinforcement interrupted by these openings. The flexural strength of a wall containing small openings was calculated for the wall as a single element rather than as a series of individual piers since the openings are generally small compared to the wall itself and are usually isolated as opposed to occurring in a regular pattern through the wall height. Failure is expected to occur due to gross, overall behavior. The additional reinforcement around the openings is normally sufficient to resist any stress concentrations.

Some of the walls of the auxiliary building are subjected to out-of-plane forces under normal operating conditions. An example of this case is an exterior wall below grade that is subjected to transverse

loads from lateral earth pressures. Out-of-plane moments due to normal operating conditions were available from the results of Bechtel's static analyses performed on their finite element model. The presence of out-of-plane moments about a horizontal axis through the wall is expected to influence the capacity of the wall to resist the in-plane overturning moment due to horizontal seismic response of the building. The procedure used to account for the effects of out-of-plane moments on the wall overturning moment capacities is described in Appendix C.

Capacities for the selected shear walls determined in accordance with ACI 349-80 are presented in Tables III-4-1 and III-4-2. The possibility of failure due to in-plane shear or overturning was considered for these walls. Shear capacities for the walls whose code margins are governed by shear are listed in Table III-4-1 while overturning capacities for the walls whose code margins are governed by overturning are listed in Table III-4-2. Applied in-plane shear and overturning loads due to seismic and normal operating condition loads are also listed in these tables. These loads were calculated as described in Section 3.3.3. Applied loads due to dead, live, jacking preload, and settlement load cases were combined to create the most adverse loading condition on the walls. That is, if the force due to the live or settlement load cases tended to reduce the effect of the force due to seismic, it was not included for conservatism.

The code margins for the selected shear walls were developed from the calculated loads and capacities and are listed in Tables III-4-1 and III-4-2. The code margin, CM, is defined as the ratio of the code capacity to the applied load. The applied load is specified by the load combination given in Section 7.1 of Volume I and is taken as the sum of the applied loads due to the seismic and normal operating condition.

CM = Code Margin = $\frac{C}{P}$

C = Element code capacity

P = Applied load due to the combined normal operating condition and seismic load cases = $P_{NOL} + P_{SME}$

P_{NOL} = Applied load due to normal operating condition loads

P_{SME} = Applied load due to the SME

In general, the walls are subjected to axial loads occurring simultaneously with the shears and overturning moments. The magnitudes of the axial loads can have an influence on the shear and overturning capacities. Code margins were determined based on the capacities and loads under consideration (shear or overturning) with the effect of the axial load included in the capacities.

For each of the selected shear walls, a factor F_{SME} is also listed in Tables III-4-1 and III-4-2. This term is the factor by which the SME ground motion would have to be multiplied to cause loads equal to the code capacities:

$$F_{SME} = \frac{C - P_{NOL}}{P_{SME}}$$

When the effect of axial load was included in the capacity, this equation was modified to account for the influence of the axial load due to seismic response. F_{SME} factors less than the code margins occur when the seismic axial load tends to reduce the capacity against shear or overturning moment. As an example, derivation of the F_{SME} factor for the wall on Line A from Elevation 568'-0" to Elevation 584'-0" (wall identification number 1) is as follows:

M_{SME} = Overturning moment due to the SME factored by F_{SME}
= $235{,}000F_{SME}$ k-ft

M_{NOL} = Overturning moment at normal operating conditions
= 2650 k-ft

$M_{NET} = M_{SME} + M_{NOL}$
= $235{,}000F_{SME} + 2650$

M_U = Overturning moment capacity per Equation 4-5 including the effects of the axial load due to the SME factored by F_{SME}

= $-361F^2_{SME} - 39{,}700F_{SME} + 365{,}000$ k-ft

$M_U = M_{NET}$

$-361F^2_{SME} - 39{,}700F_{SME} + 365{,}000 = 235{,}000F_{SME} + 2650$

$-361F^2_{SME} - 275{,}000F_{SME} + 362{,}000 = 0$

$F_{SME} = 1.3$

4.2 DIAPHRAGM CAPACITY OF EXISTING STRUCTURE

Capacities of diaphragms for in-plane shear and moment are not directly addressed by ACI 349-80. However, it is common to design concrete diaphragms by the same provisions as those used for shear walls because of similarities in geometry and loading. Section 11.8 of Reference 22 specifies the same limiting shear stress for shear walls and diaphragms. Consequently, in-plane shear and flexural capacities of the diaphragms selected for evaluation were calculated in the same manner as the corresponding capacities of the shear walls. The slabs must also transmit out-of-plane shears due to vertical forces. Because the in-plane concrete shear strength was determined in accordance with Sections 11.10.2 to 11.10.8 of ACI 349-80, Section 11.10.1 eliminates the need to consider interaction between in-plane and out-of-plane shear.

The diaphragms of the main auxiliary building selected for evaluation correspond to locations where structural steel beams or girders are embedded in the slab parallel to the applied shear force. Where this condition occurs, typical details call for the bottom layer slab reinforcement normal to the beam to be discontinued at the beam web with only the top layer being continuous across the beam. Some diaphragms have holes burned through the beam web to permit passage of alternate bottom slab reinforement bars. These slabs were not included in the SMR since they are expected to have higher capacities than the

typical case where no bottom reinforcing steel is continuous through the web. For the typical case, the concrete depth effective in transmitting shear is reduced to the thickness over the top flange of the beam. An example of this condition is the slab adjacent to the wall on Line 8.7 of Elevation 614'-0". The top of the concrete slab, 2'-0" and 1'-9" thick, is located at Elevation 616'-6" while the top of the W27x177 and W24x100 girders is located at Elevation 615'-6".

At these local diaphragm conditions, the shear capacity was determined for the slab over the top beam flange using the code provisions for shear walls previously described. Only the concrete thickness above the top beam flange and the top layer of slab reinforcement were considered effective in resisting diaphragm shear force. Additional resistance provided by bond between the concrete and the beam web was conservatively neglected.

Embedded beams do not span along the entire length of the diaphragm adjacent to the wall on Line A at Elevation 614'-0". The shear strength calculated for this diaphragm is a weighted average of the portions of slab with and without the embedded beams. This shear strength is expected to be conservative since it is based in part on local cracking of the concrete and yielding of the reinforcement over the embedded beam. However, the presence of slab without embedded beams is expected to make gross failure of the diaphragm, which is associated with greater strength, less likely. Also, loads and capacities were determined for the slab portions separated by the opening between Lines 6.2 and 6.9. This leads to conservative results since the embedded beams are actually outside of the portion for which the loads were defined. This conservatism was retained since the loads must pass across the embedded beam flanges.

Results presented for the diaphragm adjacent to the wall on Line A at Elevation 646'-0" are conservative. Large openings in this region reduce the diaphragm area available to transmit load to the wall. The applied load was based on the load distributions developed using the rigid diaphragm approximation. However, the slab openings will increase the local flexibility of the diaphragm in this region. Inclusion of this local flexibility will reduce the shear acting on this part of the diaphragm.

The diaphragms in the control tower adjacent to Line 7.8 at Elevations 659'-0" and 674'-6" were evaluated for their ability to transfer in-plane moment between the control tower and the EPA. The slabs of the EPA have substantial reinforcement concentrated at their north and south boundaries. However, some of this reinforcement is hooked into the wall on Line 7.8 with the remainder continuous into the control tower slab. Resistance to the in-plane moment at the control tower - EPA interface is provided by this continuous chord reinforcement, distributed E-W slab reinforcement, and the wall on Line 7.8 which will be bent out-of-plane. Due to the greater flexibility of the wall compared to that of the slab, any resistance provided by the wall was conservatively neglected. Seismic forces acting at this location were taken directly from the forces in the horizontal elements of the dynamic model representing the connectivity between the control tower and the east EPA. SRSS seismic axial load and in-plane moments were applied as discussed in Section 3.3.3. The in-plane moment capacities of the slabs at these interfaces were determined in the same manner as the overturning moment capacities of the shear walls. This diaphragm section is not symmetrically reinforced for in-plane loading so the in-plane moment capacity for the loading that produces compression on the south edge of the section is different from the capacity for the loading that produces compression on the north edge of the section. The lower code margin occurs when the south edge is in compression. However, the in-plane moment due to normal operating conditions causes compression on the north edge and will increase the seismic moment that the section can withstand. The negative value for the in-plane moment at normal operating conditions is retained as shown in Table III-4-4.

The applied in-plane moment and moment capacity for the diaphragm section along Line 7.8 at Elevation 704'-0" were calculated for the portion of the roof slab above the control tower between Lines H and K_c. Any interaction between this slab and the portion of slab north of Line H was neglected. This is conservative since the slab north of Line H will help to resist the applied moment due to continuity at the interface between these slabs. Also, additional resistance provided by the walls of the control tower on Lines H and K_c was conservatively neglected. In reality, these walls will be effective as flanges and their inclusion would significantly increase the in-plane diaphragm moment capacity and code margin.

Loads due to the SME and normal operating conditions, code capacities, code margins, CM, and F_{SME} factors are listed in Table III-4-3 for diaphragms whose capacities are controlled by shear and in Table III-4-4 for diaphragms whose capacities are controlled by in-plane moment. The code margins and F_{SME} factors were determined in the same manner as for the shear walls.

4.3 EFFECTS OF REINFORCEMENT BAR CUTTING ON EXISTING STRUCTURE

The shear wall and diaphragm capacities were based on information available from the structural drawings for the selected elements. The presence of small and large openings indicated on the structural drawings was accounted for in the development of these capacities. Available nonconformance reports noting deviations from the construction specifications were reviewed to verify that there were no gross deviations that would significantly influence the capacity of the selected structural elements. The calculated wall capacities do not include the effect of any minor deviations. The capacities reported in Tables III-4-1 to III-4-4 also do not address the reduction in strength due to reinforcement cutting permitted by Reference 21 since the exact location and number of reinforcement bars cut within this allowance was unavailable. Per Section 2.1 of Appendix E of Reference 21, one bar could be cut each way, each face, with the radial distance to the next cut bar on the same face, in the same direction, no less than five feet. Per Section 2.2 of Appendix E of

Reference 21, two bars could be cut each way, each face, with the radial distance to the next cut bar on the same face, in the same direction, no less than 10 feet. Additional limitations are noted in Section 7.2 of Volume I.

To determine the effect of the reinforcement cutting allowance and non-conformances on the shear capacity of the walls, the wall with the lowest code margin against shear, which is on Line G from Elevation 568'-0" to Elevation 584'-0", was recalculated. The effect of reinforcement cutting is expected to be dependent on the crack pattern that leads to failure of the wall. If a crack crosses a horizontal bar where it has been cut or where it does not have sufficient development length from the cut to develop its yield strength, then the effectiveness of that bar may be significantly reduced. As an approximation, a crack was assumed to form at a 45 degree angle from horizontal through the story height of the wall noted above. This angle is approximately consistent with the crack angle assumed in the derivation of the shear strength provided by web reinforcement of concrete beams. For the worst case of horizontal bars cut at both faces every five feet along the assumed crack, the reinforcement area effective in resisting shear was modified and the total wall shear strength recalculated. No non-conformances were reported for the wall at this story. Using the revised shear strength, a code margin of 1.2 was determined for this wall compared to 1.4 as originally calculated.

To determine the effect of the reinforcement cutting allowance and the non-conformances on the overturning moment capacity of the walls, the wall with the lowest code margin against overturning, which is the wall on Line H at Elevation 568'-0", was treated similarly. It was assumed that vertical bars at each face were cut every five feet along a horizontal plane. No non-conformances were reported for the wall at this story. Using the effective reinforcement area, the overturning moment was recalculated. A code margin of 1.2 corresponds to this revised capacity compared to 1.3 as originally calculated.

The diaphragm section exhibiting the lowest code margin, the diaphragm along Line 7.8 at Elevation 659'-0", was evaluated to determine the effect of the reinforcement cutting allowance similar to the shear walls. Since this section is governed by in-plane moment, the approach developed to reevaluate the shear walls governed by overturning was used. Only the distributed slab reinforcement was considered to be subject to cutting since bundled reinforcement is specifically excluded from the cutting allowance. Using the in-plane moment capacity calculated in a manner similar to the shear walls, a code margin of 1.3 was found for this diaphragm. This value is the same as originally calculated.

The code margins against both shear and overturning moment for the walls and in-plane moment for the diaphragms were still found to be greater than unity when the reinforcement cutting allowance and non-conformances were considered for the selected examples. It can be concluded that the cutting allowance and the non-conformances do not adversely affect the results of this study for the walls and diaphragms of the auxiliary building.

4.4 UNDERPINNING WALL CAPACITIES

Evaluation of the underpinning walls was conducted on the basis of the preliminary design configuration transmitted as a part of Reference 23 with additional data supplied by References 24 and 25. The underpinning wall on Column Line K_c of the control tower and the wall beneath the east EPA were selected for study. The code margins of these walls were determined using the same methodology and criteria developed for the shear walls described in Section 4.1. Both walls were found to be governed by overturning moment. The overturning moment capacities were determined using the approach described in Section 4.1 which applies the basic flexural strength design principles of ACI 349-80. The influence of the axial load and out-of-plane moments on the overturning moment capacities were compared to the applied overturning moments due to the SME and loads occurring at normal operating conditions to arrive at code margins. Applied loads, code capacities, code margins, and F_{SME}

factors are listed in Table III-4-5. Loads and capacities for shear acting on the walls were determined using the approach described in Section 4.1. Resulting code margins against shear were found to be greater than those against overturning.

The connectors providing load transfer between the underpinning walls and the existing structure were also evaluated. The connectors to be used for the control tower underpinning are 1.375-inch diameter Williams hollow-core rockbolts. The strength of these rockbolts was based on information contained in Reference 26. The connectors to be used for the EPA underpinning are 2.75-inch diameter bars fabricated from A588 steel which has a minimum specified yield strength of 50 ksi.

Capacities of the underpinning connectors at the interfaces to the existing structure were determined using the strength provisions of ACI 349-80. Connector capacities were evaluated for the interfaces between the existing structure and the underpinning walls beneath Column Line K_c of the control tower and the east EPA. The connectors were found to be governed by shear. Their shear capacities were based on the shear-friction provisions contained in ACI 349-80. As noted in Section 12.2.1 of Reference 27, axial compression acting at a construction joint increases the shear friction capacity available. This additional capacity was accounted for in determining the shear capacities at the interfaces between the underpinning walls and the existing structure. The possibility of a tensile axial load due to seismic response reducing the axial compression occurring under normal operating conditions was included. Including the shear friction capacity of both the connectors and the axial compression, the shear capacities at the interfaces were calculated by the following equation:

$$V_u = (A_v \times f_y + N), \text{ lb} \qquad (4\text{-}6)$$

A_{vf} = Total connector area, in^2

f_y = Connector yield stress, psi

N = Axial load, positive in compression, lb

ϕ = Strength reduction factor

μ = 1.0 for concrete-to-concrete interfaces

For the Williams rockbolts at the control underpinning wall on Column Line K_c, the product of the connector area and the yield stress for a single rockbolt was taken to be the "maximum working load to elastic limit" specified in Reference 26. Applied shear loads, code capacities, code margins, and F_{SME} factors for the connectors evaluated are listed in Table III-4-6. The connectors for the underpinning wall beneath the East EPA were found to be subjected to significant out-of-plane seismic response. The shear due to the SME listed in Table III-4-6 reports the net effect due to both in-plane and out-of-plane shear. Code margins for the connectors subjected to overturning and out-of-plane moments were found to be greater than the code margins for shear.

4.5 STRUCTURAL STEEL CAPACITY OF EXISTING STRUCTURE

Resistance to E-W seismic response for the main structural steel framing above Elevation 659'-0" is provided by seven rigid frames at column lines AA, A, B, C, D, E, F, and G. These rigid frames are composed of columns on Lines 5.6 and 7.4 with a constant five-foot deep girder spanning between them at Elevation 704'-0". The columns and girders were fabricated from steel plate conforming to ASTM A441 specifications. The columns taper in depth from a maximum of five feet at the connection to the girder-column joint detail to a minimum of 20 inches at the base connection. The north-south direction vertical braced frames at column line 5.6 and 7.4 provide lateral support to these columns in its weak axis at the eaves and at Elevation 682'-0". The columns are anchored to the slab at Elevation 659'-0" by a heavy W14 rolled section embedded in the concrete. Two types of rigid frames, F-1 and F-2 as shown on the structural drawings, were employed. Rigid Frame F-2 was built-up from steel plate of greater thickness than that of Rigid Frame F-1.

The frame on Line B was selected as being representative of Rigid Frame F-1 and the frame on Line F was selected as being representative of Rigid Frame F-2. Stresses due to normal operating loads and the SME were calculated using elastic section properties. Acceptance criteria for structural steel members used in this evaluation typically consisted of the allowable stresses specified in Part 1 of the AISC Code (Reference 18) factored by 1.6 as permitted by the Standard Review Plan for steel structures subjected to normal operating and extreme environmental loads. For conservatism, the factored allowable stresses were taken to be no greater than the minimum specified material yield strength. Allowable shear stresses on structural steel members were specified to be 0.55 times the minimum material yield stress in accordance with Section 2.5 of the AISC specifications. Because the minimum specified yield strength for members fabricated from A441 steel was not called out on the structural drawings available, the minimum value based on the availability listed in Table 1 of Appendix A of the AISC Manual of Steel Construction (Reference 18) for the given plate thickness was conservatively used.

Since the girders and columns of the rigid frames were generally subjected to combined axial load and bending moment, stresses were checked by the interaction equations for combined axial compression and bending in Section 1-6 of the AISC Specification. The stresses and their corresponding factored allowable values are listed in Table III-4-7. The code margin, CM, for each member is the ratio of the maximum value permitted for the interaction equation (which is unity) to the sum of the terms of the interaction equation. Code margins and F_{SME} factors for the members of the rigid frames included in this evaluation are listed in Table III-4-8.

The column axial compressive forces due to normal operating condition are 126 kips and 1055 kips for the selected representative F-1 and F-2 frames. The corresponding SME induced column axial tensile forces are 49 kips and 343 kips. The lower bound code margin for column uplift of F-1 and F-2 frames are 2.6 and 3.1, respectively. Additional

uplift resistance available at the column base connection was conservatively neglected. The F_{SME} factors are the same as code margins for column uplift.

The girders of F-1 frames are field spliced to the column-haunch section by using 1-inch diameter A490 high strength bolts. Analysis of this splice connection of a typical rigid frame at Line B revealed that shear capacity of the A490 bolts governs the flange as well as the web splices. The web splice has a code margin of 5.8 and a F_{SME} of 14. The 34-A490 bolts at the flange have a factored allowable shear of 941 kips. The tensile/compressive forces in the flange due to moment and axial force in the girder are 183 kips for operating condition and 196 kips for SME. Thus, the calculated code margin is 2.5 and F_{SME} is 3.9. Code margins and F_{SME} factors for the high-strength bolts were based on allowable stresses contained in the AISC code increased by a factor of 1.6. These code margins are of sufficient magnitude such that the possibility of a moderate reduction in the bolt material yield stress due to heat treatment should not lead to a code margin less than unity.

Resistance to N-S seismic response of the structural steel framing consists of vertical braced frames on Lines 5.6 and 7.4. These braced frames are composed of cross-braced 8x8x1 double angles interconnecting the columns of the rigid frames and the horizontal struts. The diagonal bracing was typically composed of A36 steel which has a minimum specified yield strength of 36 ksi. As with the rigid frames, stresses due to normal operating loads and the SME were determined elastically and compared to AISC allowables factored by 1.6. The braces were checked in both tension and compression. Although the SME causes forces in the braces that can be either tensile or compressive, different members were found to be controlling in tension and compression because of different forces occurring in the members due to dead, live, jacking preload, and settlement loads. For both tension and compression, the critical braces are located between Lines C and D and between Elevations 656'-0" and 681'-10" in the vertical direction. Forces in these members

due to normal operating loads and the SME and their factored code allowables are listed in Table III-4-9 along with the corresponding code margins and F_{SME} factors. The diagonal braces were typically connected to their end details by eight 1.125-inch diameter A490 bolts. The loads and corresponding capacities for friction-type bolted connections are listed in Table III-4-9 for the braces evaluated. These allowable bolt stresses were based on allowable values specified in the AISC Code increased by a factor of 1.6. The calculated code margins and F_{SME} factors in Table III-4-9 are of sufficient magnitude such that the possibility of a moderate reduction in the bolt material yield stress due to heat treatment should not lead to values less than unity.

The steel floor framing at Elevation 704'-0" is tied to the reinforced concrete wall of the control tower at various locations along Line H. The steel embedment is fabricated of plates and consists of an anchor plate, embedded plates, and backing plate. The void space of the embedment was fully grouted. The embedment located at Lines 5.6 and H was evaluated for gross pullout, punching and shear. Resultant forces (axial and shear forces) acting on the embedment due to normal operating loads and the SME were determined and the major contributor was found to be the SME. The pullout and shear capacities of the embedment were evaluated in accordance with ACI 349-80 requirements. The code margin and F_{SME} for pullout of the embedment were found to be 6.1 and 6.4. The shear force is transferred to the reinforced concrete matrix by the embedment plate bearing against the concrete. The shear code margin, CM, and F_{SME} determined based on concrete bearing strength are 5.8 and 5.9, respectively.

4.6 SOIL BEARING AND STRUCTURE STABILITY CAPACITY

Factors of safety for soil bearing pressures for net dead, live, and seismic loads reported in the FSAR (Reference 1) range from 2.4 for the area under the control tower to 45 under the main auxiliary building based on an ultimate soil bearing capacity of 44,000 lb/ft^2. SME

shears, overturning moments, and axial loads for both the control tower and main auxiliary building are less than the corresponding FSAR loads at the building-foundation locations so that larger factors of safety would be expected for SME loads. The upper bound EPA soil stiffness used for the SMR results in higher loads at the EPA structure foundation interface than were reported in the FSAR. The SME loads are considered quite conservative in this region since the evaluation was done using response computed for the upper bound relative EPA stiffness. This assumption maximizes the loads which could conceivably be transmitted through the EPA foundations. Using the upper bound relative EPA stiffness dynamic SME loads together with the net dead and live load bearing stress of 4300 lb/ft^2 listed in the FSAR, a margin of 2.0 against ultimate soil bearing capacity failure is indicated.

Since the SME overall overturning moments and base shears are less than the corresponding FSAR loads, factors of safety for structure stability against sliding and overturning are greater than the corresponding FSAR values.

4.7 CAPACITY OF DIAPHRAGM INCLUDING DESIGN MODIFICATIONS

Modifications intended to increase the structural capacity of the slab diaphragm at Elevation 659'-0" between Column Lines G and H are currently being designed. In the existing configuration, the slab spans between the control tower wall on Column Line H and the south fuel pool wall on Column Line G with additional vertical support given by structural steel beams. Openings in the slab are provided for the stairs and an elevator shaft. Walls enclose the west staircase and the safety equipment room.

The slab and the walls at this portion of the structure transmit loads between the main auxiliary building and the control tower. The modifications are being designed to increase the structure capacity available to resist axial load in the N-S direction and in-plane moment. Conceptual drawings available indicate that these modifications consist of 1.5-inch thick by 3-foot wide steel plates added at the east and west edges of the slab between Column Lines G and H_K. The plates are fabricated from A588 steel. The conceptual drawings show the plates being anchored to the slab at the south corners of the fuel pool and the south exterior walls of the EPA.

Due to the presence of the fuel pool, N-S forces transmitted by this diaphragm must be collected by the slab and walls located on the east and west sides of the fuel pool. The slab openings for the stairs and elevator tend to concentrate these forces in the slab sections and interior walls at the east and west sides of this diaphragm. The resulting N-S stress distributions due to the N-S diaphragm axial load and in-plane moment are not easily predicted by simplified methods.

To provide a more accurate prediction of the stress distribution through this diaphragm, a finite element substructure model representing the slab and walls between Column Lines G and H was developed as part of the SMR. The slab was modeled by plane stress membrane elements. The walls were represented by truss or beam elements having stiffness properties approximating the additional resistances developed. The steel plate to be added as part of the design modifications were included as truss elements. Applied loadings due to the SME were based on overall loads from the response spectrum analyses acting on the element corresponding to this diaphragm in the auxiliary building dynamic model. These loads were applied statically at the substructure model boundary at Column Line G. Appropriate resisting boundary conditions were established at the model boundary along Column Line H.

Examination of the resulting stress distributions predicted by the substructure model indicated that the highest stresses occur in the slab between the east stair/elevator opening and the east slab edge. Tensile yielding of the slab rebar and the steel plate is expected to initiate at an E-W section through this portion of the slab. For conservatism, the code margin for this diaphragm was based upon the local capacity of the slab between the east stair opening and the east slab edge rather than the overall capacity of the entire slab width.

Results from the diaphragm substructure analyses were used to define the local N-S axial loads and in-plane moments acting on the critical E-W section through the portion of slab being evaluated. For the SME, the local axial load and in-plane moment were found to be 2090 k and 1550 k-ft, respectively. Using reported element stresses from Bechtel's static analyses, the local axial load and in-plane moment occurring at normal operating conditions were estimated to be 222 k and 117 k-ft. The net local axial load and in-plane moment used to determine the diaphragm code margin were, therefore, 2310 k and 1730 k-ft, respectively.

The critical slab section was evaluated for its ability to resist the net applied tensile axial load and in-plane moment acting concurrently. Because the axial load is the dominant term, the code margin was based on the available tensile axial load capacity corresponding to the known applied in-plane moment. The tensile axial load capacity contributed by the slab given the known applied in-plane moment was determined by applying the basic design principles of ACI 349-80. Use of the basic ACI 349-80 design principles for the determination of member capacity under combined axial load and flexure has previously been described in Section 4.1. Discussion in Section 5.2.10 of Reference 20 indicates that general procedures such as the ACI approach are applicable to determine strength in the presence of tensile axial load. The steel plate is fully yielded when the ultimate strength of the section is attained, so the capacity of the plate was included in the tensile axial

load capacity. The plate capacity was based on the yield strength associated with the 1.5-inch thick by 3-foot wide section. It was assumed that the connection details for the plate anchorages will have sufficient strength to develop this plate capacity and that the anchorages will be located so as to eliminate eccentricities leading to the introduction of bending moment into the plate. The code tensile axial load capacity corresponding to the known applied in-plane moment, including a strength reduction factor of 0.9, was found to be 2910. Comparison of this capacity to the applied net axial load of 2310 gives a code margin of 1.3 for this diaphragm including the design modification. The F_{SME} factor for this diaphragm was found to be 1.2. As previously noted, the diaphragm capacity was conservatively based on the local capacity of the slab portion evaluated and did not include the possibility of stress redistribution to other portions of the diaphragm not stressed to yield.

4.8 EFFECTS OF THERMAL GRADIENTS

Some of the exterior walls and diaphragms whose code margins were evaluated as part of the SMR are subjected to thermal gradients at normal operating conditions. These thermal gradients can introduce additional moments on the structural members due to restraint imposed by their supports against the thermal curvature. Design thermal gradients for the walls and slabs evaluated in the SMR were transmitted by Reference 29. These values were based on the most severe combination of interior operating temperature and the worst effective winter exterior temperature.

An approach for determining the additional moment and stresses acting on containment walls due to a thermal gradient is presented in Reference 30. A step-by-step procedure for incorporating thermal gradient effects into the evaluation of reinforced concrete cross-sections is developed in Reference 31. In this procedure, thermal gradient effects are considered in a manner similar to that described in Reference 30. The treatment of thermal gradients contained in References 30 and 31 was

included in a study described in Appendix C to determine the effect of out-of-plane moments on in-plane wall and diaphragm capacities. Based upon the results of this study, it was determined that the effect of out-of-plane moments and thermal gradients on the in-plane moment capacities could be adequately represented by the simplified method described in Appendix C.

Table III-4-1

Code Margins and F_{SME} Factors For Shear Walls Governed By Shear

Wall	Wall ID No.(1)	V_{SME} (k)	V_{NOL} (k)	V_{NET} (k)	V_u (k)	CM	F_{SME}
Line G, EL 568'-0 to EL 584'-0 (3)	2	3460	1240	4700	6560(2)	1.4	1.4
Line 5.6, EL 568'-0 to EL 584'-0	4	5930	2990	8920	16,900	1.9	2.3
Line A, EL 584'-0 to EL 599'-0	5	7420	2140	9560	29,400	3.1	3.7
Line G, EL 584'-0 to EL 599'-0(3)	6	1260	842	2100	3370(2)	1.6	1.6
Line 5.6, Between Lines C & G, EL 584'-0 to EL 599'-0	8	2340	1360	3700	6530	1.8	2.2
Line A, EL 599'-0 to EL 614'-0	10	6580	1740	8320	29,400	3.5	4.2
Line 5.6, Between Lines C & G, EL 599'-0 to EL 614'-0	11	2540	1650	4190	7500	1.8	2.3
Line A, EL 614'-0 to EL 634'-6	13	5460	66	5530	27,800	5.0	5.1
Line H, EL 614'-0 to EL 634'-6 (3)	14	1510	27	1540	5280	3.4	3.5
Line K_c, EL 614'-0 to EL 634'-6 (3)	15	250	369	619	1520	2.5	4.6
Line 8.7, EL 614'-0 to EL 634'-6	17	2860	297	3160	7950	2.5	2.7
Line H, EL 634'-6 to EL 646'-0 (3)	19	900	69	969	2310	2.4	2.5
Line H, EL 646'-0 to EL 659'-0 (3)	21	3100	181	3280	13,300	4.1	4.2
Line 7.8, EL 646'-0 to EL 659'-0 (3)	22	1220	411	1630	3340	2.0	2.4
Line H, EL 659'-0 to EL 674'-6 (3)	23	2880	130	3010	13,900	4.6	4.8
Line 7.8, EL 659'-0 to EL 674'-6 (3)	24	1320	164	1480	2780	1.9	2.0

Note: (1) - See Figures II-4-1 to II-4-8 for locations at walls corresponding to wall identification numbers.
(2) - Concrete shear strength determined in accordance with Section 11-10-6 of ACI 349-80
(3) - This wall consists of a series of piers. Load and capacity are reported for the controlling pier only.

V_{SME} = Shear due to SME
V_{NOL} = Shear due to normal operating loads
V_{NET} = $V_{SME} + V_{NOL}$
V_u = Code ultimate strength shear capacity
CM = Code margin

Table III-4-2

Code Margins and F_{SME} Factors For Shear Walls Governed By Overturning Moment

Wall	Wall ID No. (1)	M_{SME} (k-ft)	M_{NOL} (k-ft)	M_{NET} (k-ft)	M_u (k-ft)	CM	F_{SME}
Line A, EL 568' - 0" to EL 584' - 0"	1	235,000	2,650	238,000	328,000	1.4	1.3
Line H, EL 568' - 0" to EL 584' - 0"	3	392,000	1,630	394,000	506,000	1.3	1.3
Line H, EL 584' - 0" to EL 599' - 0"	7	275,000	11,400	286,000	730,000	2.6	2.6
Line 8.7, EL 584' - 0" to EL 599' - 0"	9	153,000	6,390	159,000	290,000	1.8	1.8
Line 8.7, EL 599' - 0" to EL 614' - 0"	12	112,000	6,390	118,000	292,000	2.5	2.4
Line 7.8, EL 614' - 0" to EL 634' - 6"	16	116,000	7,590	124,000	266,000	2.1	2.1
N-S Exterior Wall of East EPA, EL 628' - 6" to EL 642' - 7"	18	4,070	330	4,400	18,500	4.2	2.0
Line 7.8, EL 634' - 6" to EL 646' - 0"	20	107,000	6,920	114,000	255,000	2.3	2.3

Note: (1) See Figures II-4-1 to II-4-8 for locations of walls corresponding to wall identification numbers

M_{SME} = Overturning moment due to SME

M_{NOL} = Overturning moment due to normal operating loads

M_{NET} = M_{SME} + M_{NOL}

M_u = Code ultimate overturning moment capacity

CM = Code margin

Table III-4-3

Code Margins and F_{SME} Factors for Diaphragms Governed by Shear

Diaphragm	Diaphragm ID No.(1)	V_{SME} (k)	V_{NOL} (k)	V_{NET} (k)	V_u (k)	CM	F_{SME}
Line A, EL 614' - 0"(2)	1	562	454	1020	2770	1.7	2.3
Line 8.7, EL 614' - 0"(2)	2	348	148	496	782	1.6	1.8
Line K_C, EL 634' - 6"	3	533	31	564	4750	8.4	8.9
Line A, EL 646' - 0"	4	616	41	657	953	1.5	1.5
Line E, EL 646' - 0"	5	637	351	988	2650	2.7	3.5
Line 5.3, EL 704' - 0"	10	1700	90	1790	5390	3.0	3.1

Notes: (1) - See Figures II-4-1 to II-4-8 for locations of diaphragms corresponding to diaphragm identification numbers

(2) - This diaphragm consists of a series of sections separated by openings. Load and capacity are reported for the controlling section only

V_{SME} = Shear due to SME

V_{NOL} = Shear due to normal operating loads

V_{NET} = V_{SME} + V_{NOL}

V_u = Code ultimate shear strength capacity

CM = Code margin

Table III-4-4

Code Margins and F_{SME} Factors For Diaphragms Governed By In-Plane Moment

Diaphragm	Diaphragm ID No.(1)	M_{SME} (k-ft)	M_{NOL} (k-ft)	M_{NET} (k-ft)	M_u (k-ft)	CM	F_{SME}
Line 7.8, EL 659' - 0"	6	41,100	-864(2)	40,200	52,800	1.3	1.3
Line 6.6, EL 674' - 6"	7	23,700	2000	25,700	58,000	2.3	2.1
Line 7.8, EL 674' - 6"	8	31,600	420	32,000	63,500	2.0	1.9
Line 6.6, EL 704' - 0"	9	53,600	3480	57,100	87,800	1.5	1.6

Notes: (1) - See Figures II-4-1 to II-4-8 for locations of diaphragms corresponding to diaphragm identification numbers

(2) - Diaphragm moment capacity is dependent on the direction of the applied load because reinforcement layout is not symmetric. See discussion in Section 4.3.

M_{SME} = In-plane moment due to SME

M_{NOL} = In-plane moment due to normal operating loads

M_{NET} = $M_{SME} + M_{NOL}$

M_u = Code ultimate in-plane moment capacity

CM = Code margin

Underpinning Wall Code Margins and F_{SME} Factors

Underpinning Wall	M_{SME} (k-ft)	M_{NOL} (k-ft)	M_{NET} (k-ft)	M_u (k-ft)	CM	F_{SME}
Control Tower, Line K_c at El 556'-0	712,000	3,500	716,000	1,250,000	1.7	1.7
East EPA at El 571'-0	61,700	212,000	274,000	776,000	2.8	2.6

M_{SME} = Overturning moment due to SME

M_{NOL} = Overturning moment due to normal operating loads

M_{NET} = $M_{SME} + M_{NOL}$

M_u = Code ultimate overturning moment capacity

CM = Code margin

Underpinning Wall Connector Code Margins and F_{SME} Factors

Underpinning Wall	V_{SME} (k)	V_{NOL} (k)	V_{NET} (k)	V_u (k)	CM	F_{SME}
Control Tower, Line K_c	7440	37	7480	11,600	1.6	1.5
East EPA (1)	67	36	103	272	2.6	2.5

Notes: (1) - Values listed for most highly stressed bolt.

V_{SME} = Shear due to SME

V_{NOL} = Shear due to normal operating loads

V_{NET} = $V_{SME} + V_{NOL}$

V_u = Code ultimate strength shear capacity

CM = Code margin

Table III-4-7

Rigid Frame Stresses and Their Factored Allowable Values

Frame Type	Member	Axial Compressive Stress (Ksi), f_a		Factored Code Allowable Compressive Stress (Ksi)	Strong Axis Bending Stress (Ksi), f_{bx}		Factored Code Allowable Stress, F_{bx} (3) (Ksi)	Weak Axis Bending Stress (Ksi), f_{by}		Factored Code Allowable Stress, F_{by} (3) (Ksi)
		Normal Operating Condition	SME		Normal Operating Condition	SME		Normal Operating Condition	SME	
F-2	Column, (1) Top	5.0	1.3	40.3	12.6	3.7	42	1.8	0.2	42
	Column, (1) Base	7.4	2.1	40.3	12.6	7.1	42	1.6	4.1	42
	Girder (2)	0.3	0.1	38.3	18.0	5.1	42	0.02	0.3	42
F-1	Column, (2) Base	1.5	0.3	37.0	4.1	9.8	46	0.7	3.2	46
	Girder (2)	0.3	0.6	40.8	4.0	4.1	46	---	---	--

Notes: (1) Section is governed by AISC equation (1.6 - 1b)

(2) Section is governed by AISC equation (1.6 - 2)

(3) Conservatively limited to a maximum value equal to the minimum specified material yield strength.

Table III-4-8

Rigid Frame Code Margins and F_{SME} Factors

Frame	Member	Code Margin[1]	F_{SME}	Remark
F-2	Column, Top	1.7	4.2	Governed by AISC Eq. (1.6 -1b)
	Column, Base	1.2	1.5	Governed by AISC Eq. (1.6 -1b)
	Girder	1.8	4.3	Governed by AISC Eq. (1.6 -2)
F-1	Column, Base	2.3	2.9	Governed by AISC Eq. (1.6 - 1b)
	Girder	5.0	8.8	Governed by AISC Eq. (1.6 - 2)

Notes: (1) Factored code allowable bending stresses conservatively limited to a maximum value equal to the minimum specified material yield strength.

Table III-4-9
Braced Frame Code Margins and F_{SME} Factors

Member Description	Axial Tension (+) or Compression (-), Kips		Member			Connection		
	Operating Condition	SME	Factored Code Allowable Force, Kips	Code Margin	F_{SME}	Factored Code Allowable Force, Kips	Code Margin	F_{SME}
Diagonal bracing located between column lines C and D and between Elevations 659' - 0" and 681' - 10"(1)	51.1	±211.5	1036.8	3.9	4.7	560	2.1	2.4
	-128.3	±237.9	816.0	2.2	2.9	560	1.5	1.8

Notes: (1) Each braced panel consists of a pair of cross-braced members. One diagonal brace is loaded in tension under normal operating conditions while the other is loaded in compression. The brace of this panel in tension at normal operating conditions is the critical element for diagonal braces in tension and the brace in compression at normal operating conditions is the critical element for diagonal braces in compression

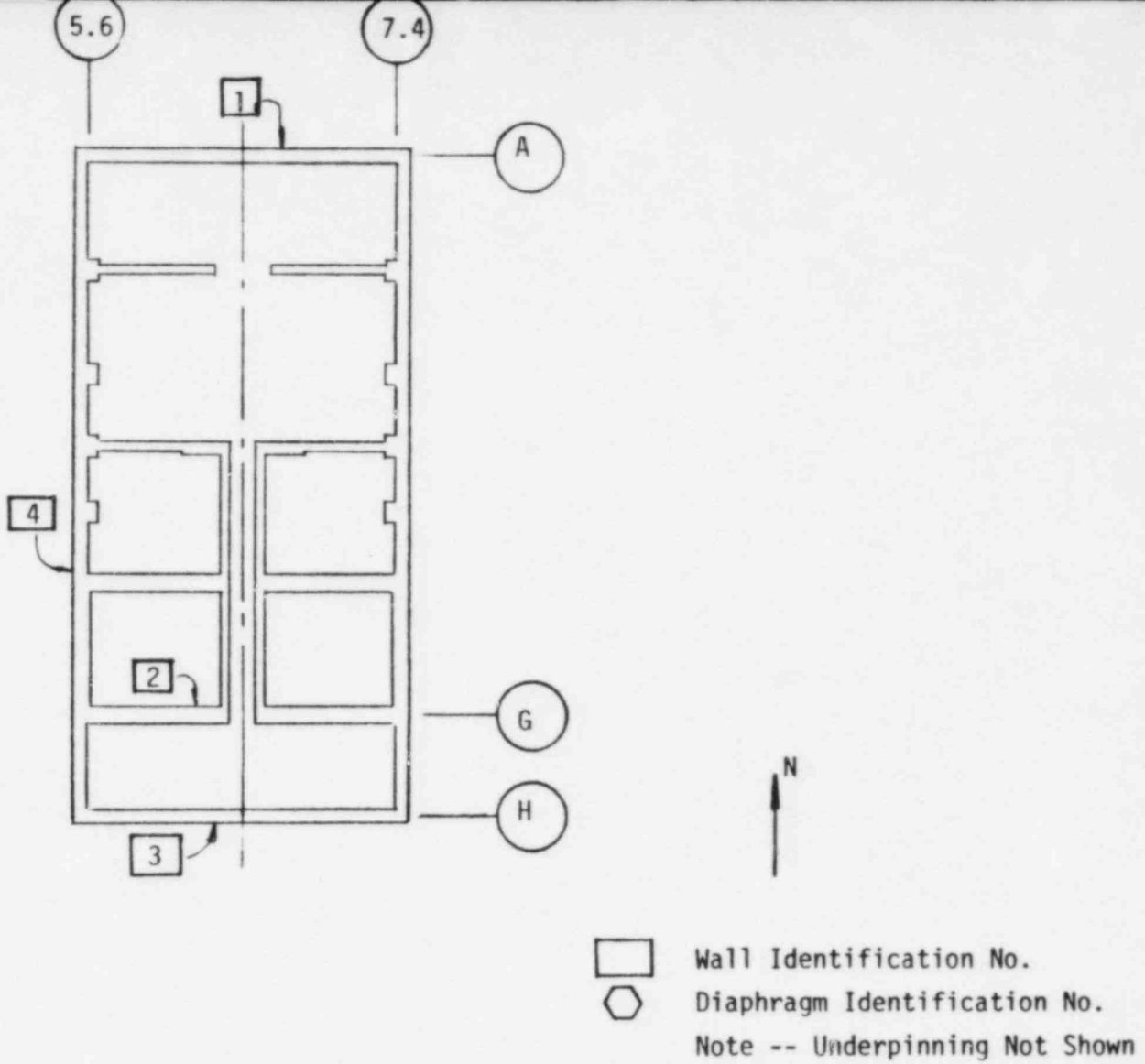

FIGURE III-4-1. AUXILIARY BUILDING PLAN, ELEVATION 568' - 0"

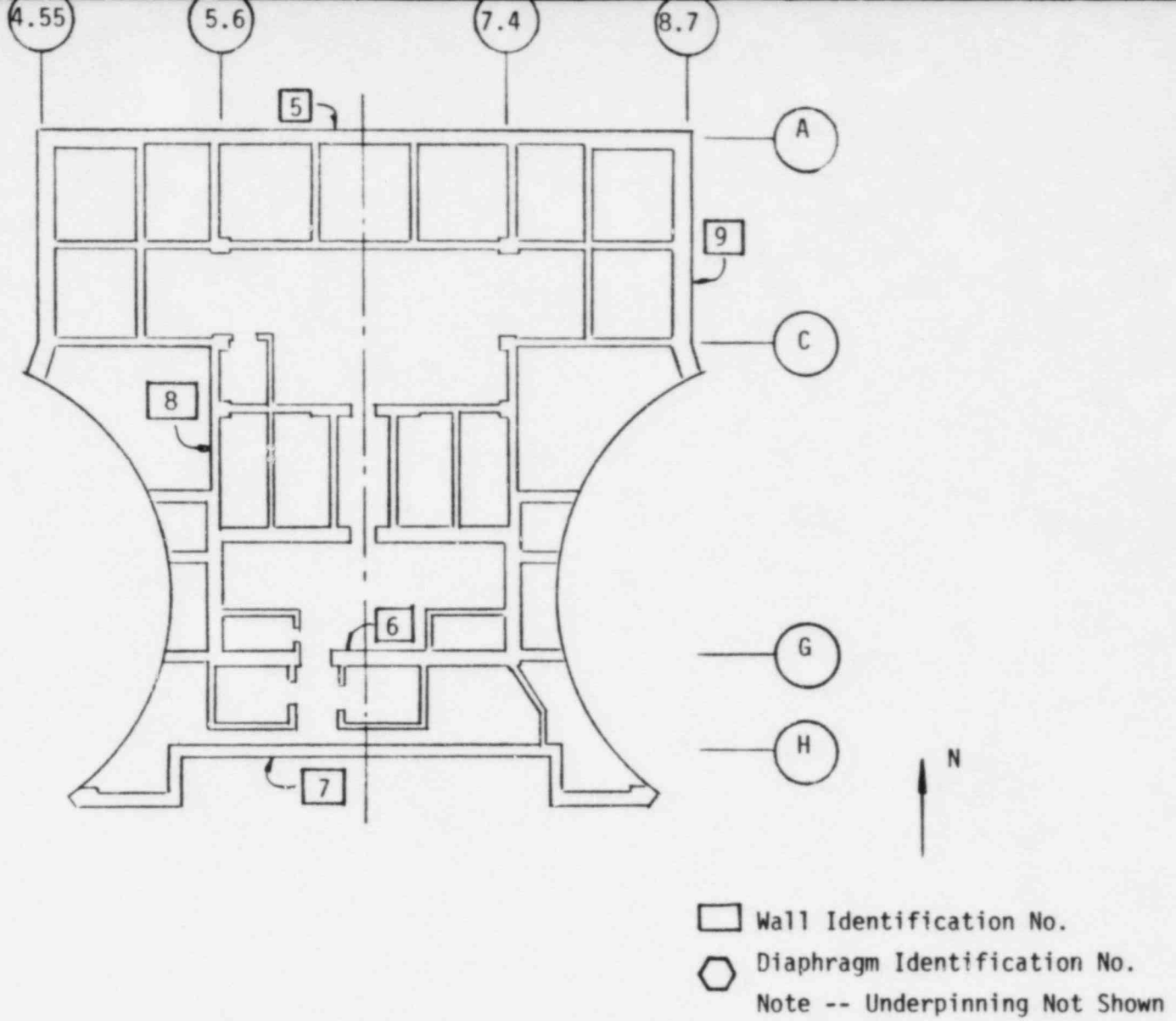

FIGURE III-4-2. AUXILIARY BUILDING PLAN, ELEVATION 584' - 0"

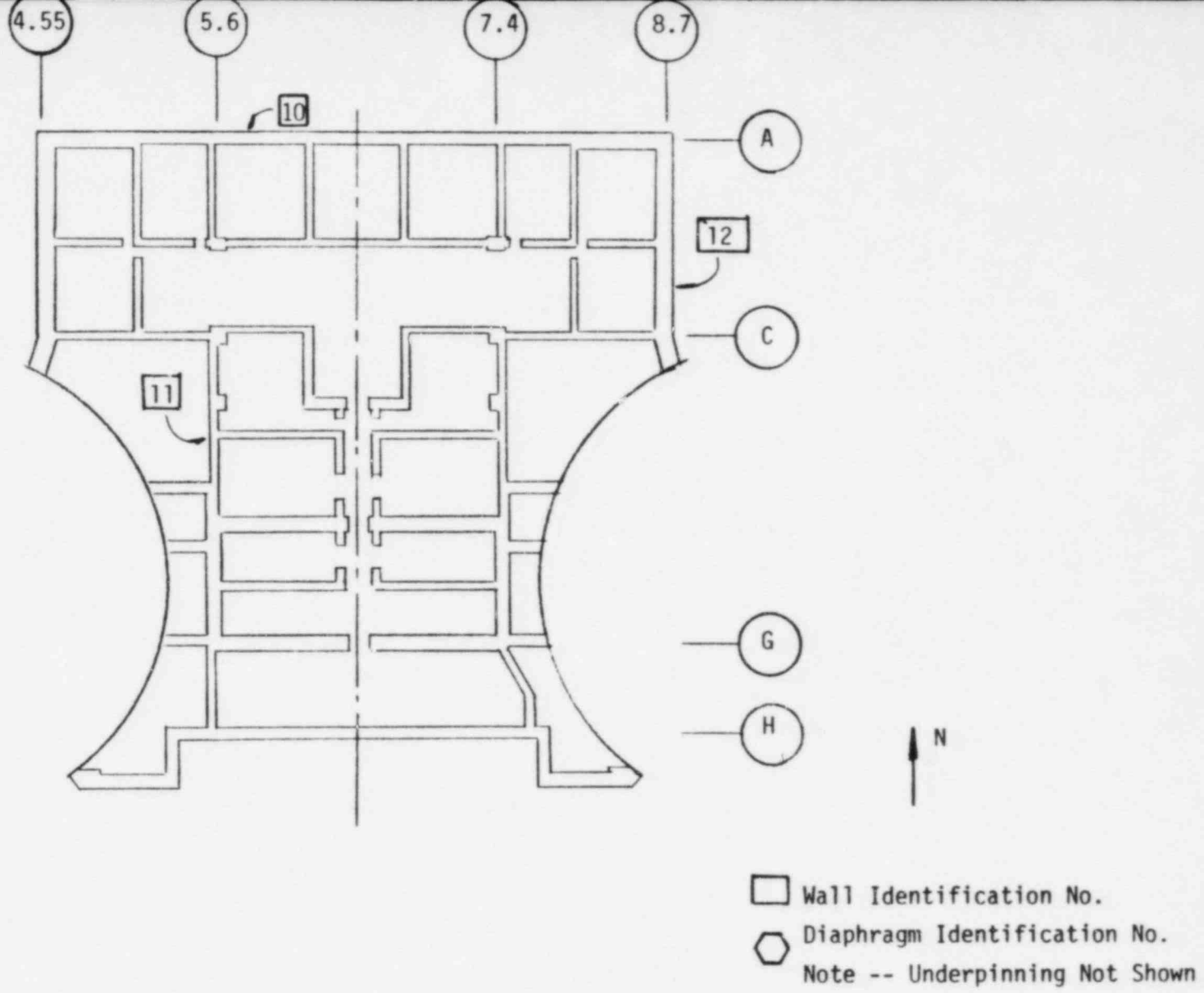

FIGURE III-4-3. AUXILIARY BUILDING PLAN, ELEVATION 599' - 0"

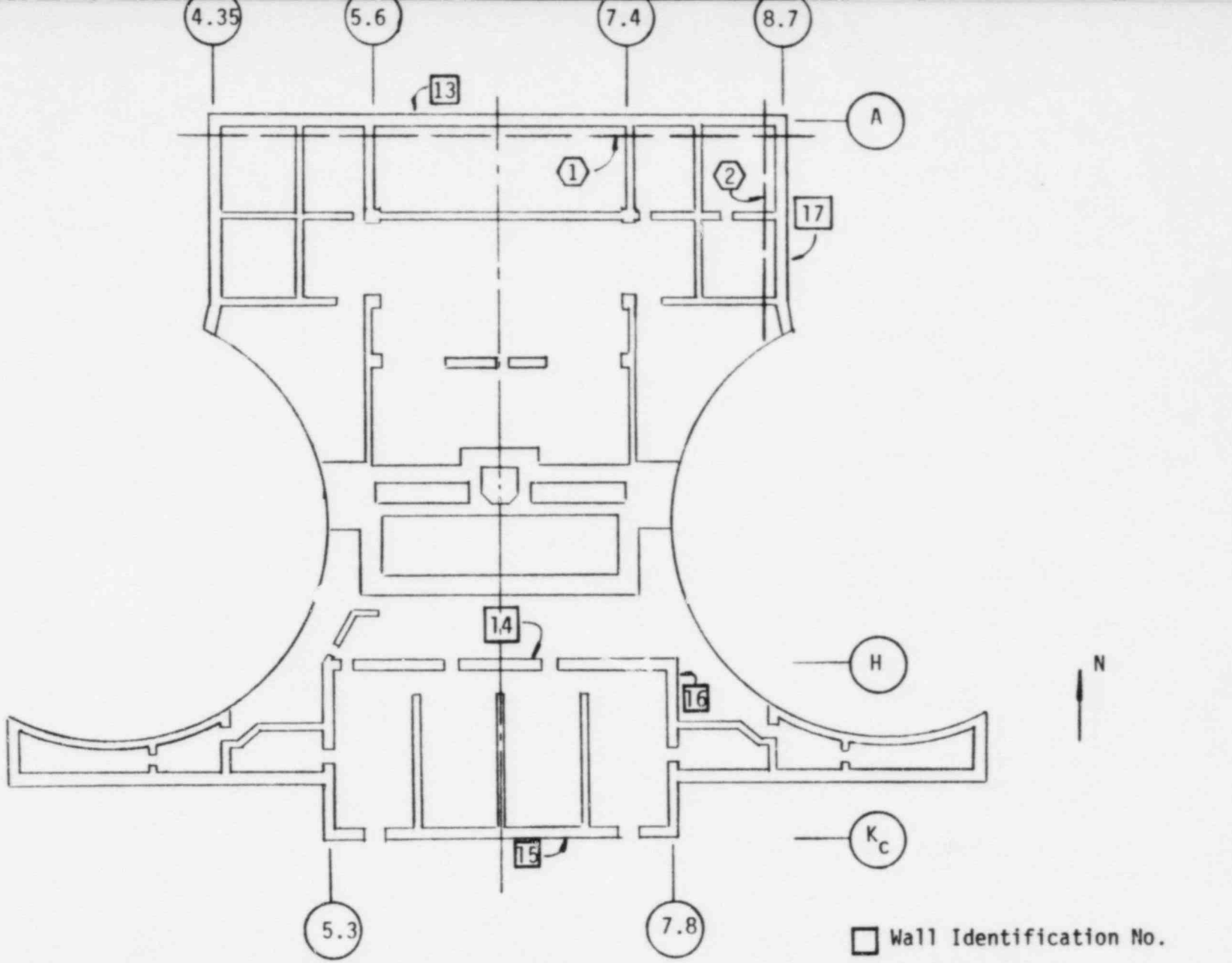

FIGURE III-4-4. AUXILIARY BUILDING PLAN, ELEVATION 614'-0

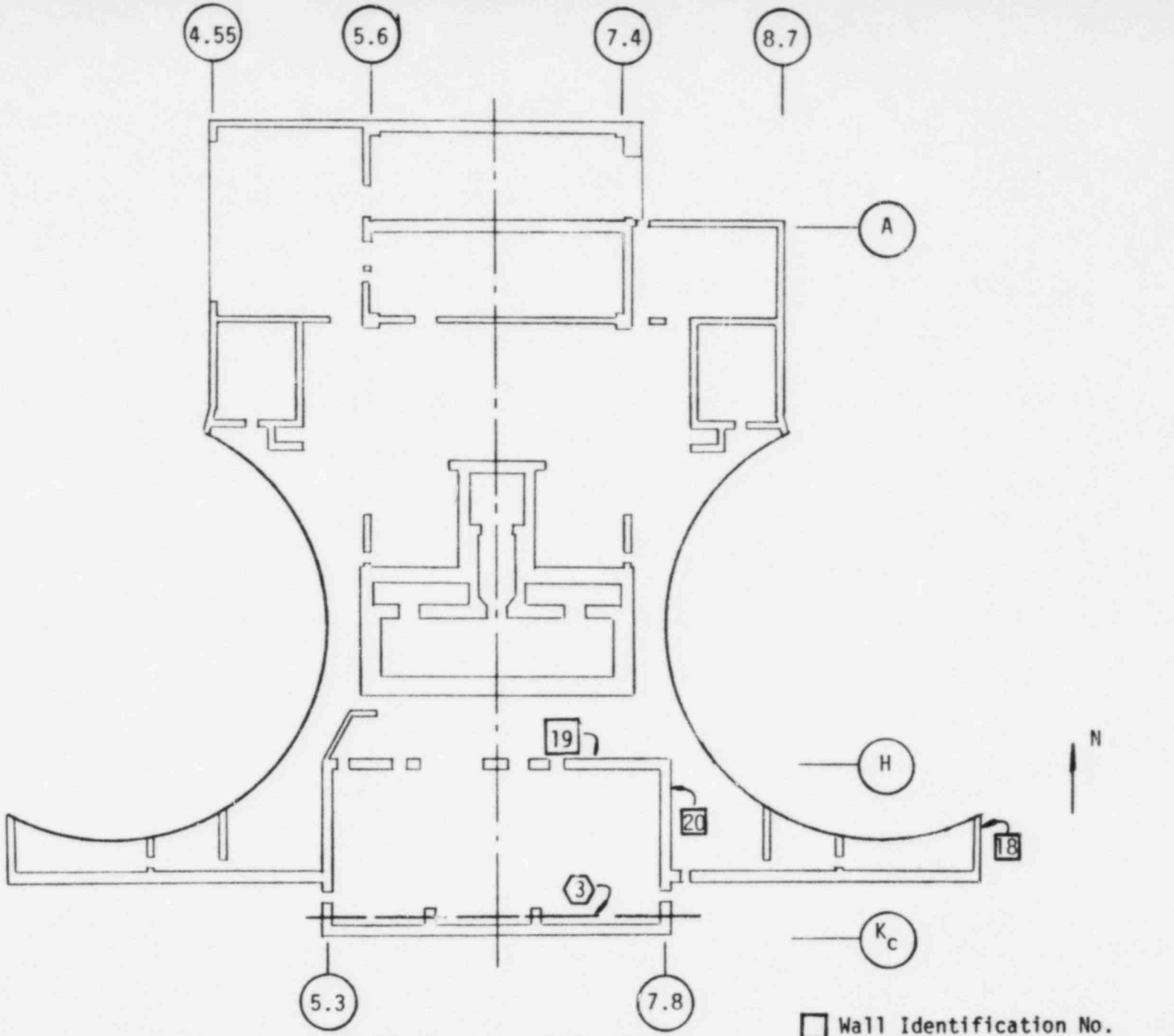

FIGURE III-4-5. AUXILIARY BUILDING PLAN, ELEVATION 634'-6"

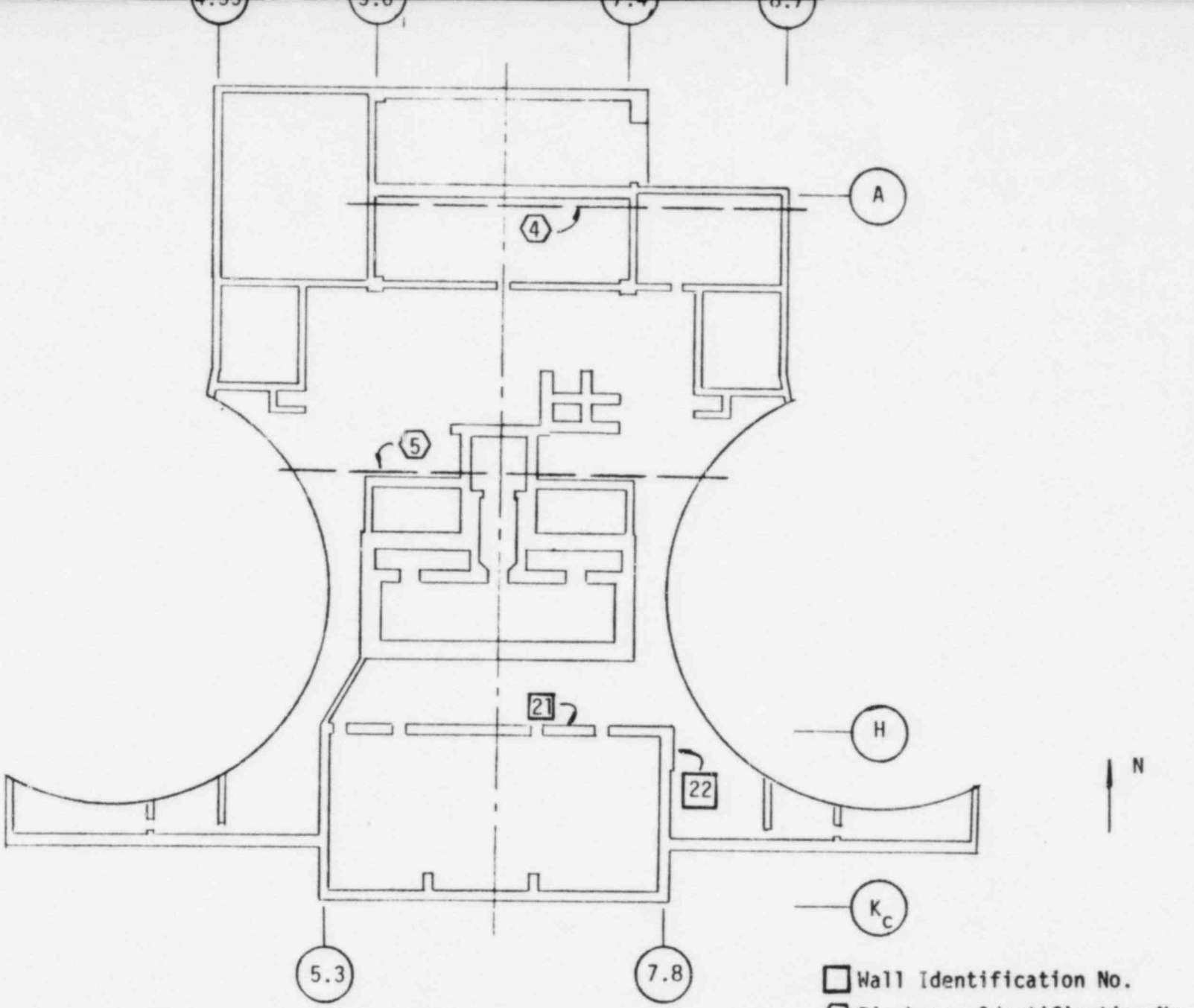

FIGURE III-4-6. AUXILIARY BUILDING PLAN, ELEVATION 646'-0"

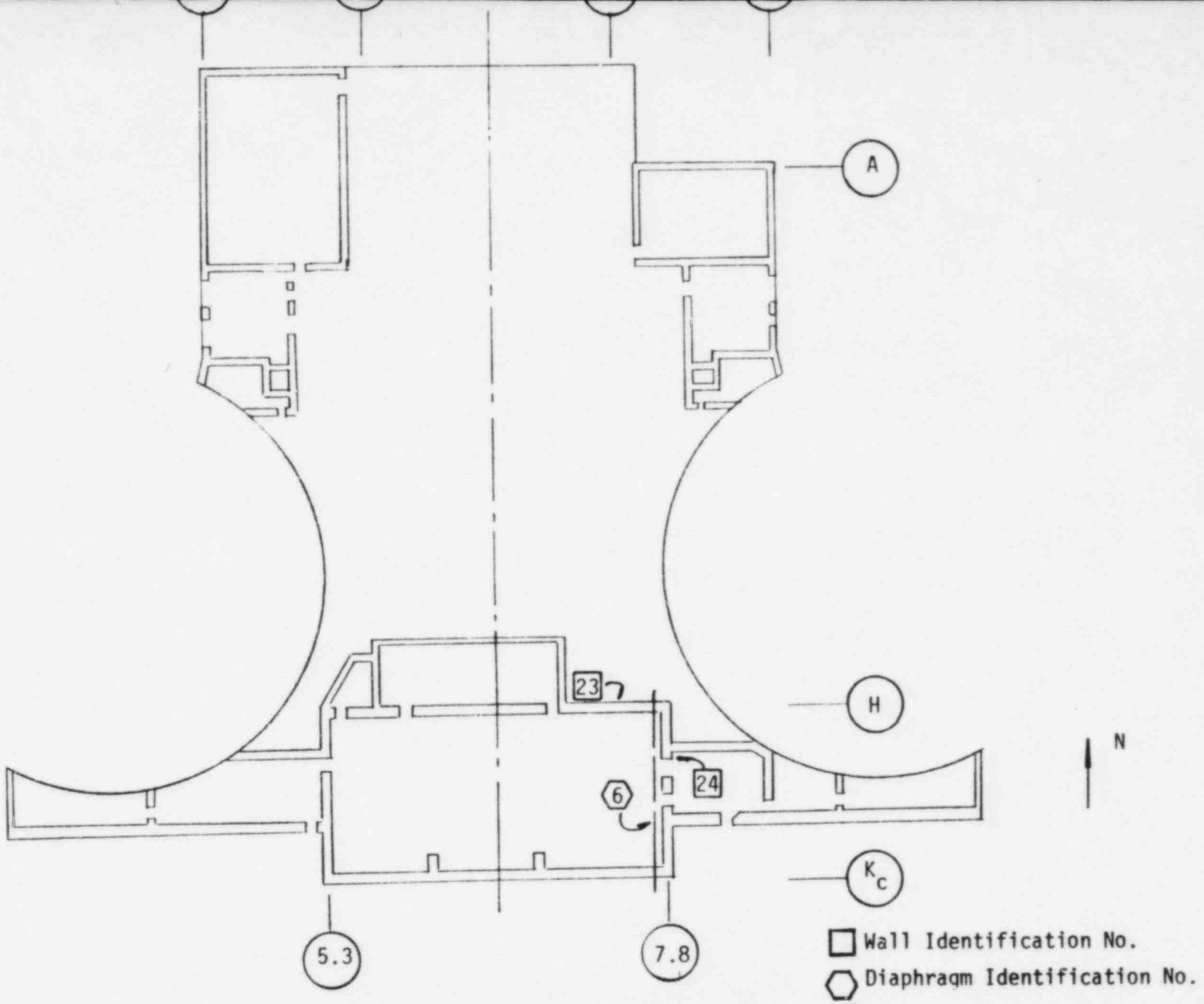

FIGURE III-4-7. AUXILIARY BUILDING PLAN, ELEVATION 659'-0"

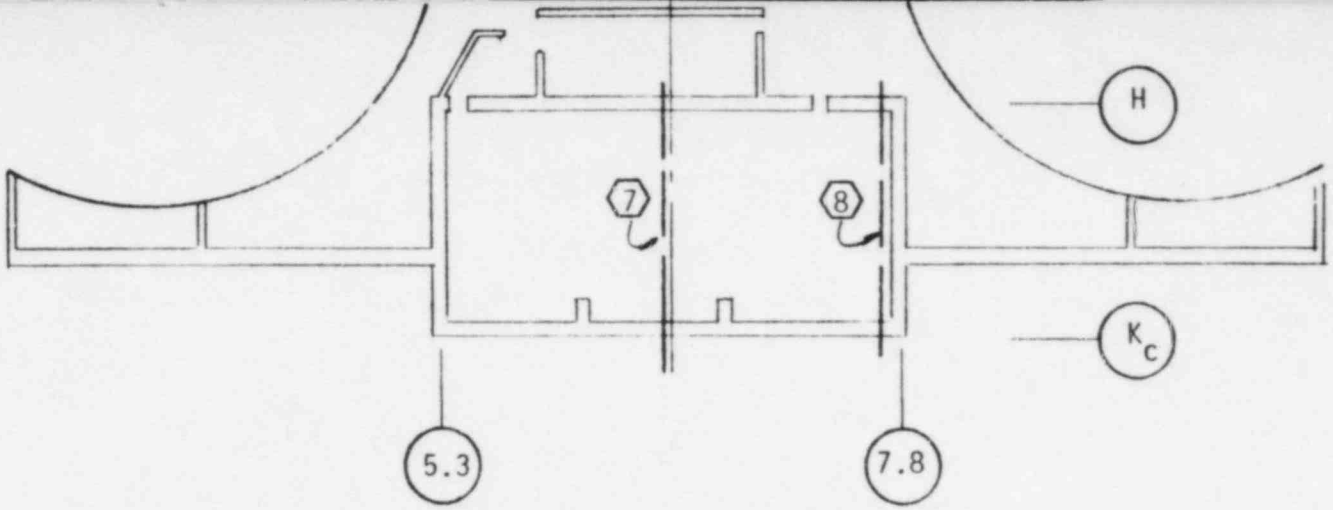

Elevation 674'-6"

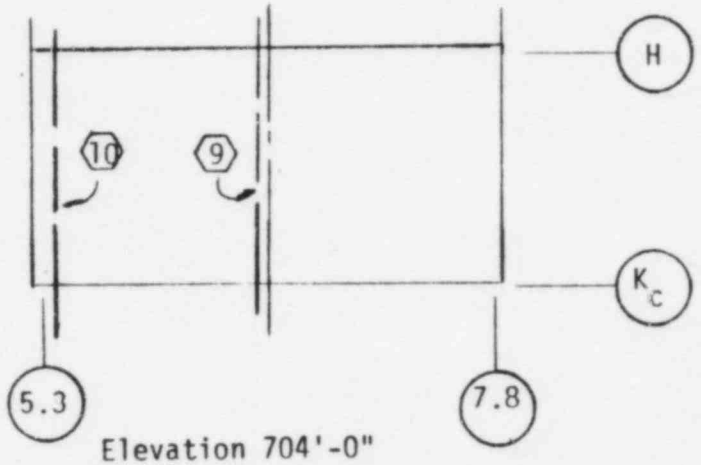

Elevation 704'-0"

Wall Identification No.

Diaphragm Identification No.

FIGURE III-4-8. AUXILIARY BUILDING PLAN, ELEVATIONS 674'-6" AND 704'-0"

5. INPUT TO EQUIPMENT

Seismic input to equipment for the SME was specified by in-structure response spectra. These spectra were generated by time history analysis using the coupled equations of motion of the structure as discussed in Section 8 of Volume I of this report. The time history input used was an artificial earthquake whose response spectra essentially envelop the SME ground response spectra at the original ground location. The development of the artificial earthquake is discussed in Section 2 of Volume I of this report. The spectra developed for the auxiliary building considered the effects of multidirection excitation, the range of soil characteristics previously discussed, and the torsional response of the structure.

In-structure response spectra were developed for all locations of critical equipment within the main auxiliary building, the control tower, and the EPA. Due to the symmetry of the structure, the seismic response of the structure and hence the excitation input to the equipment is virtually identical for corresponding locations in the east and west EPA. Consequently, only one set of spectra which is applicable to both EPA was generated. Spectra were generated for the lower bound, intermediate, and upper bound soil conditions. These spectra were smoothed and the peaks broadened $\pm$ 10 percent as discussed in Section 8 of Volume I. Final spectra were developed from an envelope of the three soil conditions. The in-structure response spectra developed for the auxiliary building complex include the effects of the torsional response of the structure. The method of accounting for the torsional components is described in Section 8.1 of Volume I. Enveloped in-structure reseponse spectra for the N-S, E-W, and vertical directions for equipment damping ratios of 2, 3, 4, and 7 percent of critical are shown in Figures III-B-1 through III-B-5.

The vertical spectra as shown are applicable for piping and equipment located adjacent to major walls or on rigid slabs. For flexible floor slabs within the auxiliary building, vertical input to equipment for the SME was determined by means of Vertical Amplification Factors (VAFs). These factors were developed from analyses of selected flexible floor slabs throughout the structure as described in Appendix A of Volume I of this report.

Damping ratios of 2 through 7 percent of critical are considered appropriate for the respose of piping and equipment for the SMR. In-structure response spectra for the auxiliary building are shown in Appendix B of this report.

6. SUMMARY

As part of the Seismic Margin Review (SMR) conducted for Midland, the ability of the auxiliary building structure to withstand seismic excitation was investigated. The evalution was conducted using new seismic response loads developed for the SME together with design dead and live loads (including jacking loads). Included in the evaluation was the underpinning under the control tower and electrical penetration areas. The underpinning was designed for 1.5 times the calculated FSAR loads. The SME seismic loads were developed using a site specific earthquake for Midland as well as new soil-structure interaction parameters which reflect the site layering characteristics. Margins against code allowable values were calculated for selected elements throughout the structure.

The seismic excitation of the structure was specified in terms of site specific response spectra developed for the original ground location. These spectra have a peak ground acceleration of approximately 0.13g. The vertical component was specified as 2/3 of horizontal.

Three soil profiles representing soft site, stiff site and intermediate soil conditions were used in the analysis. Layered site analyses were used to develop the soil impedance functions for the structure using an equivalent rectangular foundation plan. Effective shear moduli (G_{eff}) were calculated based on elastic half-space formulae by maintaining the same stiffness values as those obtained for the layered site analyses for each of the three soil profiles. In order to account for uncertainties in the soil data, global stiffness and damping parameters were developed based on a lower bound of 0.6 G_{eff} for the soft soil profile and 1.3 G_{eff} for the stiff soil profile. These parameters were then adjusted to account for effects such as embedment and the presence of the railroad bay which were not included in the

layered site analyses. Damping values were conservatively limited to 75 percent of theoretical elastic half-space values for all degrees-of-freedom except rocking which were limited to 50 percent of theoretical.

The dynamic analysis model of the structure used for the SMR evaluation was the same model used for the seismic design. This is a multi-stick lumped-mass model with plate finite elements used to model areas of the building of particular concern. As part of the SMR evaluation, the model was reviewed for the general methodology used in its development and for adequacy to characterize the seismic response of the structure.

Because of some uncertainty regarding the effects of various possible modeling assumptions on the soil stiffnesses under the EPA, parametric studies were conducted to determine the influence of these assumptions on the structure response. In-structure response spectra as well as the seismic structural responses were compared for three cases of soil stiffness approximations under the wings. The results indicated the overall structure response was not sensitive to the different modeling assumptions. Slightly higher in-structure response spectra were developed for the lower bound EPA stiffness case. However, in-structure loads in the vicinity of the EPA and underpinning were maximized for the upper bound EPA stiffness case. Worst case conditions were used for the SMR.

Composite modal damping ratios were computed for the combined soil-structure model by matching structure response defined by both structure accelerations and in-structure response spectra at a number of loctions using the same time-history input for both the coupled equations of motion and modal analysis. Structural damping based on seven percent of critical was used throughout the structure.

Structural loads were determined using response spectrum modal analysis. Modal responses were combined on an SRSS basis except for closely spaced modes which were combined by the absolute sum. The responses to three directions of input motion were calculated independently and combined by the SRSS method.

In general, the upper bound soil condition resulted in maximum structural loads. Depending on the location within the structure, the upper or lower bound EPA stiffness case could control. The code margin evaluation was based on the maximum load condition in all instances. When compared with seismic design loads, the maximum SME loads were generally found to be lower with the exception of torsional response, overturning moments in the control tower about the N-S axis, and the loads in the EPA.

Overall seismic loads determined by the structure response spectrum analyses were distributed to the resisting structural elements by methods appropriate to the load-resisting system being evaluated. For the main auxiliary building and the control tower which are composed of concrete shear walls and diaphragms, load distributions to the individual walls were developed using the rigid diaphragm approximation. Seismic shears and overturning moments were distributed to the individual walls in proportion to their relative rigidities. These relative rigidities were derived using element story stiffnesses developed in the determination of the design dynamic model stiffness properties. Seismic loads acting on the diaphragms were determined using information available from the load distributions to the individual walls or from loads in the elements of the dynamic model. Seismic loads acting on members of the EPA evaluated in this study were taken directly from the results of the response spectrum analyses for the appropriate elements of the dynamic model. Seismic loads acting on the control tower underpinning walls were calculated as part of the load distribution for the main auxiliary building and the rest of the control tower. Loads on the EPA underpinning walls were determined by resolving the reactions from the beam and boundary elements at the wall boundaries into overall seismic loads. For the structural steel framing above Elevation 659'-0", a comparison of the individual modal responses was made. Because response in a horizontal direction for the element modeling this framing occurs primarily in a single mode, it was determined that scale factors could be developed to ratio member forces due to the design OBE from Bechtel's static finite

element model. This approach accounts for member forces due to inertial loads and differential displacements between the main auxiliary building and the control tower. The scale factors were based on SRSS forces in the elements modeling the steel framing due to the SME and the design OBE. Seismic loads acting on the members evaluated in this study were combined with loads due to normal operating conditions predicted by Bechtel's static analyses.

Capacities for the shear walls were developed in accordance with the ultimate strength design provisions contained in ACI 349-80. Shear walls were checked for their ability to resist in-plane shears and overturning moments. Code margins and F_{SME} factors were determined for the selected walls based on comparisons of the loads due to seismic and normal operating conditions and the code ultimate strength capacities. The lowest code margins calculated were found to be 1.4 for walls governed by shear and 1.3 for walls governed by overturning. The SME would have to be increased by at least a factor of 1.3 before the code margin for any wall would be exceeded. To account for the effects of the reinforcement cutting allowance and available non-conformance reports indicating deviations from the construction specifications, the governing walls were re-evaluated assuming the worst case possible due to these field conditions. A code margin of 1.2 was calculated both for walls governed by shear and overturning moment.

Diaphragm capacities were determined using ACI 349-80 criteria developed for shear walls. Capacities of diaphragms in the main auxiliary building were found to be influenced by the presence of structural steel beams embedded in the concrete slabs. Capacities of the diaphragms at the control tower-penetration wing interfaces were found to be influenced by reinforcement detailing in these regions. The lowest code margin for diaphragms governed by shear was found to be 1.5. The lowest code margin for diaphragms governed by in-plane moment was found to be 1.3. For any existing diaphragm to reach code capacity, the SME would have to be increased by a factor of 1.3.

Modifications intended to increase the capacity of the slab diaphragm at Elevation 659'-0" between Column Lines G and H are currently being designed. Preliminary drawings available indicate that these modifications consist of steel plates anchored to the slab. The plates provide additional tensile capacity to resist N-S axial load and in-plane moment. The diaphragm evaluation was conservatively based on the load failure of a portion of the diaphragm rather than the overall failure of the diaphragm as a whole. The diaphragm code margin including the design modifications was found to be 1.3. The SME would have to be increased by a factor of 1.2 before the code capacity would be reached for this element.

Capacities of both the underpinning walls and their connectors to the existing structure were determined. The walls themselves were evaluated using the same acceptance criteria developed for the shear walls. Shear strengths of the connectors between the underpinning walls and the existing structure were calculated using the shear-friction provisions of ACI 349-80. The lowest underpinning wall code margin at 1.6 was found to occur for one of the interfaces to the existing structure. The SME would have to be increased by a factor of 1.5 before the code capacity would be exceeded.

The structural steel framing above Elevation 659'-0" of the main auxiliary building was typically evaluated using allowable stresses specified by the AISC code increased by a factor of 1.6 for stresses due to loads from normal operating plus extreme environmental conditions as permitted by the Standard Review Plan. Member stresses due to loads from normal operating conditions and the SME were calculated using elastic section properties. The lowest code margins for the E-W rigid frames and the N-S vertical braced frames were found to be 1.2 and 2.2, respectively. Bolted connection details occurring at the ends of the diagonal bracing and at splices for girders of the rigid frames were also evaluated. The lowest code margin was found to be 1.5. This code margin is of sufficient

magnitude such that the possibility of moderately reduced bolt material yield strengths due to heat treatment will not lead to a code margin less than unity. The SME would have to be increased by a factor of 1.5 before the code capacity of any steel member would be reached.

Code margins for the selected structural elements were all conservatively based on minimum specified material strengths and maximum seismic load cases. Reductions in loads to account for inelastic energy dissipation were not used for the auxiliary building. All code margins were determined to be greater than unity. Before code capacity is reached for any auxiliary building element investigated, the SME would have to be increased by a factor of 1.2. It can, therefore, be concluded that the auxiliary building has more than sufficient structural capacity to resist the SME based on code criteria and significantly higher capacity before failure is expected.

In-structure response spectra were generated for the auxiliary building SMR by time history analyses using the coupled equations of motion. Envelopes of spectra for the three soil cases were generated for the two horizontal and vertical directions. Vertical amplification factors to account for the vertical response of flexible floor slabs were also developed for use in the evaluation of piping and equipment located near the centers of the flexible slabs. The effects of out-of-plane moments and thermal gradients on in-plane wall and diaphragm capacities were considered.

REFERENCES

1. Final Safety Analysis Report (FSAR), Midland Plant - Units 1 and 2, Consumers Power Company.

2. TID-7024, Nuclear Reactors and Earthquakes, Lockheed Aircraft Corporation and Holmes and Narver, Inc., August 1963.

3. Site Specific Response Spectra, Midland Plant - Units 1 and 2, Part I, Response Spectra - Safe Shutdown Earthquake, Original Ground Surface, Weston Geophysical Corp., prepared for Consumers Power Company, February 1981.

4. Site Specific Response Spectra, Midland Plant - Units 1 and 2, Part II, Response Spectra - Applicable for the Top of Fill Material at the Plant Site, Weston Geophysical Corp., prepared for Consumers Power Copany, April 1981.

5. Draft, Site Specific Response Spectra, Midland Plant - Units 1 and 2, Part III, Seismic Hazard Analysis, Weston Geophysical Corp. prepared for Consumers Power Company, Revision 1, May 1982.

6. Wesley, D. A., Campbell, R. D., Kennedy, R. P., Kincaid, R. H., and P. S. Hashimoto, "Seismic Margin Review, Midland Energy Center, Volume I, Methodology & Criteria", February, 1983, SMA 13701.05R003 (Volume I).

7. Wong,. H. L. and J. E. Luco, "Soil-Structure Interaction: A Linear Continuum Mechanics Approach (CLASSI), Report, CE, Department of Civil Engineering, University of Southern California, Los Angeles, California, 1980.

8. Woodward-McNeill and Associates, "Development of Soil-Structure Interaction Parameters Proposed Units 2 and 3, San Onofre Nuclear Generating Station", San Onofre, California, January 1974.

9. Richart, F. E., Hall, Jr. R. and R. A. Woods, Vibrations of Soils and Foundations, Prentice-Hall, Inc., New Jersey, 1970.

10. Kausel, E., and R. Ushijima, "Vertical and Torsional Stiffness of Cylindrical Footings", Massachusetts Institute of Technology, Research Report R79-6, February, 1979.

11. Veletsos, A. S., and Y. T. Wei, "Lateral and Rocking Vibration of Footings", Journal of the Soil Mechanics and Foundations Division, Proceedings of ASCE, EM5, pp 1381-1395, October, 1971.

12. Luco, J. E., and R. A. Westmann, "Dynamic Response of Circular Footings", Journal of the Engineering Mechanics Division, Proceedings of ASCE, EM5, pp 1381-1395, October, 1971.

REFERENCES (Continued)

13. Bechtel Submittal to NRC "Auxiliary Building Seismic Model Revision 3 for Midland Units 1 and 2 Consumers Power Company", September 28, 1981.

14. Johnson, J. J., "SOILST - A Computer Program for Soil-Structure Interaction Analyses", General Atomic Company, GA-A15067, April 1979.

15. Derecho, A. T., et. al., "Analysis and Design of Small Reinforced Concrete Buildings for Earthquake Forces", Portland Cement Association, 1974.

16. Letter correspondence from E. M. Hughes to R. P. Kennedy, April 20, 1982, Subject: Midland Plant Units 1 and 2, Consumers Power Company, Bechtel Job 7220, Seismic Margin Analysis.

17. ACI 349-80, "Code Requirements for Nuclear Safety Related Concrete Structures", American Concrete Institute, 1980.

18. AISC, "Specification for the Design, Fabrication, and Erection of Structural Steel for Buildings", American Institute of Steel Construction, 1980.

19. Cardenas, A. E., et. al., "Design Provisions for Shear Walls", ACI Journal, March, 1973.

20. Bresler, B. (ed), Reinforced Concrete Engineering, John Wiley and Sons, Inc., 1974.

21. Bechtel Associates Professional Corporation, "Technical Specifications for Forming, Placing, Finishing and Curing of Concrete for the Consumers Power Company Midland Plant - Midland, Michigan", Spec. 7220-C-231Q, Revision 21, September 28, 1981.

22. "Tentative Provisions for the Development of Seismic Regulations for Buildings", National Bureau of Standards Special Publication 510, Applied Technology Council.

23. Bechtel letter correspondence from E. M. Hughes to R. P. Kennedy, August 26, 1982, Subject: Midland Plant Units 1 and 2, Consumers Power Company, Bechtel Job 7220, Seismic Margin Analysis.

24. Personal communication between P. S. Hashimoto (SMA) and M. DasGupta (Bechtel), September 22, 1982.

25. Personal communication between W. H. Tong (SMA) and J. Ross (Bechtel), December 13, 1982.

REFERENCES (Continued)

26. William Forms Engineering Corporation, Concrete Form Hardware and Rock Bolts, Product Catalog No. 418, 1981.

27. Park, R. and T. Paulay, Reinforced Concrete Structures, John Wiley and Sons, 1975.

28. Letter correspondence from J. W. Cook to H. R. Denton, May 7, 1982, CPC Serial 17209, Subject: Closure of December 4, 1981 Hearing Open Item Concerning Soil Impedance Functions of the Auxiliary Building Electrical Penetration Wings.

29. Letter correspondence from N. W. Swanberg (Bechtel) to D. A. Wesley (SMA), April 6, 1983, Subject: Design Thermal Gradients.

30. Gurfinkel, G., "Thermal Effects in Walls of Nuclear Containments - Elastic and Inelastic Behavior", First International Conference on Structural Mechanics in Reactor Technology, Berlin, Germany, September 20-24, 1971.

31. Kohli, T. D. and O. Gurbuz, "Optimum Design of Reinforced Concrete for Nuclear Containments, Including Thermal Effects", Second ASCE Specialty Conference on Structural Design of Nuclear Plant Facilities, New Orleans, Louisiana, December 8-10, 1975.

APPENDIX III-A

TYPICAL CALCULATION OF SOIL IMPEDANCES

TABLE OF CONTENTS

APPENDIX A

This appendix presents illustrative calculations showing the development of typical soil impedances (including embedment effects) for the auxiliary building based on the results of CLASSI layered site analyses. The basic methodology used to account for soil-structure interaction was previously presented in Volume I of this report (Methodology and Criteria, Reference III-A-1) and will not be repeated here.

The east-west translational soil impedances for the intermediate soil case are developed in this appendix. The development of the soil impedances for other structure degrees-of-freedom and soil cases was done in a similar manner.

A.1 DEVELOPMENT OF EFFECTIVE SOIL SHEAR MODULUS

Figure III-A-1 (repeated from Figure III-2-9) presents the CLASSI layered site results for E-W translation. An initial estimate of the fundamental east-west translation structure frequency was f = 2.75 Hz with an uncertainty range from 0.7f to 1.35f. This frequency estimate was subsequently compared to the actual fundamental east-west translational frequency of the structure of 2.66 Hz.

For a range of 0.7 f to 1.35 f (Figure III-A-1),

$K(CLASSI) = 3.65 \times 10^6$ K/ft

For the idealized 140'x236' foundation (Figure III-2-1), determine an equivalent radius based on stiffness equivalence between a circle and a rectangle. Using Table III-2-3 for horizontal motion:

$$R_{eq} = (1+\nu)\ \beta_x\ \sqrt{BL}\quad (7-8\nu)/(16\ (1-\nu))$$

$$B/L = 140/236 = 0.59 \longrightarrow \beta_x = 1.01$$

Noting that the Auxiliary Building is founded at Elevation 562' (Figure III-1-6) let

$\nu = 0.42$, $W_s = 135$ pcf (represents average soil properties below Elevation 562')

$$R_{eq} = (1.42)\ 1.01\ \sqrt{140(236)}\quad (7-8(0.42))/(16(1-0.42))$$

$$R_{eq} = 102.3 \text{ ft.}$$

Initially assume a trial G_{eff} of:

$$G_{eff} = 7100 \text{ ksf}$$

Calculate the effective shear wave velocity from:

$$V_s = \sqrt{G_{eff}\ (g)/W_s}$$

$$V_s = \sqrt{7100(32.2)/0.135} = 1300 \text{ fps.}$$

Find the dimensionless soil-structure frequency by:

$$f_o = f\, R_{eq}/V_s$$

$$f_o = 2.75(102)/1300 = 0.22$$

From Figure III-A-2, determine the frequency dependent coefficient, k_1

$$k_1 \approx 0.96$$

Using Table III-2-3, determine G_{eff} from:

$$G_{eff} = K(CLASSI)/(k_1\, 2(1+\nu)\, \beta_x\, \sqrt{BL}\,)$$

$$G_{eff} = 3.65 \times 10^6/(0.96(2)(1.42)(1.01)\, \sqrt{140(236)})$$

G_{eff} = 7,290 ksf (Estimate of $G_{eff} \approx$ 7100 ksf was reasonable and second trial is unnecessary)

Using a similar procedure for north-south translation and torsion, results showed an average G_{eff} = 7100 ksf best represented the equivalent half-space properties for these degrees-of-freedom.

A.2 LAYERING FACTORS

From Figure III-A-1, determine the layered site damping for the frequency range of 0.7f to 1.35f.

$$C^*(CLASSI) = 0.95 \times 10^6 \text{ k-sec-rad/ft}$$

Remove CLASSI frequency normalization by:

$$C'(CLASSI) = C^*(CLASSI)/(2\pi)$$

$$C'(CLASSI) = 0.95 \times 10^6/(2\pi) = 1.51 \times 10^5 \text{ k-sec/ft}$$

From Figure III-A-2, determine the frequency dependent coefficient, C_1.

$$C_1 \approx 0.60 \qquad (f_o \approx 0.22)$$

Remove the 5 percent soil material damping from the CLASSI damping coefficient by:

$$C(CLASSI) = C'(CLASSI) - (2\beta)\, K(CLASSI)/(2\pi f)$$

$$C(CLASSI) = 1.51 \times 10^5 - (0.1)\, 3.65 \times 10^6/(2\pi(2.75))$$

$$C(CLASSI) = 1.30 \times 10^5 \text{ k-sec/ft}$$

Determine the equivalent thecretical elastic half-space damping coefficient from:

$$C(EHS) = C_1\, K_{static}\, R_{eq}/V_s$$

where: $K_{static} = K(CLASSI)/k_1 = \dfrac{3.65 \times 10^6}{0.96}$

$$K_{static} = 3.80 \times 10^6 \text{ k/ft}$$

$$C(EHS) = 0.60\ (3.80 \times 10^6)(102.3)/1300$$

$$C(EHS) = 1.79 \times 10^5 \text{ k-sec/ft}$$

Determine the layering factor, F_{Layer} from:

$$F_{Layer} = C(CLASS I)/C(EHS)$$

$$F_{Layer} = 1.30 \times 10^5 / 1.79 \times 10^5 = 0.73$$

Using a similar procedure for north-south translation, vertical translation and torsion, the results showed an average $F_{Layer} \approx 0.75$ best represented site conditions for these degrees-of-freedom.

A.3 UNEMBEDDED SOIL SPRINGS

Determine equivalent rectangles for the actual foundation geometry shown in Figure III-2-1. As discussed in Section 2.1.4 of this report, structure geometric properties are required for two cases.

Case 1: Structure geometric properties including the effect of the railroad bay on the overall geometry.

$I = 6.94 \times 10^7$ ft^4 (Neglects entrapped soil)

$A = 32{,}904$ ft^2 (Includes entrapped soil)

Determine an equivalent rectangle based on equivalence of rocking inertias about north-south axis and area equivalence.

$$\left.\begin{aligned} I &= LB^3/12 \\ A &= BL \end{aligned}\right\} \quad \text{For a rectangle}$$

Solving for B and reformulating:

$$B_1 = \sqrt{12I/A} = \sqrt{12(6.94\times10^7)/32,904}$$

$$B_1 = 159.1 \text{ ft}$$

$$L_1 = 32,904/159.1 = 206.8 \text{ ft}$$

Case 2: Structure geometric properties neglecting the effect of the railroad bay

$$I = 6.37\times10^7 \text{ ft}^4 \text{ (Neglects entrapped soil)}$$

$$A = 29,416 \text{ ft}^2 \text{ (Includes entrapped soil)}$$

Determine equivalent rectangles for this case.

$$B_2 = \sqrt{12(6.37\times10^7)/29,416}$$

$$B_2 = 161.2 \text{ ft}$$

$$L_2 = 29,416/161.2 = 182.5 \text{ ft}$$

Determine the overall unembedded foundation stiffness, K*, based on the actual foundation geometry including the railroad bay. Using Table III-2-3:

$$K^* = k_1\, 2(1+\nu)(G_{eff})\, \beta_{x_1} \sqrt{B_1 L_1}$$

$$B_1/L_1 = 159.1/206.8 = 0.77 \longrightarrow \beta_{x_1} = 1.00$$

$$K^* = 0.96(2)(1.42)(7100)(1.00) \quad \sqrt{159.1(206.8)}$$

$$K^* = 3.51 \times 10^6 \text{ k/ft}$$

Determine the overall unembedded foundation stiffness, K', based on the actual foundation geometry neglecting the railroad bay.

$$B_2/L_2 = 161.2/182.5 = 0.88 \longrightarrow \beta_x = 0.99$$

$$K' = 0.96(2)(1.42)(7100)(0.99) \quad \sqrt{161.2(182.5)}$$

$$K' = 3.29 \times 10^6 \text{ k/ft}$$

Determine the global soil stiffness from:

$$K_G = K' + (K^* - K') \, G_{eff} \text{ (railroad bay)}/G_{eff} \text{ (Section A.1)}$$

G_{eff} (railroad bay) = 2300 ksf based on backfill soil data for the auxiliary building and strain degradation effects of 53 percent. G_{eff} (Section A.1) = 7100 ksf.

$$K_G = 3.29 \times 10^6 + (3.51 \times 10^6 - 3.29 \times 10^6) \, 2300/7100$$

$K_G = 3.36 \times 10^6$ k/ft is the unembedded east-west translation soil spring.

A.4 UNEMBEDDED DASHPOT

The fundamental equation for an unembedded dashpot is:

$$C^* = (C_1 \ K_T \ (\text{Static}) \ R_{eq}/V_s) \ F_{Layer}$$

The equivalent radius, R_{eq}, is redetermined based on the actual foundation geometry for the overall structure. As before:

$$R_{eq} = (1+\nu) \ \beta_x \ \sqrt{BL} \quad (7-8\nu)/(16 \ (1-\nu))$$

Using Case 1 results (Section A.3),

$$R_{eq} = (1.42)(1.00) \quad \sqrt{159.1(206.8)} \quad (7-8(0.42))/(16 \ (1-0.42))$$

$$R_{eq} = 101 \text{ ft}$$

Determine K_T (Static) by:

$$K_T \ (\text{Static}) = K_G \ (\text{Section A.3})/k_1$$

where $k_1 = 0.96$ (Section A.1)

$$K_T \ (\text{Static}) = 3.36 \times 10^6/0.96 = 3.50 \times 10^6 \text{ k/ft}$$

$$C^* = (0.60 \ (3.50 \times 10^6)(101)/1300) \quad (0.75)$$

$C^* = 1.22 \times 10^5$ k-sec/ft is the unembedded east-west translational dashpot.

A.5 EMBEDMENT EFFECTS

Embedment effects for the unembedded soil stiffness are of the form:

$$F_{emb_1} = (1+(\alpha_i-1)\ (G_1/G_2)j)$$

The average high strain soil shear modulus for soil adjacent to the auxiliary building is G_1 = 2300 ksf as presented in the previous section. Soil beneath the structure is best represented by G_2 = 7100 ksf.

In the east-west direction, the auxiliary building is unembedded in the vicinity of the reactor buildings (Figure III-2-1) above Elevation 580'. The effective soil surcharge, due to the reactor building weight, is determined by calculating an equivalent free-column height of the soil required to equal the reactor building weight.

$$W\ (\text{Reactor}) \approx 106{,}000 \text{ kips}$$

$$A\ (\text{Reactor}) = \pi R^2 = \pi(62)^2 = 1.21\times10^4 \text{ ft}^2$$

$$q_{eff} = W(\text{Reactor})/A(\text{Reactor}) = 106{,}000/1.21\times10^4 = 8.78 \text{ ksf}$$

$$H_{eq} = q_{eff}/W_s = 8.78/0.135 = 65 \text{ feet}$$

$$W_s = 0.135 \text{ k/ft}^3 \text{ (Section A.1)}$$

Approximate this surcharge effect by an equivalent free-column of soil from Elevation 580' to Elevation 634' (Top-of-Grade).

Summarizing soil conditions next to structure (east-west motion):

For approximately 1/3 of total structure length,

a. Soil is in contact with the auxiliary building from Elevation 562' to Elevation 634'.

For approximately 2/3 of the total structure length, the reactor buildings are adjacent to the auxiliary building.

b. For this case, soil is in contact with the auxiliary building from Elevation 562' to Elevation 580'.

c. An equivalent free soil column approximating surcharge effects exists from Elevation 580' to Elevation 634'

Calculate the areas of the structure that are in actual contact with the side soil and not in contact with side soil. The approximate structure length is 207 feet.

$$A_{Free} = 2\ (2/3\ (207)(634-580)) = 14,904\ ft^2$$

$$A_{Contact} = 2((2/3\ (207)(580-562) + 1/3\ (207)(634-562)) = 14,904\ ft^2$$

Determine embedment coefficients j and α_i from Figures III-A-3 and III-A-4 (from Reference A-3).

Total soil depth, H = 634 - 562 = 72 ft.

R_{eq} = 101 ft. (Section A.4)

H/R = 72/101 = 0.71

$a_o = 2\pi f_o$ ($f_o \approx 0.22$ - Section A.1)

$a_o = 2\pi(0.22) = 1.38$

From Figure III-A-4,

$\alpha_i = 1.75$

Based upon a weighted average depth of embedment soil surrounding the auxiliary building of 69 feet as compared to a full embedment depth of 72 feet, an average contact angle of 345^o where embedment exists was determined (see Figure III-A-3).

Using Figure III-A-3,

a. "Recommended" Curve: j = 0.48 for soil in contact with the structure.

b. "Free" Curve: j = 0.38 for a free soil column.

Weighting the "j" factors by the areas of the structure in contact with the soil and not in contact with the soil, determine j(best) by:

$$j(best) = (0.48(14,904) + 0.38(14,904))/(2(14,904))$$

$$j(best) = 0.43$$

Calculate translation embedment factor by:

$$F_{emb_1} = (1+(1.75-1)\ 2300/7100\ (0.43))$$

F_{emb_1} = 1.10 - east-west translation

The calculation of the embedment factor for damping is similar.
F_{emb} (damping) = 1.24.

A.6 EMBEDDED SOIL SPRINGS AND DASHPOTS

Final embedded soil spring:

$$K(embedded) = K_G\ F_{emb}\ (stiffness) = (3.36x10^6)(1.10)$$

where: K_G is from Section A.3
F_{emb} is from Section A.5

$K(embedded) = 3.70x10^6$k/ft - final embedded soil stiffness, east-west translation

Final embedded dashpot:

$$C(\text{embedded}) = C^* F_{emb}\ (\text{damping}) + C(5\%)$$

where

$C(5\%) = 0.1\ K_T\ (\text{embedded})/(2\pi f)$

$f = 2.75$ Hz (Section A.1)

$k_1 = 0.96$ (Section A.1)

$C^* = 1.22 \times 10^5$ k-ft/sec (Section A.4)

$F_{emb}\ (\text{damping}) = 1.24$ (Section A.5)

$K_T\ (\text{embedded}) = K(\text{embedded})/k_1$

$$C(\text{embedded}) = 1.22 \times 10^5 (1.24) + 0.1\ (3.70 \times 10^6)/(0.96(2)\,\pi\,(2.75))$$

$C(\text{embedded}) = 1.73 \times 10^6$ k-sec/ft. - final embedded dashpot, east-west translation

FIGURE III-A-1. EAST-WEST TRANSLATION SOIL IMPEDANCE
INTERMEDIATE CASE LAYERED SOIL PROFILE

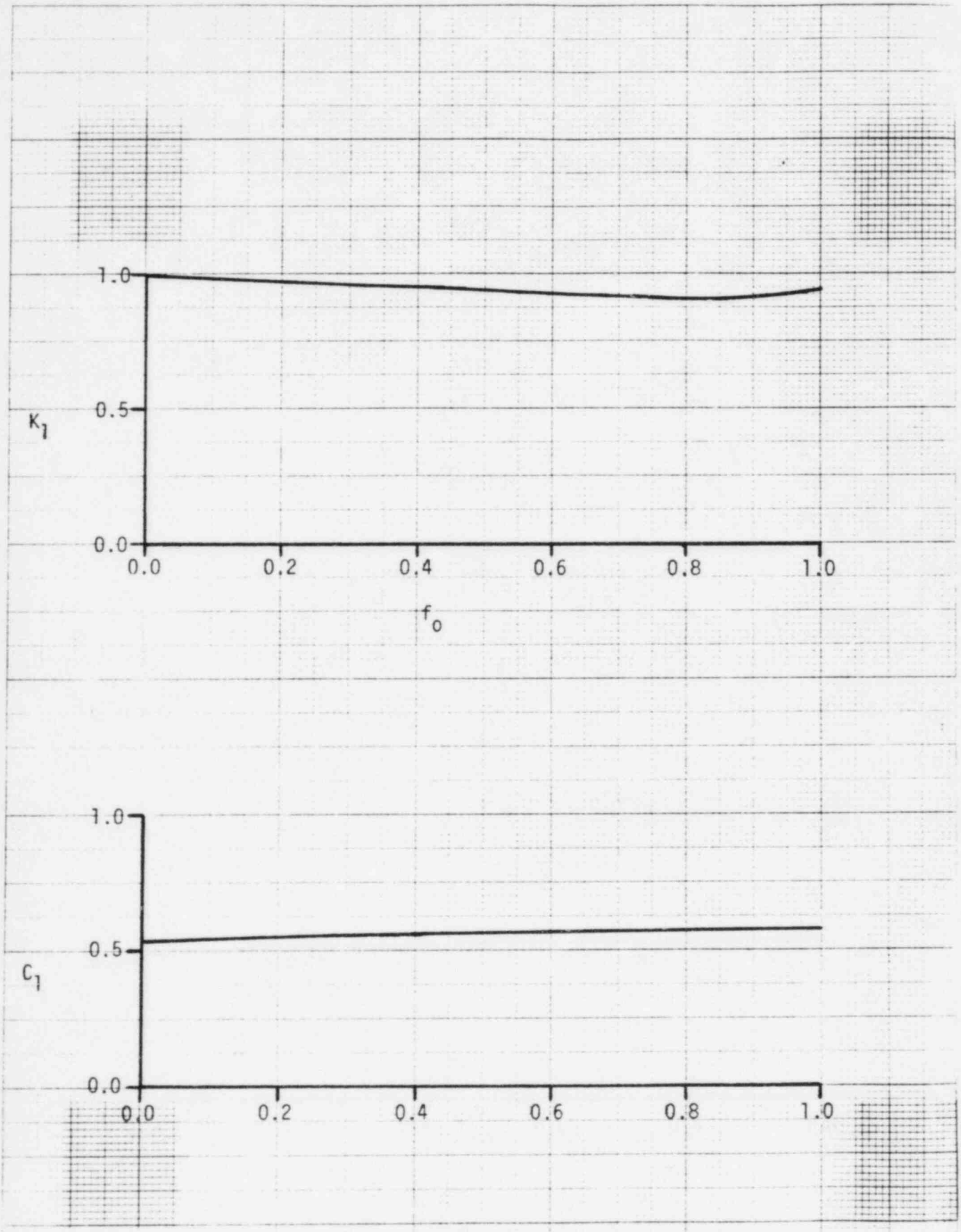

FIGURE III-A-2. HORIZONTAL TRANSLATION STIFFNESS AND DAMPING COEFFICIENTS FOR A CIRCULAR FOUNDATION ON AN ELASTIC HALF-SPACE (FROM REFERENCE A-2)

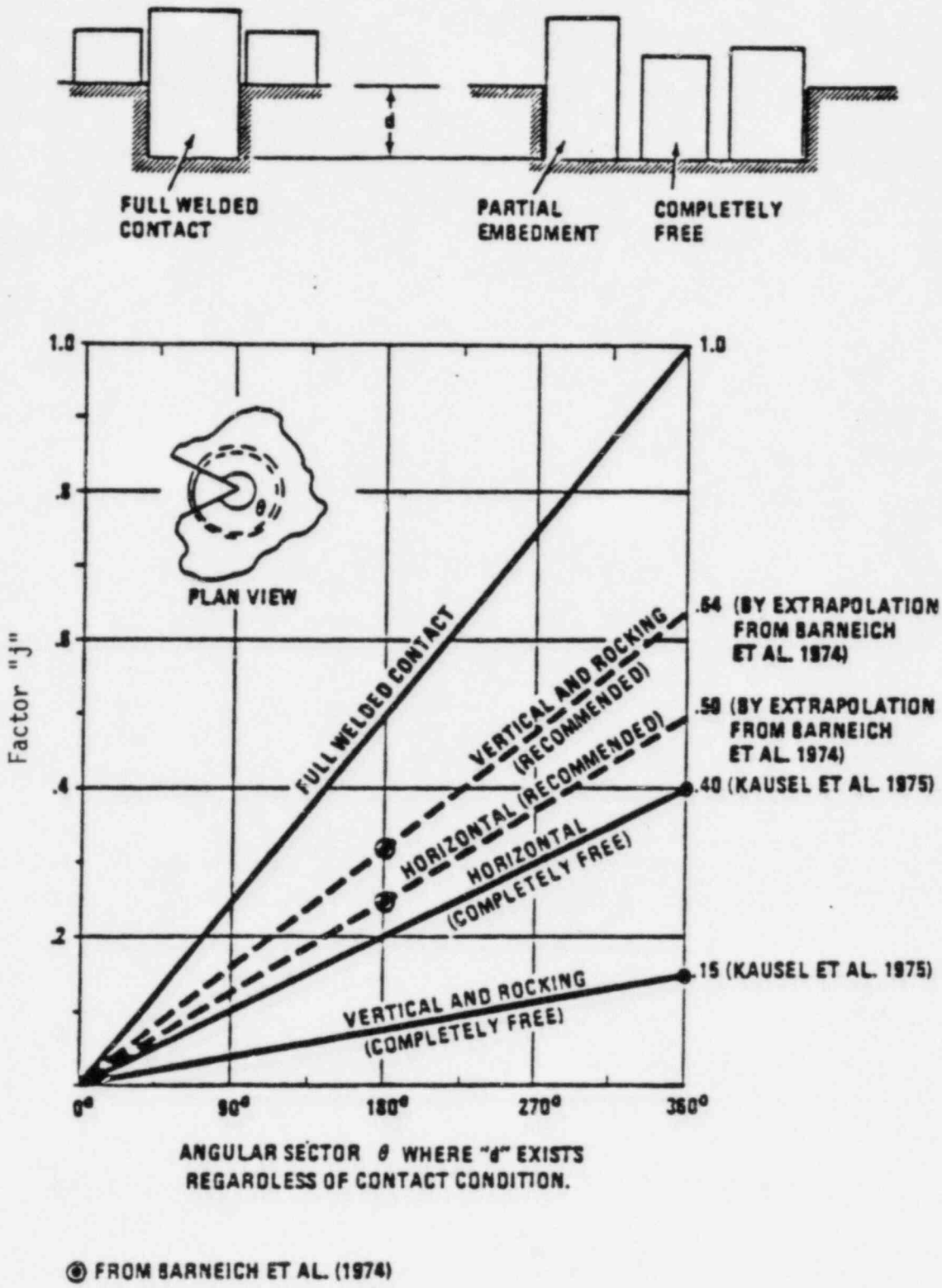

FIGURE III-A-3. EMBEDDED FOUNDATIONS, IMPEDANCE CORRECTION FACTOR j for SHALLOW EMBEDMENT (from Reference A-3)

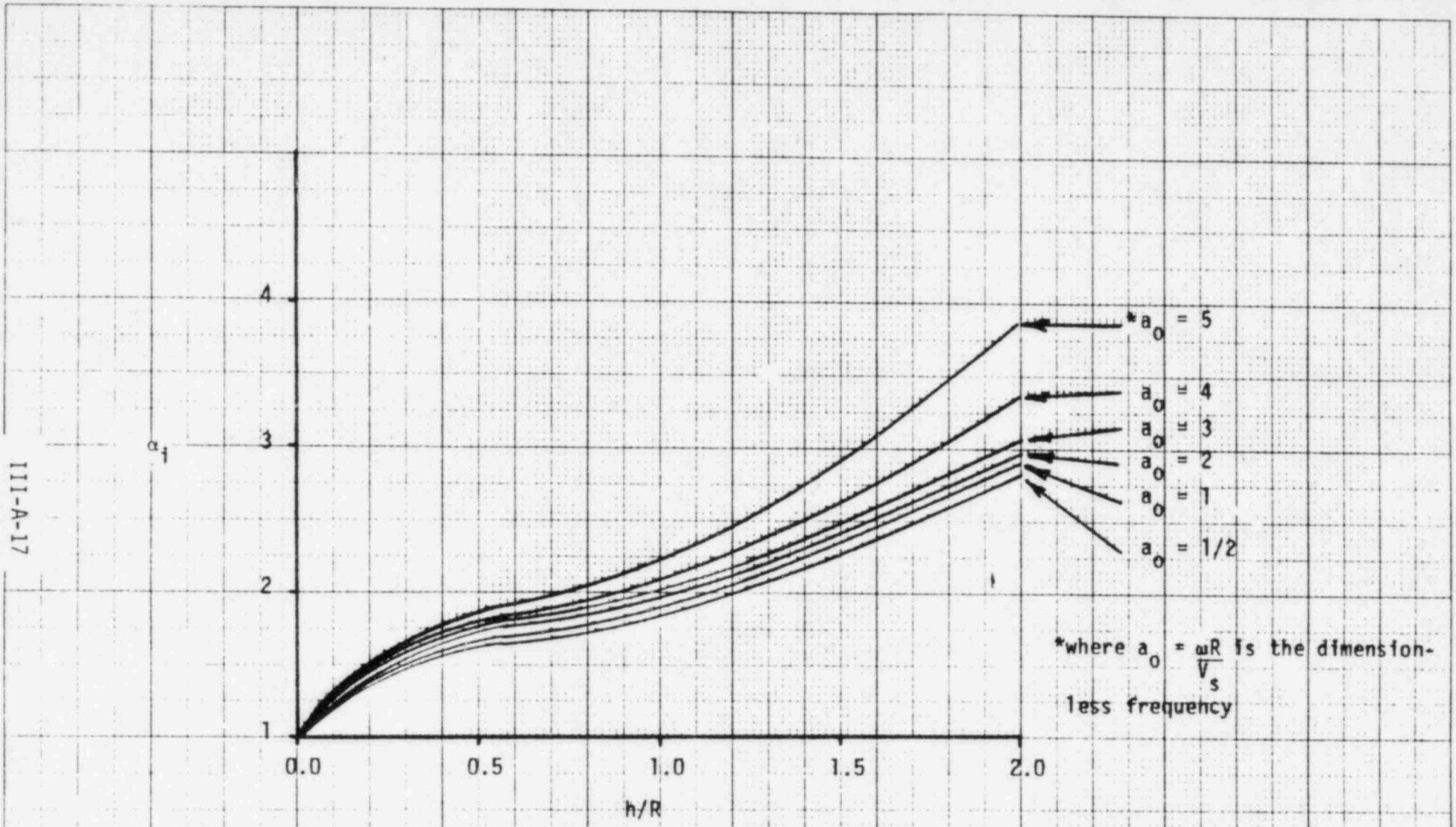

FIGURE III-A-4. NORMALIZED EMBEDMENT STIFFNESS COEFFICIENT, α_1

REFERENCES

A-1. Wesley, D. A., Campbell, R. D., Kennedy, R. P., Kincaid, R. H., and P. S. Hashimoto, "Seismic Margin Review, Midland Energy Center, Volume I, Methodology and Criteria", February, 1983, SMA 13701.05R003 (Volume I).

A-2. Kausel, E., and R. Ushijima, "Vertical and Torsional Stiffness of Cylindrical Footings", Massachusetts Institute of Technology, Research Report R79-6, February, 1979.

A-3. Bechtel submittal to NRC "Auxiliary Building Seismic Model Revision 3 for Midland Plants 1 and Consumers Power Company", September 28, 1981.

APPENDIX III-B

AUXILIARY BUILDING IN-STRUCTURE RESPONSE SPECTRA

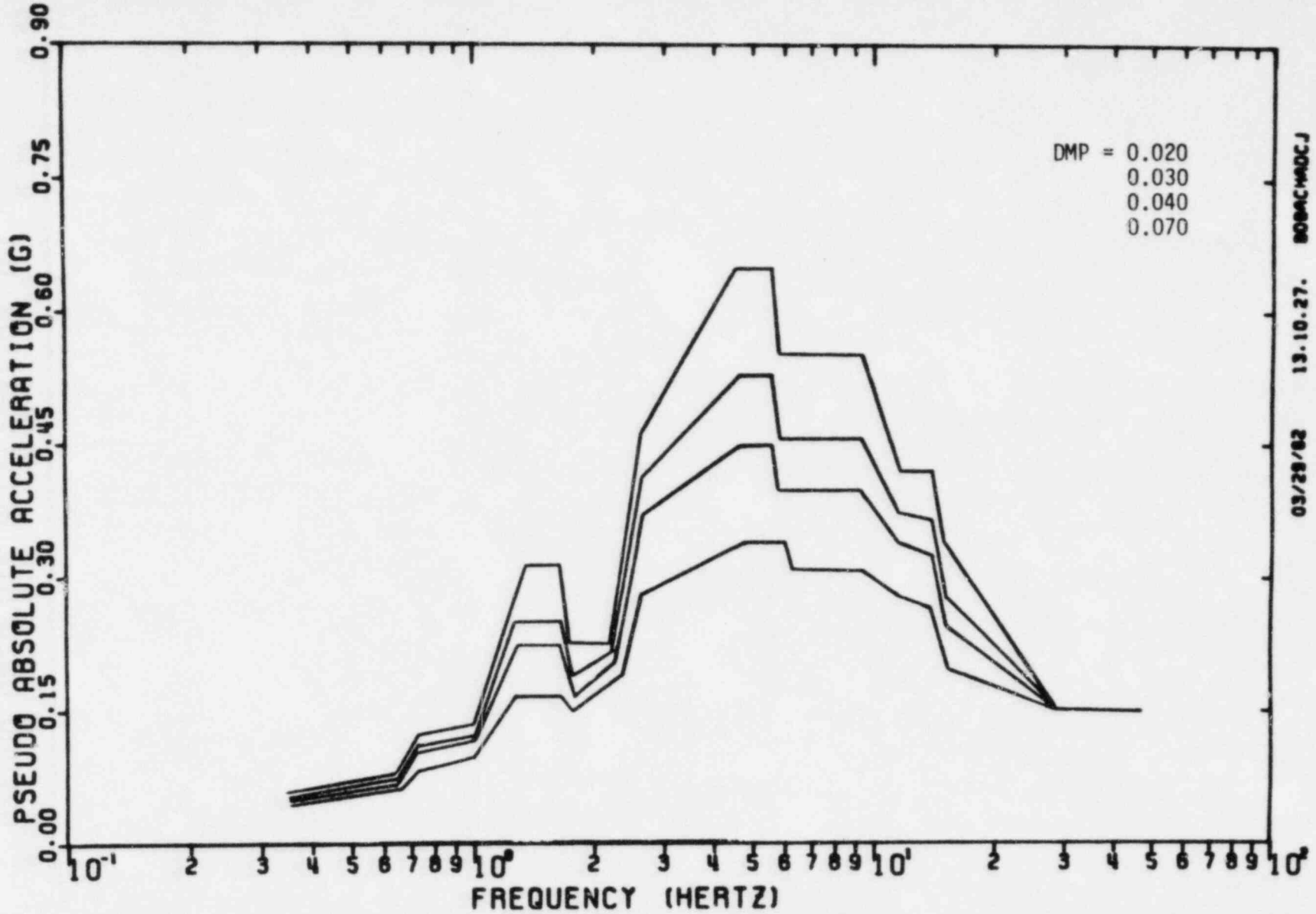

FIGURE III-B-1. Enveloped SRSS Combined Response Spectra
Main Auxiliary Building, Elevation 565' - 0"
North-South Direction

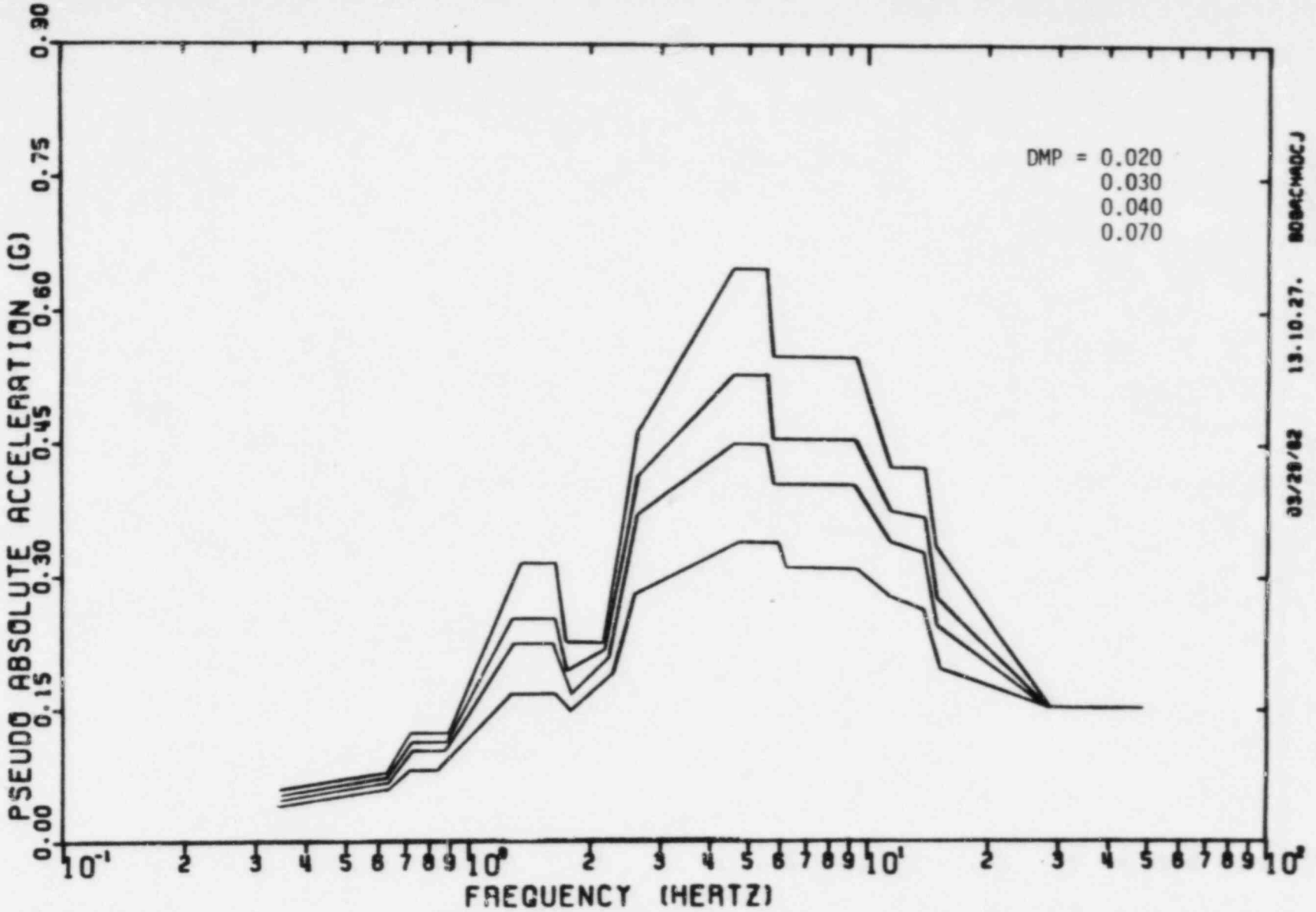

FIGURE III-B-2. Enveloped SRSS Combined Response Spectra
Main Auxiliary Building, Elevation 565' - 0"
East-West Direction

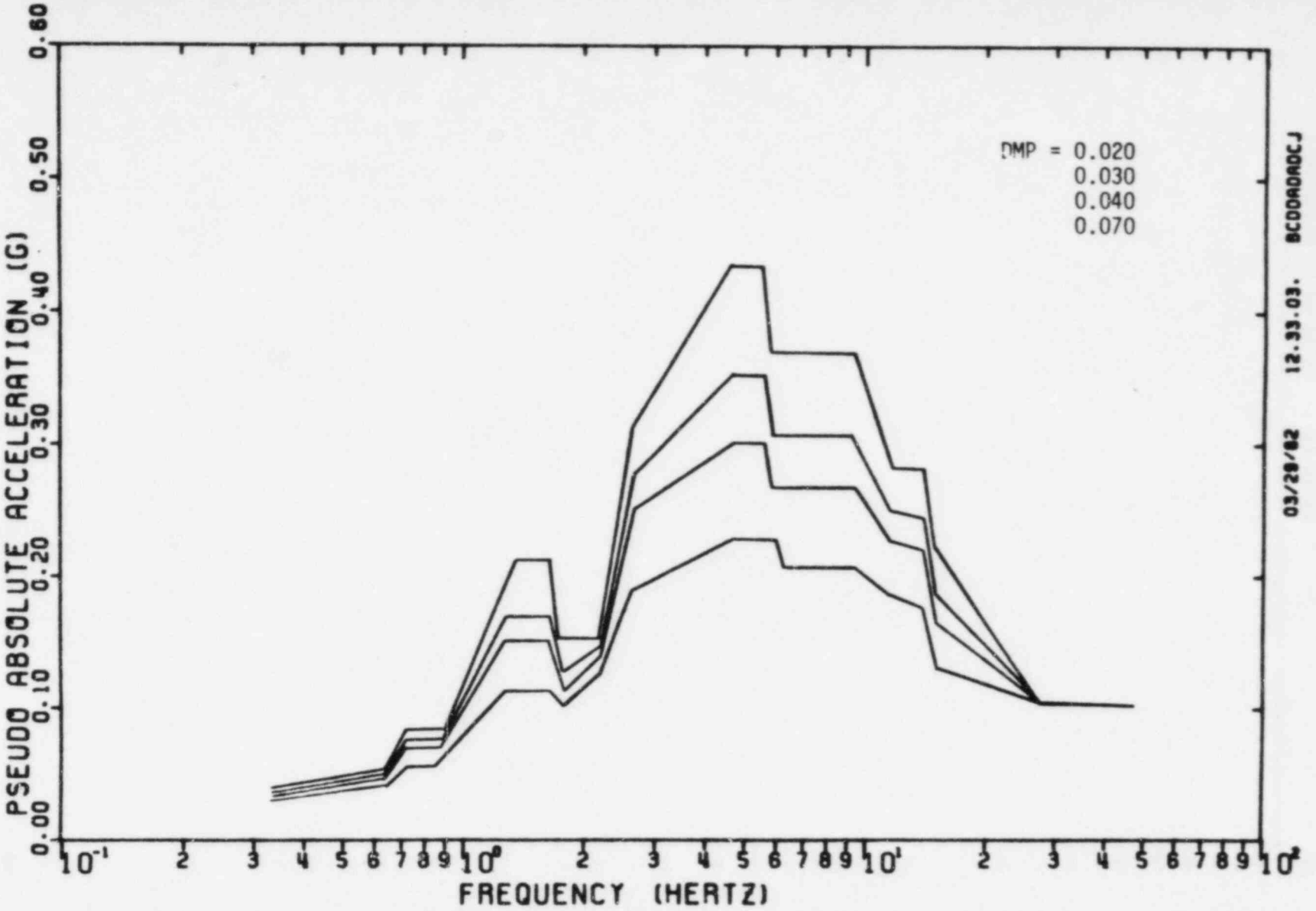

FIGURE III-B-3. Enveloped SRSS Combined Response Spectra
Main Auxiliary Building, Elevation 565'-0"
Vertical Direction

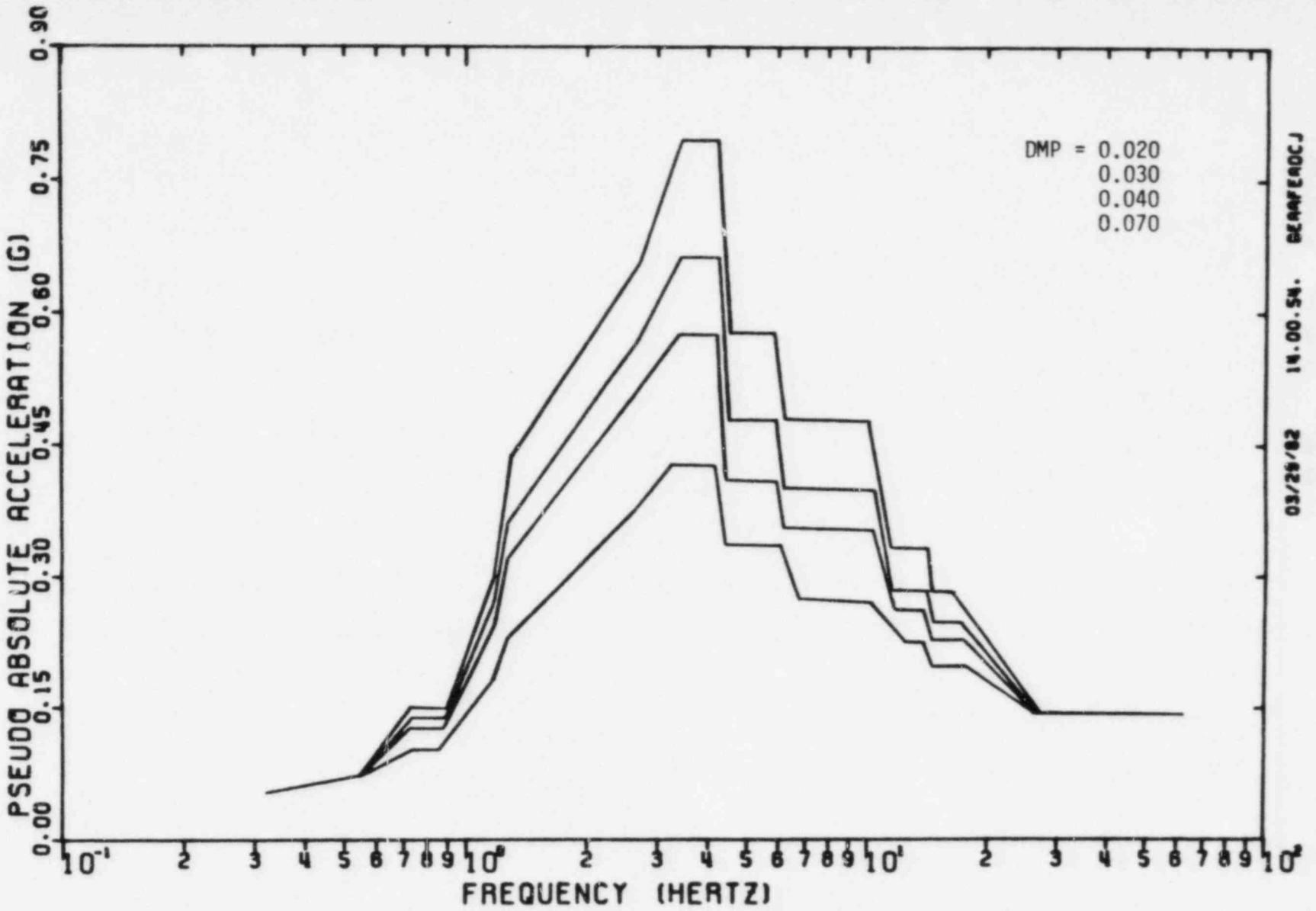

FIGURE III-B-4. Enveloped SRSS Combined Response Spectra
Main Auxiliary Building, Elevation 584'-0"
North-South Direction

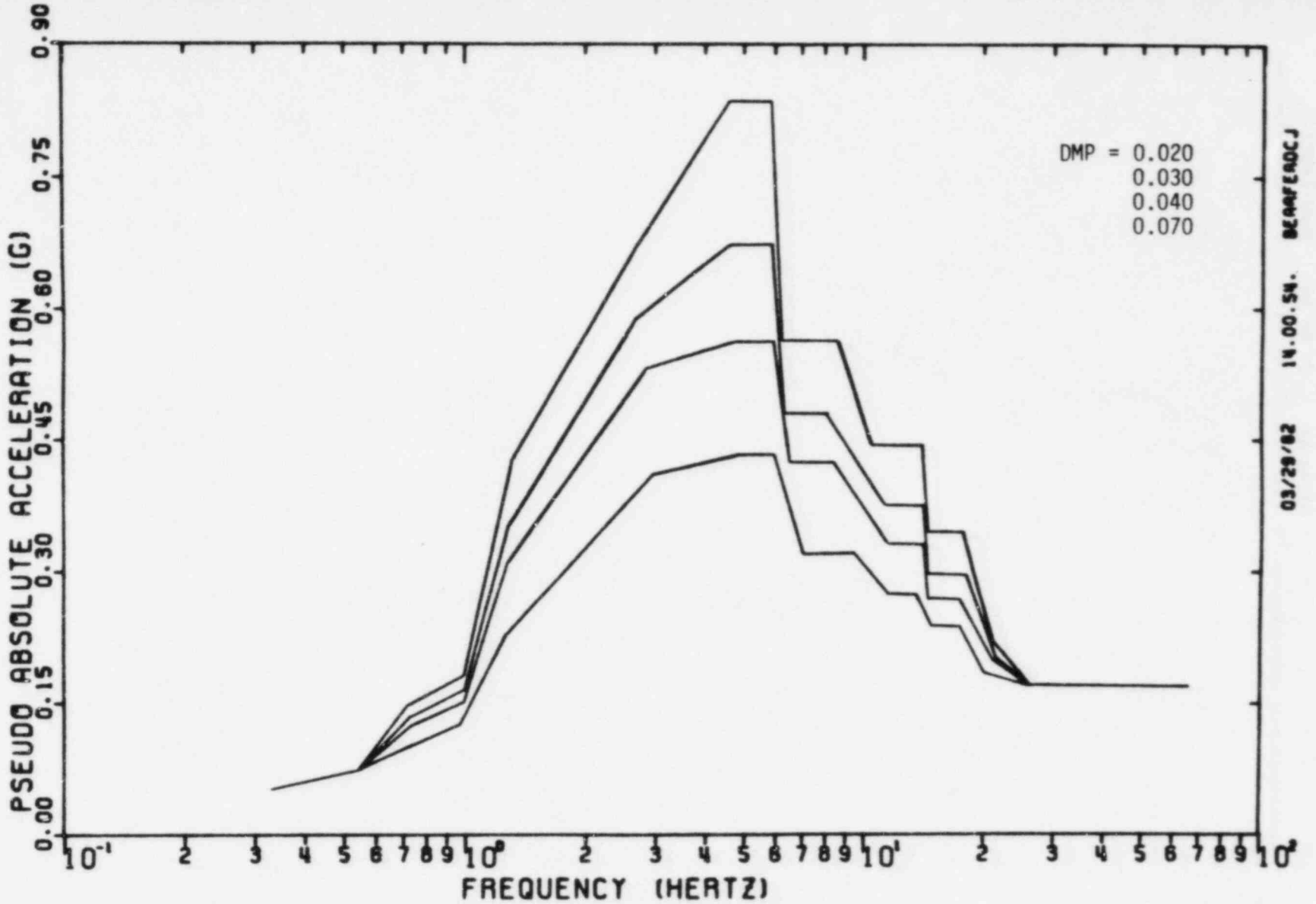

FIGURE III-B-5. Enveloped SRSS Combined Response Spectra
Main Auxiliary Building, Elevation 584' - 0"
East-West Direction

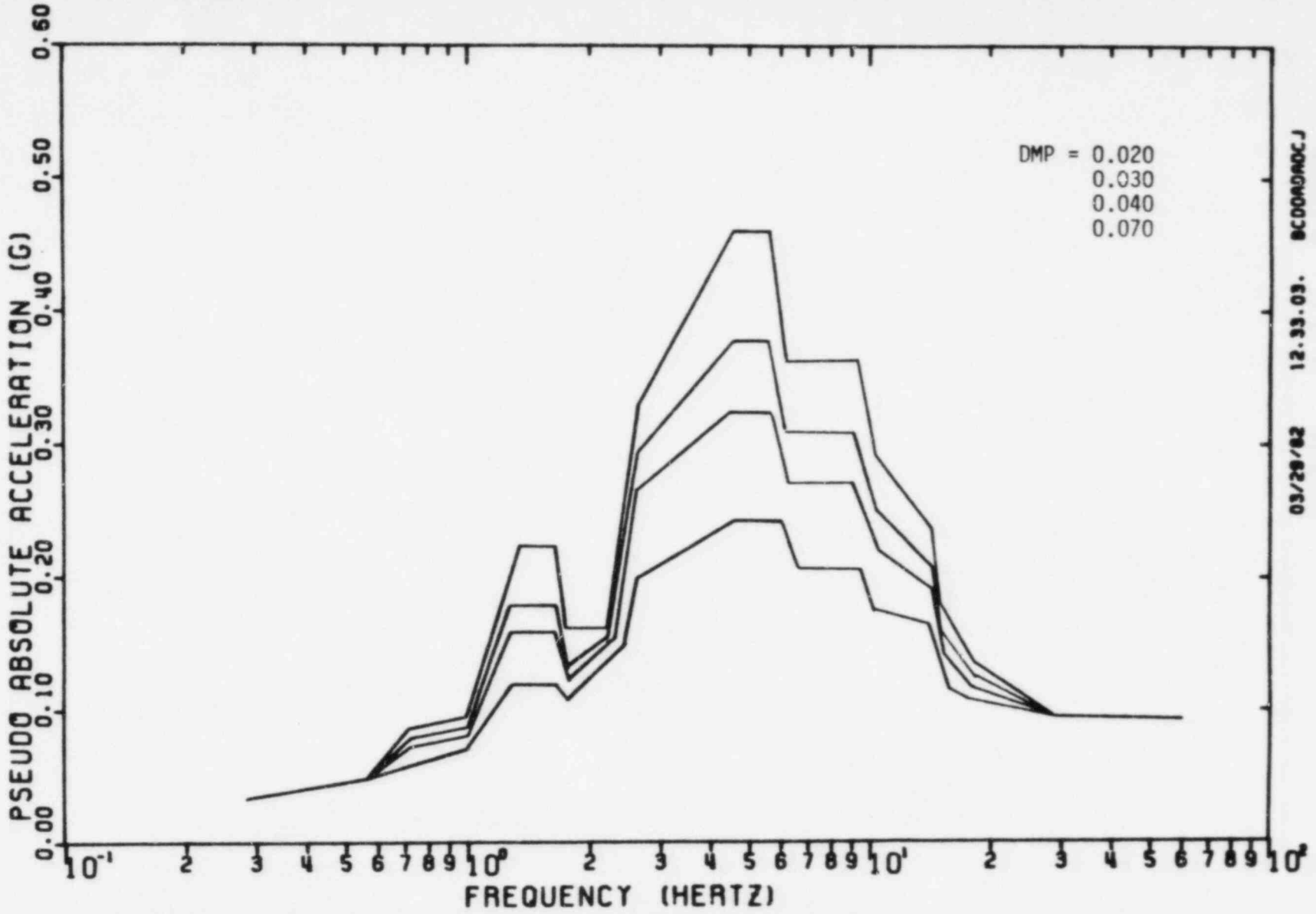

FIGURE III-B-6. Enveloped SRSS Combined Response Spectra
Main Auxiliary Building, Elevation 584'-0"
Vertical Direction

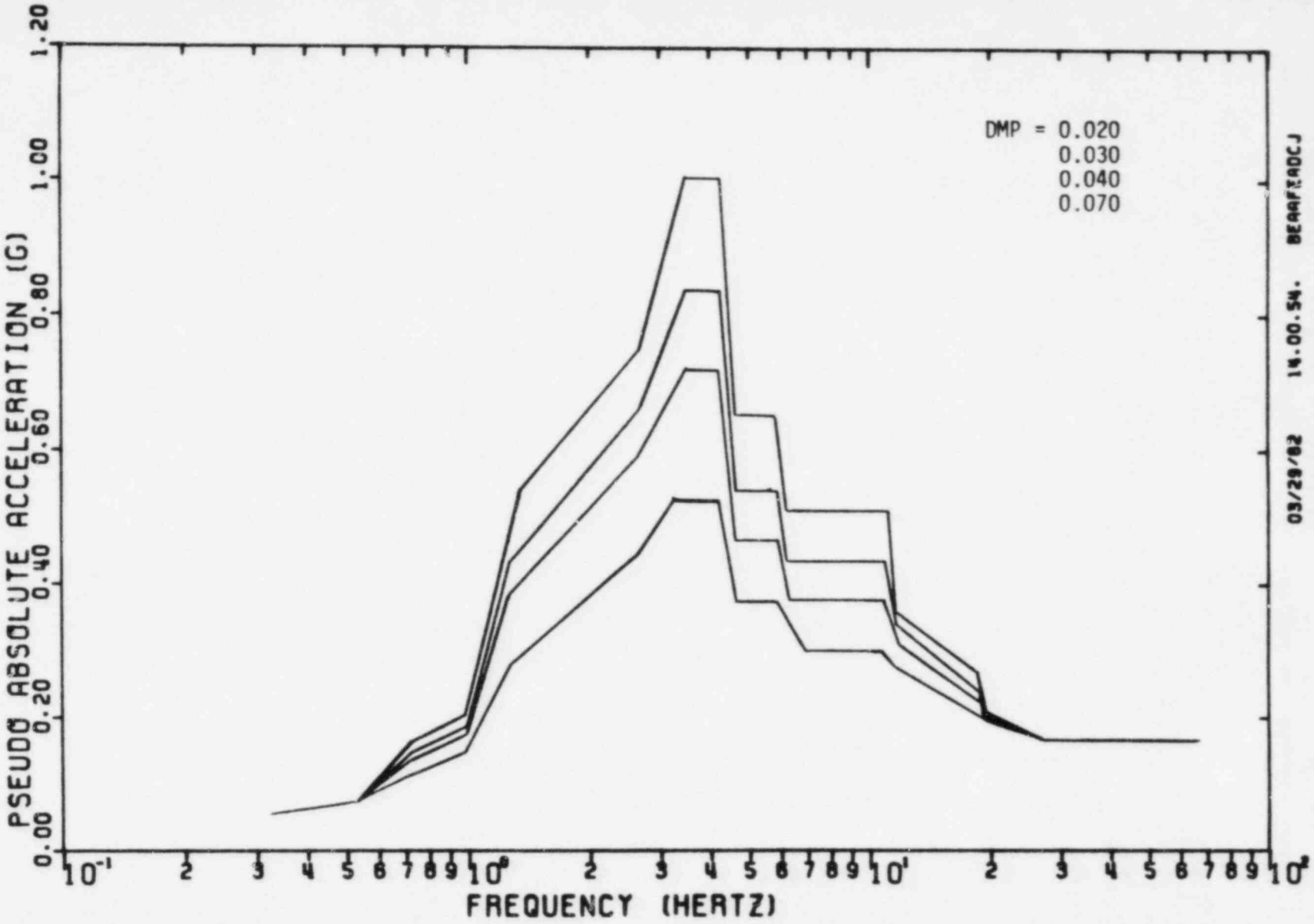

FIGURE III-B-7. Enveloped SRSS Combined Response Spectra
Main Auxiliary Building, Elevation 599' - 0"
North-South Direction

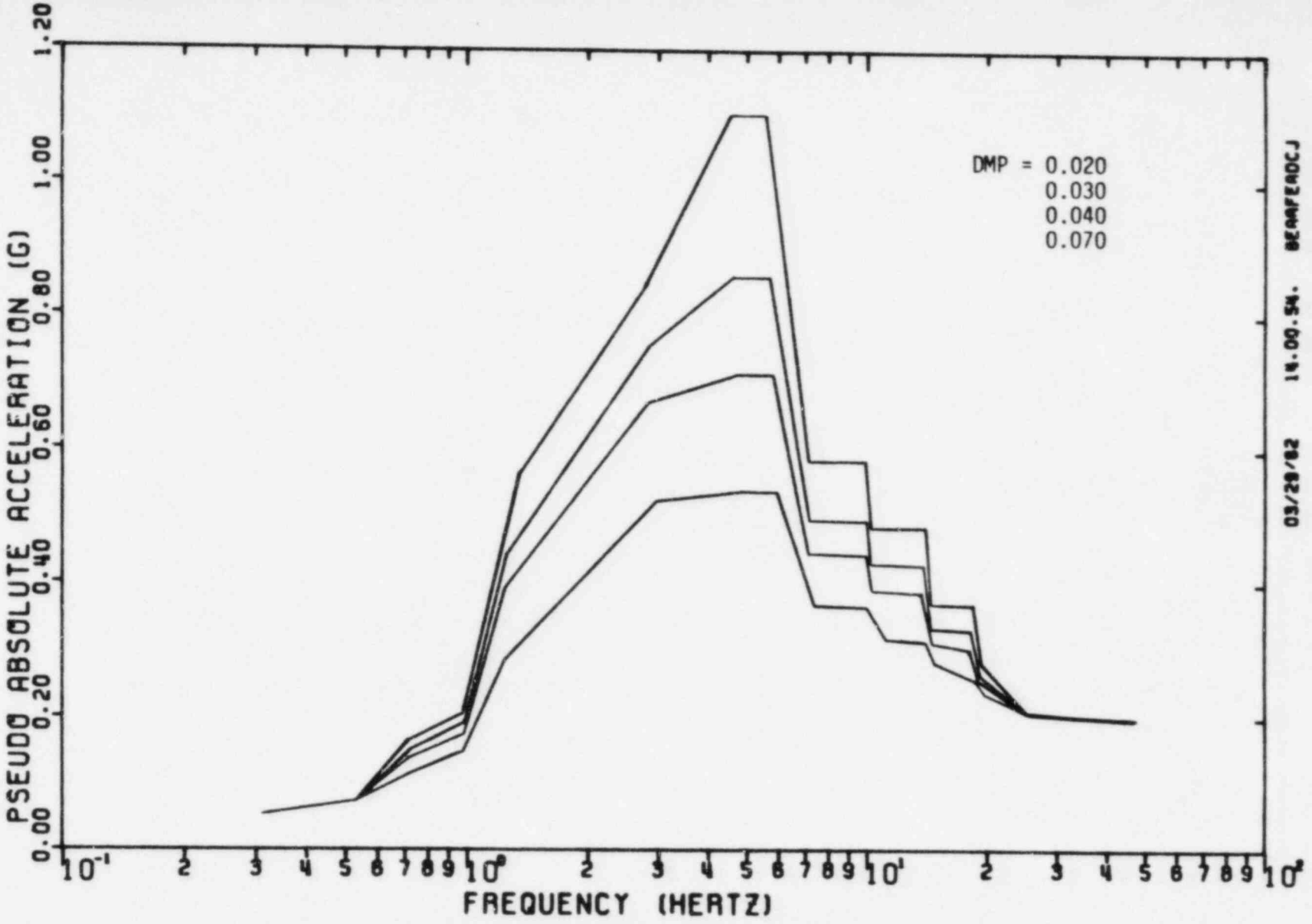

FIGURE III-B-8. Enveloped SRSS Combined Response Spectra
Main Auxiliary Building Elevation 599' - 0"
East-West Direction

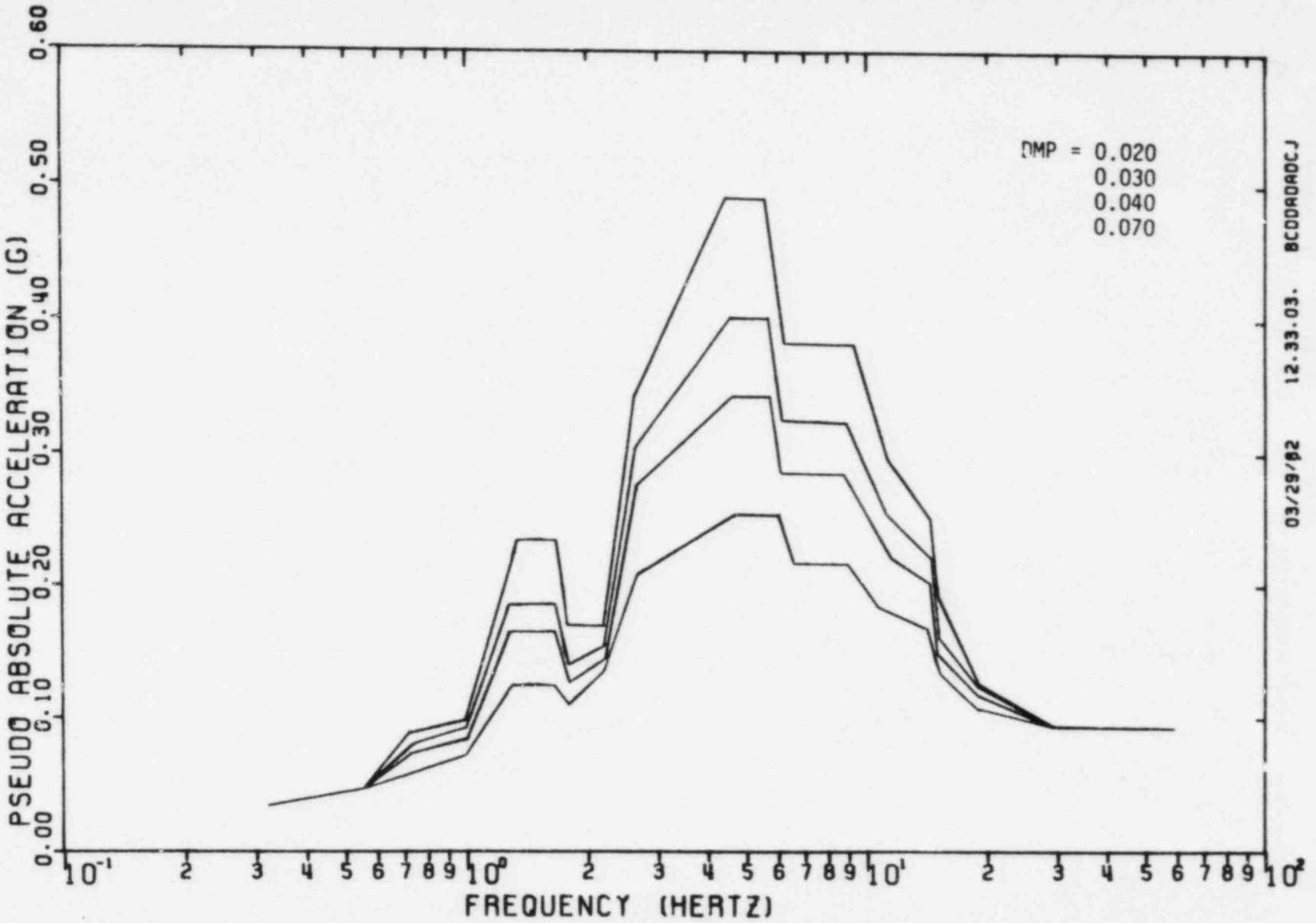

FIGURE III-B-9. Enveloped SRSS Combined Response Spectra
Main Auxiliary Building, Elevation 599'-0"
Vertical Direction

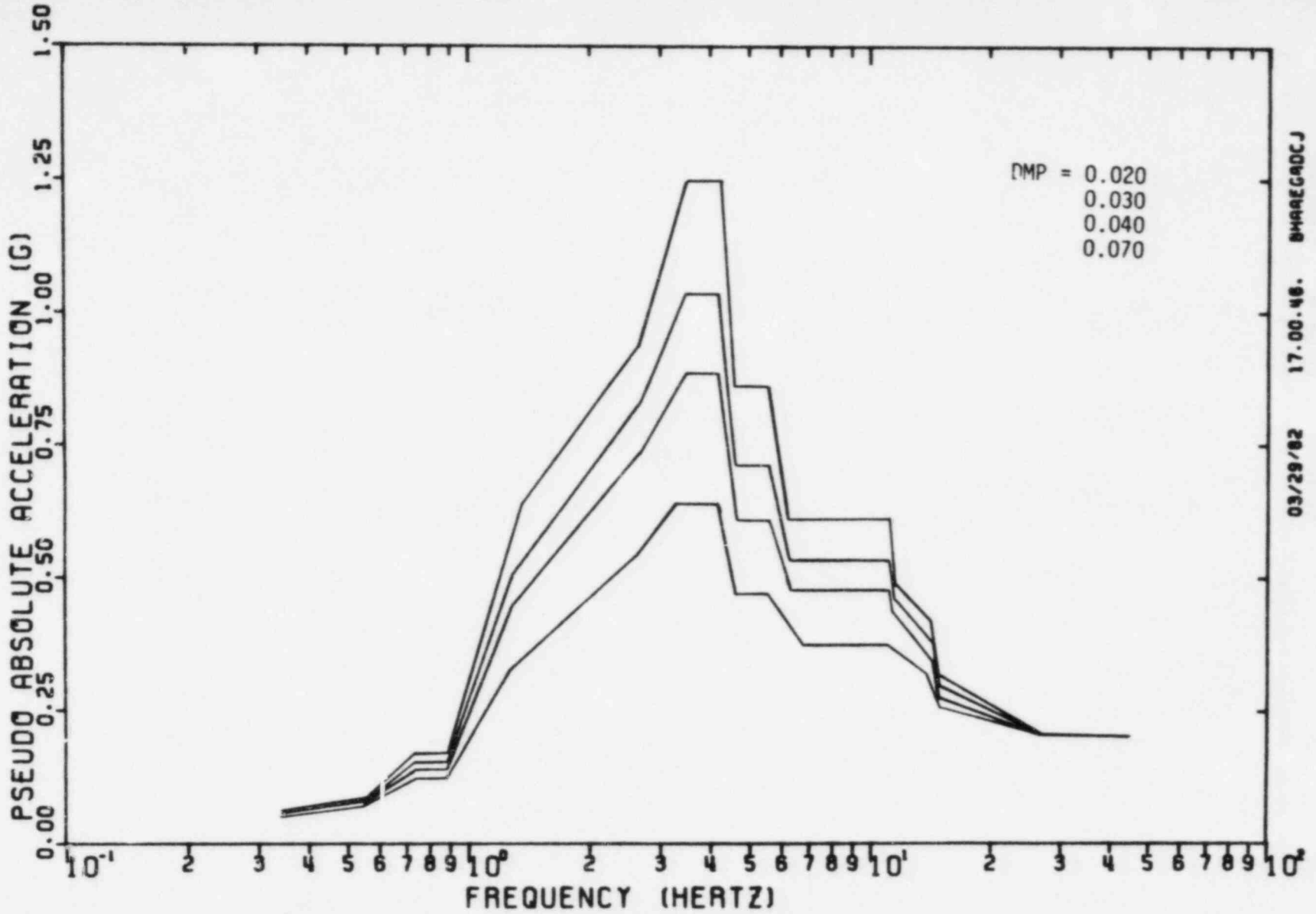

FIGURE III-B-10. Enveloped SRSS Combined Response Spectra
Main Auxiliary Building, Elevation 614'-0"
North-South Direction

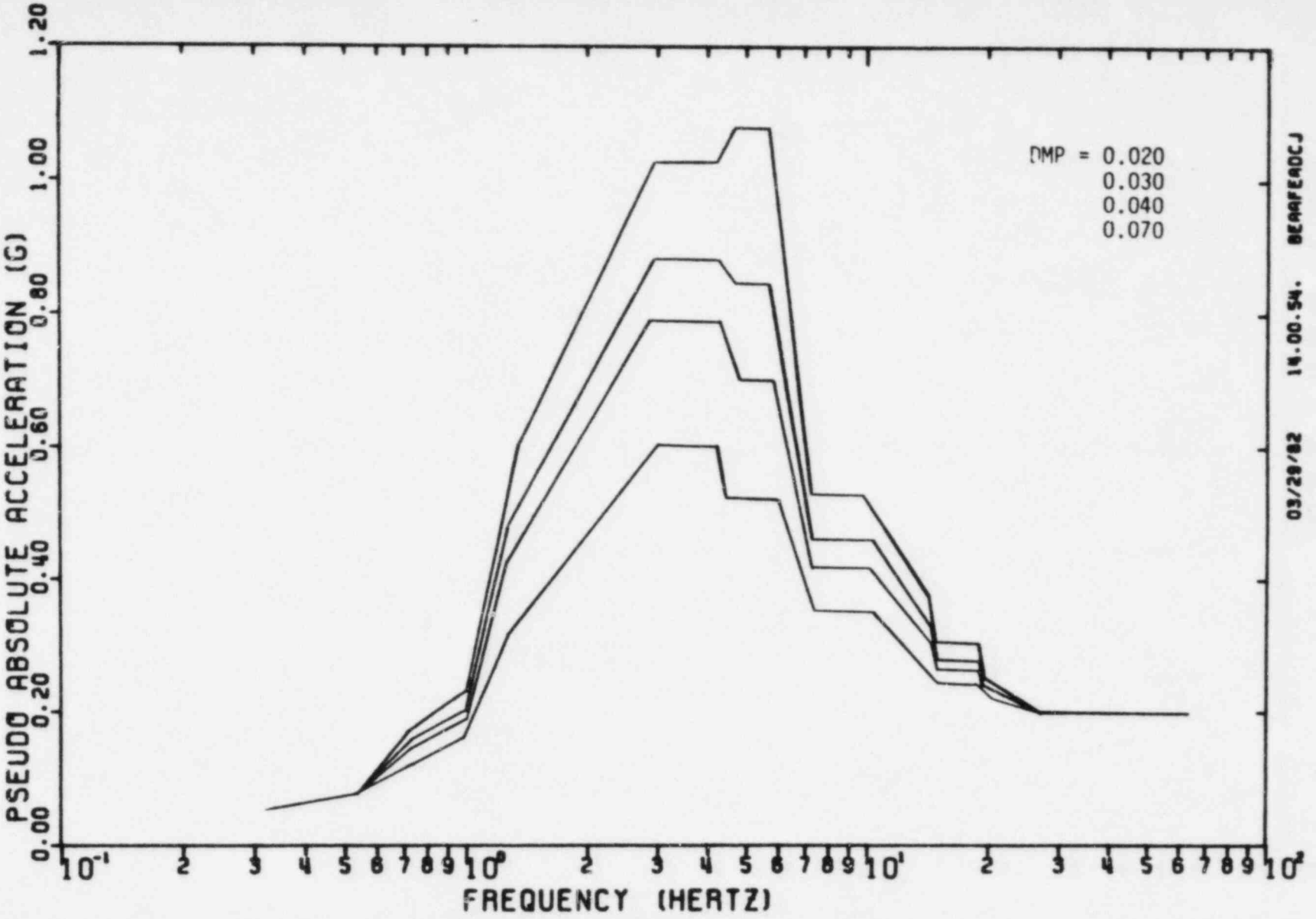

FIGURE III-B-11. Enveloped SRSS Combined Response Spectra
Main Auxiliary Building, Elevation 614'-0"
East-West Direction

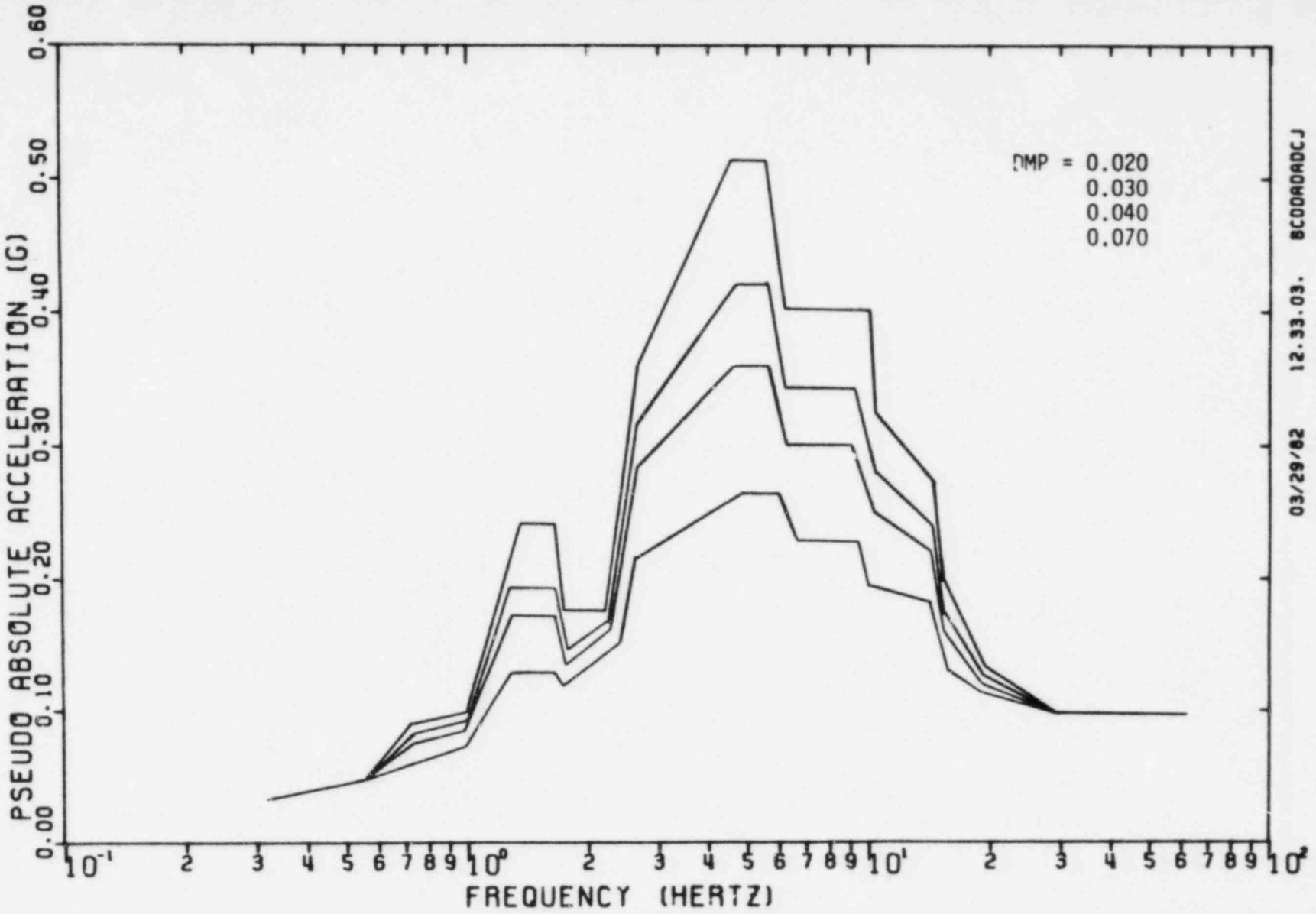

FIGURE III-B-12. Enveloped SRSS Combined Response Spectra
Main Auxiliary Building, Elevation 614'-0"
Vertical Direction

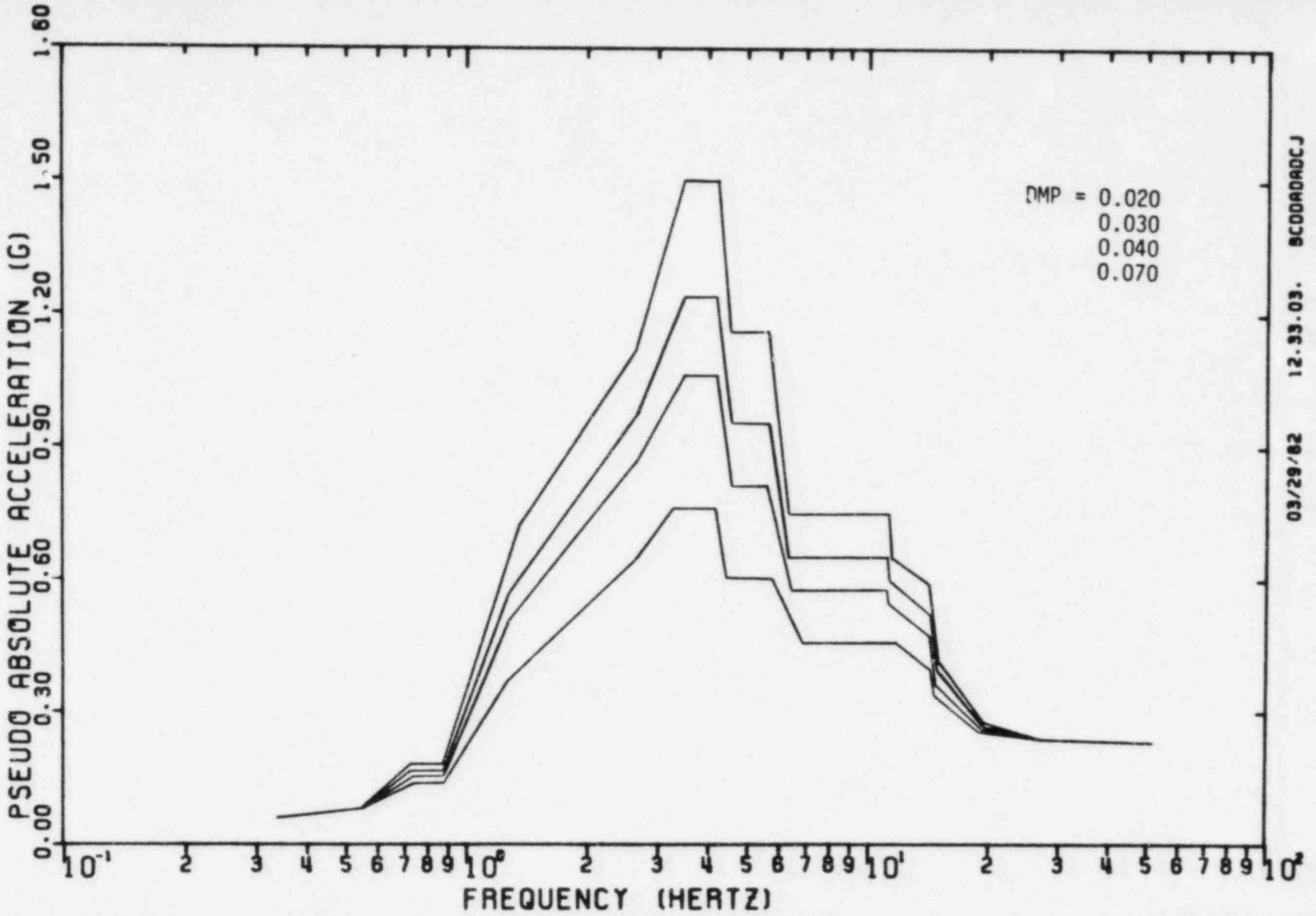

FIGURE III-B-13. Enveloped SRSS Combined Response Spectra
Main Auxiliary Building, Elevation 634'-6"
North-South Direction

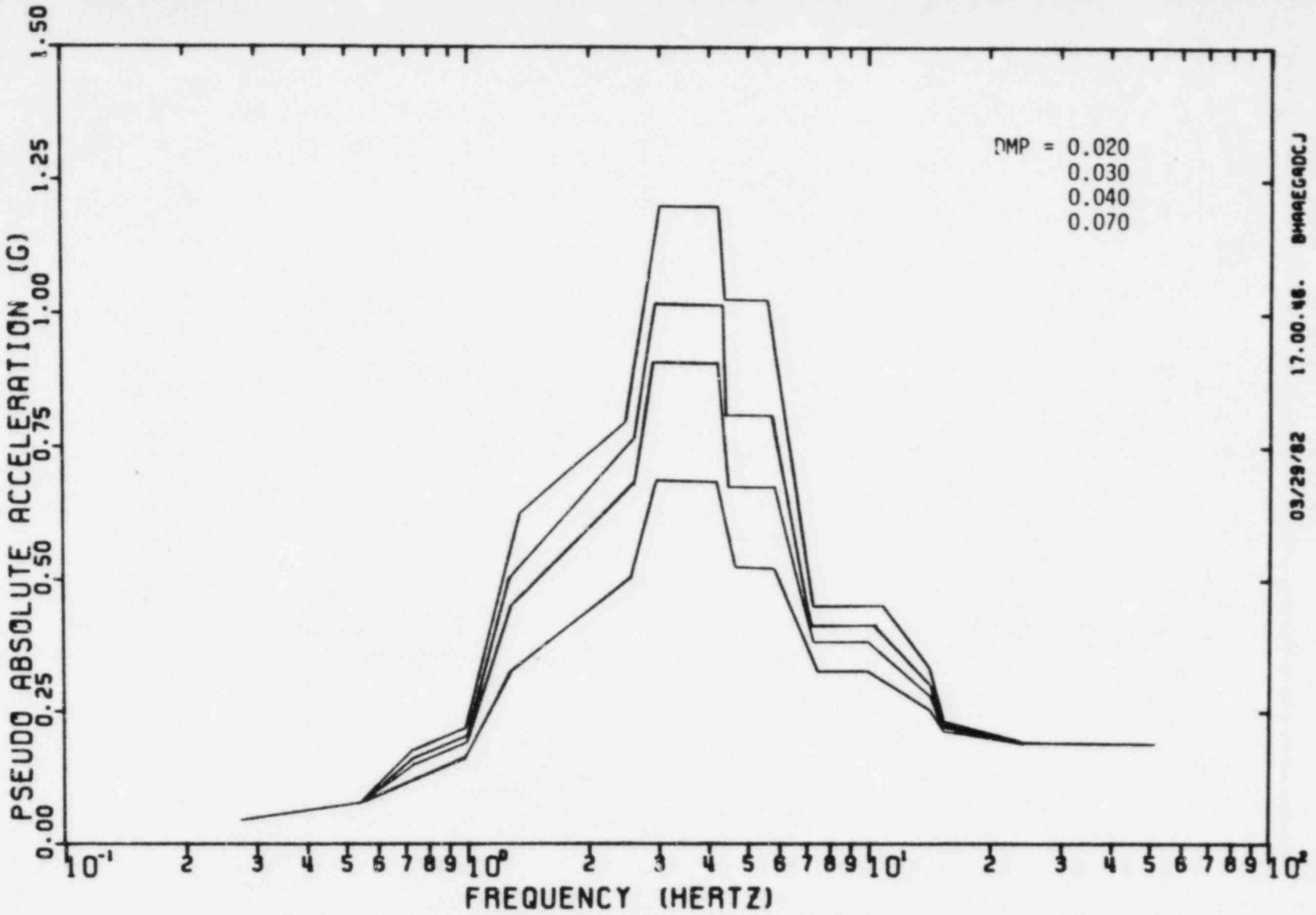

FIGURE III-B-14. Enveloped SRSS Combined Response Spectra
Main Auxiliary Building, Elevation 634'-6"
East-West Direction

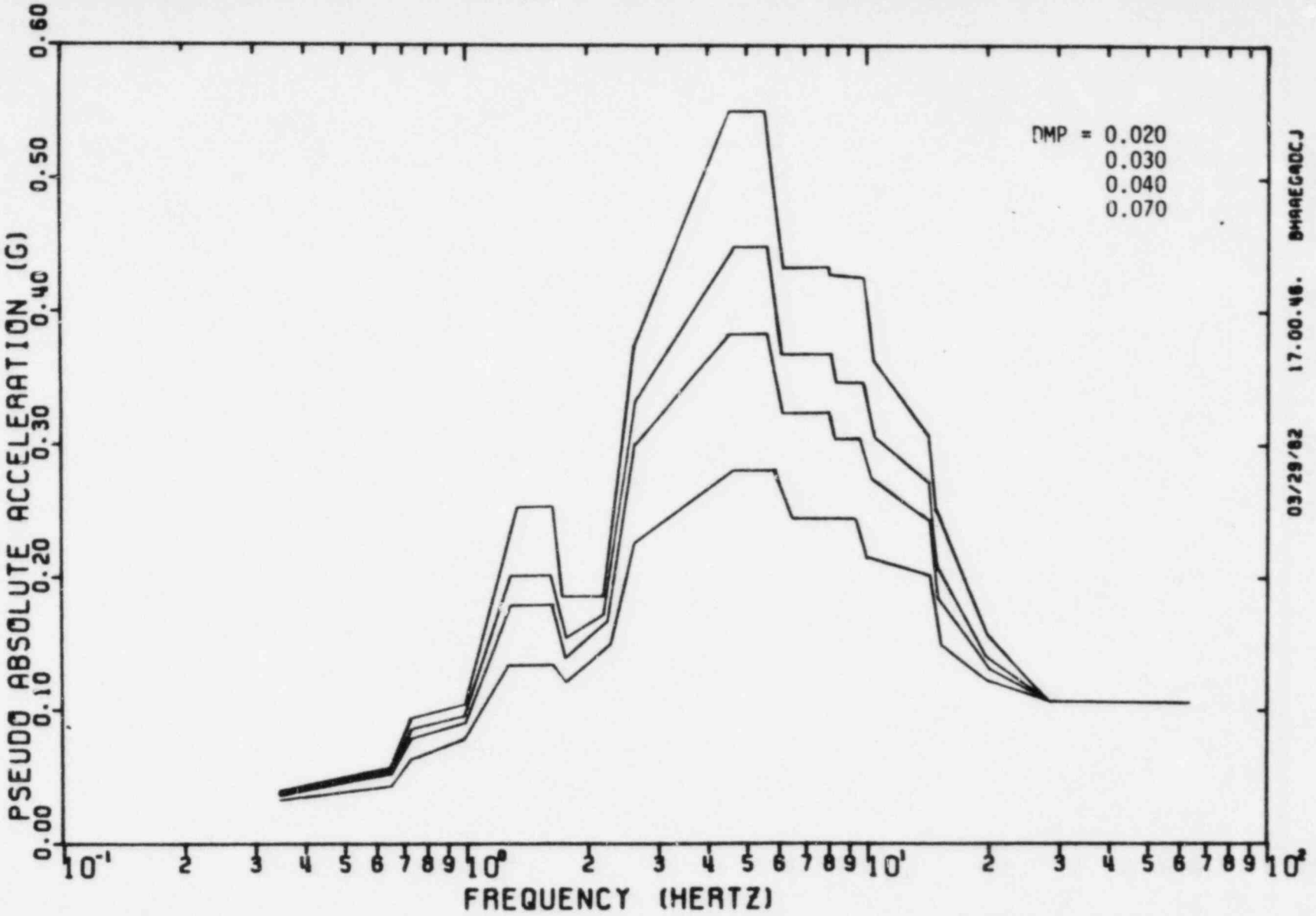

FIGURE III-B-15. Enveloped SRSS Combined Response Spectra
Main Auxiliary Building, Elevation 634'-6"
Vertical Direction

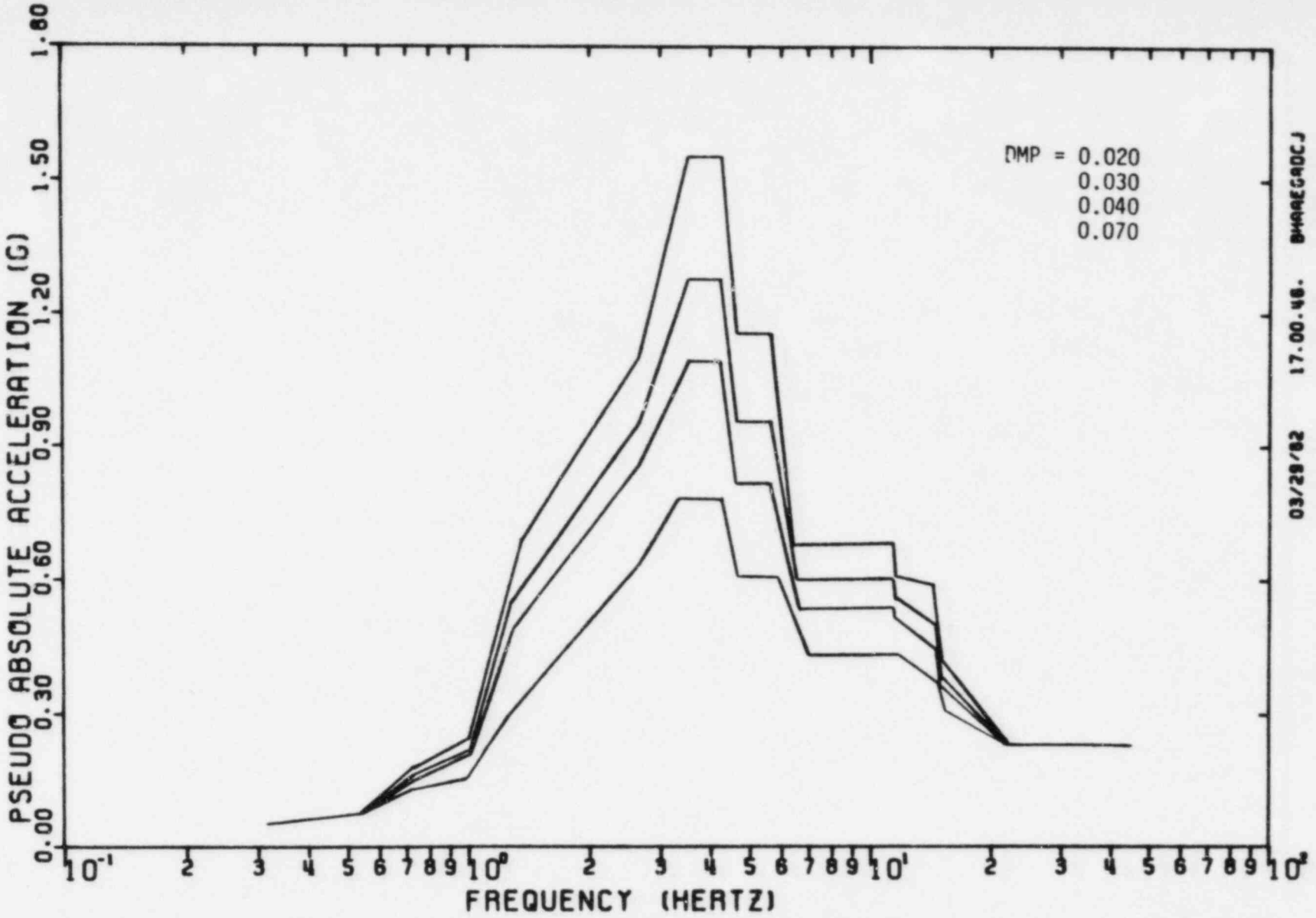

FIGURE III-B-16. Enveloped SRSS Combined Response Spectra
Main Auxiliary Building, Elevation 646'-0"
North-South Direction

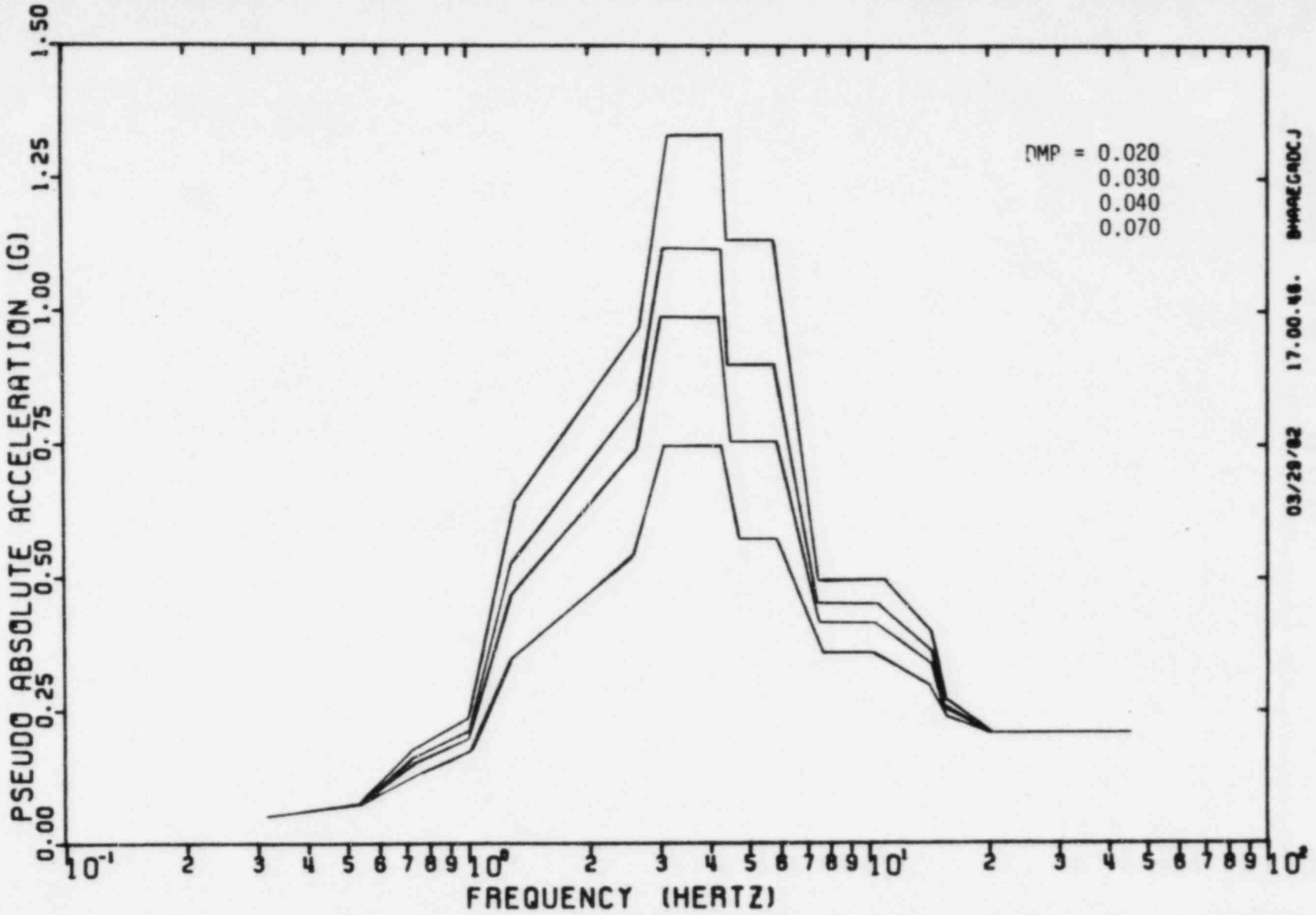

FIGURE III-B-17. Enveloped SRSS Combined Response Spectra
Main Auxiliary Building, Elevation 646'-0"
East-West Direction

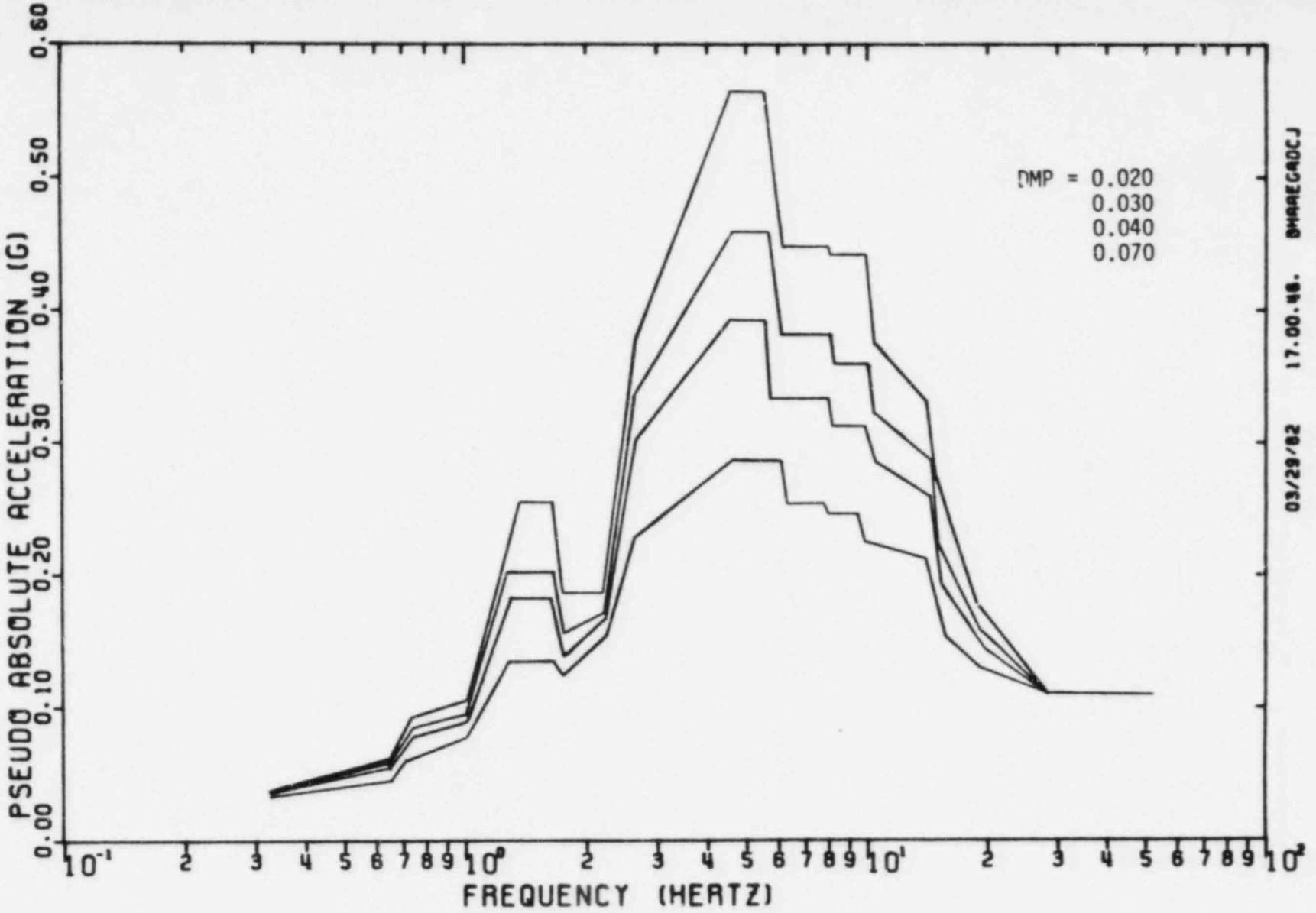

FIGURE III-B-18. Enveloped SRSS Combined Response Spectra
Main Auxiliary Building, Elevation 646'-0"
Vertical Direction

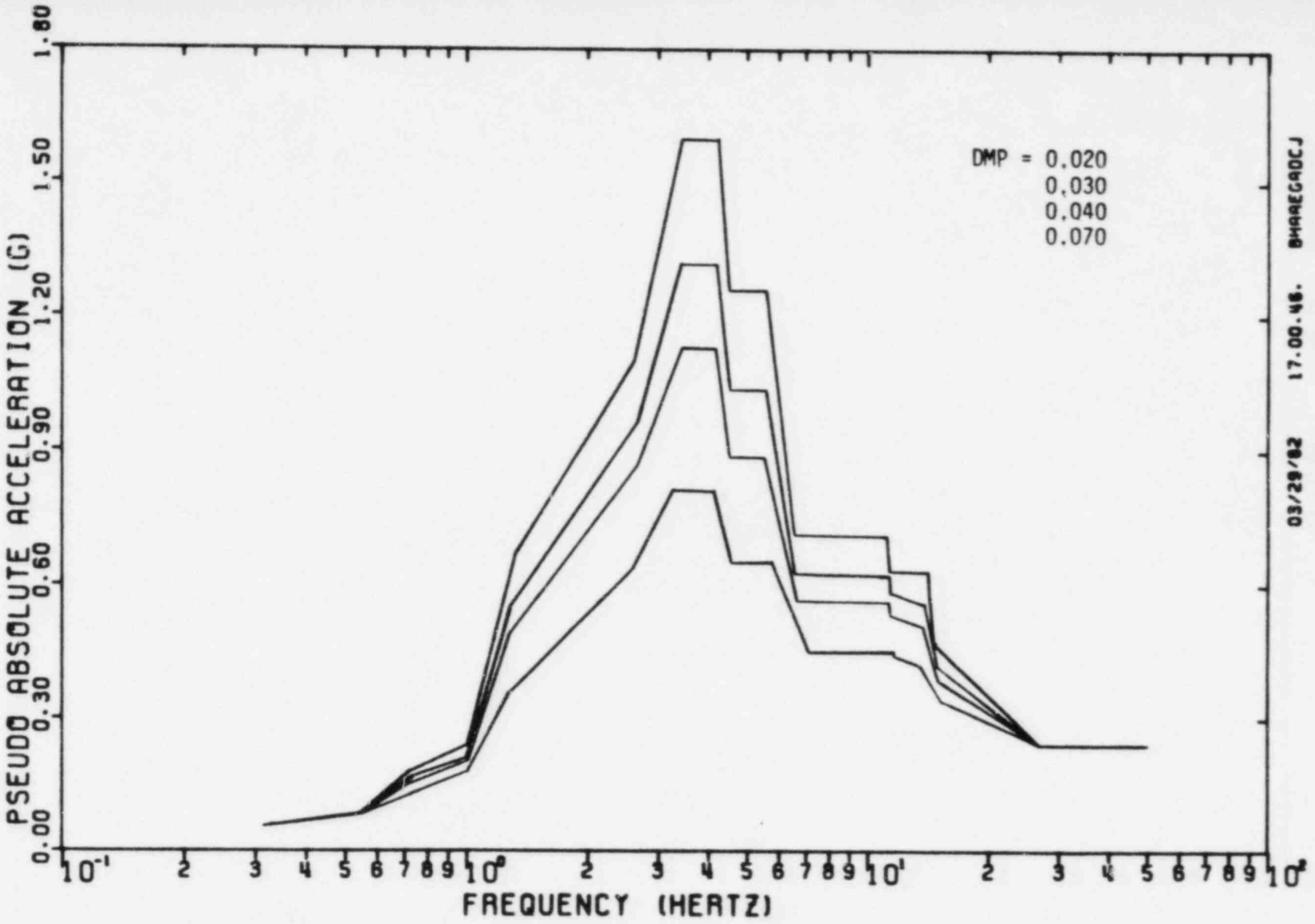

FIGURE III-B-19. Enveloped SRSS Combined Response Spectra
Main Auxiliary Building, Elevation 659' - 0"
North-South Direction

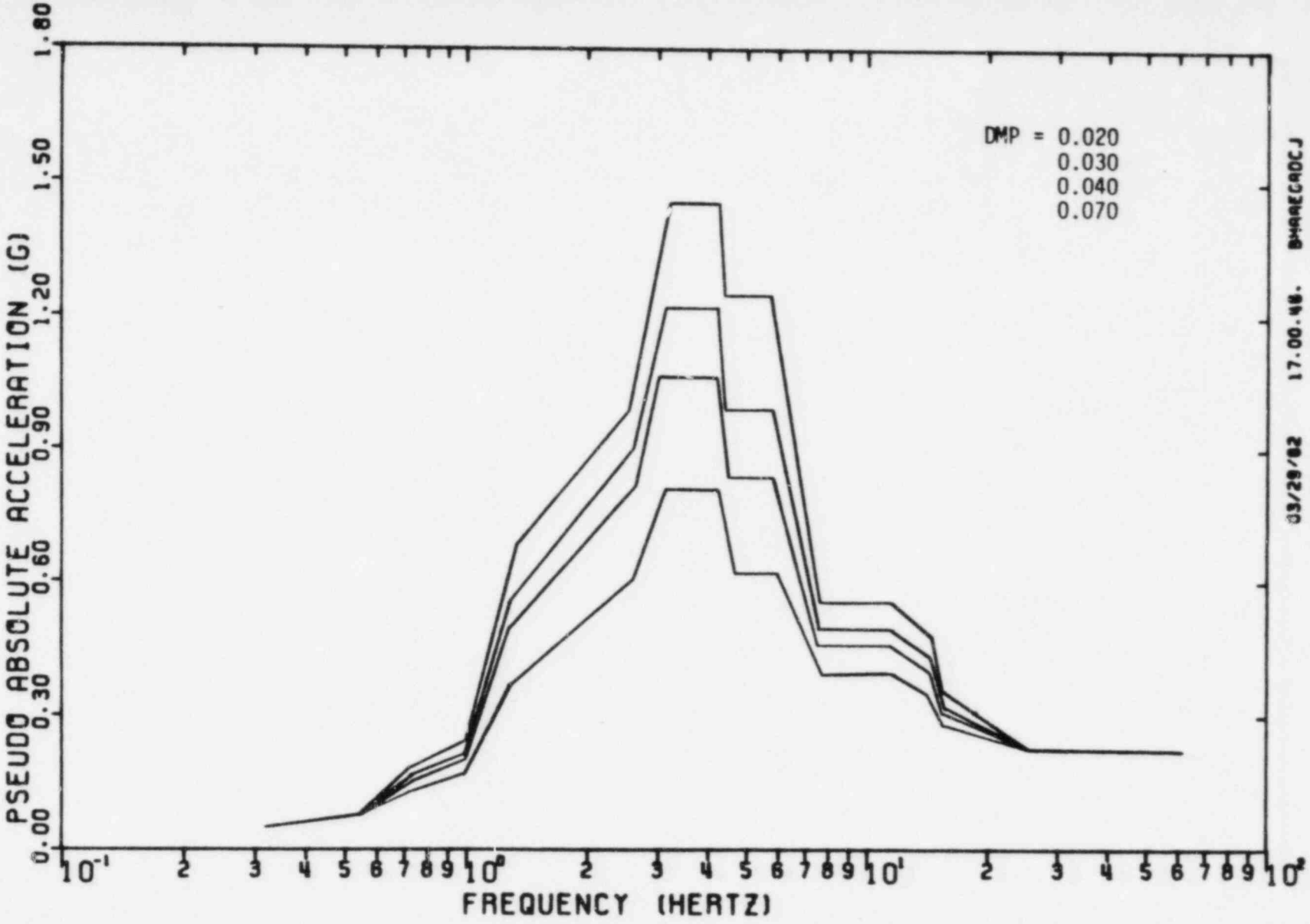

FIGURE III-B-20. Enveloped SRSS Combined Response Spectra
Main Auxiliary Building, Elevation 659' - 0"
East-West Direction

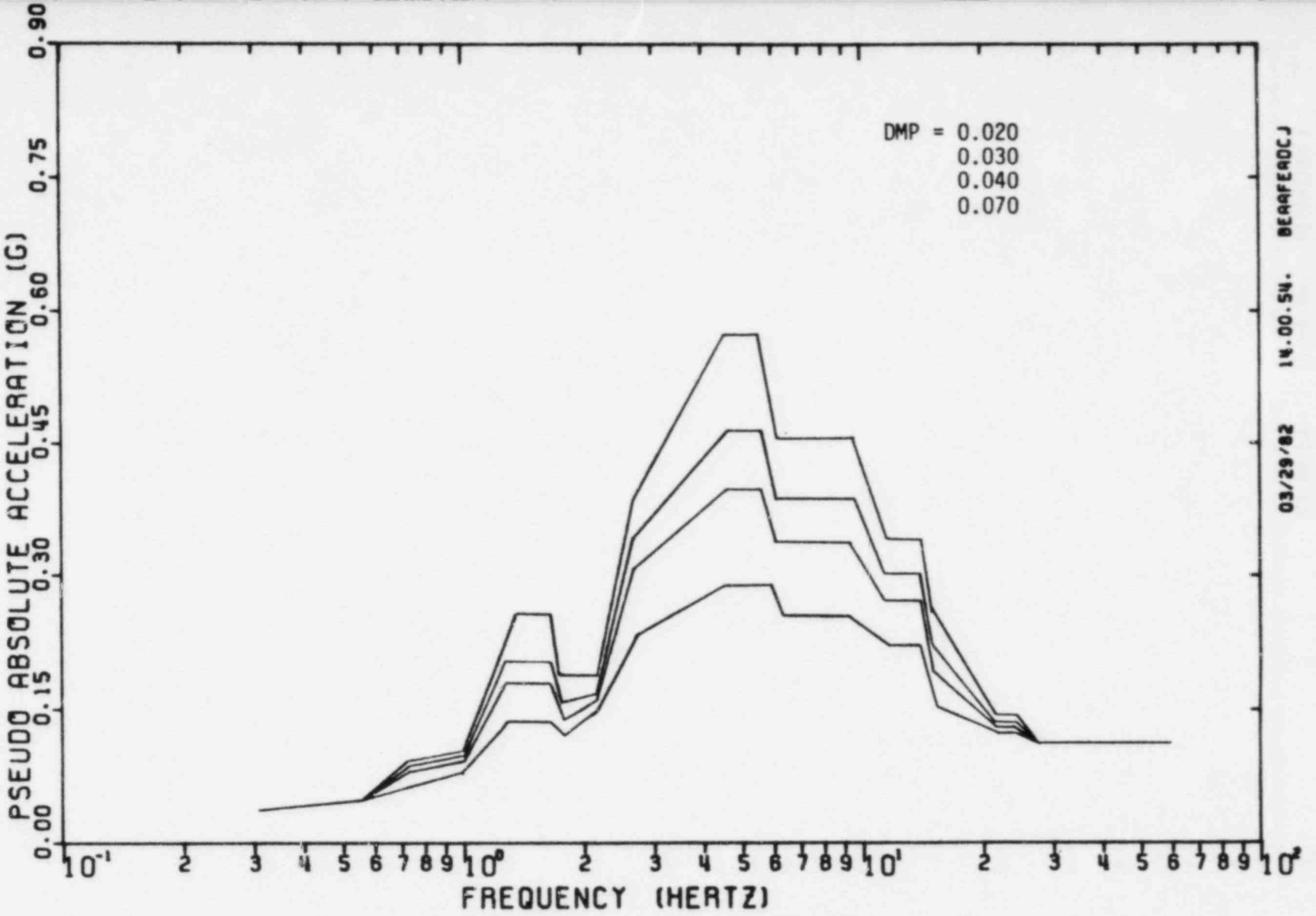

FIGURE III-B-21. Enveloped SRSS Combined Response Spectra
Main Auxiliary Building, Elevation 659' - 0"
Vertical Direction

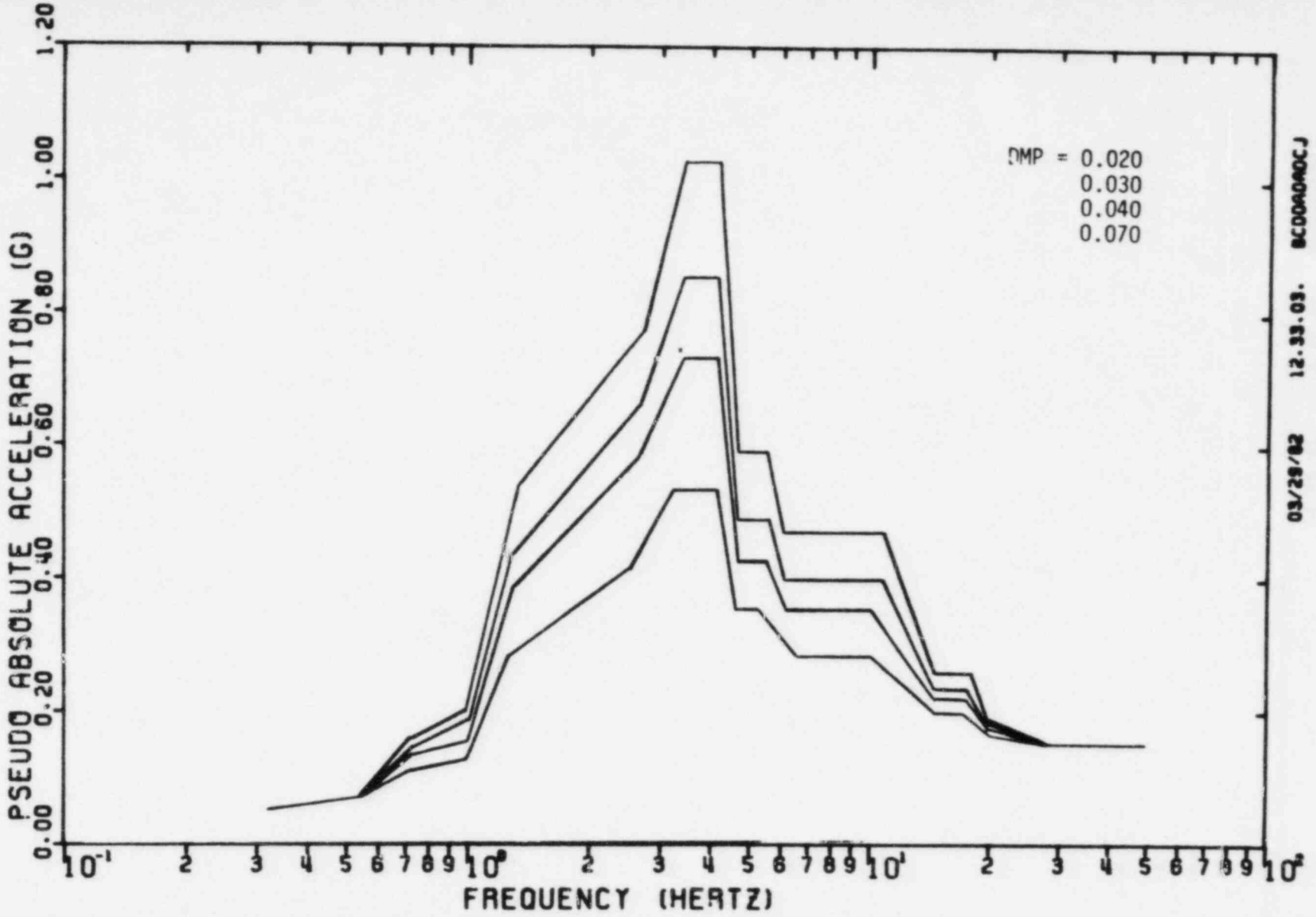

FIGURE III-B-22. Enveloped SRSS Combined Response Spectra
Control Tower, Elevation 614'-0"
North-South Direction

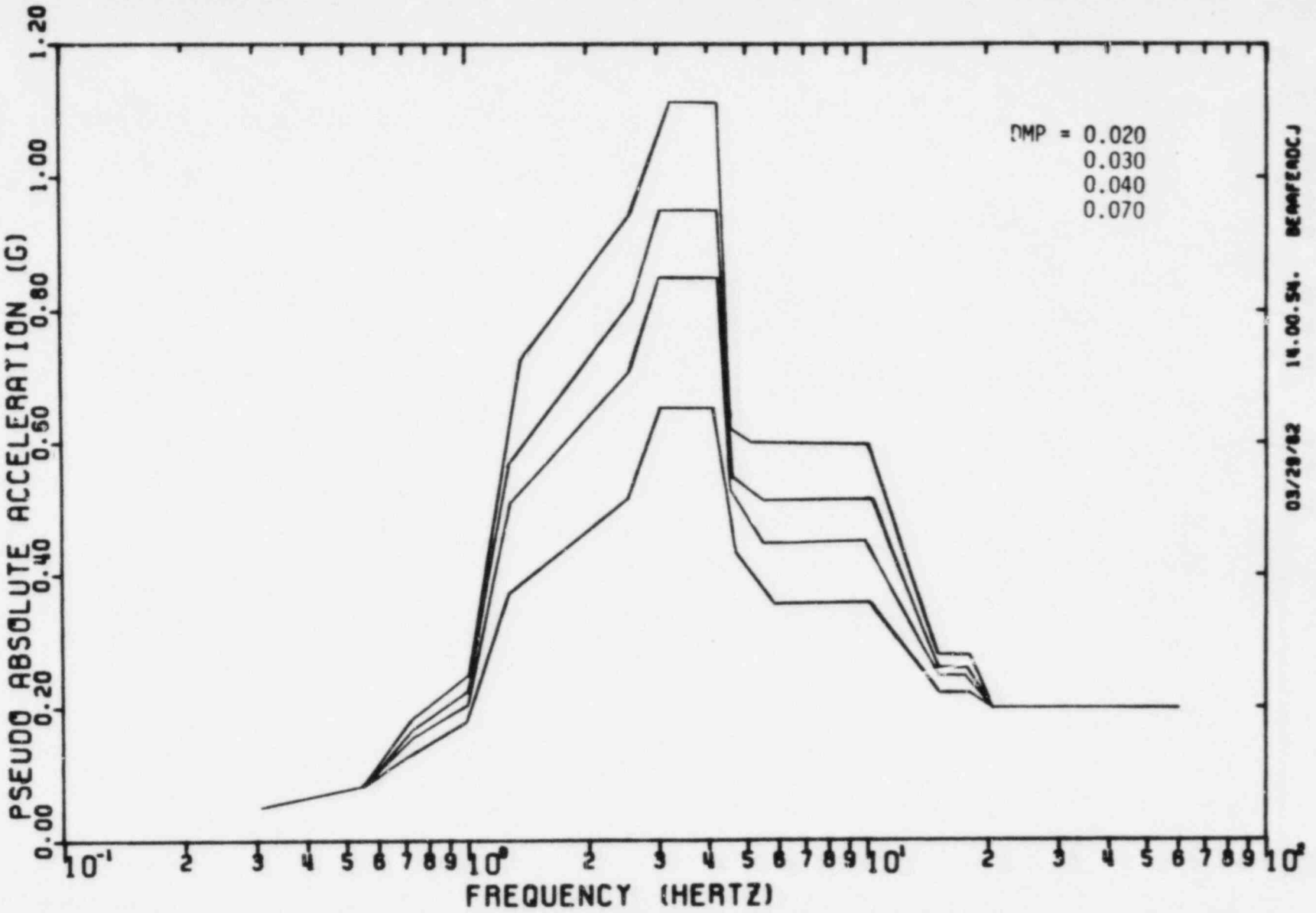

FIGURE III-B-23. Enveloped SRSS Combined Response Spectra
Control Tower, Elevation 614'-0"
East-West Direction

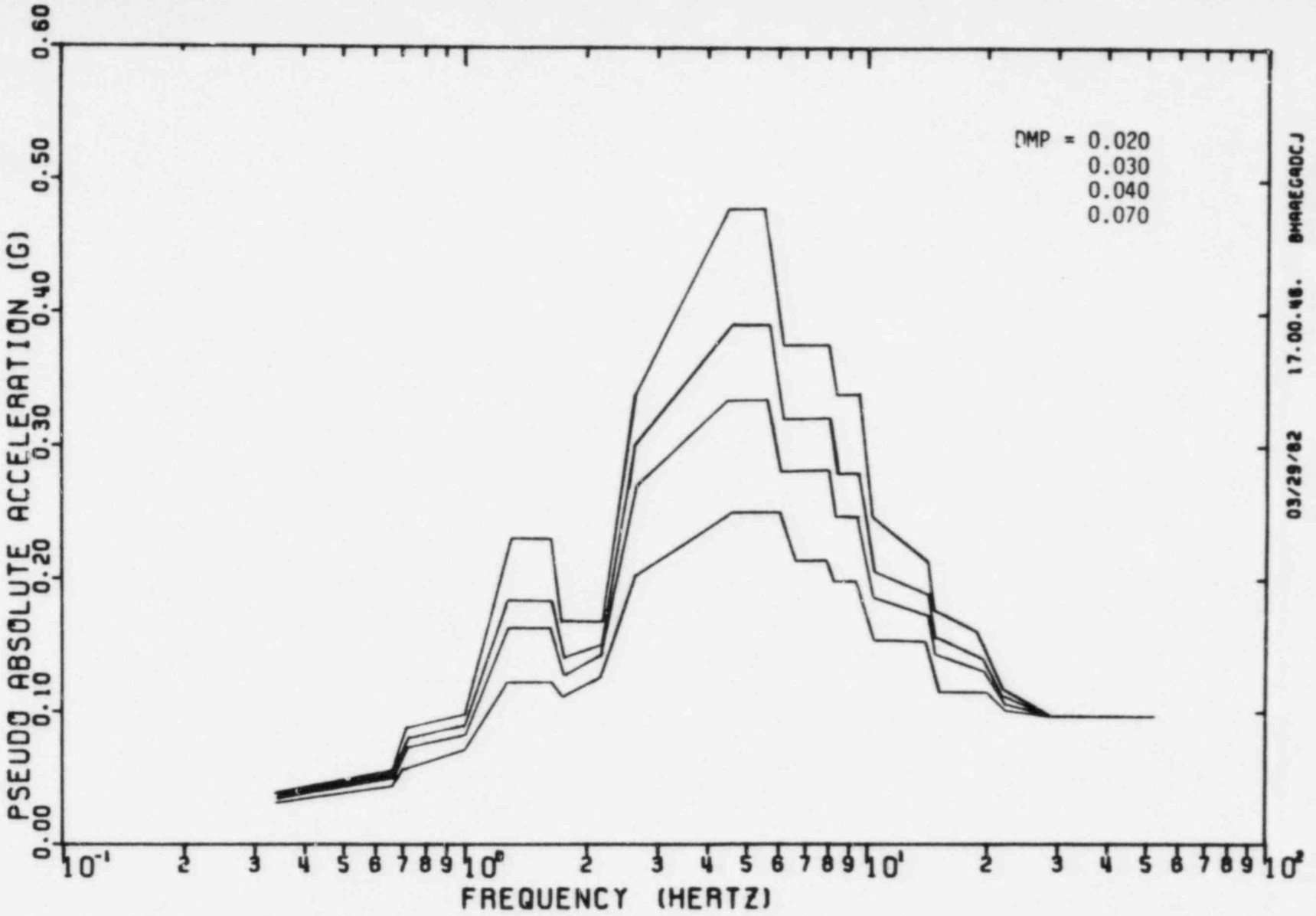

FIGURE III-B-24. Enveloped SRSS Combined Response Spectra
Control Tower, Elevation 614'-0"
Vertical Direction

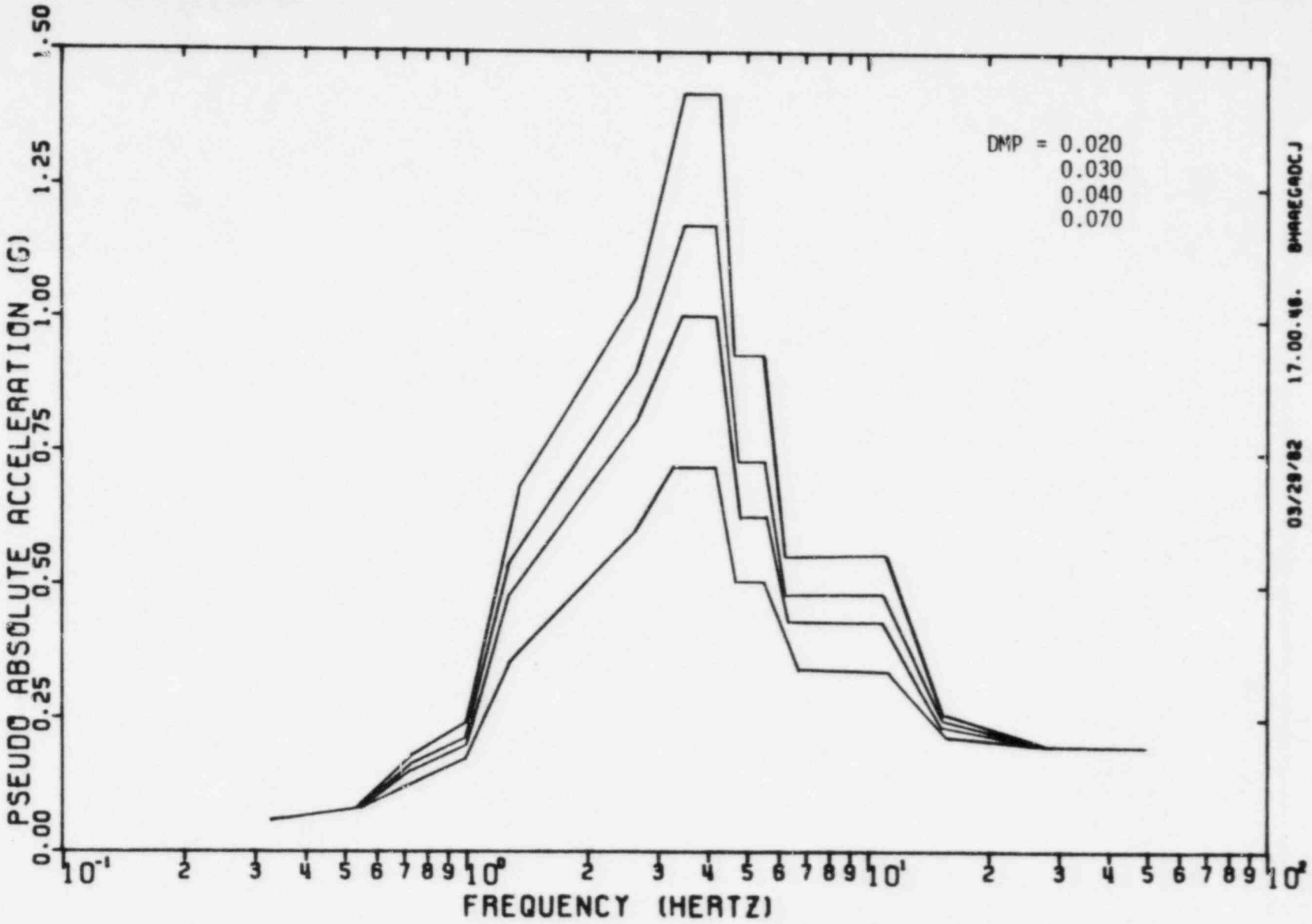

FIGURE III-B-25. Enveloped SRSS Combined Response Spectra
Control Tower, Elevation 634' - 6",
North-South Direction

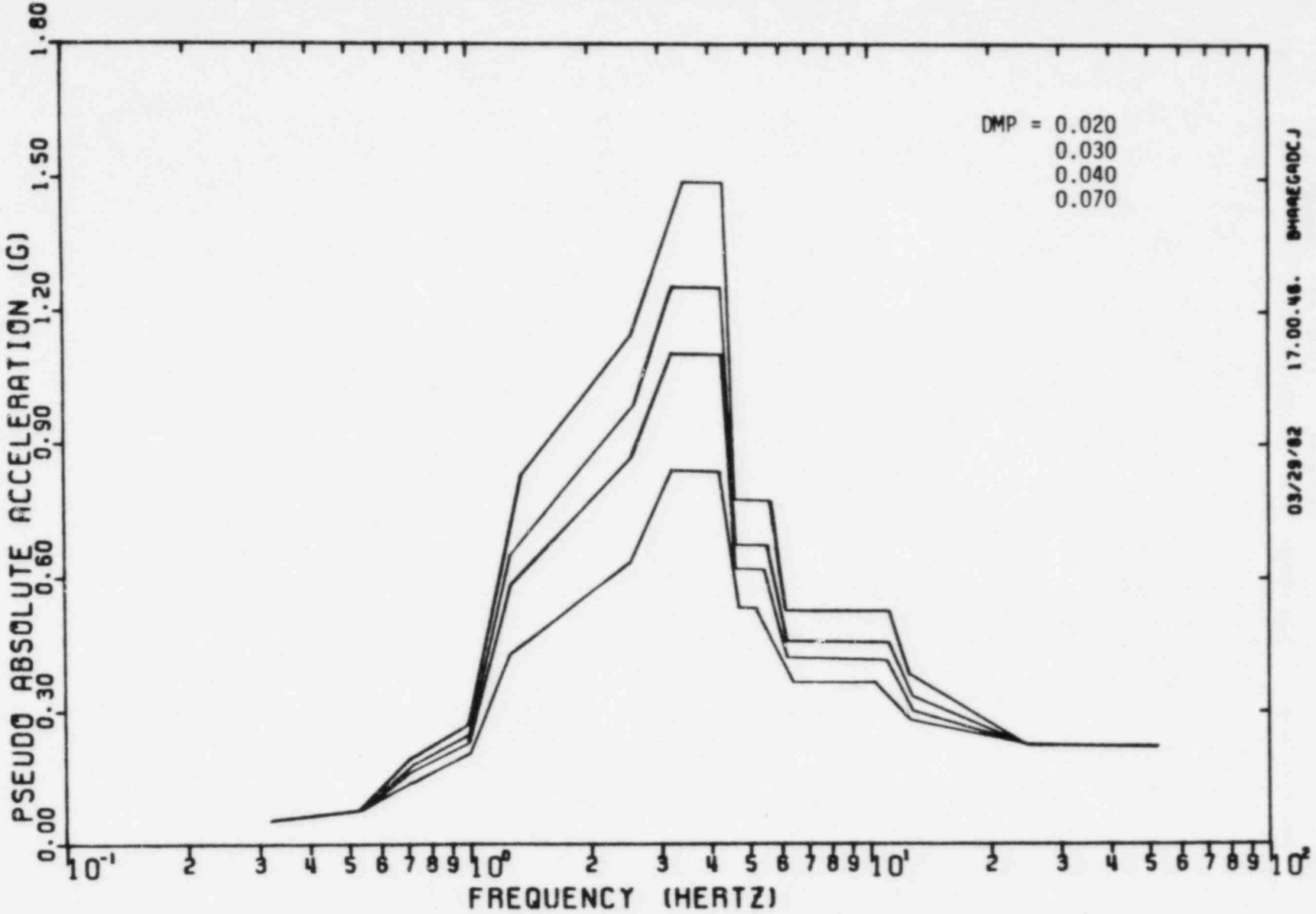

FIGURE III-B-26. Enveloped SRSS Combined Response Spectra
Control Tower, Elevation 634' - 6",
East-West Direction

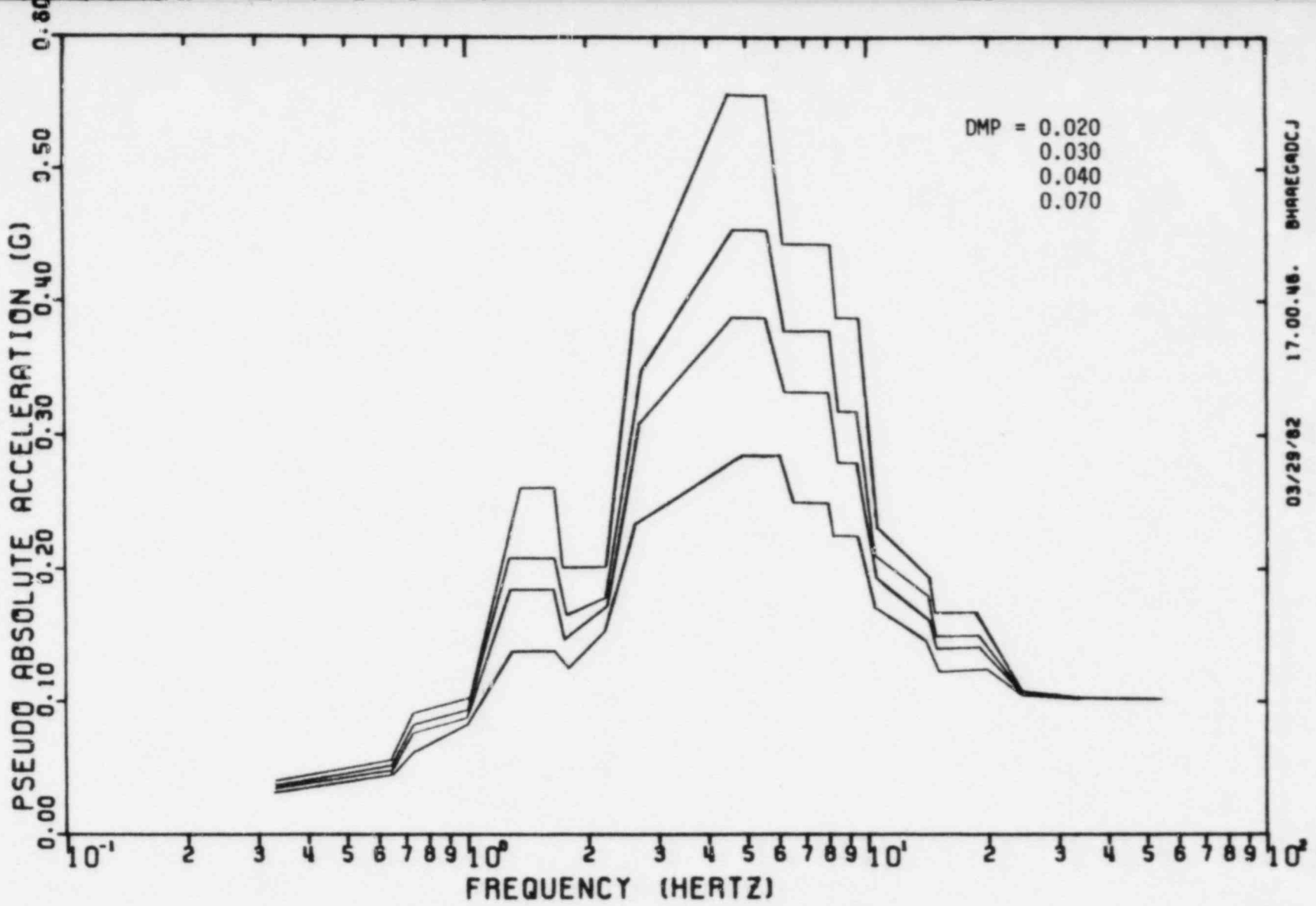

FIGURE III-B-27. Enveloped SRSS Combined Response Spectra
Control Tower, Elevation 634' - 6"
Vertical Direction

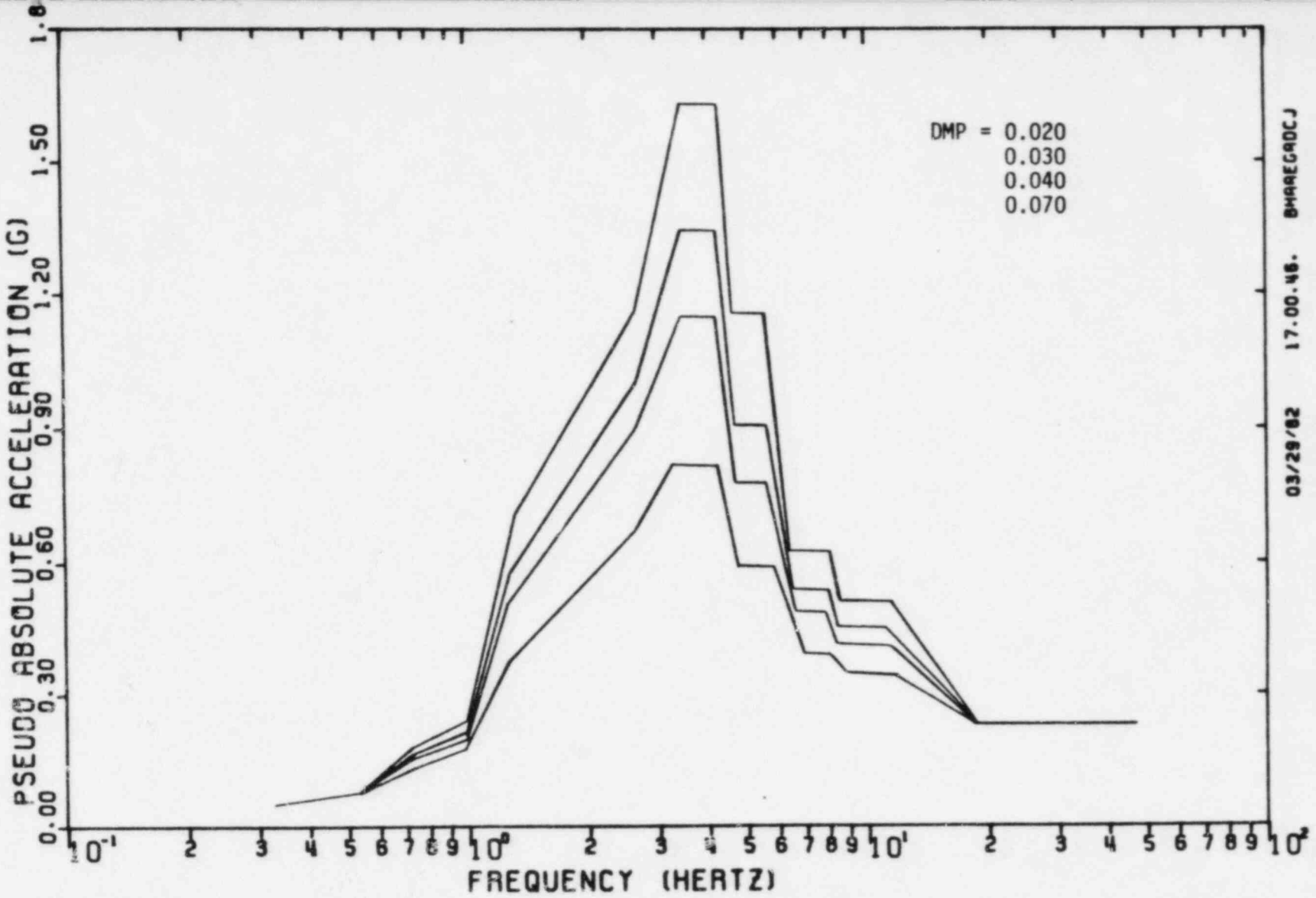

FIGURE III-B-28. Enveloped SRSS Combined Response Spectra
Control Tower, Elevation 646' - 0"
North-South Direction

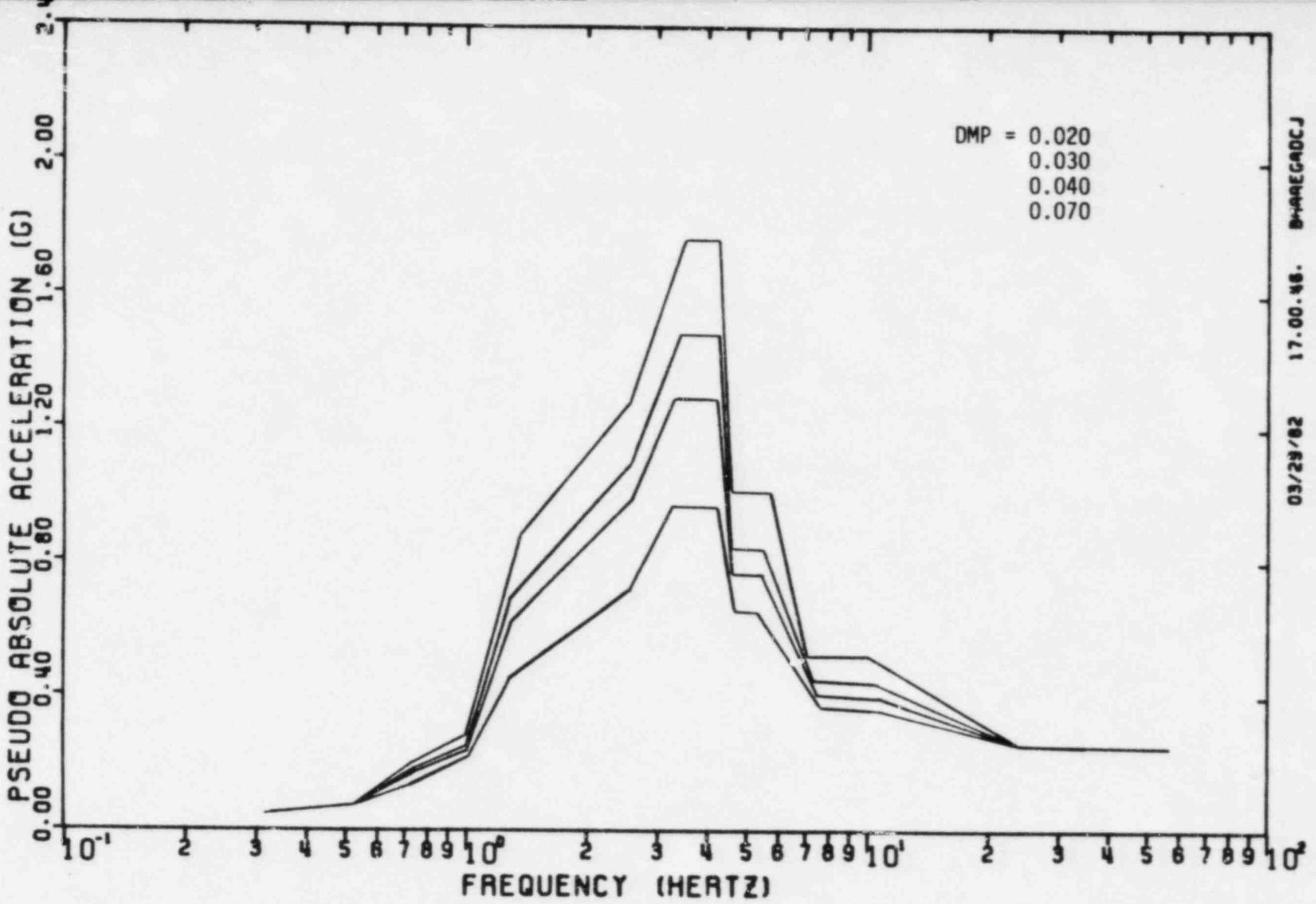

FIGURE III-B-29. Enveloped SRSS Combined Response Spectra
Control Tower, Elevation 646' - 0"
East-West Direction

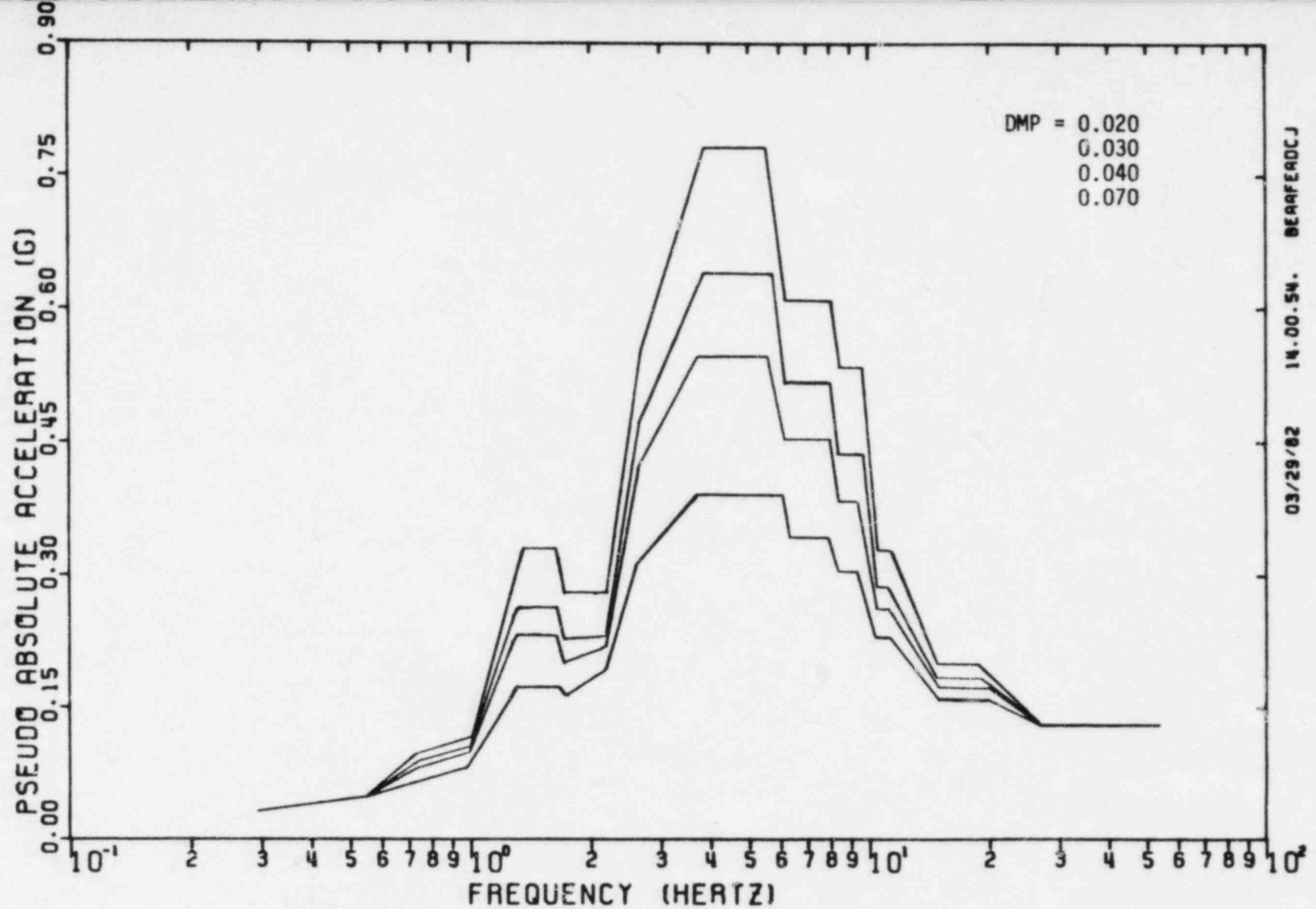

FIGURE III-B-30. Enveloped SRSS Combined Response Spectra
Control Tower, Elevation 646' - 0"
Vertical Direction

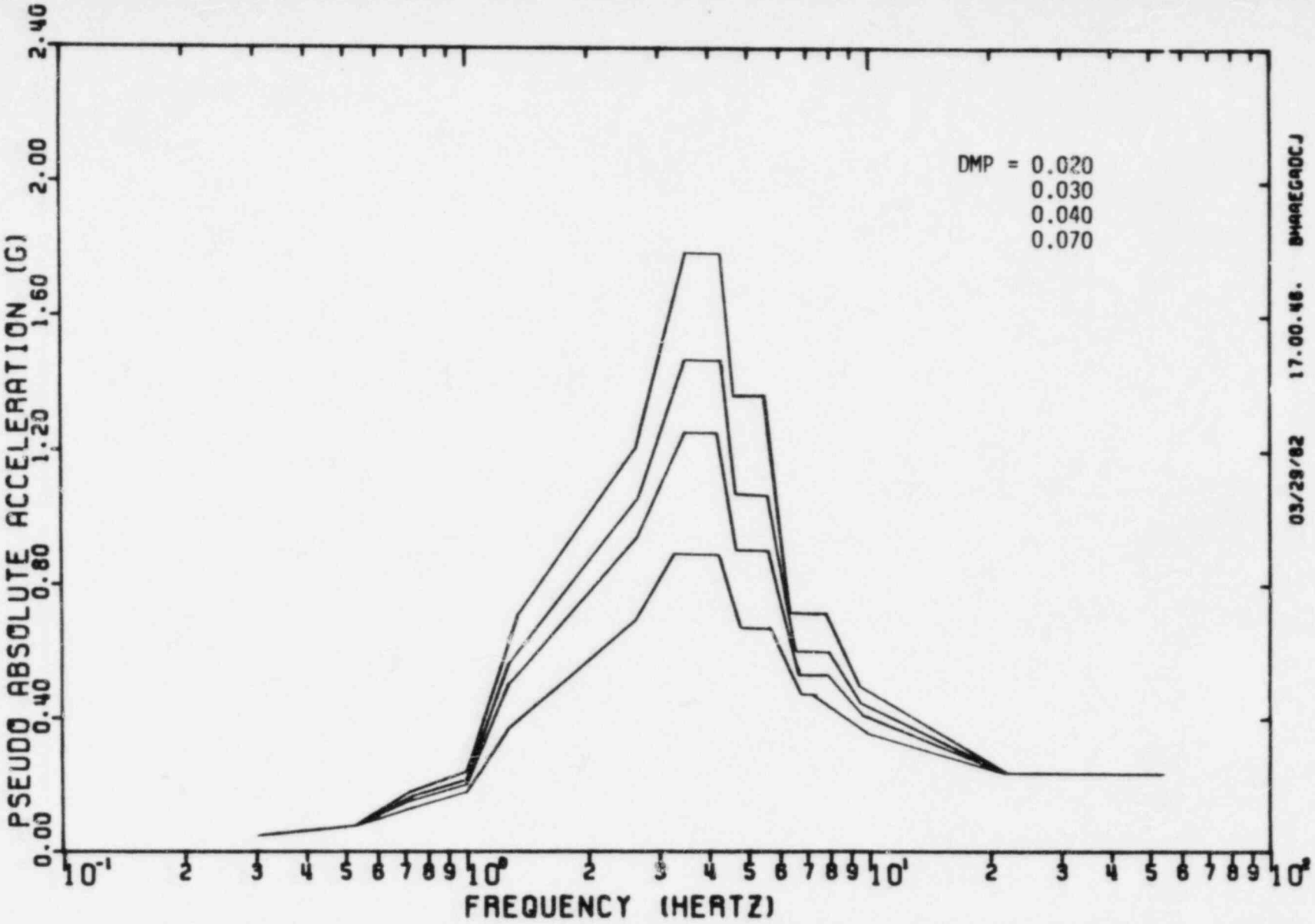

FIGURE III-B-31. Enveloped SRSS Combined Response Spectra
Control Tower, Elevation 659'-0"
North-South Direction

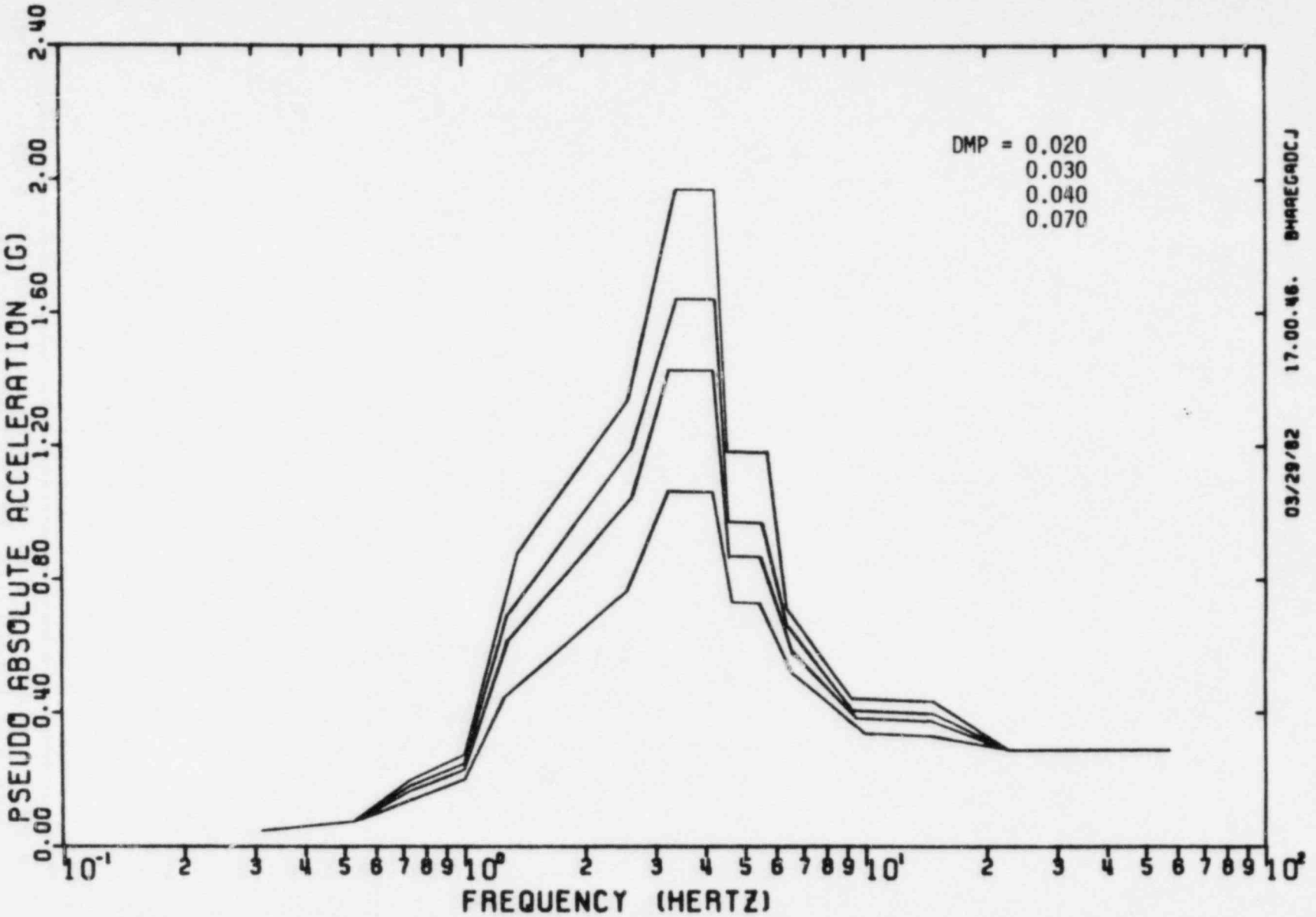

FIGURE III-B-32. Enveloped SRSS Combined Response Spectra
Control Tower, Elevation 659'-0"
East-West Direction

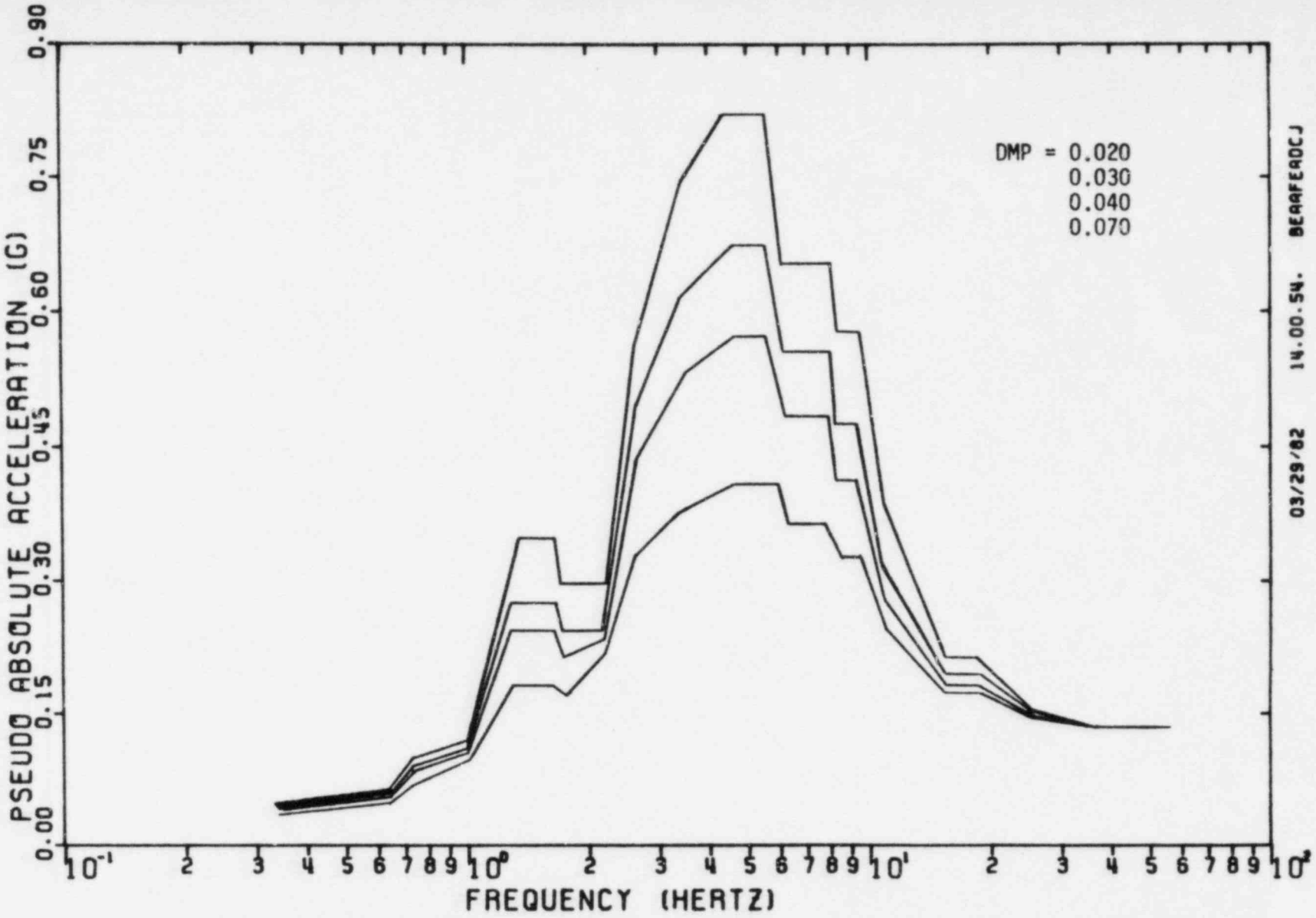

FIGURE III-B-33. Enveloped SRSS Combined Response Spectra
Control Tower, Elevation 659'-0"
Vertical Direction

FIGURE III-B-34. Enveloped SRSS Combined Response Spectra
Control Tower, Elevation 674' - 6"
North-South Direction

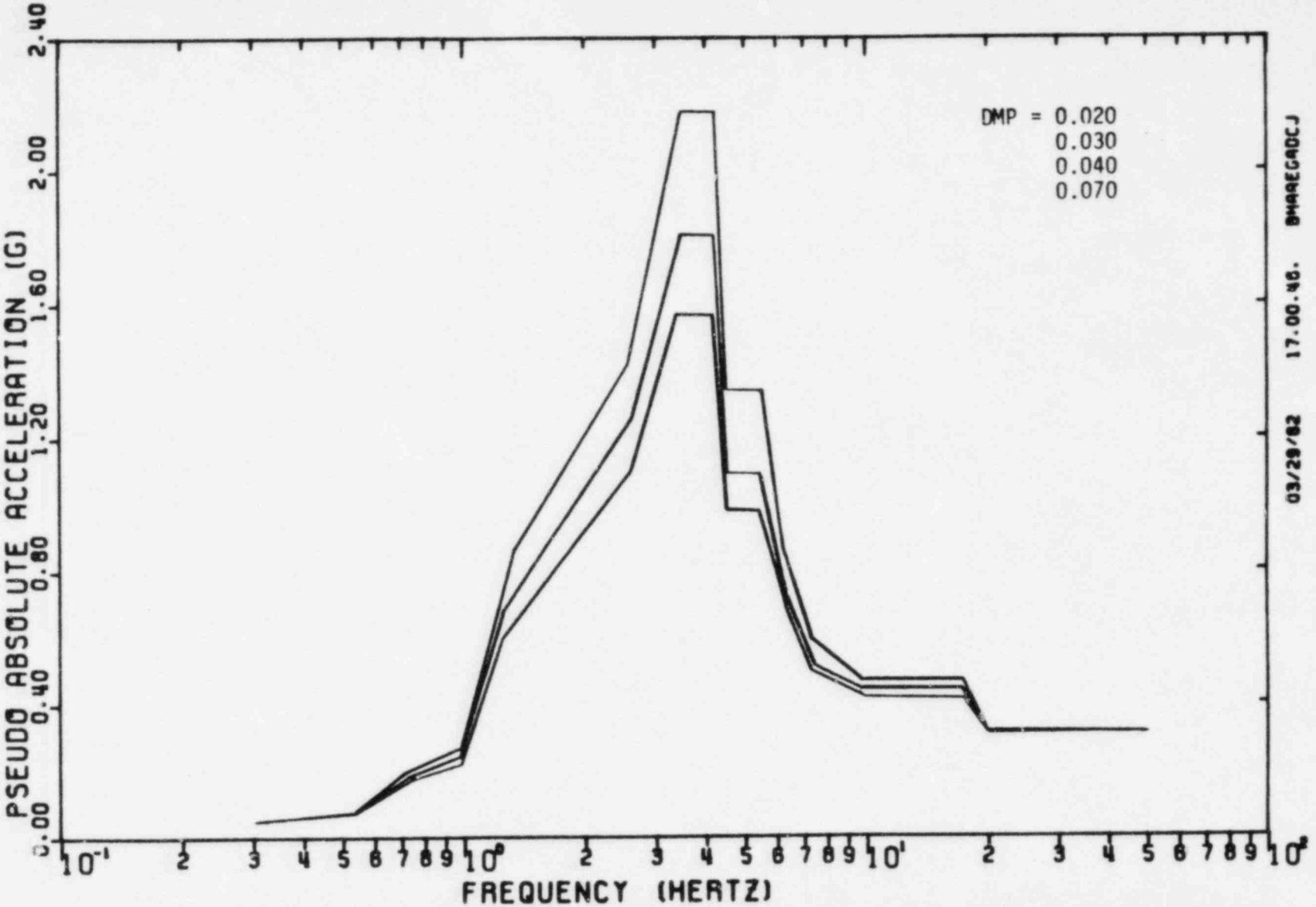

FIGURE III-B-35. Enveloped SRSS Combined Response Spectra
Control Tower, Elevation 674' - 6"
East-West Direction

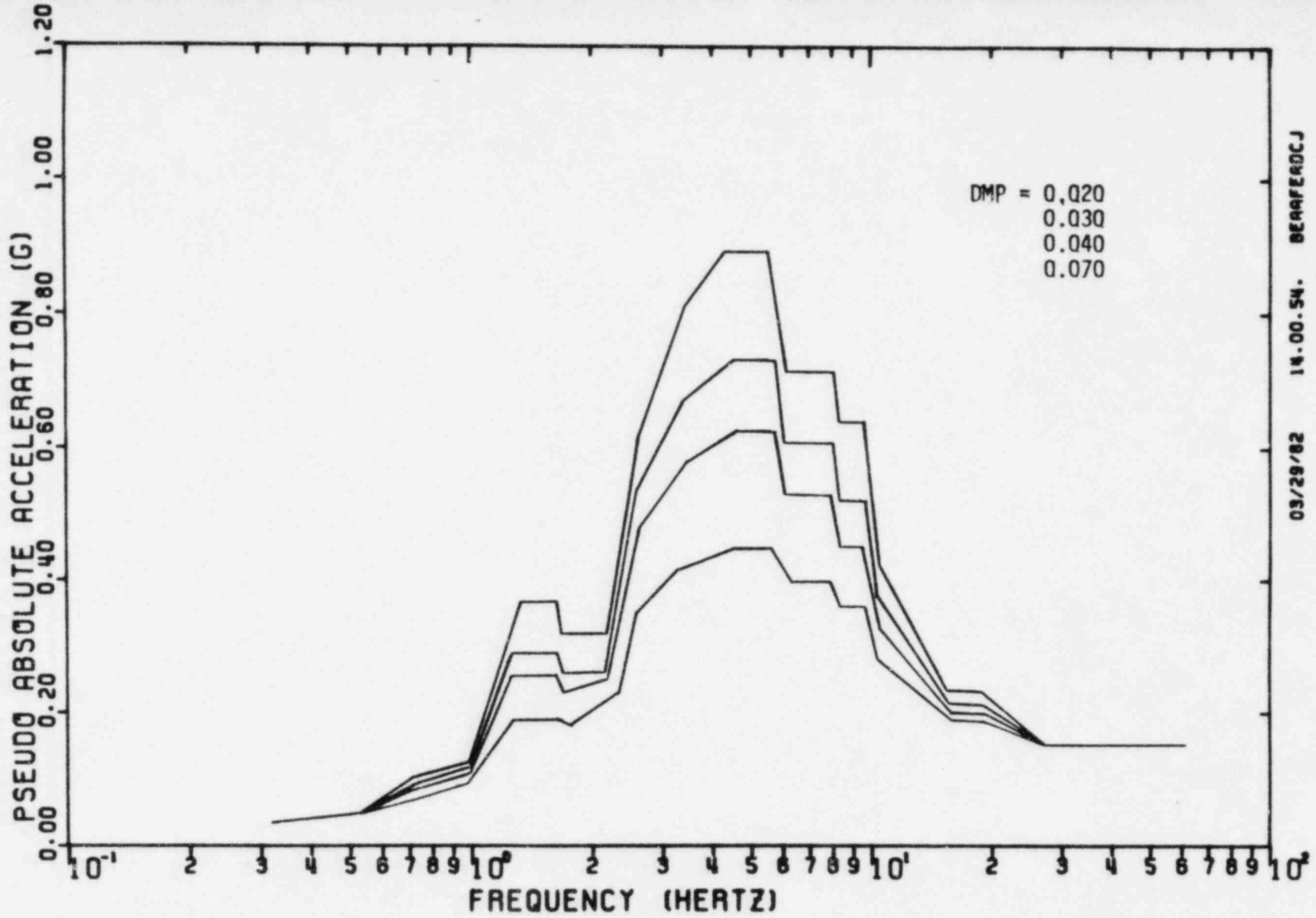

FIGURE III-B-36. Enveloped SRSS Combined Response Spectra
Control Tower, Elevation 674'-6"
Vertical Direction

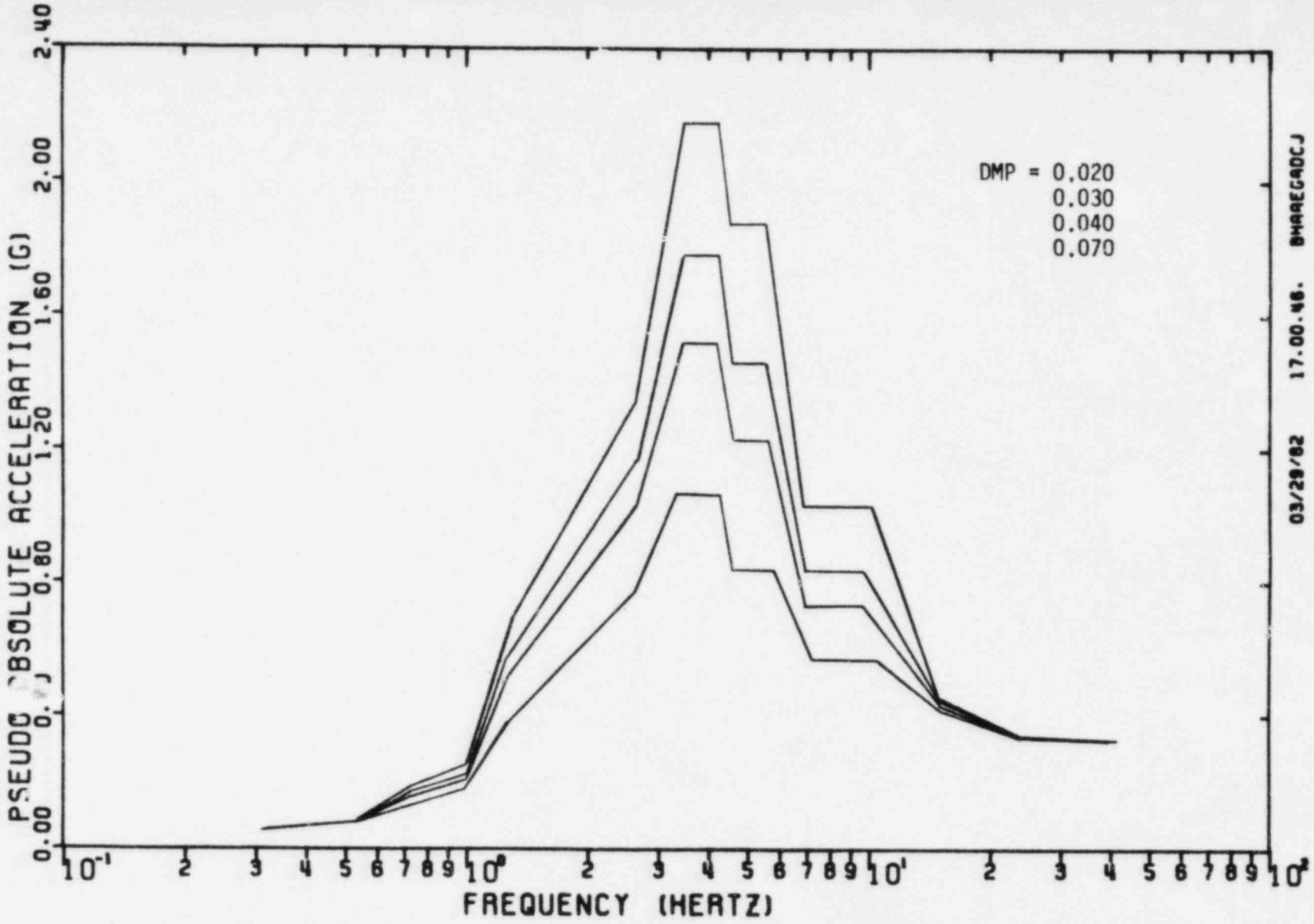

FIGURE III-B-37. Enveloped SRSS Combined Response Spectra
Control Tower, Elevation 685'-0"
North-South Direction

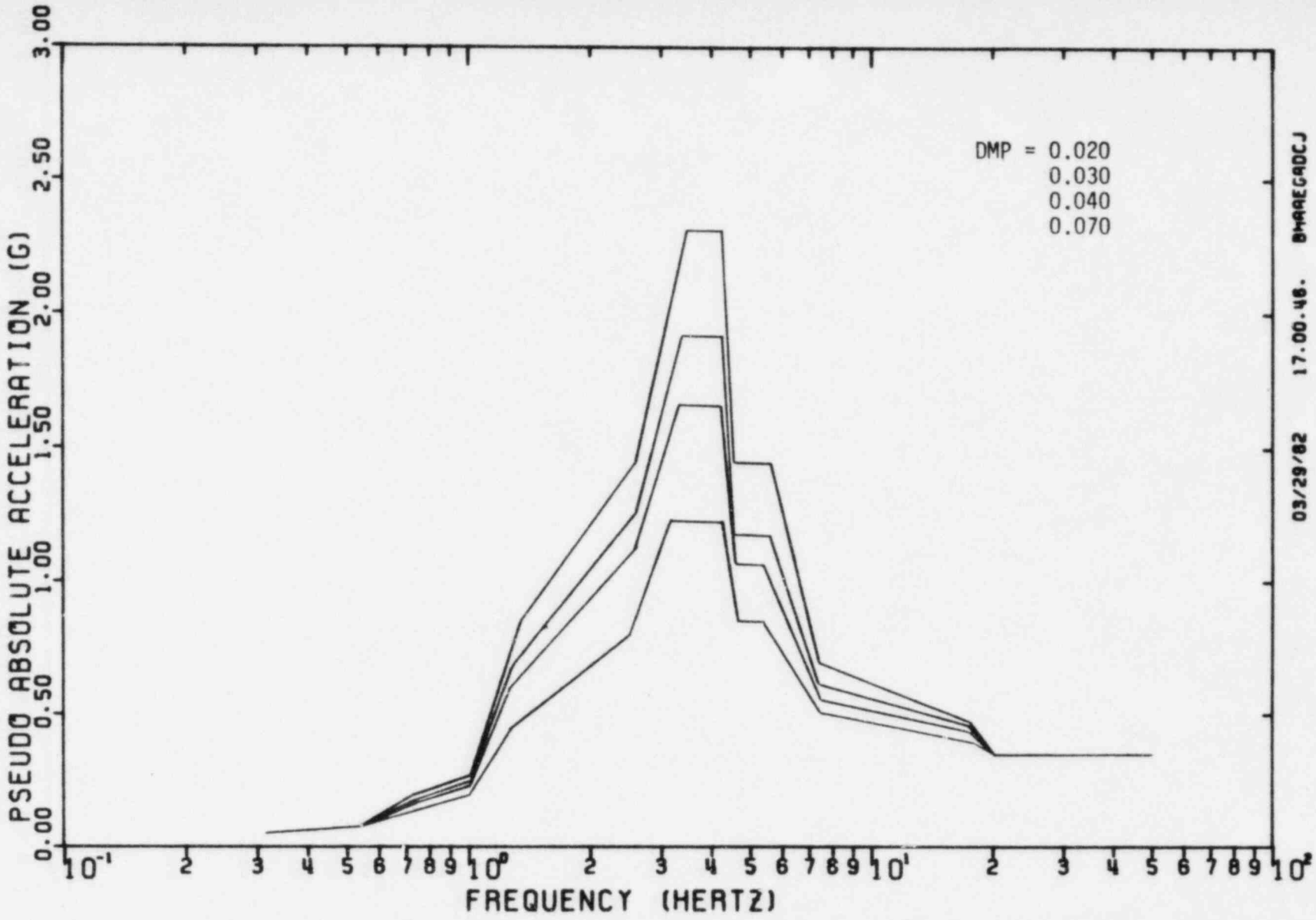

FIGURE III-B-38. Enveloped SRSS Combined Response Spectra
Control Tower, Elevation 685'-0"
East-West Direction

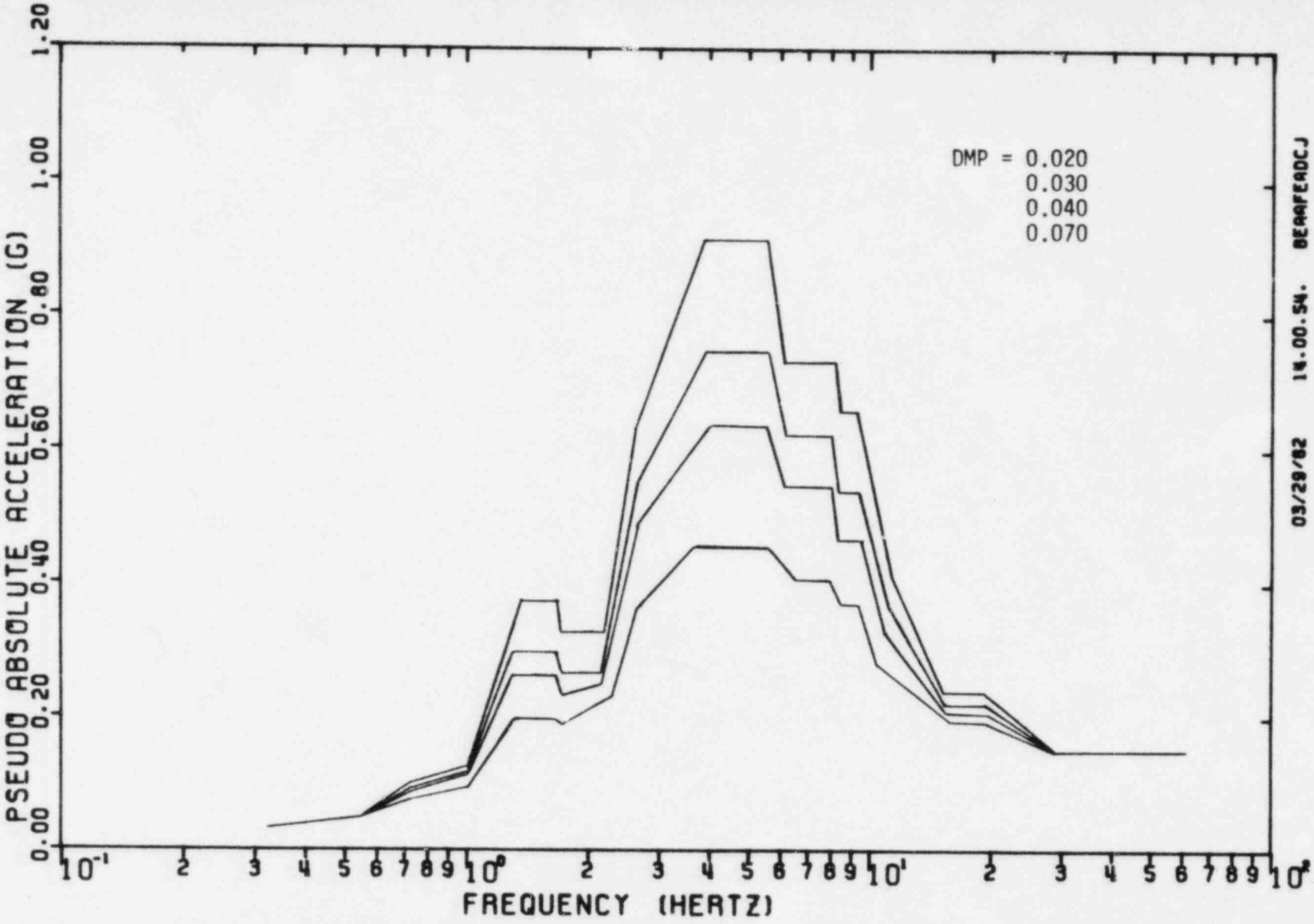

FIGURE III-B-39. Enveloped SRSS Combined Response Spectra
Control Tower, Elevation 685'-0"
Vertical Direction

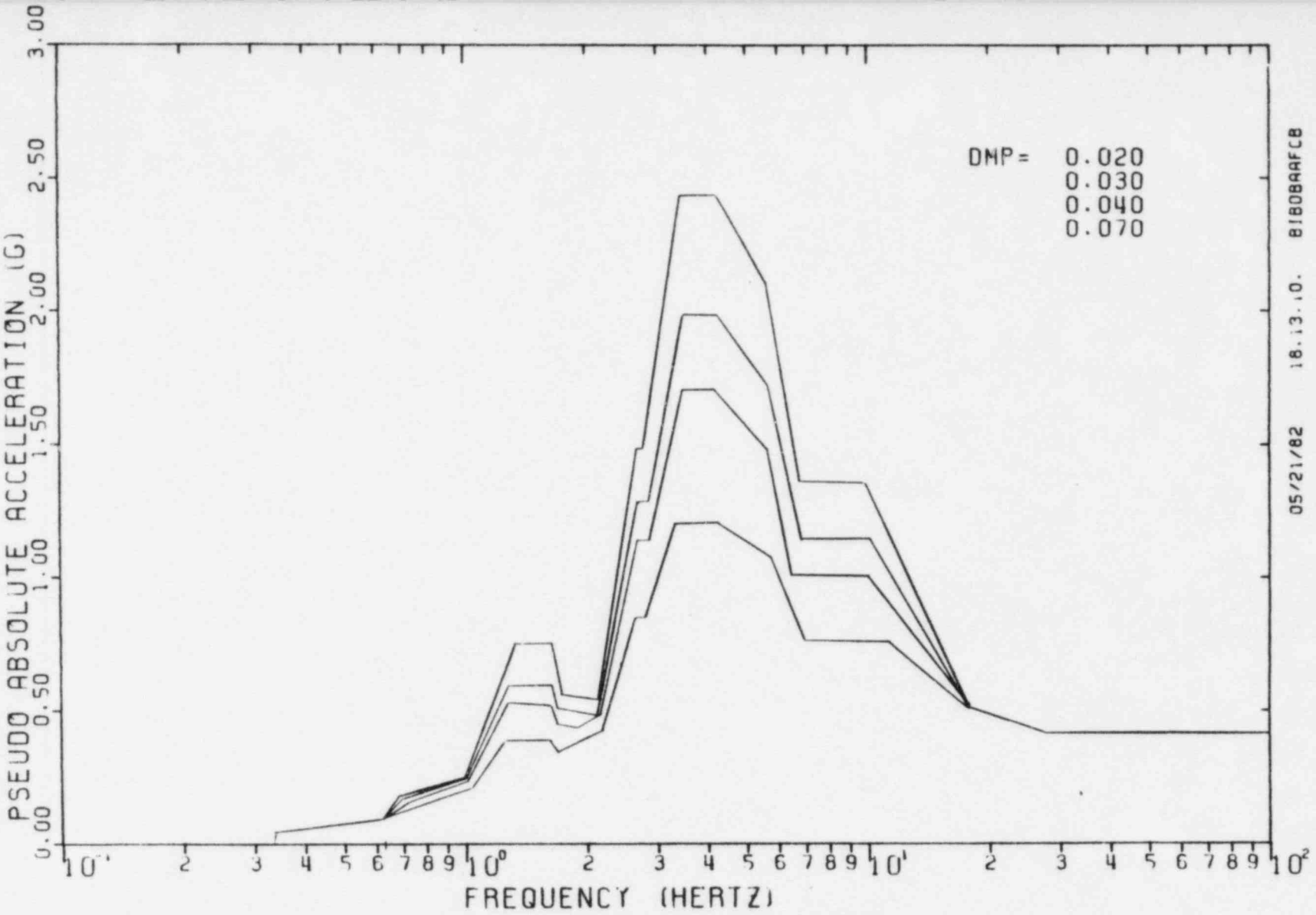

FIGURE III-B-40. ENVELOPED SRSS RESPONSE SPECTRA CONTROL TOWER, ELEVATION 704' NORTH-SOUTH DIRECTION

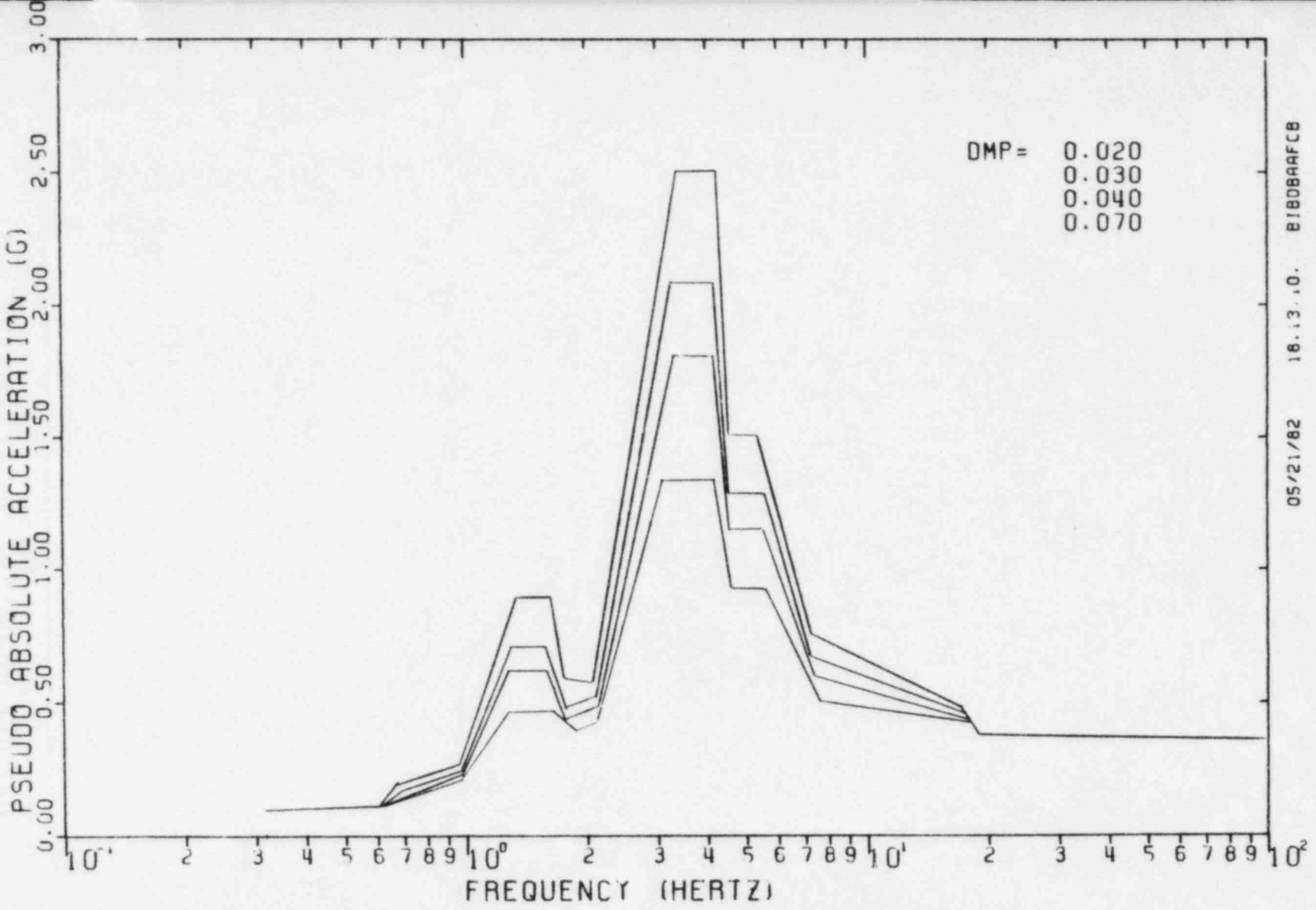

FIGURE III-B-41. ENVELOPED SRSS RESPONSE SPECTRA CONTROL TOWER, ELEVATION 704' EAST-WEST DIRECTION

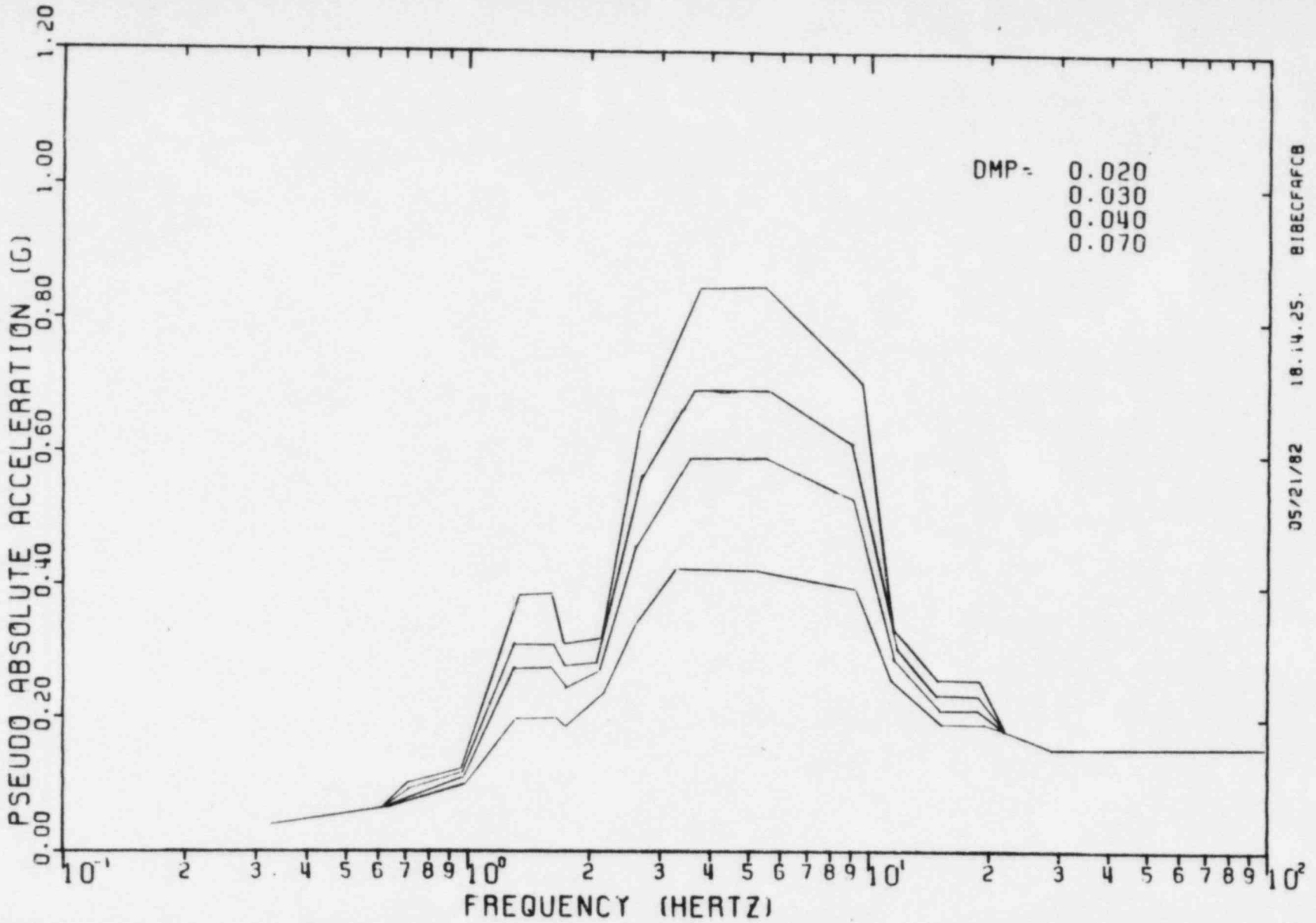

FIGURE III-B-42. ENVELOPED SRSS RESPONSE SPECTRA CONTROL TOWER, ELEVATION 704' VERTICAL DIRECTION

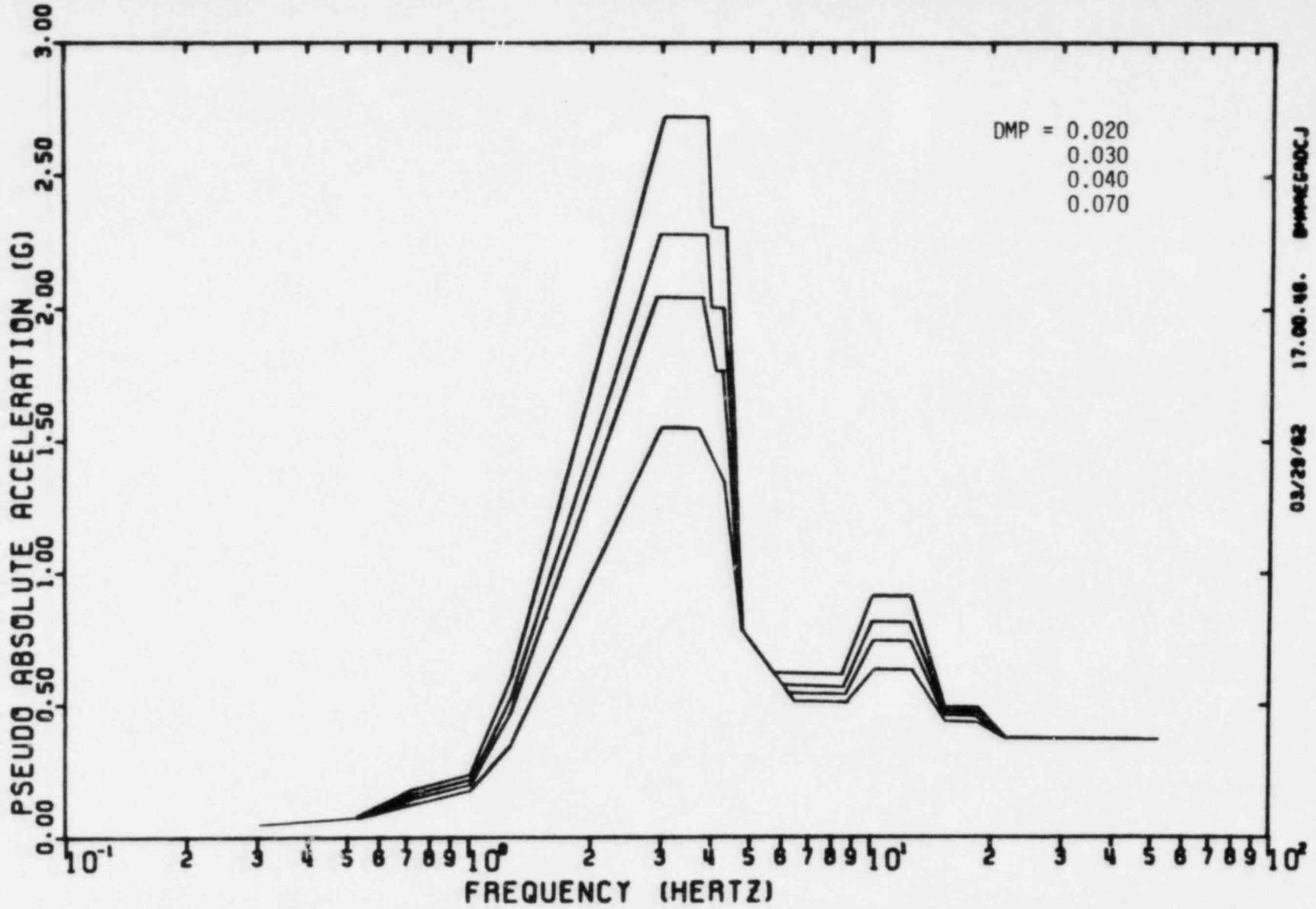

FIGURE III-B-43. Enveloped SRSS Combined Response Spectra
Auxiliary Building East/West Wings, Elevation 614'-0"
North-South Direction

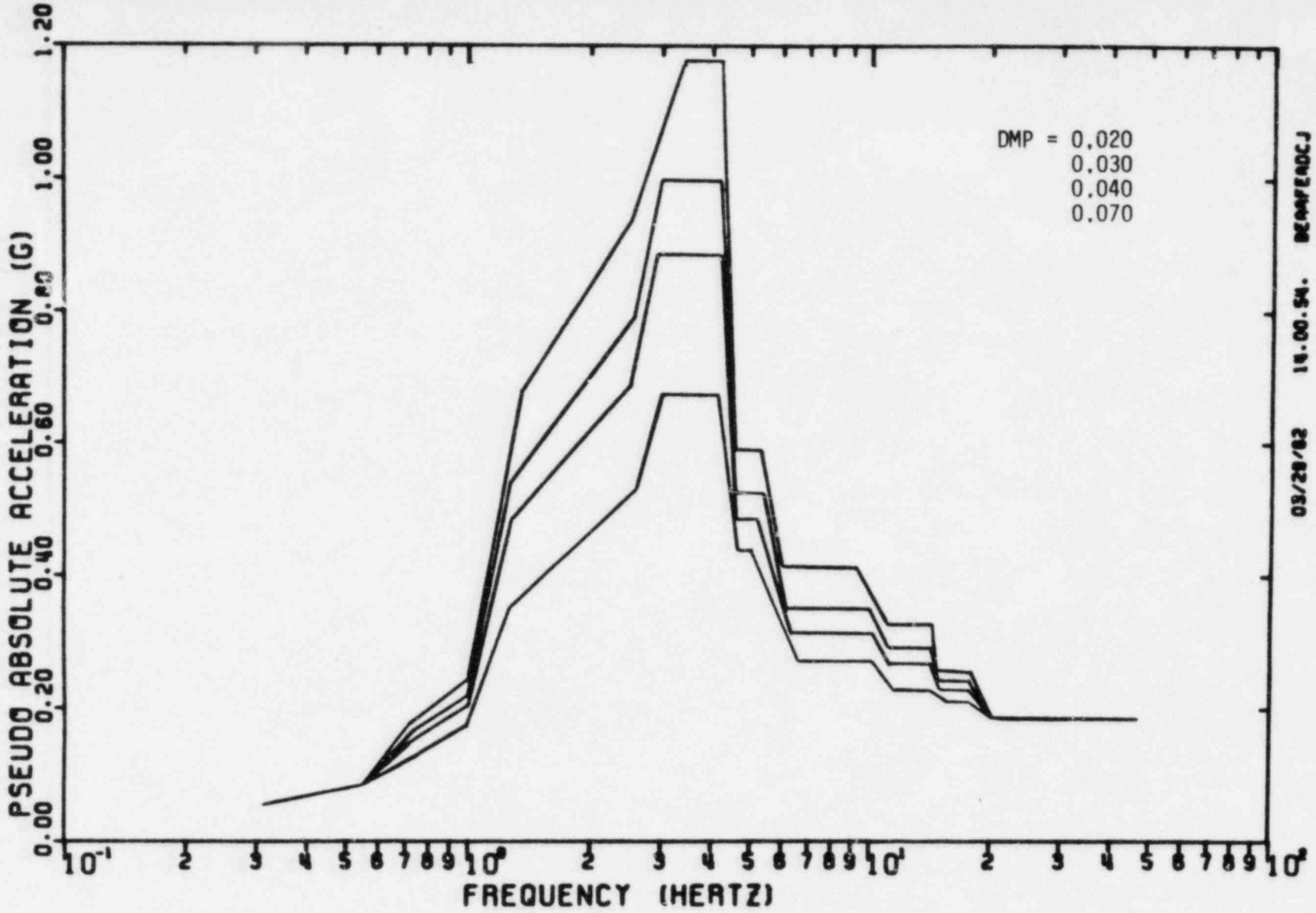

FIGURE III-B-44. Enveloped SRSS Combined Response Spectra
Auxiliary Building East/West Wings, Elevation 614'-0"
East-West Direction

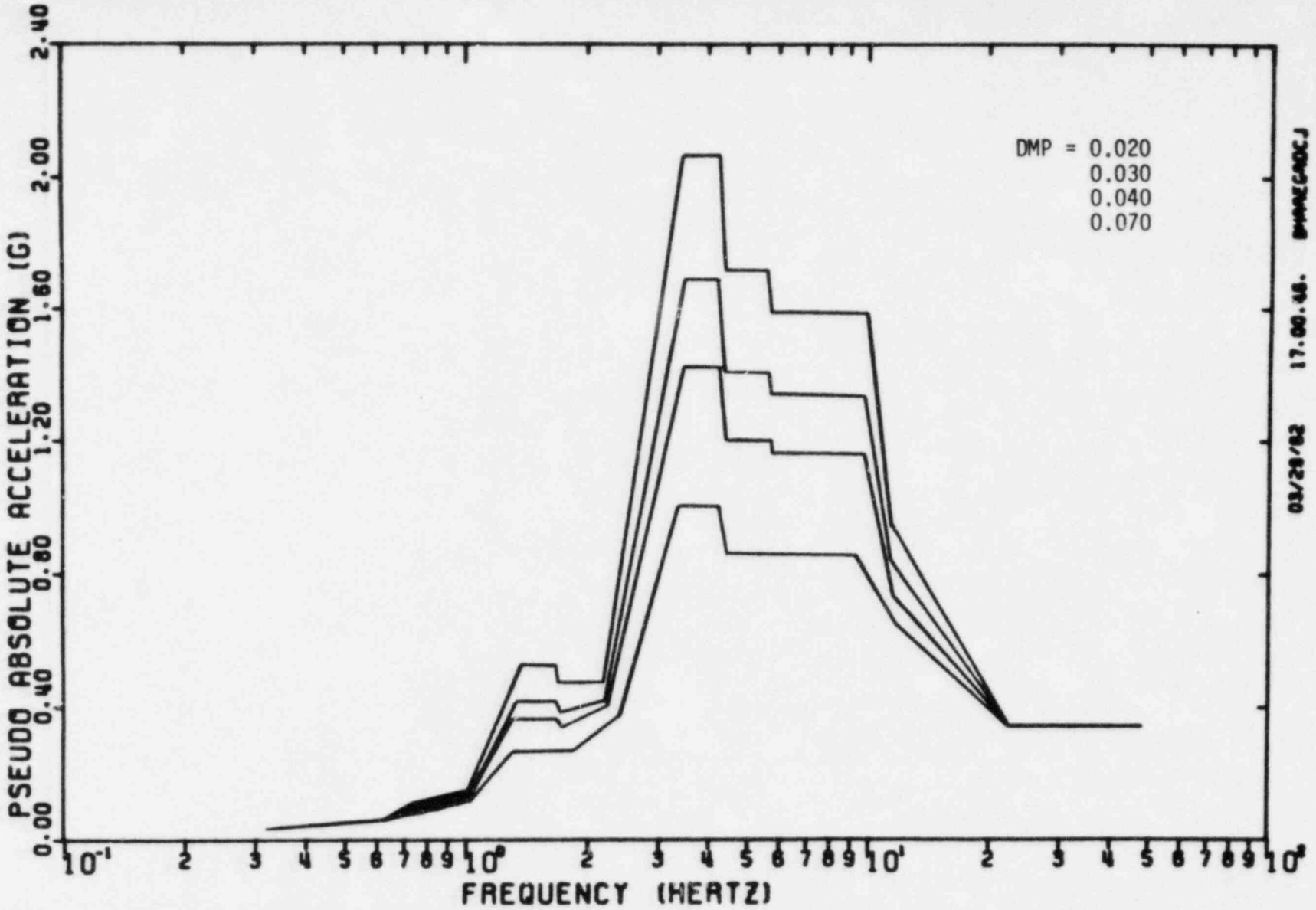

FIGURE III-B-45. Enveloped SRSS Combined Response Spectra
Auxiliary Building East/West Wings, Elevation 614'-0"
Vertical Direction

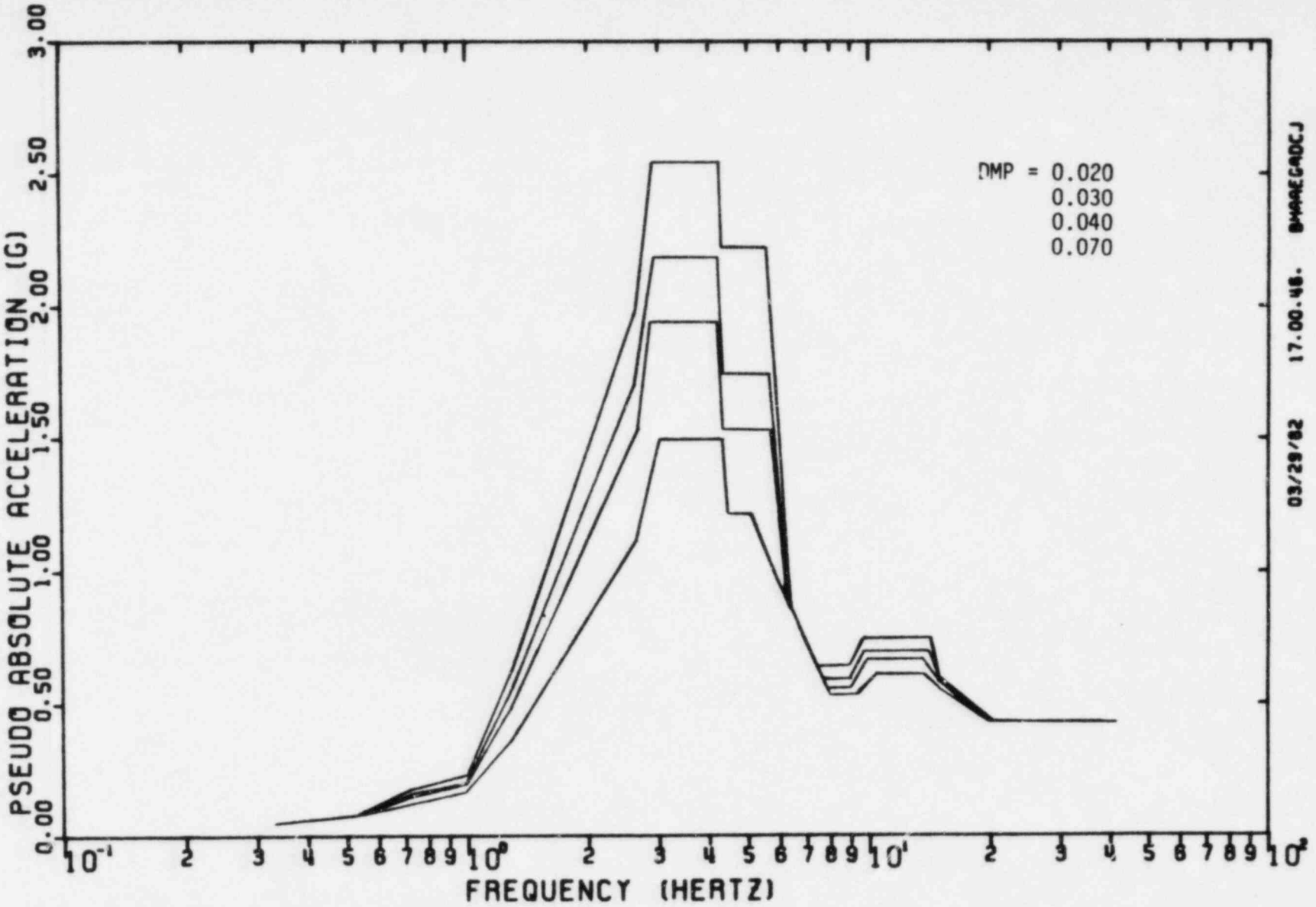

FIGURE III-B-46. Enveloped SRSS Combined Response Spectra
Auxiliary Building, East/West Wings, Elevation 642'-7"
North-South Direction

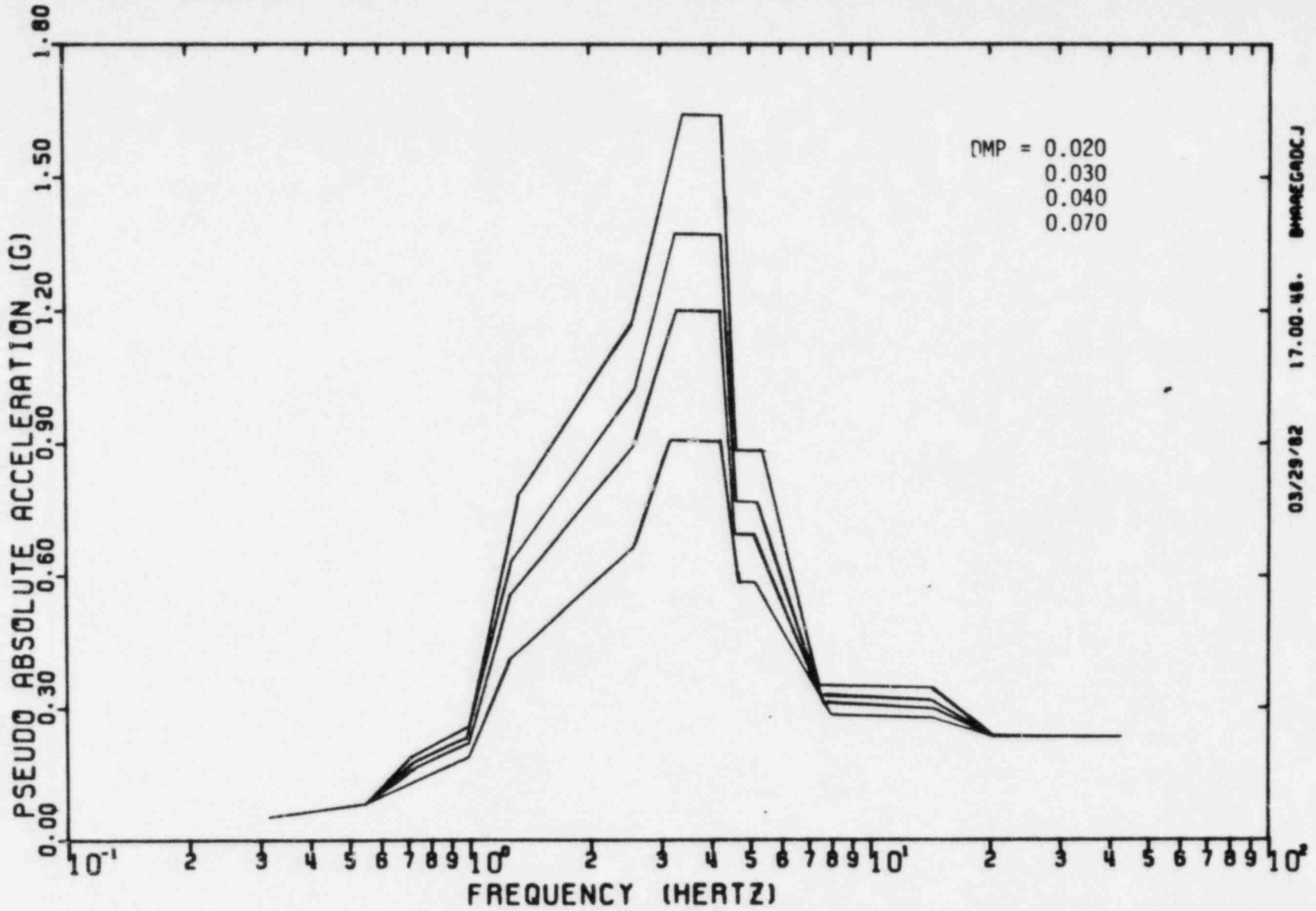

FIGURE III-B-47. Median Soil Case, SRSS Combined Response Spectra
Auxiliary Building, East/West Wings, Elevation 642'-7"
East-West Direction

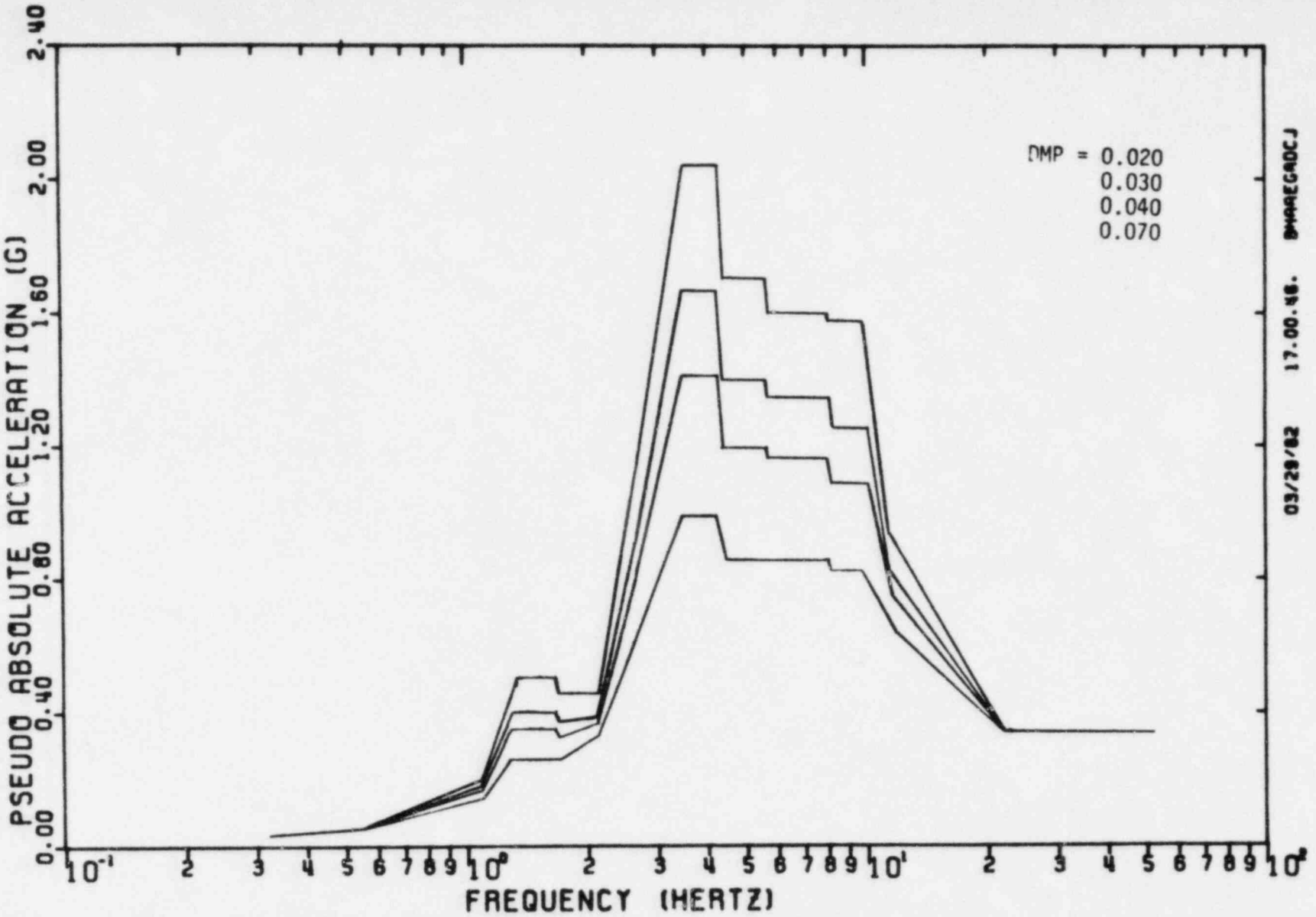

FIGURE III-B-48. Enveloped SRSS Combined Response Spectra
Auxiliary Building, East/West Wings, Elevation 642'-7"
Vertical Direction

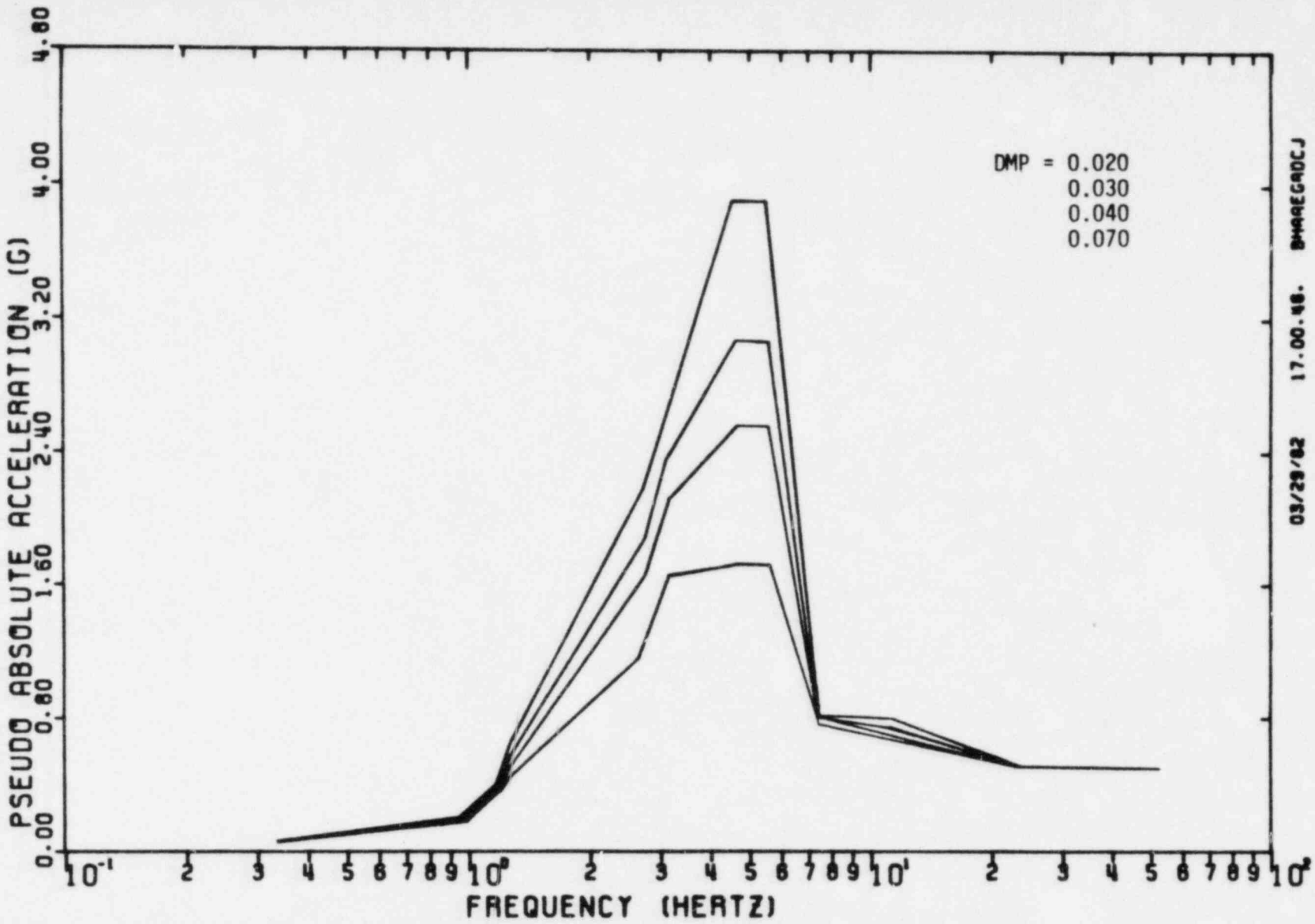

FIGURE III-B-49. Enveloped SRSS Combined Response Spectra
East Penetration Wing, Elevation 659' - 0"
North-South Direction

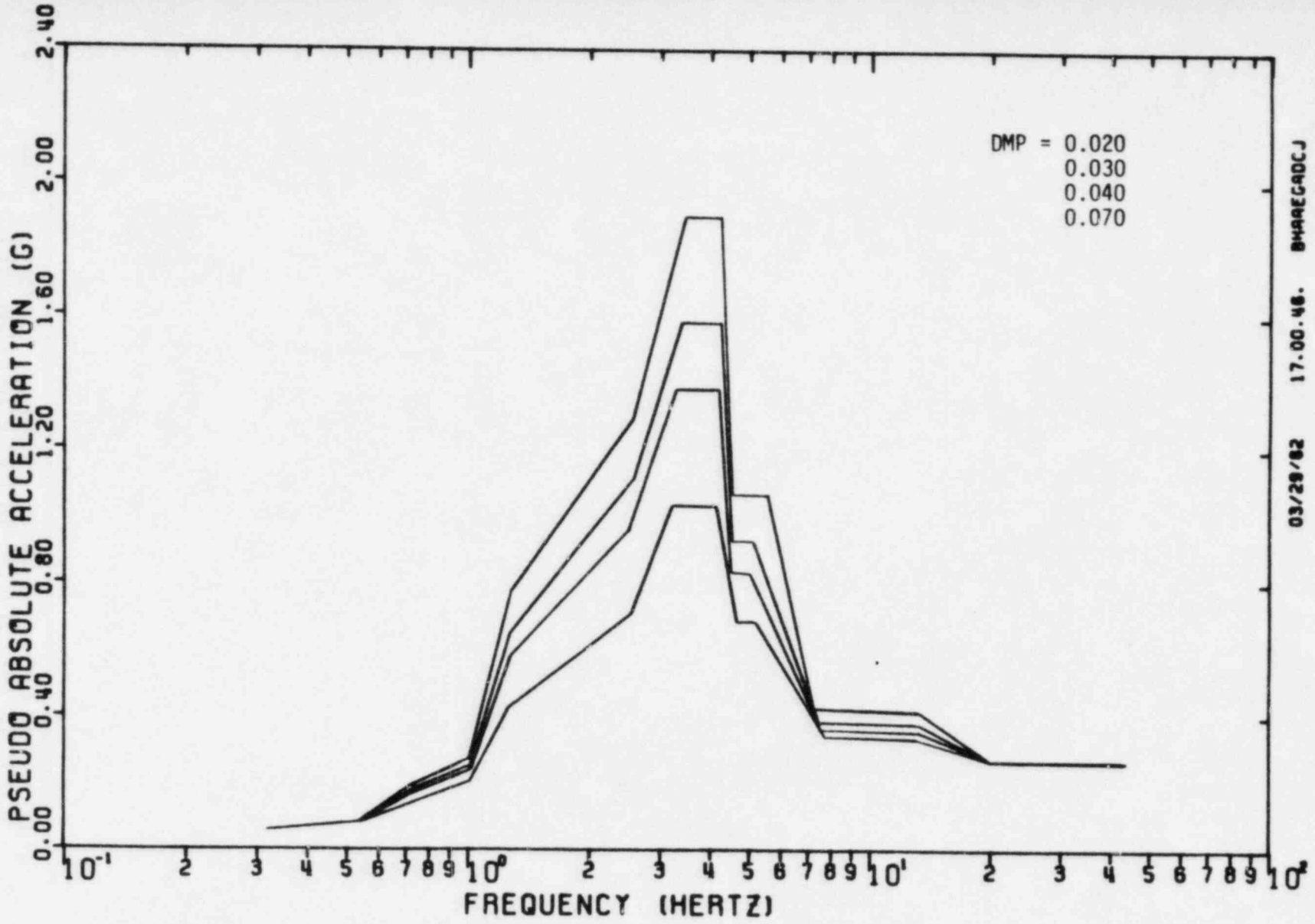

FIGURE III-B-50. Enveloped SRSS Combined Response Spectra
East Penetration Wing, Elevation 659' - 0"
East-West Direction

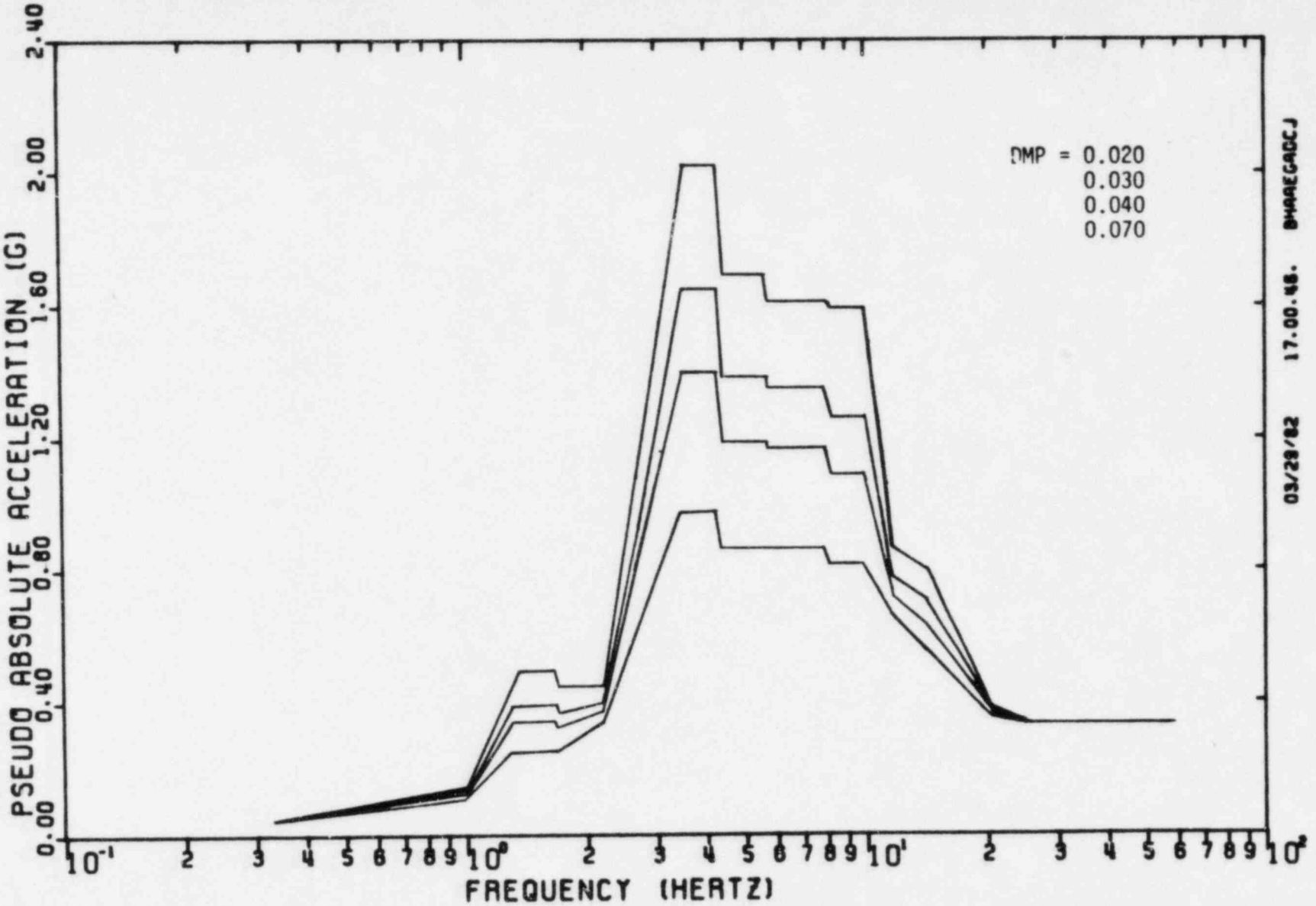

FIGURE III-B-51. Enveloped SRSS Combined Response Spectra
Auxiliary Building, East/West Wings, Elevation 659'-0"
Vertical Direction

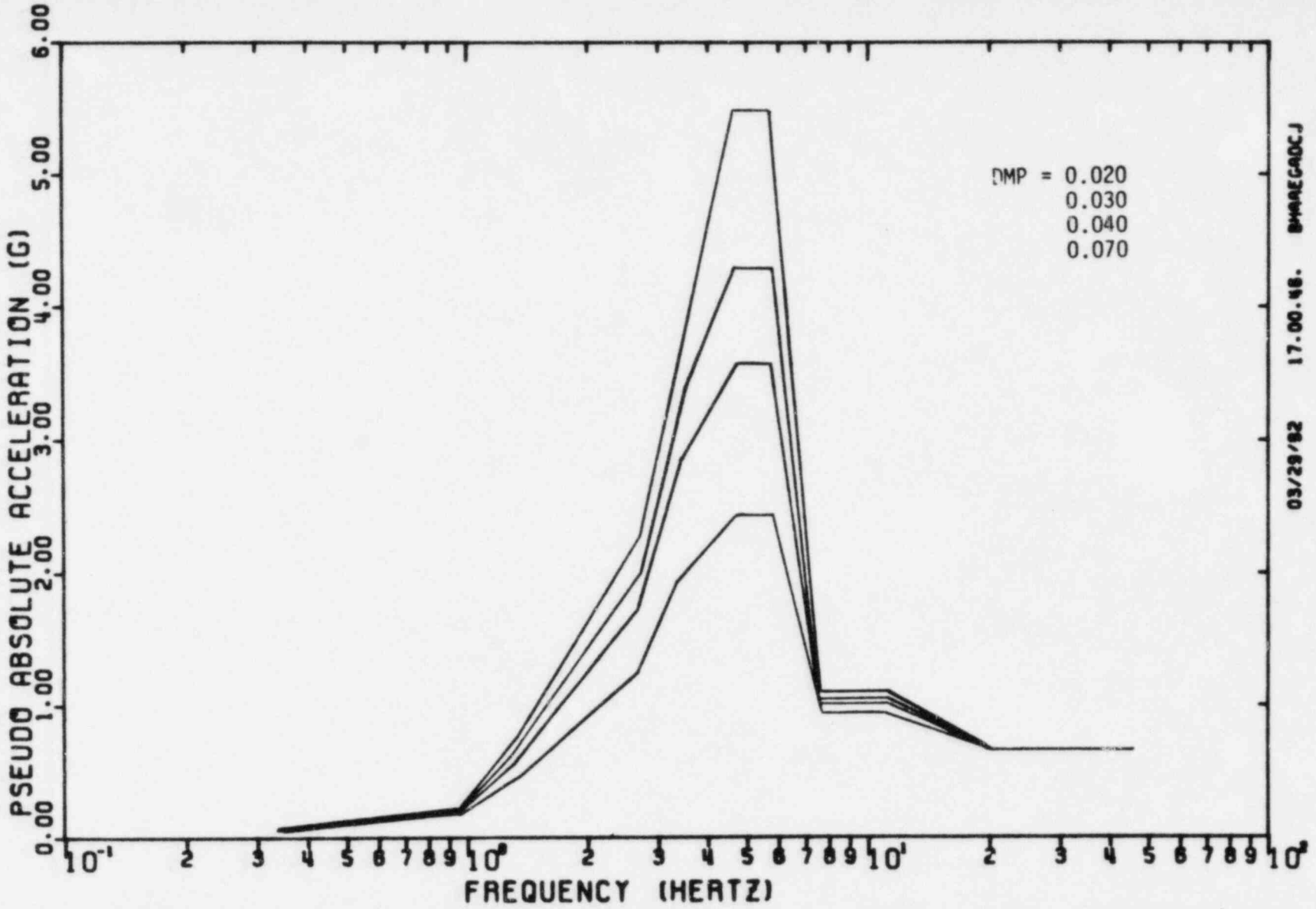

FIGURE III-B-52. Enveloped SRSS Combined Response Spectra
Auxiliary Building, East/West Wings, Elevation 674'-6"
North-South Direction

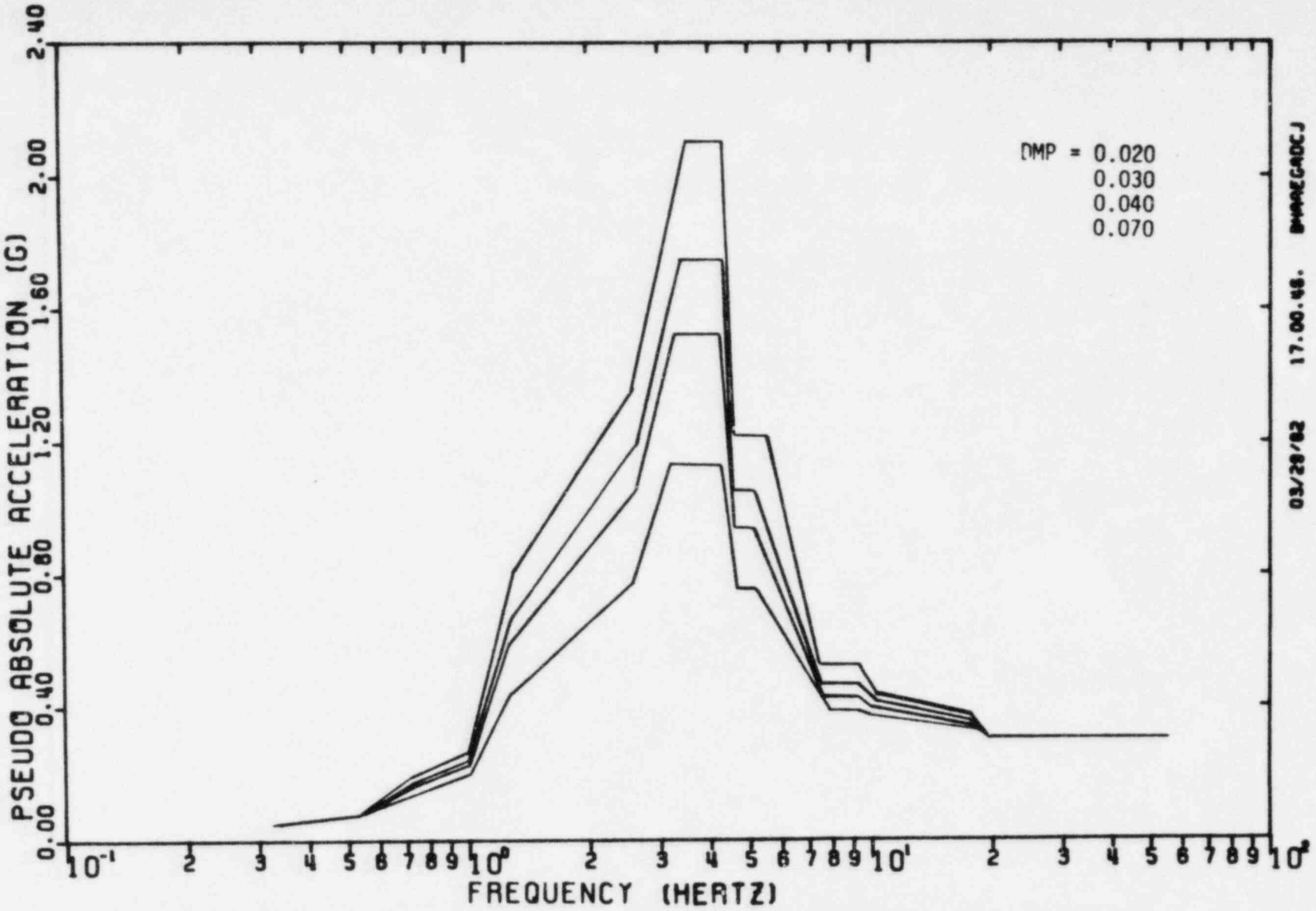

FIGURE III-B-53. Enveloped SRSS Combined Response Spectra
Auxiliary Building, East/West Wings, Elevation 674'-6"
East-West Direction

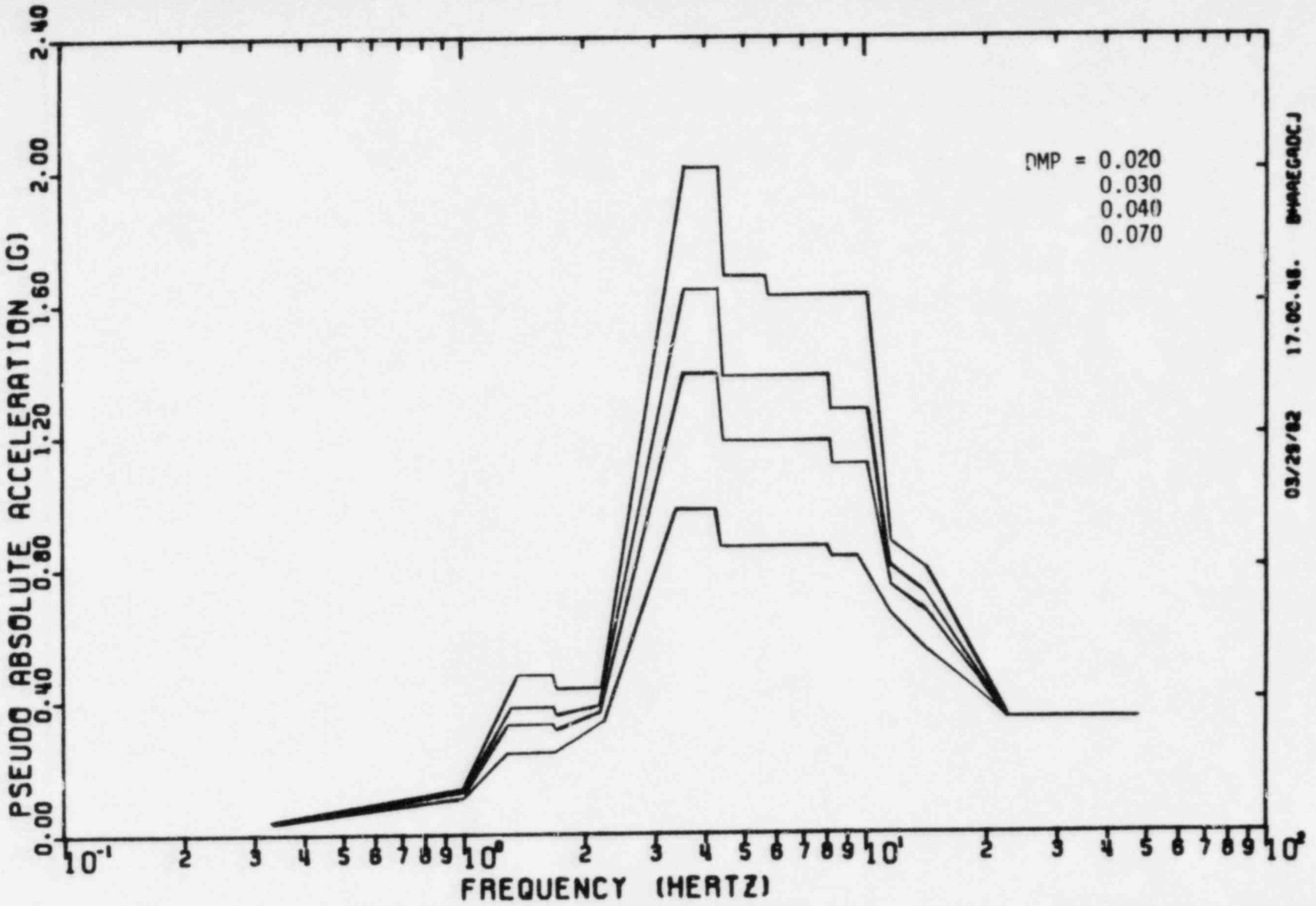

FIGURE III-B-54. Enveloped SRSS Combined Response Spectra
Auxiliary Building, East/West Wings, Elevation 674'-6"
Vertical Direction

APPENDIX III-C

EFFECTS OF OUT-OF-PLANE MOMENTS INCLUDING THERMAL GRADIENTS ON SHEAR WALL OVERTURNING MOMENT CAPACITY

TABLE OF CONTENTS

APPENDIX III-C

Reference 19 presented Equations 4-4 and 4-5 to determine the flexural strength of rectangular shear walls containing uniformly distributed vertical reinforcement. These equations are appropriate for walls subjected to in-plane loads only. Application of out-of-plane moments due to mechanical loads will cause additional stresses that can influence the capacity of the wall available to resist the in-plane overturning moment due to horizontal seismic response of the building. Inclusion of a thermal gradient across the wall can introduce additional out-of-plane moments due to restraint against the thermal curvature provided by the structural supports. This appendix describes the manner in which the effect of the out-of-plane moments including thermal gradient effects on the wall overturning moment capacity was considered.

C.1 EQUIVALENT YIELD STRESS

Examination of Equations 4-4 and 4-5 indicates that the shear wall overturning moment capacity is dependent on the product of the total vertical reinforcement area A_s and the specified reinforcement yield strength f_y. For a unit length of wall not subjected to an out-of-plane moment about a horizontal axis through the wall the pure tensile axial load capacity for the unit length P_{uo} is available to resist the overturning moment.

P_{uo} = Pure tensile axial load capacity of a unit length of wall

$P_{uo} = A_{SL} f_y$

A_{SL} = Vertical reinforcement area per unit length of wall

If an out-of-plane moment acts on the unit wall length, then the tensile axial load capacity P_u available to resist the overturning moment is reduced to some value less than P_{uo}.

The effect of the out-of-plane moments on the wall overturning moment capacity can be accounted for by the definition of an equivalent yield stress f_{ye}. For a unit length of wall, the tensile axial load capacity P_u available when the known out-of-plane moment acts simultaneously can be determined by considering axial load-moment interaction. Different methods permitted by ACI 349 for treating axial load-moment interaction are described in Section C.2. The equivalent yield stress can then be calculated from the available tensile axial load capacity P_u.

f_{ye} = Equivalent yield stress

$$f_{ye} = \frac{P_u}{A_{SL}}$$

P_u = Tensile axial load capacity for a unit length of wall available when the out-of-plane moment occurs simultaneously

To account for the effect of out-of-plane moments in the SMR, the equivalent yield stress f_{ye}, calculated as described above, was substituted for the specified reinforcement yield stress f_y in determining the shear wall overturning moment code capacities. The tensile axial load capacities P_u were determined using the simplified ACI assumptions described in Section C.2.1. As shown in Section C.3, use of these assumptions lead to tensile axial load capacities nearly the same as those predicted by more sophisticated methods including thermal gradient effects.

Although out-of-plane moments typically vary along the length of a wall, the equivalent yield stress was conservatively based on the largest moment predicted by the elements modeling the wall at the story under consideration. Development of the equivalent yield stress is appropriate since the effects of the seismic overturning moments are generally more significant than the effects of the out-of-plane moments, given the conservative nature of the overturning resistances calculated.

Use of the equivalent yield stress accounts for the gradual development of tensile reinforcement yield under increasing in-plane moment that is inherent in Equation 4-5. Attainment of the tensile capacity at a local section of the wall does not necessarily imply failure since additional in-plane moment resistance is available through stress redistribution. Failure occurs for the wall as a whole as predicted by the basic design principles of ACI 349-80.

C.2 TENSILE AXIAL LOAD-MOMENT INTERACTION

Provisions for the design of reinforced concrete members subjected to flexure and axial loads are contained in Section 10 of ACI 349-80. Design assumptions permitted in this code are described in Section 10.2. Members designed in accordance with this section of the code are required to satisfy force equilibrium and strain compatibility. A linear strain distribution can be assumed. The maximum usable concrete compressive strain is limited 0.003 in/in while the concrete tensile strength must be neglected. The reinforcement stress-strain relationship is represented as being elastic-perfectly plastic.

Tensile axial load-moment interaction curves determined using different methods permitted by the code are compared in Section C.3. The procedures used to develop the interaction curves by these different methods are described below. Section C.2.1 describes the application of the simplified assumptions permitted by Section 10.2.7 of ACI 349-80. The code also permits the use of any concrete compressive stress-strain relationship that results in a prediction of strength in substantial agreement with comprehensive tests. The use of the parabolic-linear concrete stress-strain relationship is contained in Section C.2.2. The procedure developed to accomodate the effects of thermal gradients is described in Section C.2.3.

C.2.1 Tensile Axial Load Capacity Using Simplified Assumptions of ACI 349-80. Section 10.2.7

Simplified assumptions to determine the concrete compressive stress distribution are contained in Section 10.2.6 of ACI 349-80. These assumptions were used to develop one of the interaction curves compared in Section C.3. The stress was assumed to be a uniform value of 0.85 f'_c where f'_c is the minimum specified concrete compressive strength. This stress was taken to act over a depth of $\beta_1 c$ fom the extreme compressive fiber, where c is the distance from the extreme compressive fiber to the neutral axis and β_1 is a factor that is a function of the concrete compressive strength.

Discussion in Section 5.2.10 of Reference 20 indicates that general procedures such as this approach are applicable to determine strength under combined axial tension and bending. The rectangular concrete stress block assumption was used to determine the tensile axial load capacity of a unit length of wall given the known out-of-plane mechanical moment. The strain distribution was defined by the maximum usable concrete compressive strain of 0.003 in/in and the distance to the neutral axis c. Concrete and reinforcement forces were then expressed in terms of the distance to the neutral axis c. Equating the internal moment resistance provided by the concrete and reinforcement to the applied out-of-plane moment led to the solution for c. The axial tension capacity given the applied mechanical out-of-plane moment was then calculated as the sum of the concrete and reinforcement forces. This approach was used to determine the equivalent yield stress for code margin calculations.

C.2.2 Tensile Axial Load Capacity Using the Parabolic-Linear Concrete Stress-Strain Relationship

Section 10.2.6 of ACI 349-80 permits any concrete compressive stress-strain relationship that results in a prediction of strength in substantial agreement with comprehensive tests. Reference C-3 notes that an acceptable relationship is parabolic to a strain of 0.002 in/in, at

which the concrete stress is 0.85 f'_c, with a linear reduction in stress at greater strains. The parabolic-linear concrete stress-strain relationship used by Reference C-2 is shown in Figure III-C-1.

The parabolic-linear concrete stress-strain relationship was used in conjunction with the other requirements of ACI 349-80 Section 10.2 to determine the tensile axial load capacities corresponding to the known mechanical out-of-plane moments for the comparison in Section C.3. Ultimate strength conditions occur when the maximum usable concrete compressive strain of 0.003 in/in is attained. Under combined axial tension and moment, large strains in the reinforcement can occur. Although ACI 349-80 Section 10.2 sets no limit on the maximum permissible reinforcement strain, a value of 0.05 in/in was used. This strain limit is conservatively less than the minimum specified value of 7 percent for bar sizes #11 and larger and 9 percent for bar sizes #10 and smaller for ASTM A615, Grade 60 reinforcement (from Reference C-4).

The tensile axial load capacities corresponding to the known mechanical out-of-plane moments were found by satisfying the conditions of force equilibrium and strain compatibility. The linear strain distribution at ultimate strength conditions was defined by the maximum allowable concrete or reinforcement strain and the unknown distance to the neutral axis c. Similar to the solution using the simplified assumptions described in Section C.2.1, the concrete and reinforcement forces were determined from the strain distribution using the stress-strain relationship and expressed in terms of the distance to the neutral axis c. Equating the internal moment resistance provided by the concrete and reinforcement to the applied out-of-plane moment led to the solution for c. The axial tension capacity given the applied mechanical out-of-plane moment was then calculated as the sum of the concrete and reinforcement forces.

C.2.3 Tensile Axial Load Capacity Including Thermal Gradient

Some of the exterior walls and slabs evaluated as part of the SMR are subjected to thermal gradients at normal operating conditions. These thermal gradients can introduce additional out-of-plane moments on the walls and slabs due to restraint against the thermal curvature imposed by their supports. The effect of the thermal gradients on the tensile axial load capacity was also considered.

An approach for determining the additional moment and stresses on containment walls due to a thermal gradient was presented in Reference C-1. A step-by-step procedure to incorporate thermal gradient effects into the evaluation of reinforced concrete cross-sections was developed in Reference C-2. In this procedure, thermal gradient effects were considered in a manner similar to that described in Reference C-1. It was assumed that no change occurred in axial force under thermal effects due to the lack of restraint against axial deformations. The change in curvature due to the thermal gradient was defined as:

$\Delta\phi_T$ = Change in curvature due to a thermal gradient, in^{-1}

$$\Delta\phi_T = \frac{\alpha\Delta T}{t}$$

α = Coefficient of thermal expansion, $in/in/^oF$

ΔT = Thermal differential between the inside and outside member forces, ^oF

t = Member thickness, in

Many of the same assumptions previously described in Section C.2.1 and C.2.2 were adopted in Reference C-2. Strains were taken to be linearly distributed. The parabolic-linear concrete compressive stress-strain relationship shown in Figure III-C-1 was used while the concrete tensile strength was neglected. The reinforcement stress-strain relationship was represented as being elastic-perfectly plastic. The solution techniques involved the satisfaction of force equilibrium and strain compatibility.

To include the effect of thermal gradients on the tensile axial load capacities, the approach described in Section C.2.2 was modified to include the treatment of the thermal gradients as described in References C-1 and C-2. A trial-and-error solution was developed to determine the tensile axial force that, when combined with the known mechanical out-of-plane moment and the thermal gradient would cause the maximum permissible concrete or reinforcement strains to be attained. The material strain limitations used were noted in Section C.2.2. This solution involved the following steps:

1. Define the strain distribution at ultimate strength conditions by assuming that the maximum allowable concrete or reinforcement strain is reached. Assume a value for the curvature ϕ_f including the thermal gradient at ultimate strength conditions.

2. Determine the axial force P_f and moment M_f corresponding to the strain distribution defined in (1) by utilizing the material stress-strain relationships.

3. Determine the curvature without the thermal gradient ϕ_i by deducting the change in curvature due to the thermal gradient $\Delta\phi_T$ from the value at ultimate strength condition ϕ_f.

   $$\phi_i = \phi_f - \Delta\phi_T$$

4. Given ϕ_i, determine the strain distribution that produces an axial force of P_f using the material stress-strain relationships. This step is a consequence of the assumption that the axial force does not change under the application of the thermal gradient.

5. Calculate the moment without the thermal gradient M_i from the strain distribution found in (4). The additional moment due to the thermal gradient can be found by:

   ΔM_T = Additional momnt due to the thermal gradient

   $\Delta M_T = M_f - M_i$

6. Compare M_i to the known mechanical out-of-plane moment. If they are not equal, repeat steps (1) to (6) using a different assumed curvature at ultimate strength conditions ϕf.

7. If M_i is equal to the known mechanical out-of-plane moment, then the tensile axial load capacity is P_f. In other words, if the mechanical out-of-plane moment is a value M_i, then the application of a tensile axial force P and the thermal gradient will cause the section to reach ultimate strength conditions.

This solution procedure satisfies the general requirements of Appendix A of ACI 349-80. A coefficient of thermal expansion α of 5.5×10^{-6} in/in/^{o}F was used in accordance with Section A.3.3 (d) of the code.

C.3 COMPARISON OF RESULTS

To determine the effect of different representations of the concrete stress distribution and the inclusion of a thermal gradient, the tensile axial load out-of-plane mechanical moment interaction curves were developed for a selected wall section. The wall chosen for evaluation was the south wall of the diesel generator building. This wall is representative of the walls evaluated in the SMR. This wall is 30 inches thick and reinforced by #8 vertical bars spaced 12 inches apart at both faces. The thermal gradient of 61^{o}F transmitted by Reference 29 was based on the most severe combination of interior operating temperature and the worst effective winter exterior temperature.

The interaction curve determined using the simplified ACI 349-80 assumptions described in Section C.2.1 is plotted on Figure III-C-2. Also plotted on this figure is the interaction curve found by using the parabolic-linear concrete stress-strain relationship and including the thermal gradient as noted in Section C.2.3. For the latter curve, the moment values plotted are the mechanical out-of-plane moments that lead to ultimate strength conditions when combined with the thermal gradient and the corresponding tensile axial load capacities. The interaction curves developed using the parabolic-linear concrete stress-strain relationship with and without the thermal gradient are nearly the same.

The interaction curves shown in Figure III-C-2 lie very close to each other. Based upon this comparison for the selected representative wall, it can be concluded that the use of the simplified ACI assumptions to determine the tensile axial load capacity corresponding to a known out-of-plane mechanical moment provides an adequate approximation to a more sophisticated method including the thermal gradient. The simplified ACI assumptions were used to define the equivalent reinforcement yield stress f_{ye} included in the wall and diaphragm in-plane moment capacity evaluation.

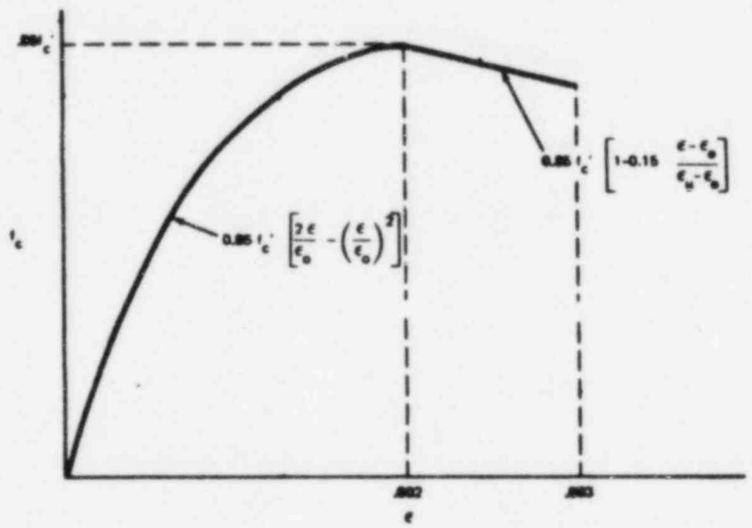

FIGURE III-C-1. PARABOLIC-LINEAR CONCRETE STRESS-STRAIN RELATIONSHIP (FROM REFERENCE 31)

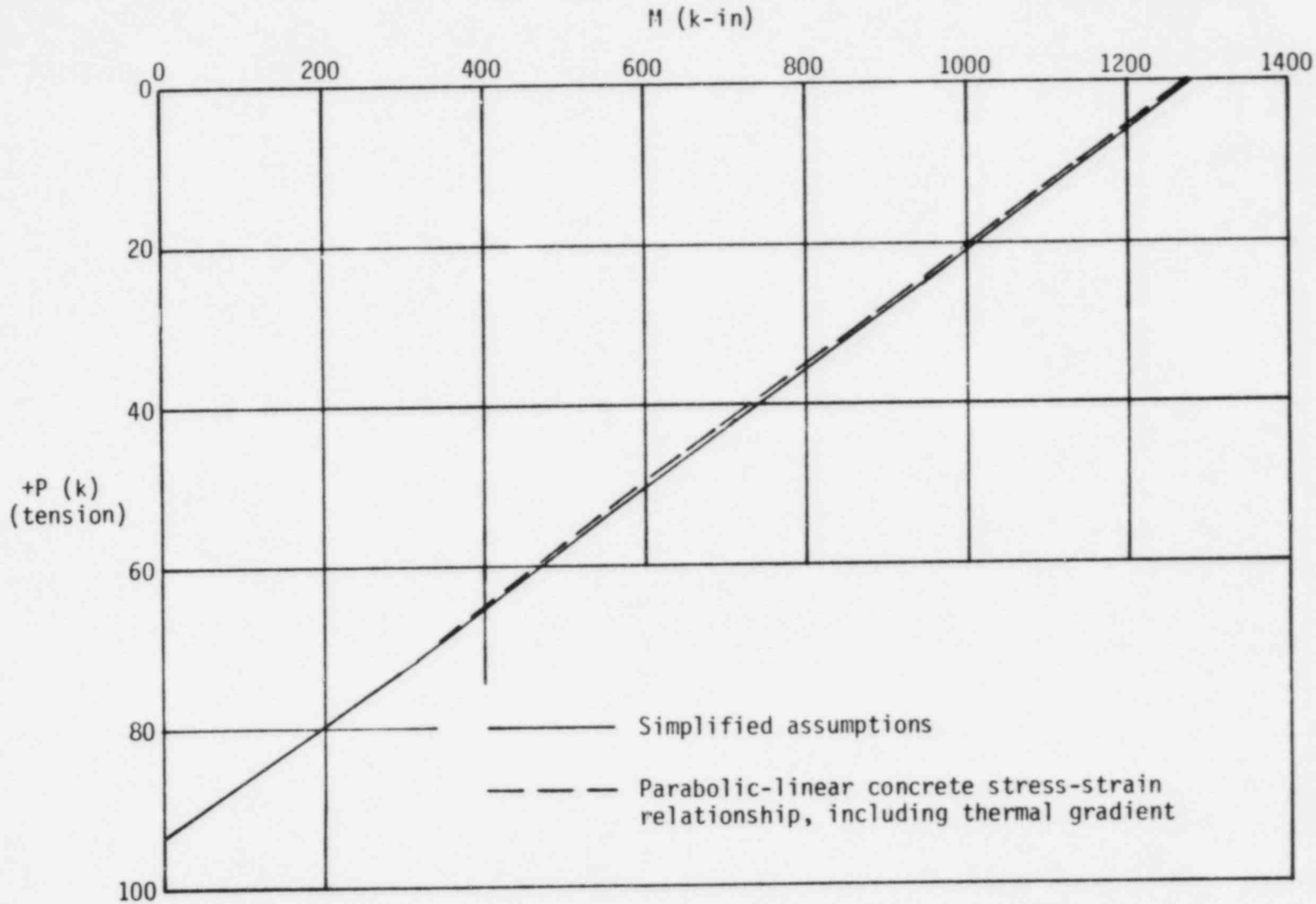

FIGURE III-C-2. COMPARISON OF INTERACTION CURVES USING DIFFERENT APPROACHES

REFERENCES

C-1 Gurfinkel, G., "Thermal Effects in Walls of Nuclear Containments - Elastic and Inelastic Behavior", First International Conference on Structural Mechanics in Reactor Technology, Berlin, Germany, September 20-24, 1971.

C-2 Kohli, T. D. and O. Gurbuz, "Optimum Design of Reinforced Concrete for Nuclear Containments, Including Thermal Effects", Second ASCE Specialty Conference on Structural Design of Nuclear Plant Facilities, New Orleans, Louisiana, December 8-10, 1975.

C-3 Structural Analysis and Design of Nuclear Plant Facilities, American Society of Civil Engineers, 1980.

C-4 Final Safety Analysis Report (FSAR), Midland Plant - Units 1 and 2, Consumers Power Company.